



**Appraisal of the stability of a road tunnel based on microfracture
distribution and total displacement of the rock mass**

by

Mrs Vhutali Carol Madanda

Student number: 14488523

Submitted in accordance with the requirements for the degree of

Doctor of Philosophy

In the subject

Mining Engineering (Rock Engineering)

at the

School of Engineering

College of Science, Engineering, and Technology

University of South Africa

Supervisor: Prof Francois Mulenga

Co-Supervisor: Dr Fhatuwani Sengani

(July 2023)

Declaration

Name: Mrs Vhutali Carol Madanda

Student Number: 14488523

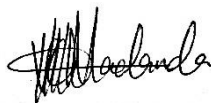
Degree: Doctor of Philosophy

Title: Appraisal of the stability of a road tunnel based on microfracture distribution and total displacement of the rock mass

I declare that the above thesis is my own work and that all the sources that I have used or quoted have been indicated and acknowledged by means of complete references.

I further declare that I submitted the thesis to originality checking software and that it falls within the accepted requirements for originality.

I further declare that I have not previously submitted this work, or part of it, for examination at Unisa for another qualification or at any other higher education institution.



Signature

10 July 2023

Date

Abstract

Appraisal of the stability of a road tunnel based on microfracture distribution and total displacement of the rock mass.

In tunnelling, instability is always a major concern for the safety of people and equipment. Tunnels are designed to maintain a specific profile; however, deterioration tends to occur over time due to factors such as age and wear, water infiltration, chemical attack, ground movements and poor maintenance.

The main objective of this thesis was to predict the effects of fracturing on road tunnel stability. This was achieved through the application of finite element modelling approaches and linear regression analysis technique. A predictive model was developed using supervised machine learning algorithm. This was done to predict the fracturing along the road tunnels using the Hendrik Verwoerd tunnels as case studies. The predictive model showed that shallow tunnels can be classified into three zones based on the fracturing intensity. For road tunnels, the middle portion is characterised by little or no fracturing (Zone 1). The intensity of fracturing increases when moving outside of the tunnel. Moderately fractured zone was referred to as Zone 2 and highly fracture zone was referred to as Zone 3 in this thesis.

The effect of fracturing for each zone was analysed and support lining was proposed to cater for the three zones. According to the suggested support lining strategy, zone 1 inside a new road tunnel should have lining that is 0.3 meters thick if the overall lining for the tunnel is intended to be 0.3 meters thick. Zones 2 and 3 should have linings that are respectively 0.4 (i.e., 0.3 + 0.1) and 0.5 (i.e., 0.3 + 0.2) meters thick. Each zone was assessed individually, and support capacity diagrams were used to validate the proposed support.

Keywords: Tunnelling, tunnel stability, machine learning, thin section, microcracks, fracture propagation, jointed rock mass, tunnel lining

List of Publications

The following articles have been published or submitted to peer-reviewed journals in fulfilment of the requirements for the degree of Doctor of Philosophy.

Published:

Madanda, V.C., Sengani, F. and Mulenga, F., 2023. Applications of Fuzzy Theory-Based Approaches in Tunnelling Geomechanics: a State-of-the-Art Review. *Mining, Metallurgy & Exploration*, pp.1-19.

Submitted for review:

Madanda, V.C., Mulenga, F.K., Sengani F., 2023. Effects of fracture distribution on tunnel stability. (*Geotechnical and Geological Engineering*)

Madanda, V.C., Mulenga, F.K., Sengani F., 2023. Predicting fracture distribution along road tunnels. (*Geotechnical and Geological Engineering*)

Dedication

I dedicate this thesis to my husband, parents and siblings for their endless love, encouragement and support in my pursuit for education. Lastly, to everyone who played part in making this thesis a success, I appreciate your efforts.

Acknowledgments

First and foremost, I would like to register my profound gratitude to the Almighty God for grace, good health, strength, wisdom and understanding to further my education and complete my Doctor of Philosophy degree.

I wish to acknowledge my supervisors Professor Francois Mulenga from University of South Africa and Dr Fhatuwani Sengani from University of Limpopo who made this work possible. Their guidance and advises carried me through all the stages of writing my thesis. I appreciate your immense contributions, commitment, and support towards my studies. I also would like to thank University of South Africa for funding this research.

I would like to give a special thanks to my husband Mr. Samuel Madanda for his endless support and sacrifices towards my studies. I am also grateful to my amazing parents and sisters (Mr. Humbulani & Mrs. Livhuwani Netshilaphala, Mrs. KP Munyai and Ms. L Netshilaphala) who are the source of any success in my life. May the Almighty God shower you with blessings.

Finally, I would like to express my gratitude to my extended family, friends and colleagues in the Department of Mining Engineering, University of South Africa, for their moral support.

Table of Contents

Declaration.....	i
Abstract.....	ii
List of Publications.....	iii
Dedication.....	iv
Acknowledgments.....	v
Table of Contents.....	vi
List of Figures.....	x
List of Tables.....	xvi
List of Abbreviations.....	xvii
List of Symbols.....	xviii
1. Chapter 1: Introduction.....	1
1.1. Research context.....	1
1.2. Problem statement.....	3
1.3. Research objectives.....	5
1.4. Contribution to the body of knowledge.....	6
1.5. Location of the study.....	7
1.6. Layout of the thesis.....	9
2. Chapter 2: Literature Review.....	11
2.1. Traditional methods of rock mass classification.....	11
2.1.1. Barton's Q-system.....	12
2.1.2. Bieniawski's geomechanics classification.....	15
2.1.3. Laubscher's Mining Rock Mass Classification.....	16
2.1.4. Geological strength index.....	17
2.2. Fuzzy set theory.....	24

2.2.1.	Fuzzy logic	26
2.2.2.	Fuzzy inference techniques and their application in mining geomechanics	27
2.3.	Innovative application of fuzzy inference system in mining geomechanics	33
2.3.1.	Slope stability analysis	33
2.3.2.	Stability analysis of tunnels under construction	34
2.3.3.	Stress analysis in tunnels.....	35
2.3.4.	Tunnel convergence.....	36
2.4.	Recent case studies on FIS applications in tunnelling	38
2.5.	Ground characteristics and support reaction curves.....	40
2.6.	Comparison of measurement methods for tunnel convergence..	42
2.6.1.	Method 1: Total station.....	42
2.6.2.	Method 2: Laser scanner.....	44
2.6.3.	Method 3: Photogrammetry	45
2.6.4.	Method 4: Wireless sensors	46
2.6.5.	General conclusions of the four tunnel convergence measurement techniques.	47
2.7.	Concluding remarks.....	48
3.	Chapter 3: Materials and Methodology.....	51
3.1.	Introduction	51
3.2.	Field observations and measurements	52
3.2.1.	Observations	53
3.2.2.	Field measurements.....	54
3.3.	Laboratory experiments and analysis	59
3.4.	Data analysis using Machine Learning	62
3.5.	Numerical simulation work.....	64

3.5.1.	Estimating rock mass properties using RocLab	65
3.5.2.	Kinematic analysis.....	68
3.5.3.	Rock slope stability analysis.....	70
3.6.	Strength reduction factor.....	71
3.7.	Tunnel deformation analysis using RS2.....	72
3.8.	Limitations and challenges.....	77
4.	Chapter 4: Field Observations and Measurements	79
4.1.	Introduction	79
4.2.	Observations.....	80
4.2.1.	Observations on Tunnel One	80
4.2.2.	Observations on Tunnel Two	83
4.3.	Field measurements and analysis	85
4.3.1.	Rock mass rating using GSI for Tunnel One	86
4.3.2.	Rock mass rating using GSI for Tunnel Two	87
4.3.3.	Rock mass properties estimation for Tunnel One	88
4.3.4.	Rock mass properties estimation for Tunnel Two	91
4.4.	Structural analysis and development of joint sets	95
4.4.1.	Developing joint sets of the tunnels.....	96
4.4.2.	Kinematic failure analysis.....	96
4.5.	Establishing the rock mass failure models	102
4.5.1.	Toppling Analysis	102
4.5.2.	Wedge analysis (for single and multi-tetrahedral wedges) .	103
4.5.3.	Planar failure	104
4.6.	Conclusion	106
5.	Chapter 5: Developing an Empirical Chart for Fracturing Distribution in Shallow Tunnels.....	108

5.1.	Introduction	108
5.2.	Micro-fracturing analysis	110
5.2.1.	Micro-fracturing analysis on the right side of tunnel one. ...	110
5.2.2.	Micro-fracturing analysis on the left side of tunnel one.....	114
5.3.	Rock failure analysis on a large scale.....	118
5.4.	Development of an empirical chart of fracture distribution	119
5.5.	Conclusion	124
6.	Chapter 6: Effects of Fracture Distribution on Tunnel Stability	126
6.1.	Introduction	126
6.2.	Effects of fracturing on shallow tunnels using Optum G2.....	126
6.3.	Effects of fracture distribution on strength factor and total displacement in shallow tunnels	133
6.3.1.	Total displacement around the tunnel in RS2.....	134
6.3.2.	Total displacement around the tunnel in RS2.....	137
6.4.	Design of tunnel lining based on factor of safety.	143
6.5.	Conclusions	150
7.	Chapter 7: Conclusions and Recommendations for Future Research... ..	151
7.1.	Summary of the thesis	151
7.2.	Techniques, analysis, and findings	154
7.3.	Original contribution	156
7.4.	Overall conclusion of the thesis	156
7.5.	Recommended future research.	158
	LIST OF REFERENCES	159
	APPENDIX.....	178

List of Figures

Figure 1.1: Ground characteristic curve (GCC) and support reaction line (SRL) in the graphical representation of convergence-confinement (Sandrone and Labiouse, 2010).....	4
Figure 1.2: Hendrik Verwoerd tunnels in Limpopo (Google Maps, 2022)...	8
Figure 2.1: Estimated support categories based on tunnelling quality index Q (Grimstad and Barton, 1993).....	14
Figure 2.2: GSI estimates correlated with geological observations (Stacey, 2001).....	21
Figure 2.3: An example of using the GSI Chart.....	22
Figure 2.4: Crisp set and fuzzy set illustrated (After Chetan, 2021)	25
Figure 2.5: Fuzzy logic process (After Murnawan et al., 2021)	26
Figure 2.6: Results of the proposed system, 3D FDM, and characteristic curve method are compared (Rangel et al., 2005).....	35
Figure 2.7: Structure of the ANFIS model for crown convergence prediction (Adoko and Wu, 2012)	38
Figure 2.8: Ground reaction curve (GRC) and Support Reaction Curve (SRC) (Lu et al., 2022).....	41
Figure 2.9: Schematic illustration of the total station measurement set-up with four different instrument positions (Erlandsson, 2020)	43
Figure 2.10: Schematic illustration of the laser scanner setup with three different instrument positions (Erlandsson, 2020)	45
Figure 2.11: Schematic illustration of capturing photos for the photogrammetry method (Erlandsson, 2020).....	46
Figure 3.1: Areal map of the study area (Google Maps, 2022)	53
Figure 3.2: Geological tools used for field measurements. (a) Tape measurement, (b) Geological hammer, (c) Sample bag, (d) Clino ruler, (e) Compass, (f) Field notebook and pen	55
Figure 3.3: Jointed rock mass in the periphery of the tunnels	55
Figure 3.4: Scanline mapping technique for geotechnical data collection (Chaminé et al., 2015)	58

Figure 3.5: Scanline mapping and terminologies for rock mass properties (After Harrison and Hudson, 1997)	58
Figure 3.6: Scanline mapping in the periphery of the tunnels	59
Figure 3.7: Thin section preparation at the laboratory. (a) Cutting machine, (b) Drying process, (c) Course and fine silicon carbide powder, and (d) Polishing	60
Figure 3.8: Schematic diagram of thin section preparation. (a) Sample block with one polished side fixed on glass, (b) Final 35µm thick section of the sample block, (c) Thin section covered by glass on both sides (Sturm, 2010)	61
Figure 3.9: Machine Learning Flowchart (Modified after MathWorks, 2022)	63
Figure 3.10: Estimating intact uniaxial compressive strength in RocLab .	66
Figure 3.11: Choosing GSI number in RocLab	67
Figure 3.12: Choosing the mean constant value (m_i) in RocLab	67
Figure 3.13: Choosing disturbance factor (D) in RocLab	68
Figure 3.14: Rock mass strength parameters estimated in RocLab.....	68
Figure 3.15: Creating a DIPS file.	69
Figure 3.16: Example of scatter plots and contour plots in DIPS	70
Figure 3.17: Example of major plane plots in DIPS.....	70
Figure 3.18: Strength reduction factor simulation running on Optum G2 .	71
Figure 3.19: Example of SRF simulation on tunnel in Optum G2.....	72
Figure 3.20: Starting a new project in RS2	73
Figure 3.21: General project settings in RS2	73
Figure 3.22: Defining the arch and external boundary	74
Figure 3.23: Excavation and external boundary defined.	74
Figure 3.24: Illustration of how joint properties and joint network are defined in RS2	75
Figure 3.25: Mesh set up in RS2.....	75
Figure 3.26: Field stress set up in RS2	76

Figure 3.27: Defining rock mass properties in RS2.....	76
Figure 3.28: Example of computing in RS2.....	77
Figure 4.1: Rock mass conditions on the right side (A) and the left side (B) of Tunnel One	81
Figure 4.2: Rock mass conditions in the vicinity of Tunnel One: (a) Blocky weathered ground supported with wire mesh; (b) Fractured rock on the top of the tunnel; (c) Evidence of rock fall from the top of the tunnel; and (d) Evidence of rock fall on the left side of the tunnel	82
Figure 4.3: Evidence of water seepage in Tunnel One	83
Figure 4.4: Rock Mass conditions in the vicinity of Tunnel Two. (a) blocky rock mass supported with rock bolts and wire mesh; (b) blocky side wall with evidence of vegetation; (c) blocky rock mass around the tunnel entrance; (d) evidence of rock falls	84
Figure 4.5: Evidence of water seepage in Tunnel Two	85
Figure 4.6: GSI rock mass rating on tunnel one: (a) tunnel one with all three sides visible, (b)Top portion of tunnel one, (c) right side of tunnel one, (d) left side of tunnel one.....	86
Figure 4.7: GSI rock mass rating on Tunnel Two: (a) tunnel one with all three sides visible, (b) left side of tunnel two, (c) top portion of tunnel two, (d) right side of tunnel two.....	88
Figure 4.8: GSI estimation for the rock mass slope of Tunnel One.....	89
Figure 4.9: Principal stresses for the Tunnel One slope	91
Figure 4.10: Normal stress vs shear stress for Tunnel One.....	91
Figure 4.11: GSI estimation for tunnel two rock mass slope	92
Figure 4.12: Principal stresses for the Tunnel Two slope	94
Figure 4.13:Normal stress vs shear stress for Tunnel Two.....	94
Figure 4.14: Scanline mapping in the vicinity of the tunnels	95
Figure 4.15: Pole plots of mapped discontinuities.....	97
Figure 4.16: Contour plots of mapped discontinuities	98
Figure 4.17: Contour plot with mean discontinuity planes and face planes	98
Figure 4.18: Planar failure analysis using DIPS.....	99

Figure 4.19: Toppling failure analysis using DIPS.....	100
Figure 4.20: Wedge failure analysis using DIPS	101
Figure 4.21: Schematic illustration of toppling failure (Cundall, 1971) ...	103
Figure 4.22: Wedge failure using deterministic analysis using Swedge.	104
Figure 4.23: Simulated representation of plane failure using deterministic analysis.....	105
Figure 4.24: Simulation of planar failure on the rock slope in the periphery of the tunnels	106
Figure 5.1: Microcracks at Point 1 on the right side of Tunnel One.....	111
Figure 5.2: Microcracks at Point 2 on the right side of Tunnel One.....	111
Figure 5.3: Microcracks at Point 3 on the right side of Tunnel One.....	112
Figure 5.4: Microcracks at Point 7 on the right side of Tunnel One.....	112
Figure 5.5: Microcracks at Point 8 on the right side of Tunnel One.....	113
Figure 5.6: Microcracks at Point 13 on the right side of Tunnel One.....	113
Figure 5.7: Microcracks at Point 14 on the right side of Tunnel One.....	114
Figure 5.8: Microcracks at Point 1 on the left side of Tunnel One.....	115
Figure 5.9: Microcracks at Point 2 on the left side of Tunnel One.....	116
Figure 5.10: Microcracks at Point 3 on the left side of Tunnel One.....	116
Figure 5.11: Microcracks at Point 5 on the left side of Tunnel One.....	117
Figure 5.12: Microcracks at Point 6 on the left side of Tunnel One.....	117
Figure 5.13: Microcracks at Point 10 on the left side of Tunnel One.....	118
Figure 5.14: Rock fracturing from micro to macro scale (Modified after Ghamgosar, 2017).....	119
Figure 5.15: Predictive chart of fracture distribution in shallow tunnels..	123
Figure 6.1: Tunnel simulation dimensions.....	127
Figure 6.2: Fracture distribution in Zone 1 using Optum G2	128
Figure 6.3: Fracture distribution in Zone 2 using Optum G2	129

Figure 6.4: Fracture distribution in Zone 3 using Optum G2	130
Figure 6.5: Strength reduction factor and fracture distribution along tunnel one.....	132
Figure 6.6: Predictive chart of fracture distribution and relative strength reduction factor per zone in shallow tunnels	133
Figure 6.7: Section view of fracture distribution along the tunnel in different zones	134
Figure 6.8: Simulated strength factor in various stages of Zone 1	135
Figure 6.9: Simulated strength factor in various stages of Zone 2	135
Figure 6.10: Simulated strength factor in various stages of Zone 3	136
Figure 6.11: Total displacement analysis on three sides of the tunnel...	137
Figure 6.12: Simulated total displacement in Zone 1 using RS2.....	138
Figure 6.13: Simulated total displacement in Zone 2 using RS2.....	138
Figure 6.14: Simulated total displacement in Zone 3 using RS2.....	139
Figure 6.15: Total displacement on the tunnel crown Zone 1	139
Figure 6.16: Total displacement on the tunnel crown Zone 2	140
Figure 6.17: Total displacement on the tunnel crown in Zone 3.....	140
Figure 6.18: Total displacement on the tunnel crown.....	141
Figure 6.19: Total displacement on the left sidewall	142
Figure 6.20: Total displacement on the right sidewall	142
Figure 6.21: Major Principal stress in Zone 1 before and after support installation.....	144
Figure 6.22: Total displacement in Zone 1 before and after support installation.....	144
Figure 6.23: Support capacity diagrams for Zone 1	145
Figure 6.24: Major principal stress in Zone 2 before and after support installation.....	146
Figure 6.25: Total displacement in Zone 2 before and after support installation.....	146

Figure 6.26: Major principal stress in Zone 3 before support installation	146
Figure 6.27: Total displacement in Zone 3 before and after support installation.....	147
Figure 6.28: Support capacity diagrams for Zone 2	147
Figure 6.29: Support capacity diagrams for Zone 3	148
Figure 6.30: Points evaluated before and after support installation.	148

List of Tables

Table 2.1: Description and ratings table for joint water reduction factor (Barton et al., 1974)	13
Table 2.2: GSI values and corresponding quality of rock mass (Hoek, 1994)	23
Table 2.3: Fuzzy inference system applied in mining geomechanics.....	31
Table 2.4: Performance of the prediction model (Adoko and Wu, 2012)..	39
Table 2.5: Uncertainty at 95% confidence and cost for four deformation measurement methods (After Erlandsson, 2020).....	47
Table 3.1: Field measurement geotechnical parameters	56
Table 3.2: Mechanical properties of the rock	65
Table 4.1: Rock mass properties estimation for Tunnel One through the means of RocLab.....	90
Table 4.2: Rock Mass properties estimation for Tunnel Two through the means of RocLab.....	92
Table 4.3: Joint sets developed based on mapping data	97
Table 5.1: Total number of fractures for right side of tunnel one.....	120
Table 5.2: Total number of fractures for left side of tunnel one	121
Table 5.3: Total number of fractures around tunnel one	122
Table 6.1: Strength reduction factor for fracture distribution along the tunnel	131
Table 6.2: Support design parameters.....	143
Table 6.3: Major principal stresses (in MPa) before and after support installation.....	149
Table 6.4: Total displacement (m) before and after support installation.	149

List of Abbreviations

Abbreviation	Description
FEM	Finite element method
FOS	Factor of safety
GCC	Ground characteristic curve
GSI	Geological strength index
m	Metre
ML	Machine learning
MRMR	Mining rock mass rating
Pa	Pascal
RMR	Rock mass rating
RQD	Rock quality designation
SRF	Stress reduction factor
SRL	Support reaction line
UCS	Uniaxial compressive stress

List of Symbols

Symbol	Description	Unit
J_a	Joint alteration number	Dimensionless
J_n	Joint set number	Dimensionless
J_r	Joint roughness number	Dimensionless
J_v	Volumetric joint count	Dimensionless
J_w	Joint water reduction factor	Dimensionless
σ_n	Normal stress	Pa
σ_t	Tensile strength	Pa
UCS	Uniaxial compressive strength	Pa
σ_1	Major principal stress	Pa
σ_3	Minor Principal stress	Pa
σ_{ci}	Unconfined compressive strength of the intact rock	Pa
σ_{cm}	Global strength	Pa
m	Hoek-Brown constant for the rock	Dimensionless
m_b	Material constant (rock mass)	Dimensionless
m_i	Material constant (intact rock)	Dimensionless
s	Material constant	Dimensionless
a	Material constant	Dimensionless
D	Disturbance factor	Dimensionless
ρ	Density	kg/m ³
γ	Unit weight	kN/m ³
E	Elastic modulus	GPa

ν	Poisson's ratio	Dimensionless
τ	Shear stress	Pa
ϕ	Angle of internal friction	Degrees ($^{\circ}$)
c	Cohesion	Pa

1. Chapter 1: Introduction

1.1. Research context

Tunnels are designed and constructed to serve different purposes which include but are not limited to road and railway transportation, development in mining, storage, civil defence, water, and sewage. Generally, road and railway tunnels are constructed through hills or mountainous terrains. Like any other structure, tunnels deteriorate with time. The deterioration may be due to the evolution and/or creation of micro to large geological structures such as fractures and joints in the periphery of the tunnel.

Limpopo province in South Africa has mountainous topography which has led to the construction of road tunnels through drilling and blasting techniques in the late 1960s. Fifty to sixty years later, these tunnels are still operational. However, their common challenge is tunnel convergence or deterioration as are usually experienced by road tunnels (Sandrone et al., 2007; Sandrone, 2008). To ensure daily safety, efficient maintenance practices need to be put in place considering the type of deterioration on and around the tunnel. Deterioration is expected to occur on both the rock mass around the tunnel and the support system installed in the tunnel (i.e., roof bolts and concrete lining). As such, the initial conditions of the tunnel can be used to establish the level of degradation experienced by the rock mass and the lining. By so doing, it should be possible to assess the evolution of the stability conditions of the tunnel with time. Tunnel equilibrium is significantly dependent on the interaction between the rock mass and the lining, as Sandrone and Labiouse (2010) argued.

Scholars such as Brown et al. (1983), Panet (1995), Carranza-Torres and Fairhurst (2000), and Park and Kim (2006) have conducted critical literature reviews on road tunnel deterioration. From these reviews, it appears that few methods exist for the analysis of tunnel deterioration. However, the convergence-confinement method and the rock mass classification methods are the most common due to their simplicity. Technically, the

convergence-confinement method is limited to basic assumptions of plane strain and axisymmetric conditions (Sandrone and Labiouse, 2010). Every engineering problem is basically in three-dimensions (x, y, z) coordinate system. However, for analysis the problems are usually considered as two-dimensional problems. In plane strain, the analysis of strain condition is in one plane only. Therefore, the out-of-plane displacement (strain) is, by definition, zero. In the axisymmetric condition, the geometry, material properties and loading conditions are symmetric about one axis. This symmetry axis is usually aligned with the z -axis of the cylindrical (r, θ, z) coordinate system. Deterioration of tunnels frequently occurs gradually over time. Plane strain and symmetry assumptions are made under the assumption of steady-state conditions and do not consider the effects of time-dependent phenomena like creep, relaxation, or long-term material deterioration. A consideration of appropriate material models and the use of specialised modelling techniques are required to account for time-dependent behaviour.

The rock mass classification method, on the other hand, is governed by subjective uncertainties (Nguyen, 1985; Adoko et al., 2016). For example, where the RQD approach is generally required, uncertainties results from core logging because of core handling and alteration of the degree of fracturing (Nguyen, 1985). Moreover, ambiguous words and phrases such as highly weathered, very blocky, and large water inflow are used to describe geotechnical parameters that are rated using some index values.

The limitations of the two traditional methods (convergence-confinement and rock mass classification) are well known. As a result, they cannot fully address a complex geomechanics problem like tunnel deterioration on their own (Nguyen, 1985; Adoko and Yagiz, 2018). Recent work suggests that Machine Learning together with advanced geomechanics approaches could be useful tools to analyse the effects of the main degradation processes on the long-term stability conditions of tunnels (see Adoko and Wu, 2011;

Adoko et al., 2011; Adoko and Wu, 2012; Adoko et al., 2013a & b; Adoko et al., 2016; Adoko and Yagiz, 2018).

In this thesis, this is what is explored. This thesis explores the use of microfracture distribution and total displacement of the rock mass to appraise the stability of the road tunnel. This approach is suggested to improve the design and maintenance of tunnels. The Hendrik Verwoerd tunnels along the N1 in Limpopo Province, South Africa have been identified as case studies for this thesis.

1.2. Problem statement

In tunnelling design, the selection of appropriate excavation methods and techniques is critical. This is because the potential modes of failure for the rock conditions encountered depend on the excavation techniques used. An understanding of the possible failure modes is therefore central to making informed decisions regarding support units that will maintain the required profile of the tunnel.

Generally, the tunnel profile is influenced by the intended function of the tunnel. For example, road tunnels are designed to shorten the traveling distance between two points (regions). Therefore, a road tunnel profile should accommodate at least two lanes, ventilation, drainage, and services. In addition to this, a tunnel should be designed to maintain a specific profile (i.e., size and shape) and constructed as per design. Failure to adhere to the design may compromise the safety and stability of the overall tunnel.

Any built structure including tunnels is bound to deteriorate over time (Boidy, 2002, Boydy et al., 2002). And in the case of a tunnel, the support system and the rock mass in the periphery of the tunnel are both expected to deteriorate. Several scholars (e.g., Brown et al., 1983; Panet, 1995; Carranza-Torres and Fairhurst, 2000; Park and Kim, 2006) have identified several factors that drive such deterioration. Nonetheless, it appears that water seepage, cracks, fracturing, and degrading of the rock mass around

the tunnel are the most important. This is because they are acknowledged to negatively affect the overall stability of the tunnel (Liu et al., 2017; Zhou et al., 2018; Frenelus et al., 2021).

Tunnel deterioration is primarily analysed using techniques commonly referred to as convergence methods. These methods have historically incorporated time, rock mass and lining degradations in the assessment of tunnel equilibrium conditions (Brown et al., 1983; Panet, 1995; Carranza-Torres and Fairhurst, 2000; Park and Kim 2006). Figure 1.1 illustrates the calculation of the characteristic lines for a circular tunnel. These lines are used to establish the equilibrium of a tunnel.

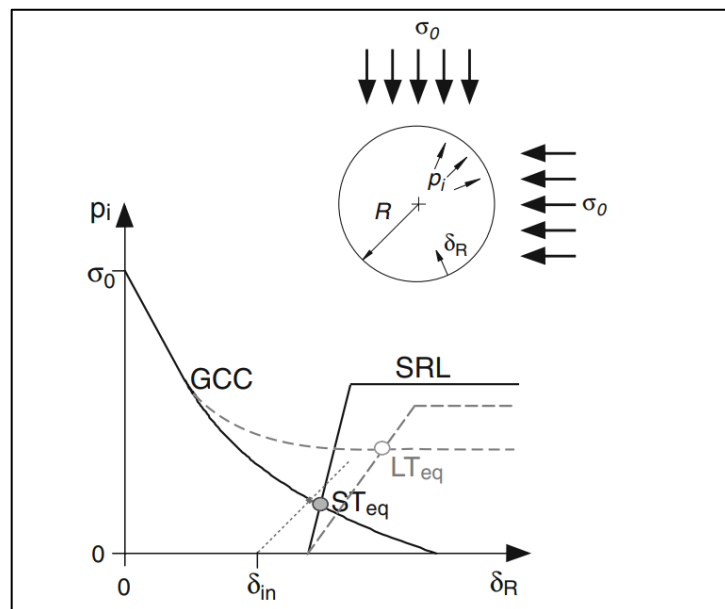


Figure 1.1: Ground characteristic curve (GCC) and support reaction line (SRL) in the graphical representation of convergence-confinement (Sandrone and Labiouse, 2010)

The response of the rock mass defines the GCC, whereas the response of the installed support is defined by the SRL. The equilibrium point related to short-term conditions is indicated by the intersection of the GCC and the SRL. The dotted lines are suggested for long-term stability where the proposed long term equilibrium point is represented by LT_{eq} in Figure 1.1.

Authors like Panet (1979), Cristescu (1985, 1988 & 1994) and Cristescu and Hunsche (1998) have contributed to developing the convergence-confinement method for tunnel deterioration. And although the method is widespread, it is based on restrictive assumptions of plane strain and axisymmetric conditions as explained in Section 1.1. The use of the convergence-confinement method alone to verify tunnel stability is constrained by these factors.

A more rigorous approach to the analysis of the long-term rock support would require a numerical model (e.g., Finite Element Method or FEM for short), machine learning and other advanced geomechanics approaches. These tools may in turn be used to interrogate the validity of the point of intersection ST_{eq} in Figure 1.1 deemed to represent the state of equilibrium of the tunnel. In this thesis, two tunnels in the Limpopo province of the Republic of South Africa are used as case studies to appraise the stability of shallow road tunnels based on microfracture distribution and total displacement of the rock mass. These tunnels have been chosen because they are on a national road that connects South Africa and Zimbabwe. Tunnels designed for a specific traffic load may have higher volumes or heavier vehicles than anticipated. When the tunnel is subjected to traffic loads that are too high and strain the structure, the deterioration process can be accelerated.

1.3. Research objectives

Road tunnels like any other structures evolve with time. They deteriorate and degrade after several years in operation and eventually lose their usability and safety levels (Sandrone and Labiouse, 2010). The continuous stability analysis of road tunnels is therefore a significant task in maintaining road safety. In this regard, microfracture distribution and total displacement of the rock mass are used to appraise the stability of road tunnels at shallow depths. Specific objectives for the doctoral thesis are to:

- assess rock mass behaviour around the periphery of the tunnels using finite element modelling approaches.
- develop a predictive model for fracture distribution along road tunnels using supervised machine learning (linear regression).
- understand the effect of fracturing on total displacement.
- recommend the best support lining for shallow road tunnels.

This research sought to answer the following research questions:

- How does the rock mass behave around shallow excavations such as road tunnels?
- How are fractures distributed along the road tunnel?
- What is the effect of fracturing on total displacement of the rock mass along the tunnel?
- Which support lining technique is best suitable for road tunnels?

The combination of finite element modelling approaches and linear regression analysis technique are anticipated to address some of the problems associated with road tunnel deterioration and equilibrium conditions. The aforementioned methods are not expected to resolve all problems associated with tunnel deterioration. Nonetheless, this study provides some additional insights into fracture distribution and its impact on strength factor and total displacement in shallow tunnels.

1.4. Contribution to the body of knowledge

Monitoring the deterioration of road tunnels is essential for the safety of individuals and vehicles using the tunnels daily. This is done to collect information that may guide future design of primary support and concrete lining for road tunnels in general. The data may also enable engineering researchers to gain a good understanding of the type and effects of deterioration processes prevalent around a tunnel for mitigation plans.

In this light, initial assumptions generally made around rock mass is that it is homogeneous. However, this doctoral research proposed to introduce a level of variability to the rock mass around the tunnel getting the underlying model closer to reality. The contribution to the body of knowledge to stem from the study is envisaged to be the development of a refined predictive model for fracture distribution along shallow road tunnels. The modelling endeavour is centred on the use of numerical methods that are gaining popularity as tools for the analysis of geo-mechanical problems. These numerical tools are explored in the study of the stability and deterioration of road tunnels.

It is relatively new to propose using microfracture analysis and total displacement of the rock mass to assess the stability of a road tunnel. This makes it possible for engineering researchers to identify and design the best support lining for specific rock mass conditions for road tunnels. Further research work can stem from the proposed approach.

1.5. Location of the study

The Hendrik Verwoerd tunnels shown in Figure 1.2 are located at coordinates (22° 54' 57" S and 29° 55' 38" E) in the Limpopo province, South Africa, along the national road N1. The tunnels were constructed in the late 1960s using the traditional drill and blast method. These tunnels have since been in operation daily. They serve as the main artery that links South Africa and Zimbabwe through the Beit bridge in the town of Musina. The stability and safety level of these tunnels are crucial because trucks and cars travel through them every day.

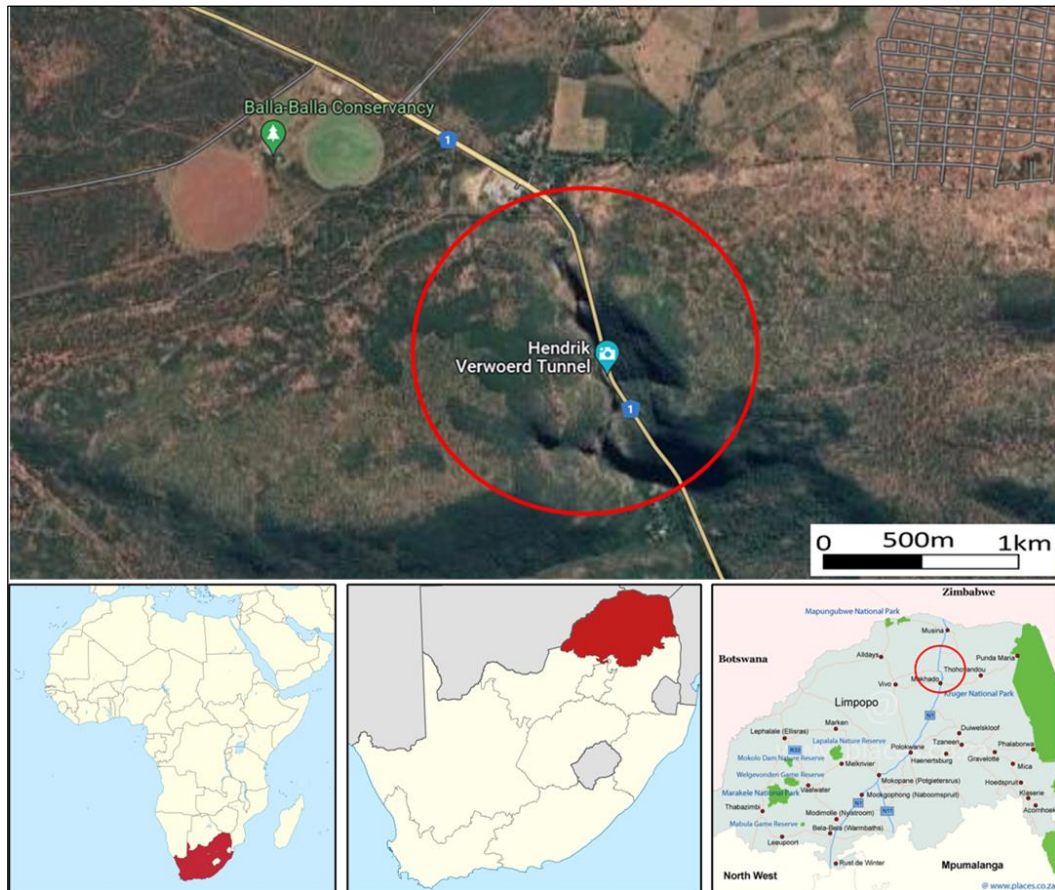


Figure 1.2: Hendrik Verwoerd tunnels in Limpopo (Google Maps, 2022)

The Hendrik Verwoerd tunnels are built in the Waterberg mountains that form part of the Soutpansberg Group of the Limpopo basin. The initial deposition of the Soutpansberg Group was basaltic lavas followed by sedimentary rock (Barker et al., 2006; Brandl, 1981 & 1986). Rocks in the Soutpansberg Group are not of economic mineralisation; they have therefore not attracted much scientific attention. Suffice it to say that these rocks form mountainous terrains with the Soutpansberg reported to have prominent faults and joints. These faults generally trend east-northeast to west-southwest thereby creating blocky rock mass (Barker et al., 2006; Brandl, 1981 & 1986).

The Hendrik Verwoerd tunnels were specifically chosen as case studies because of the inhomogeneous type of rock mass in the periphery of their location. An attempt to understand the influence of blocky ground on tunnel deterioration and equilibrium is therefore made in line with the focus set out

for this doctoral study. A combination of finite element modelling approaches and linear regression analysis technique were used to understand the phenomena.

1.6. Layout of the thesis

This thesis consists of seven chapters. The first chapter is an introduction to the thesis. It outlines the research problem, the objectives of the thesis, the area of study and the scientific contribution of the thesis.

Chapter two gives a detailed literature review of traditional methods of rock mass classification. This review is important as input data for numerical simulations is obtained in the field using these methods. Popular rock engineering methods used for tunnelling stability analysis are also reviewed. From this, the gap knowledge is identified to substantiate this study.

In Chapter three, the methodology followed for data collection is explained in detail. This includes field measurements and observations, laboratory experiments and analysis, traditional rock slope analysis, and failure probability analysis for tunnels. This is followed by Chapter four that is devoted to the description of the observed rock mass and the conditions of the tunnel. The structural analysis and development of joint sets is also presented in this chapter.

Chapter five covers the development of an empirical chart of fracturing distribution for shallow tunnels based on laboratory experiments conducted on rock samples collected in Chapter 3. Micro-fracturing and large-scale rock failure analysis is also done. Lastly, supervised machine learning (linear regression) was used to develop a predictive chart for fracture distribution along shallow road tunnels.

Chapter six focuses on analysing the effect of fracturing on tunnel stability in terms of the strength reduction factor and total displacement using Optum G2 and RS2 as rock engineering software packages. Support lining was then proposed for shallow road tunnels similar to the Hendrick Verwoerd

tunnels. Finally, conclusions and recommendations are given in Chapter seven.

2. Chapter 2: Literature Review

In this chapter, relevant rock engineering methods which are commonly used for tunnel stability analysis are reviewed. These include traditional methods of rock mass classification, fuzzy set theory, and advanced engineering systems tools.

In terms of traditional methods of rock mass classification, the focus is on four prominent methods: Barton's Q-system, Bieniawski's geomechanics classification (RMR), Laubscher's Mining Rock Mass Classification (MRMR), and Geological Strength Index (GSI). Each method is introduced in terms of its fundamental concepts as well as its applications and developments in tunnelling over the years. The literature review also covers analysis techniques applied in tunnelling to address convergence, safety, lining deterioration and overall tunnel stability. Case studies of successful application of fuzzy set theory in tunnelling are presented. Furthermore, a comparison of four methods for the measurement of tunnel convergence is conducted. The four measurement methods are total station, laser scanner, photogrammetry, and wireless sensors. The comparison is made on the basis of their reported performance as far as the accurate and precise measurements of the deformation of the tunnel walls (i.e., crown and side walls) is concerned. Finally, the chapter concludes by identifying the gap in knowledge in the analysis of the stability and deterioration of shallow road tunnels to provide ground for the doctoral study.

2.1. Traditional methods of rock mass classification

Rock masses are intersected by numerous geological discontinuities. As a result, their behaviour is no longer controlled by individual plane failure but by the combination of the existing geological disturbances. Usually, the geological discontinuities are weaker than the rock material; thus, the rock mass behaviour is highly influenced by the occurrence and frequency of

these discontinuities. Such cases call for the use of rock mass classification methods (Hudson and Harrison, 2005).

Rock mass classification assesses the intact properties of the rock, joint characteristic, and the joint boundary conditions. This section evaluates traditional methods of rock mass classification in order to classify the rock mass in the periphery of the tunnel. The following traditional rock mass classification systems are reviewed: Barton's Q-system (Barton et al., 1974); geomechanics classification system, also known as Bieniawski's RMR (Bieniawski, 1973); Mining Rock Mass classification or Laubscher's MRMR (Laubscher and Jakubec, 2001); and Geological Strength Index or GSI (Hoek, 1994).

2.1.1. Barton's Q-system

Barton's Q-system was developed with the aim to characterise rock mass and determine the preliminary empirical design for support systems in tunnels. It is based on several case histories and is widely used in the mining industry to classify rock mass around various mining excavations.

The Q-system is characterised by six parameters. These parameters are further categorised into three main qualities: the rock block size (RQD/J_n), the joint shear strength (J_r/J_a), and the confining stress (J_w/SRF). Barton et al. (1974) encapsulated all these parameters in an empirical relationship descriptive of the Q – value mathematically expressed as follows:

$$Q = \frac{RQD}{J_n} \cdot \frac{J_r}{J_a} \cdot \frac{J_w}{SRF} \quad (2.1)$$

Where RQD is the rock quality designation, J_n is the joint number, J_r is the joint roughness number, J_a is the joint alteration number, J_w is the joint water reduction factor and SRF is the stress reduction factor.

When the RQD was developed by Deere et al. (1967), it was intended to quantitatively estimate the quality of a rock mass using drill core logs (see Equation 2.2).

$$RQD = \frac{\text{Core recovered 100 mm or longer} \times 100\%}{\text{Total length of the drill run}} \quad (2.2)$$

When core logs are not available, the alternative approach proposed by Palmstrom (1982) can be adopted (see Equation 2.3 and 2.4). In this approach, visible traces of discontinuities are used to estimate the *RQD* value based on the number of discontinuities per unit volume known as volumetric joint count (J_v in Equation 2.3 and 2.4). A measuring tape about 5m to 10m long is extended against the exposed rock mass where the number of joint planes ($J_1, J_2, J_3, \dots, J_n$) crossing the tape is counted. This process should be repeated such that several *RQD* readings along surfaces with various orientations should be taken, preferably perpendicular to one another (NGI, 2015). Then, the mean *RQD* value can be utilised to determine the Q-value.

$$RQD = 115 - 3.3 J_v \quad (2.3)$$

$$J_v = \frac{1}{J_1} + \frac{1}{J_2} + \frac{1}{J_3} + \dots + \frac{1}{J_n} \quad (2.4)$$

For the remaining parameters in Equation (2.1), values are assigned using description and ratings tables from Barton et al. (1974). For example, in a tunnelling project where the rock mass conditions are dry, the index value assigned to J_w will be equal to 1.0 (see Table 2.1). Similar to this, a value is assigned to each Q system parameter based on the characteristics of the rock mass using the appropriate table.

Table 2.1: Description and ratings table for joint water reduction factor (Barton et al., 1974)

Condition of Groundwater	Head of Water (m)	Joint Water Reduction Factor J_w
Dry excavation or minor inflow 5 litres/minute locally	<10	1.0
Medium inflow, occasional outwash of joint/fissure fillings	10 – 25	0.66
Large inflow in competent ground with unfilled joints/fissures	25-100	0.5

Large inflow with considerable outwash of joint/fissure fillings	25-100	0.33
Exceptionally high inflow upon excavation, decaying with time	>100	0.2-0.1
Exceptionally high inflow continuing without noticeable decay	>100	0.1-0.05

The rock mass rating value obtained from the Q-system can be used to determine and estimate the support categories following Grimstad and Barton (1993) as shown in Figure 2.1.

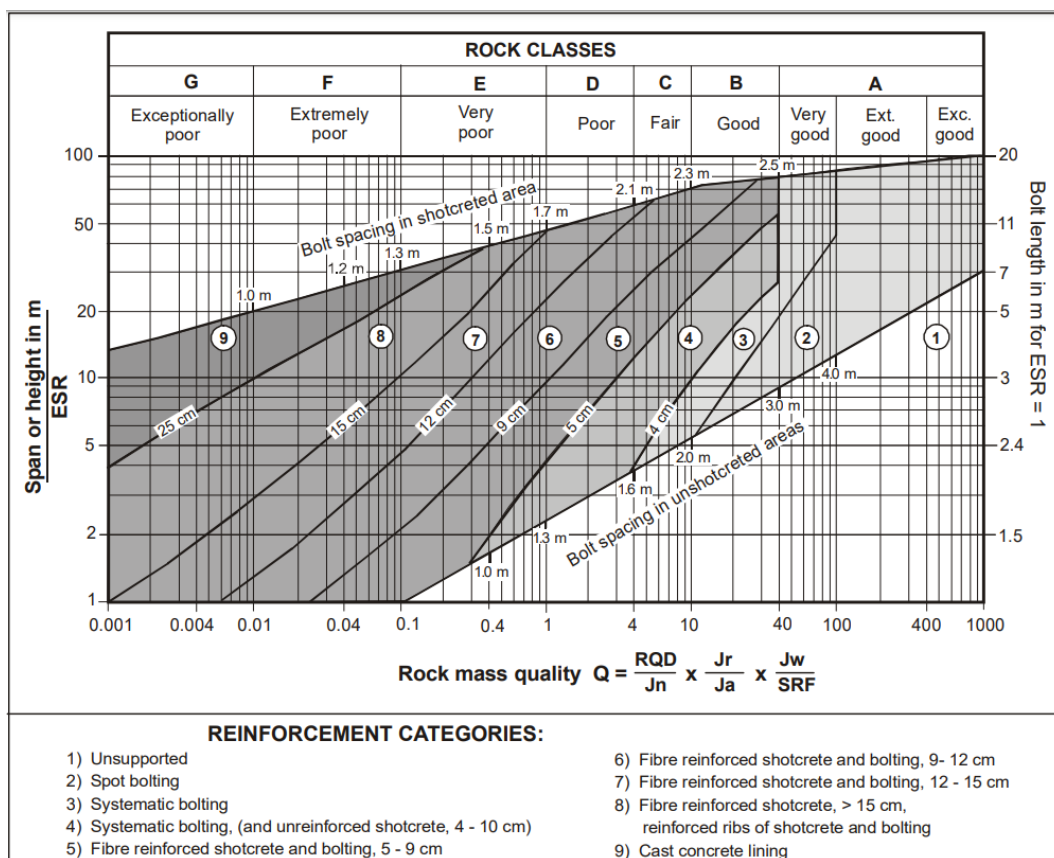


Figure 2.1: Estimated support categories based on tunnelling quality index Q (Grimstad and Barton, 1993)

According to Palmstrom and Broch (2006), the Q-system has previously been misused. However, when used with full awareness of its limitations, the Q-system can be applied to the stability analysis and the estimation of support required of shallow and deep tunnels with great success particularly in jointed rock mass. For example, in a recent study, Khadka and Maskey

(2017) resorted to the Q-system to classify the rock mass. They then analysed the stability of a tunnel and cavern and subsequently develop the support required. The empirical approach was successfully applied to the collection of rock mass data for their studies. Another example is that of Høyen et al. (2019) who also used this traditional method successfully in their tunnelling research. As an empirical method, it is evident that the Q-system is ideal for tunnelling applications. In combination with Barton's chart for support estimation, researchers can easily modify their designs for tunnel support. However, a proper description of rock mass quality is required when working on the evaluation of tunnel stability and the design of support. The Q system has been successfully applied in hard, jointed rocks with weakness zones, which make up the majority of the geological material. There are only a few examples of soft rocks with few or no joints, so other approaches to support design should be taken into consideration when evaluating support in these types of rocks. The Q-system is one such approach. Application of the Q-system in squeezing rock or extremely weak rock must be done in conjunction with deformation measurements and numerical simulations (NGI, 2015).

2.1.2. Bieniawski's geomechanics classification

Bieniawski's geomechanics classification is a system that gives a Rock Mass Rating (RMR) indicative of the quality of the rock mass. RMR combines the most important geologic characteristics of influence into one overall comprehensive index of rock mass quality. This system was introduced by Bieniawski (1973) at the South African Council of Scientific and Industrial Research (CSIR). The system is based on his empirical experience gained from numerous studies done at the time on shallow tunnels excavated in sedimentary rocks. This means that if the system is to be applied on any other rock types (e.g., metamorphic and igneous rocks) or structures (e.g., dam foundation, hill slopes), caution needs to be exercised as far as possible (Bieniawski, 1973, 1974, 1979, 1988 & 1989).

The RMR approach takes into consideration six parameters; namely, the uniaxial compressive strength (UCS) of the rock material; RQD; the spacing of discontinuities; the condition of discontinuities; groundwater conditions; and the orientation of discontinuities. The magnitude of the UCS is determined from rock samples collected from the field and prepared for laboratory uniaxial compressive testing. Each of the six parameters of the RMR is assigned a rating using the geomechanics classification chart after Bieniawski (1976 & 1989).

The initial focus of Bieniawski's (1973) RMR system was on tunnels. Several modifications were made to the RMR system (Bieniawski, 1974, 1976, 1979, 1988 & 1989). Even though the system was regularly updated, the most common error made today is that older versions are still being used (Aksoy, 2008). Although the RMR system was initially designed for tunnels, it has been used to estimate the strength and in-situ deformation modulus of rock masses as well as to design rock slopes and foundations (Zhang, 2017).

The rock mass rating system is only useful for predesign. It is clear that using the system requires a first-rate user experience. The data obtained by using the RMR system should be taken into account alongside analytical and numerical study data (Aksoy, 2008).

2.1.3. Laubscher's Mining Rock Mass Classification

Laubscher's Mining Rock Mass Rating system (or MRMR) was introduced in 1975 and subsequently updated (Laubscher, 1975, 1990 & 1993). The latest modernised version was made available by Laubscher and Jakubec (2001).

The MRMR system takes into account the same parameters found in the RMR classification covered in the previous section. However, it combines ground water and joint conditions into one single indicator. The system also omits adjustments for joint orientation and, therefore, considers four

parameters: UCS, RQD, joint spacing, joint condition and groundwater (note that joint condition and groundwater are considered collectively). The MRMR system modifies Bieniawski's basic RMR value to consider modification factors. These factors include in-situ and induced stresses, stress changes, and the effects of blasting and weathering. The MRMR value is therefore obtained by adding the four parameter ratings.

The MRMR system was originally created for caving operations, but over the years it has become a standard in all facets of mining. On numerous significant mining projects around the world today, the MRMR classification is used. Despite being relatively simple to use, it is also easily abused. The two common classification mistakes that occur most frequently in MRMR are averaging values throughout geotechnical areas and combining naturally occurring and mine-induced defects (Jakubec and Laubscher, 2000).

Understanding that rock mass competency is influenced by mining activities (e.g., blasting damage, induced stress, weathering, water) as well as by inherent geological factors (e.g., rock strength, geological discontinuities) is important. The man-made changes cannot be disregarded because they frequently have negative effects on the rock mass competency and thereby stability of the excavations. All of the crucial factors affecting the behaviour of the rock mass must be considered. Neglecting the strength reduction brought on by micro-fractures could result in significant financial losses in a mining or tunnelling project.

2.1.4. Geological strength index

Geological Strength Index (or GSI) is one key parameter needed in assessing the strength and deformability of rock using the Hoek-Brown failure criterion (Hoek, 1994). Several failure criteria exist, e.g., Hoek-Brown, Mohr-Coulomb, and extension strain. However, the Hoek-Brown failure criteria is the most widely used to assess the stability of rock mass in underground excavations. It is given as follows (Hoek, 1994):

$$\sigma_1 = \sigma_3 + \sigma_{ci} \left(m_b \frac{\sigma_3}{\sigma_{ci}} + s \right)^a \quad (2.5)$$

In Equation (2.5), σ_1 and σ_3 are respectively the major and minor principal stresses obtained at failure of a rock specimen during triaxial compressive strength testing; σ_{ci} is the UCS of the intact rock measured in the laboratory; m_b ; s and a are the parameters of Hoek-Brown failure criteria expressed as follows (Hoek, 1994):

$$m_b = m_i \exp\left(\frac{GSI-100}{28-14D}\right) \quad (2.6)$$

$$s = \exp\left(\frac{GSI-100}{9-3D}\right) \quad (2.7)$$

$$a = \frac{1}{2} + \frac{1}{6} (e^{-GSI/15} - e^{-20/3}) \quad (2.8)$$

All the above parameters are highly influenced by the rock mass characteristics. Parameter D (see Equation 2.6) is a variable affected by the intensity of disturbance on the rock mass. The recommended value of the disturbance factor is $D = 0$ for undisturbed rock mass (in-situ rock) and $D = 1$ for disturbed rock mass. The Hoek-Brown constants m_i and m_b apply to intact rock and rock mass, respectively. In simple terms, this means that the Hoek-Brown criterion is applicable to both intact rock as well as rock mass.

Hoek-Brown criteria parameters were derived from RMR before 1994. The excavation was presumed to be dry and there were no adjustments made for project-related discontinuities. As research developed in this direction, the failure criterion was modified and corrected for low values of RMR, i.e., low quality rock mass. This was to address the fact that low RMR values came with high variability and poor reproducibility. The compounding effect was that the RMR-dependent Hoek-Brown parameters was not deemed unreliable for low quality (Hoek et al., 2002 ; Hoek and Brown, 2018). This led to the development of GSI as an indicator value of which ranges from approximately 10 for extremely poor-quality rock mass to 100 for extremely strong unjointed rock mass. Therefore, the value of GSI is expected to

increase with the quality of rock mass. It was initially estimated as follows (Hoek, 1994):

$$GSI \approx RMR_{76} \approx RMR_{89} - 5 \quad (2.9)$$

In Equation (2.9), RMR_{76} represents the RMR value as introduced by Bieniawski in 1976; hence, the subscript 76. The maximum rating for ground water in this case was assigned as 10. Similarly, RMR_{89} represents the RMR value as per Bieniawski (1989). The GSI system was introduced by Hoek to quantitatively describe the rock mass quality based on geological observations and less numerical values.

The GSI system is characterised by two main parameters: surface condition of discontinuities and interlocking among the rock blocks. The surface conditions of discontinuities contrast from very good to very poor; in other words, from fresh unweathered surface to highly weathered or slicken sided surface with clay infill. Likewise, interlocking among the rock blocks refers to massive at the upper end of scale to crushed or laminated towards the low end (See Figure 2.2).

The GSI system consists of six main qualitative rock classes, including folded/laminated/sheared, blocky, very blocky, blocky/disturbed, and intact or massive. Similar to how joint conditions are categorised in the RMR system, discontinuities are divided into five surface conditions. According to Figure 2.2, these are good, very good, fair, poor, and very poor. In other words, GSI makes use of a 6 x 5 matrix. An example of how to use the GSI chart is illustrated in Figure 2.3. The rock mass in the presented example is considered to be very blocky. However, surface conditions are good hence the GSI reading is 50.

Marinos et al. (2005) are of the view that GSI was not introduced to replace the Q-system or RMR system because it does not contain support design capability. However, it was developed with a focus on the estimation of rock mass properties. The rating is based on observations of the exposed rock mass such as an outcrop or the rock mass exposed after road cut or

tunnelling. The empirical and numerical estimation of rock mass properties both are linked to the Hoek-Brown failure parameters covered in Equations (2.6) – (2.8). After a rock mass is quantified, the estimated GSI number is used to empirically estimate the rock mass properties. These rock mass properties can be used in any numerical analysis.







ROCK MASS STRUCTURE		JOINT SURFACE CONDITIONS				
		GOOD Very rough, fresh unweathered surfaces	VERY GOOD rough, slightly unweathered iron stained surfaces	FAIR Smooth, moderately weathered and altered surfaces	POOR Slack-sided, highly weathered surfaces with compact coatings or fillings of angular fragments	VERY POOR Slack-sided, or highly weathered surfaces with soft clay coatings or fillings
 INTACT OR MASSIVE - massive in situ rock masses with very few, widely spaced discontinuities		90	N/A	N/A	N/A	N/A
 BLOCKY - very well interlocked undisturbed rock mass		80	70	N/A	N/A	N/A
 VERY BLOCKY - interlocked, partially disturbed rock mass		60	50	N/A	N/A	N/A
 BLOCKY/DISTURBED - folded and/or faulted with angular blocks		40	N/A	N/A	N/A	N/A
 DISINTEGRATED - poorly interlocked, heavily broken rock mass		20	30	N/A	N/A	N/A
 FOLIATED/LAMINATED/SHEARED - complete lack of blockiness		N/A	N/A	N/A	N/A	N/A

Figure 2.2: GSI estimates correlated with geological observations (Stacey, 2001)

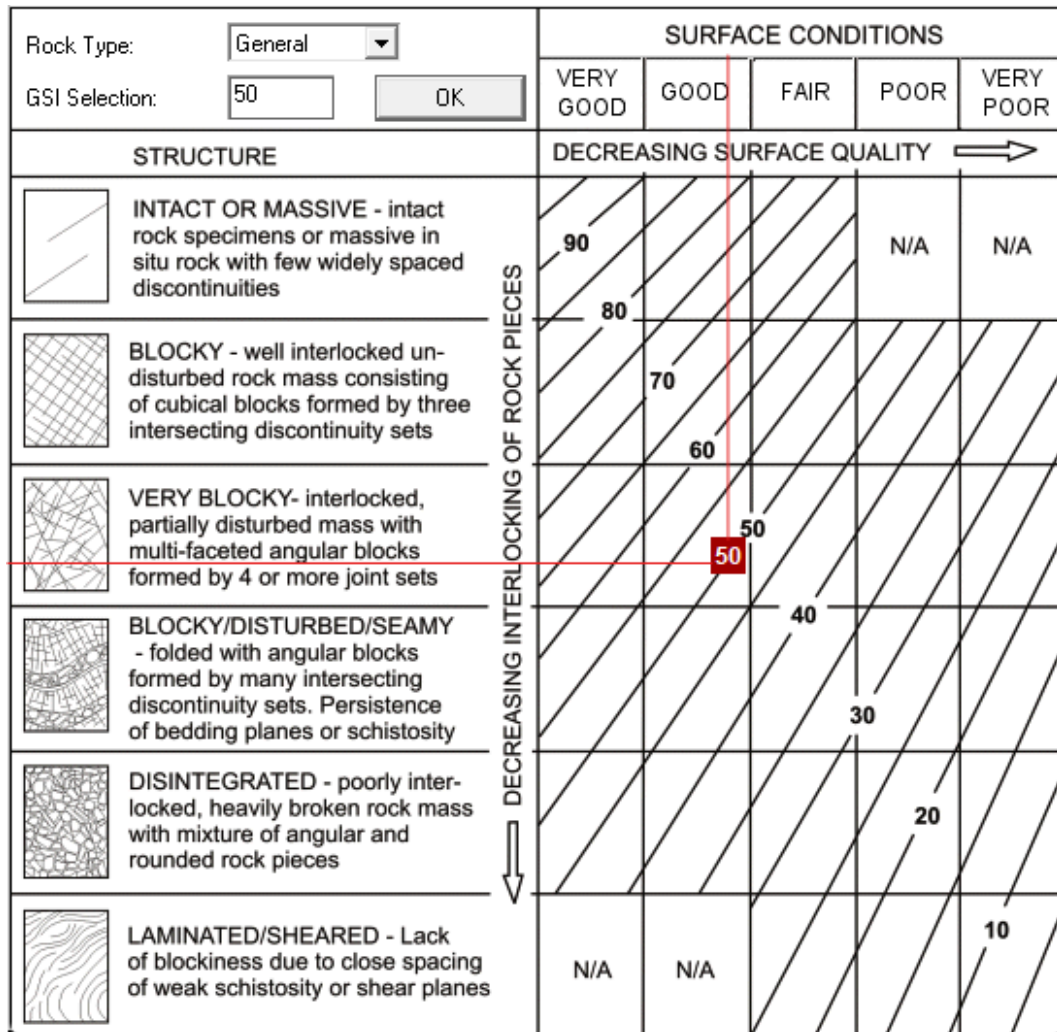


Figure 2.3: An example of using the GSI Chart.

As alluded to earlier, GSI forms part of the parameters employed when evaluating the strength and deformability of rock mass in Hoek-Brown criterion. The relationship between GSI and Hoek-Brown failure parameters m_b , s and a can be expressed for rock mass and intact rock using the following empirical expressions (Hoek, 1994):

$$m_b = m_i \exp\left(\frac{GSI-100}{28}\right) \quad (2.10)$$

$$s = \exp\left(\frac{GSI-100}{9}\right) \quad (2.11)$$

$$a = 0.5 \quad (2.12)$$

Equations (2.10) – (2.12) are valid for $GSI > 25$ (obtained from the field conditions using Figure 2.2). And for very poor-quality rock masses (i.e., $GSI < 25$), the values of s and a are defined as (Hoek, 1994):

$$s = 0 \quad (2.13)$$

$$a = 0.65 - \frac{GSI}{200} \quad (2.14)$$

Based on the value of GSI, the quality of rock mass can be determined from the classification in Table 2.2.

Table 2.2: GSI values and corresponding quality of rock mass (Hoek, 1994)

GSI	Rock mass quality
< 20	Very poor
21 – 40	Poor
41 – 55	Fair
56 – 75	Good
76 – 95	Very good

GSI is a method of characterising rock mass created in engineering rock mechanics to address the need for accurate input data. When designing slopes or tunnels in rocks, specific information about the properties of the rock mass is required as input for numerical analysis. The selection of parameters necessary for the prediction of the strength and deformability of rock masses is directly influenced by the geological makeup of the rock material as well as a visual evaluation of the rock mass. With this method, it is possible to think of a rock mass as a mechanical continuum without losing sight of the impact that geology has on its mechanical characteristics.

Marinos et al. (2005) are of the view that the choice of GSI chart for dealing with particular rock masses should not be restricted to the visual similarity with the sketches of the rock mass structure as they appear in the charts. To select the most appropriate structure, it is also necessary to carefully

read the associated descriptions. This is because the most appropriate case might be somewhere in the middle of the charts' sparse collection of sketches or descriptions.

The issue of changed ground conditions is one of the most significant contractual issues in rock construction, and particularly in tunnelling. To get around this issue, there has been a propensity to categorise the anticipated conditions as RMR or Q-system (Marinos et al., 2005). While GSI was created exclusively for the purpose of estimating rock mass strength, RMR and Q-system were created to estimate tunnel support. Therefore, GSI cannot be used to specify tunnelling conditions on its own because it is only one component of a tunnel design process.

2.2. Fuzzy set theory

Fuzzy set theory is gaining popularity due to its ability to accurately represent the complexity of tunnelling problems. The use of fuzzy-reasoning and knowledge-based representation is broad when designing model algorithms in Machine Learning (ML) and Artificial Intelligence (AI). Fuzzy sets enable one to solve problems with uncertainties, ambiguity and/or problems with incomplete information. Max Black, an American philosopher, first introduced the concept of fuzzy set by conducting an exercise on vagueness in logical analysis (Black, 1937). However, he was opposed by a traditional mathematician that he did not continue research on the concept. A few decades later, Zadeh (1965) reintroduced the concept of fuzzy set to address uncertainty. He reasoned that there are many uncertainties that cannot be tackled using only probability theory which works based on the crisp set. The difference between crisp set and fuzzy set is illustrated in Figure 2.4.

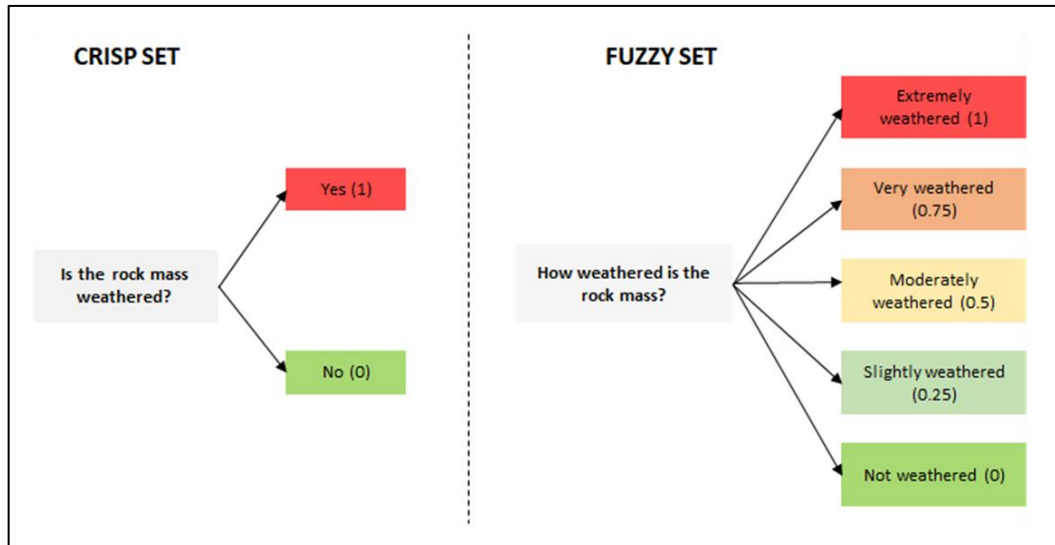


Figure 2.4: Crisp set and fuzzy set illustrated (After Chetan, 2021)

Most traditional reasoning mechanisms are crisp; in other words, they are represented by values (1) and (0) which are True/Yes and False/No respectively (see Figure 2.4). However, fuzzy sets are different because they integrate the vagueness by incorporating values between 1 and 0 to display the array of possibilities. Nguyen (1985) described fuzzy sets as a system that totally depends on the ambiguous and imprecise information in making appropriate decision. It also appears that fuzzy sets generalised the crisp set theory for them to derive a reliable and reasonable solution. For instance, considering the example in Figure 2.4, if one is to comment on the degree of weathering of a rock using a crisp set, the answer can only be yes (1) or no (0). In contrast, fuzzy set will answer the same question in a range of possibilities. One can say the rock is extremely weathered (1), very weathered (0.75), moderately weathered (0.5), slightly weathered (0.25), or not weathered (0). As a result, there is always room for uncertainty in fuzzy set logic. Systematic uncertainties occur when incorrect measurements are taken, or a model ignores certain effects. This makes it difficult to solve the problem at hand. Interestingly, several authors (e.g., Dubois and Prade, 2012; Adoko et al., 2011) have reported that fuzzy set theory can accurately represent not only systematic uncertainties but also the concepts of gradualness and bipolarity.

The subsequent sub-sections unpack the concept of fuzzy theory, fuzzy logic and typical fuzzy inference techniques suggested. Few applications of fuzzy set theory in geomechanics are also reviewed in terms of its trends and usage in slope stability analysis, stability analysis of tunnels under construction, stress analysis in tunnels and tunnel convergence analysis. Lastly, a review of recent successful and unsuccessful applications of fuzzy inference system in tunnelling geomechanics is presented with supporting case studies.

2.2.1. Fuzzy logic

Fuzzy logic refers to a computing methodology which is based on the degree of truth of a statement. In fuzzy logic, the representation of values is not limited to true (1) or false (0) like in crisp set logic. It is rather expressed by linguistic variables of true and false (1-0) (Zimmermann, 2010).

Fuzzy inference system (FIS) is the main element of a fuzzy logic; it is also referred to as fuzzy logic controller. This is because it deals with decision-making processes using IF-THEN rules of the type (If X is A then Y is B). The fuzzy logic process involves three major stages between input and output (Figure 2.5). Firstly, fuzzification stage where crisp input data or value is converted into linguistic variable through membership functions of the knowledge base. Secondly, the fuzzy inference engine evaluates the degree of input membership using fuzzy rules. This stage resembles the human decision-making process. The last process is the defuzzification of the fuzzy output into crisp values (Murnawan et al., 2021).

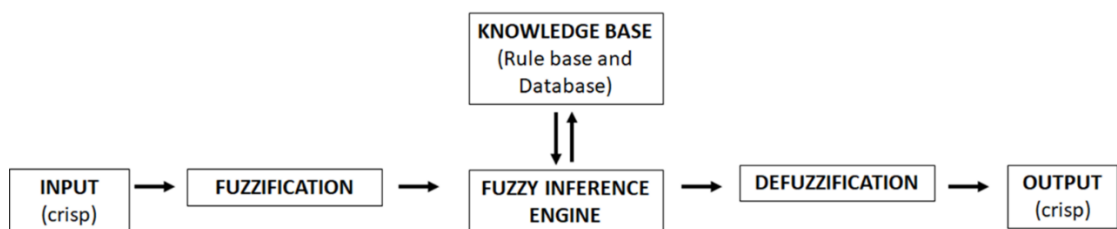


Figure 2.5: Fuzzy logic process (After Murnawan et al., 2021)

FIS was used to resolve issues of RMR in underground excavations (Adoko et al., 2011; Adoko and Wu, 2011). The technique used applied the so-called Bellman-Zadeh fuzzy aggregation scheme that is geared towards synthesising hazard index for mining excavations. The Bellman-Zadeh fuzzy aggregation scheme was applied with the purpose of evaluating the hazard index associated with mining tunnel. The same technique was also successfully implemented on rock mass classification from Bieniawski's system through integrating expert knowledge between the two concepts (conventional rock mass rating index and overlaying method). It is also used in evaluating Barton's quality index Q in Equation (2.1) provided that the information on various contributing rating parameters is fuzzy. Finally, Adoko and Wu (2011) pointed out that the Bellman-Zadeh scheme is well established in several categories of geomechanics. These includes rock mass classification, slope stability, tunnelling, foundation analysis, geotechnical project scheduling as well as costing planning.

2.2.2. Fuzzy inference techniques and their application in mining geomechanics

Basic fuzzy set systems are presented in a group of 'IF-THEN' rules to express the correlation of input and output variables in the system (Çelikyilmaz and Turksen, 2009). Computational aspects of a FIS can have a single rule with a single antecedent. For example, IF x is big, THEN y is small. The terms big and small are fuzzy and should therefore be expressed by membership functions (Monjezi et al., 2009).

FIS can also be represented by a single rule with multiple antecedents or by multiple rules with multiple antecedents. This means that for each antecedent, there will be a consequent, i.e., Rule X_n : If condition x , THEN restriction y . For example, consider the ground conditions in a tunnelling project. Rule 1 can be structured as: IF the rock mass is blocky THEN areal coverage (e.g., shotcrete or wire mesh) must be installed. Rule 2 can be: IF

the rock is intact, THEN no support is required. Rule 3: IF the rock mass is jointed, THEN cable anchors should be installed.

There can be more than one rule in a FIS; however, each rule must have its own condition and consequent. According to Yazdani-Chamzini (2014), several models have been developed to address linear and nonlinear behaviour systems. But the most important ones include the Mamdani systems, the Takagi-Sugeno-Kang (TSK) systems, and the Tsukamoto systems. These fuzzy inference systems differ regarding their rule of application (Ghasemi and Ataei, 2013).

The Mamdani system can be expressed as follows (Mamdani and Assilian, 1975):

$$\text{If } X_1 \text{ is } A_1, \text{ and } X_2 \text{ is } A_2 \text{ THEN } Y \text{ is } B \quad (2.12)$$

In Equation (2.12), both the inputs (X_1 and X_2) are fuzzy sets or fuzzy numbers. The output (B) is also a fuzzy set. The max-min inference method and the max production method are the two cases of the two input Mamdani system that make up this inference system.

The Mamdani FIS was initially introduced to create a control system by synthesizing crisp sets into linguistic control rules. The linguistic rules were constructed based on the expertise and experience of human beings (Mamdani and Assilian, 1975). In this system, the output of each rule is a fuzzy set from the output membership function. Mamdani FIS is more suitable for expert knowledge because it is more intuitive and understands the rule base easily. The final crisp output value is computed through defuzzification of the fuzzy output. Advantages of Mamdani FIS include intuitiveness, suitability for human input, understandable rule base, and widespread of acceptance (Vadapalli, 2021). It is because of the above that the Mamdani fuzzy logic system has sparked a lot of interest in the field of engineering (Azimi et al., 2010). It is said to gain popularity also because of its attractive features, its simplicity, its ability to model complex and uncertainty problems effectively, and its utilisation of expert knowledge in

decision-making which is common in the field of geomechanics and rock engineering (Adoko and Wu, 2011; Yazdani-Chamzini, 2014). Perhaps it is important to note that the Mamdani FIS has been used with success in rock slope stability assessment, burden prediction from rock geomechanical properties, tunnel convergence prediction, prediction of the blastability designation of rock, rock mass blastability, penetrability, diggability, rippability, excavability, and rock mass classification systems (Abbas et al., 2011; Monjezi and Rezaei, 2011; Azimi et al., 2010; Khademi et al., 2010; Hoseinie et al., 2009; Basarir et al., 2007; Iphar and Goktan, 2006; Sönmez et al., 2003; Gökceoğlu and Zorlu, 2004).

In comparison, the Takagi-Sugeno-Kang (TSK) system, also known as the Sugeno system, is given by (Sugeno, 1985):

$$\text{If } X_1 \text{ is } A_1, \text{ and } X_2 \text{ is } A_2 \text{ THEN } Y \text{ is } f(X_1, X_2) \quad (2.13)$$

Both the inputs of the Sugeno system (X_1 and X_2) are fuzzy sets or fuzzy numbers (Takagi and Sugeno, 1983). However, the output is a function of the inputs as specified by the inputs in the fuzzy rule. The rule has an output represented as a crisp function (Sugeno, 1985). This system uses the singleton membership function for the output variable. The output is either a linear function or a constant of the input values.

The Sugeno FIS has been found to be more computationally efficient compared to the Mamdani from the point of view of the defuzzification process (Jang and Gulley, 1997; MathWorks Inc, 2010; Blej and Azizi, 2016). This is because the Sugeno FIS uses the weighted average (Equation 2.14) or weighted sum of a few datapoints, unlike computing a centroid of two-dimensional area (Sugeno, 1985).

$$W = \frac{\sum_{i=1}^n w_i X_i}{\sum_{i=1}^n w_i} \quad (2.14)$$

Where W is the weighted average, n is the number of terms to be averaged, w_i is the weights applied to X values and X_i is the data values to be averaged.

The Sugeno FIS is also suitable for mathematical analysis, is able to adapt and optimise techniques, works well with linear techniques, and guarantees output surface continuity (Vadapalli, 2021). Finally, the Sugeno FIS has been used in the prediction of clean rock joint shear strength by Matos et al. (2019) and in rock slope stability assessment by Chen et al. (2011). Jalalifar et al. (2011) also applied the technique in conjunction with artificial neuro network to predict rock engineering classification systems such as RMR. Such a blended system is purported to produce improved models and better predictions as opposed to traditional conventional modeling methodologies. This is because the proposed weights technique was utilised in the process. Lastly, the Tsukamoto system can be defined as follows (Tsukamoto, 1979):

If X_1 is A_1 , and X_2 is A_2 THEN Y is B (2.15)

For the Tsukamoto system, both the inputs (X_1 and X_2) are fuzzy sets or fuzzy numbers. The output (B) is also a fuzzy set (Hartono, 2016). The only difference between the Mamdani and the Tsukamoto systems is that here the membership function of the output fuzzy set (B) is a monotonic function. This means that each fuzzy rule is represented by a fuzzy set with a monotonic membership function. Monotonic functions are characterised by successive values that are either increasing, decreasing or constant (Saepullah and Wahono, 2015).

Ali et al. (2012) are of the view that the Mamdani, Sugeno and Tsukamoto fuzzy models are the three fuzzy inference systems that have been widely used. They explained that the differences between the three fuzzy inference systems lie in the aggregation and defuzzification procedures as a result of their fuzzy rules. According to Adoko and Wu (2011), there are three conceptual elements defining a fuzzy inference system: the rule base, the database, and the reasoning mechanism. The rule base forms part of fuzzy rules whereas the parameters for input membership functions are established from the database. The reasoning mechanism permits opportunity for judgement of output functions using fuzzy logic and consequently making satisfactory conclusions thereof.

Fuzzy systems have also been coupled with neural networks. The combination of fuzzy systems and neural network brings about what is known as the neuro-fuzzy system. This daughter system exhibits the advantages of both parent methodologies (Adoko and Wu, 2011). An example of this combination is the Adaptive Neuro-Fuzzy Inference System (ANFIS) developed by Jang et al. (1997). ANFIS is said to work well with TSK fuzzy inference system because it permits the formation of a fuzzy rule conclusion (Walia et al., 2015).

As a final note, numerous methods of application of ANFIS in mine geomechanics are available in the literature. Although not exhaustive, one can look at applications such as modelling of tunnel boring machine performance (Grima et al., 2000); prediction of liquefaction (Rahman and Wang, 2002); interpretation of model footing response (Provenzano et al., 2004); estimation of jointed rock mass deformation modulus (Gökceoğlu et al., 2004); stability analysis of tunnel under construction (Rangel et al., 2005); assessment of potential of swelling in compacted soil (Kayadelen et al., 2009); mapping of landslide susceptibility (Sezer et al., 2011); slope stability assessment (Chen et al., 2011); estimation of convergence in tunnelling (Adoko and Wu, 2012); ANFIS model for rock burst prediction (Adoko et al., 2013a); tunnelling risk assessment (Yazdani-Chamzini, 2014); and prediction of blast-induced ground vibration (Javad et al., 2015). The history and development of applications of FIS in mining geomechanics is summarised in Table 2.3 for reference.

Table 2.3: Fuzzy inference system applied in mining geomechanics

Type of fuzzy inference system	Example of application (Author, year)
Basic fuzzy inference	Rock mass classification (Nguyen and Ashworth, 1985); Slope stability (Juang et al., 1998); Sawability classification of building stones (Tutmez et al., 2007); Risk assessment for rock stability (Wang et al., 2011)

Mamdani fuzzy models	Assessment of rock slope stability using the Fuzzy Slope Mass Rating (FSMR) system (Abbas et al., 2011); A fuzzy model for high-speed railway tunnel convergence prediction in weak rock (Adako et al., 2011); Developing a new fuzzy model to predict burden from rock geomechanical properties (Monjezi and Rezaei, 2011); Optimized Mamdani fuzzy models for predicting the strength of intact rocks and anisotropic rock masses (Asadi, 2016); Assessing subsidence susceptibility to coal mining using frequency ratio, statistical index and Mamdani fuzzy models: evidence from Raniganj coalfield, India (Rehman et al., 2020)
Sugeno fuzzy models	Rock engineering classification system (Jalalifar et al., 2011); Rock slope stability assessment (Chen et al., 2011)
Adaptive neuro fuzzy inference system	Estimation of convergence of a high-speed railway tunnel in weak rocks using an adaptive neuro-fuzzy inference system (ANFIS) approach (Adoko and Wu, 2012); Proposing a new methodology based on fuzzy logic for tunnelling risk assessment (Yazdani-Chamzini, 2014); ANFIS model for prediction of blast-induced ground vibration (Javad et al., 2015); Optimization of earth pressure balance (EPB) shield performance with adaptive neuro-fuzzy inference system and genetic algorithm (Elbaz et al., 2019)
Surrogate fuzzy models	A fuzzy surrogate modelling approach for real-time predictions in mechanized tunnelling (Cao et al., 2018)

2.3. Innovative application of fuzzy inference system in mining geomechanics

The application of FIS in rock mechanics and engineering geology has grown rapidly over the years (Sun et al., 2003; Mishra and Basu, 2013; Sari, 2016; Xie et al., 2021). This is because of its ability to tolerate a wide range of uncertainties and to describe complex and multivariable nonlinear problems. This section highlights in themes various examples where fuzzy inference systems have been used in the mining geomechanics space. Their strengths and limitations are also highlighted in each example.

2.3.1. Slope stability analysis

Fuzzy techniques have been used when analysing slope stability problems relating to surface excavations (Adoko and Wu, 2011). Indeed, the first reported attempt is a study by Kacwicz (1987) where fuzzy set theory was applied to the estimation of factor of safety for the Warsaw slope in Poland. Note that the success of this study resided in the fact that soil and rock mass parameters were incorporated as fuzzy numbers. And in another study, Zadeh (1975) was able to fully implement the method of slices (also known as Fellenius method) and the principle of extension. This enabled him to accurately predict the safety factor associated with a slope based on the intervals between the upper and lower limits of the safety factor. Finally, the membership function was enhanced with professional knowledge. This gives users the option to select the ideal safety factor.

Lastly, the study by Kacwicz (1987) prompted several scholars to try and work on the realistic implementation of FIS for predicting the safety factor. The study by Juang et al. (1998) is one of the well-known follow-up studies. The researchers considered the uncertainties inherent to soil parameters expressed as fuzzy members. The uncertainties were then discretised into a set of intervals. This led to the reduction of slope problems to a series of interval analysis that can be handled using only conventional mathematics. The approach by Juang et al. (1998) can therefore be regarded as purely

deterministic rather than probabilistic which allows for the use a computer-based program for slope stability analysis.

2.3.2. Stability analysis of tunnels under construction

Most if not all civil and mining engineering works require information relating to properties and behaviour of subsoil material. However, in tunnel construction, limited or partial information of the constraints tends to be the norm. This is evident during the construction phase when geological conditions changing with depth are sometimes not satisfactorily established. To remedy such unanticipated situations, calibrated mathematical models have been used in conjunction with continuous monitoring to predict and analyse the behaviour and stability of a tunnel under construction (see for example Gama, 2004; Mahdevvari and Torabi , 2012).

The abovementioned process is complex but effective where other techniques such as numerical, empirical, mathematical, and artificial intelligence lack precision. These methods also require knowledge and information that is uncertain during the design and construction phase of the tunnel. It is for these reasons that Rangel et al. (2005) developed an alternative strategy for the analysis of tunnel stability during the design and construction process. The strategy is a hybrid consisting of neural, neuro-fuzzy, and analytical solutions. The most important parameters considered in this technique include geostatic mean stress, ground shear strength, rock mass deformation modulus, concrete support strength, concrete support deformation modulus, displacement induced by the tunnel, and stress in the support. The system was designed such that it can reproduce the displacement induced at the periphery of the tunnel before and after support has been installed. Moreover, the system used a criterion that considers the dimensionless parameters (such as plastic factor and stiffness ratio) based on shear strength of the media. The technique was prototyped and tested using a database of 261 cases where only 45 cases were real while the remaining 216 were synthetic.

Results showed that the hybrid system by Rangel et al. (2005) can compute simultaneously the total and initial displacements, the maximum stress acting on the lining, as well as the stability of the excavation as it advances without support. The results of the proposed system, 3D FDM, and characteristic curve method are compared as indicated in Figure 2.6. In addition, the prototype can also be used in real time because of its ability to output immediate responses. The drawback of the system is that it does not consider factors such as stress path during construction. A curve or a straight line that represents stress points and changes in stress as a specimen is loaded and unloaded is the typical way to express a stress path. Furthermore, the lack of real data in the database means that the approximation of reality suffers greatly. The situation may change as more real data becomes available.

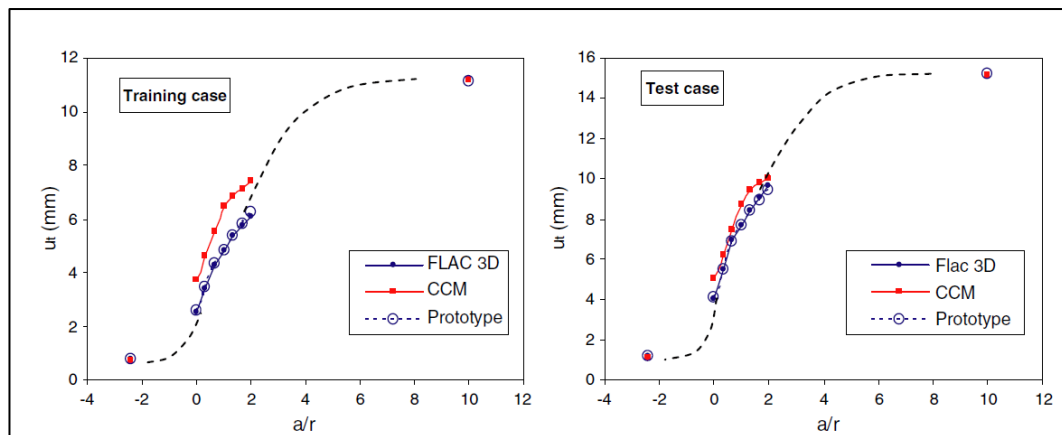


Figure 2.6: Results of the proposed system, 3D FDM, and characteristic curve method are compared (Rangel et al., 2005)

2.3.3. Stress analysis in tunnels

During tunnel construction, the redistribution of stresses in the periphery of the excavation is anticipated. As such, the prediction of earth pressure balance becomes important. Elbaz et al. (2019) developed an efficient multi-objective optimisation model integrating ANFIS and genetic algorithm (GA) to forecast shield performance during tunnel construction. The integration of GA was introduced in order to enhance the level of accuracy of ANFIS.

The proposed hybrid ANFIS-GA model was to be tested in a real fired tunnel section in Guangzhou China. Three main input parameters were considered for the purpose: cutter head torque (CT), rotational speed screw rate (SC) and cutter head rotation speed (CR). The output of interest, on the other hand, was the advance rate (AR). Elbaz et al. (2019) used the Takagi-Sugeno method to construct fuzzy rules. This is because the method is reliable and can compute efficiently synthetic systems with fuzzy rules from the input to output database. Moreover, ANFIS works very well with the Sugeno FIS (MathWorks Inc., 2010). This explains why Elbaz et al. (2019) highlighted the potential to use the hybrid ANFIS-GA model as a prediction tool for tunnelling advance rates based on the output results obtained.

Sometimes, the optimisation of fuzzy calculation for a FIS becomes inefficient when standard optimisation algorithms are used. To remedy this, GA is used instead. As outlined in MathWorks Inc. (2010), GA is more suitable for discontinuous, non-differentiable, stochastic, and highly nonlinear objective functions. Kalantary et al. (2009) exemplified this application by investigating the correlation between undrained shear strength (S_u) and the standard penetration test blow count (N_{SPT}) factor. A mathematical model that intricately defines the interdependencies of the involved variables was created using an optimised group method of data handling (GMDH) type neural network with genetic algorithm. The sensitivity analysis revealed that while plasticity index (PI) and overburden stress (δ'_n) have an impact on the function, natural moisture content has little impact on the correlation. At higher standard penetration test and lower plasticity index values, effective overburden stress has the most of an impact. Based on the above, one can conclude that hybrid models yield effective and reliable results when compared to pure fuzzy models.

2.3.4. Tunnel convergence

Tunnels should be examined for any deterioration and convergence taking place with time. Understanding the type of deterioration process and its

effects on the tunnel is critical. Together with primary support and concrete lining degradation, this information guides the safe design of tunnels.

Displacement and convergence in tunnels generally occur during construction. The convergence around a tunnel comprises two parts: plastic and elastic parts (Hazrati Aghchai et al., 2020). The elasticity component is used when analysing the stress and strain distribution around the excavation. Hazrati Aghchai et al. (2020) considered a circular tunnel under construction and analysed the elastic displacement around it. Kirsch's equation was used to determine the radial and tangential stresses. Rock mass around the tunnel was assumed to be homogenous, isotropic and in plane strain condition. Nonhydrostatic in-situ conditions were also assumed in the model analysis. Although successfully implemented, the model did not consider the time factor. This meant that it was not possible to determine how long it would take for the tunnel to reach a certain displacement factor.

Work on the integration of the time factor to the study of tunnel convergence is limited in the literature. However, a trend is emerging whereby the Mamdani technique (refer to Equation 2.15 in Section 2.2.2) is being explored to solve tunnelling convergence problems. This is ascribed to the fact that most models previous accepted for solving tunnelling convergence do not incorporate the inherent subjective uncertainties associated with rock masses (Li et al., 2006; Compilation Group, 2007; Liu et al., 2008; Kang and Wang, 2010; Wu, 2010; Dai et al., 2011; Mahdevvari and Torabi, 2012; Mao et al., 2011; Adoko and Wu, 2011). It is in this light that the pioneering work by Adoko et al. (2011) is briefly presented. In this work, a model based on the Mamdani fuzzy system algorithm was developed and implemented to predict the final ground convergence or closure at the vicinity of the tunnel. However, the approach has the drawback of only being able to predict final convergence rather than convergence as a function of time.

2.4. Recent case studies on FIS applications in tunnelling

Tunnel convergence is closely related to tunnel deformation which ultimately affects the tunnel stability and usability (Ozsan and Karakus, 2006). Adoko and Wu (2012) conducted a study on the estimation of convergence for two high-speed railway tunnels in China. Overall, more than 1000 datapoints were collected from both tunnels. The data from one tunnel was used to develop the model and that of the other was used for testing and validating the model. The model consisted of six input parameters (Figure 2.7): the surrounding rock mass rating index; the ground engineering conditions rating index; the rock density; the tunnel overburden depth; the distance between the monitoring station and the tunnel heading face; and the elapsed time after the working face passed through the monitoring station. Conversely, the two output parameters of the ANFIS-based model were the total convergence and convergence velocity of the crown sides of the tunnel (Adoko and Wu, 2012). Key performance indicators in Table 2.4 show that the model captured well factors influencing tunnel deformation such as rock mass properties and tunnel geometry.

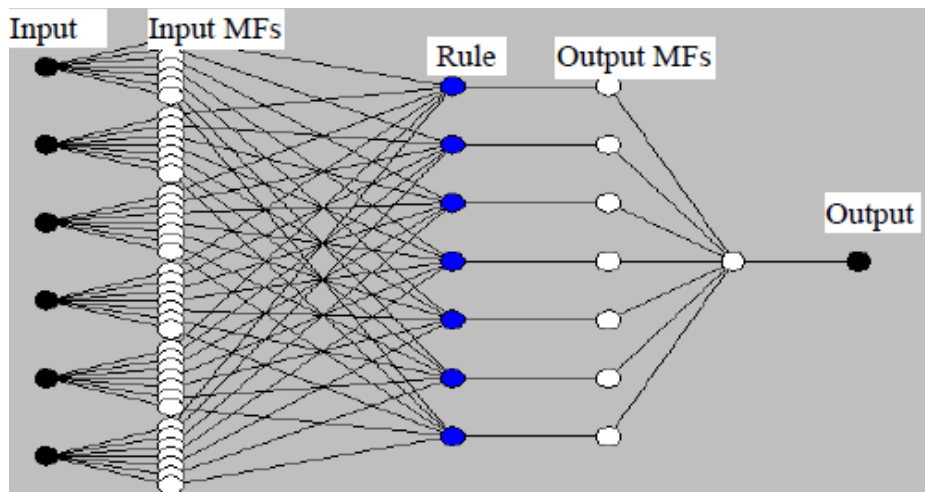


Figure 2.7: Structure of the ANFIS model for crown convergence prediction (Adoko and Wu, 2012)

Table 2.4: Performance of the prediction model (Adoko and Wu, 2012)

Position	Convergence				Convergence velocity			
	VAF (%)	RMSE (mm)	MAPE (%)	R ² (-)	VAF (%)	RMSE (mm/d)	MAPE (%)	R ² (-)
Crown	96.00	0.122	2.16	0.95	92.00	0.018	1.45	0.97
Top heading	90.80	0.243	3.25	0.98	90.23	0.201	2.78	0.96
Bottom heading	94.01	0.175	3.92	0.90	87.56	0.336	7.01	0.85

Results from the study (i.e., Adoko and Wu, 2012) also prove that the proposed model can forecast tunnel convergence with high level of accuracy. The level of accuracy is evaluated and reported in Table 2.4 as root mean square error (RMSE) and variance account for (VAF) percentage. Models that use the Takagi-Sugeno FIS like this one (i.e., Figure 2.7) show that there is enhanced accuracy for the estimated convergence velocity compared to Mamdani-based models. Indeed, in earlier study, Adoko et al. (2011) used 1000 and 135 datapoints for the Takagi-Sugeno FIS and the Mamdani FIS models respectively. The Mamdani model was built based on expertise knowledge, and hence, required a small dataset. The RMSE associated with convergence velocity was found to range between 0.4 mm/day and 2.05 mm/day while the VAR ranged between 59.23% to 78.40% for the Mamdani model. In contrast, RMSE and VAR for the Takagi-Sugeno FIS model ranged between 0.018 mm/day to 0.336 mm/day and 87.56% to 92% respectively (see Table 2.4). That is the reason why convergence velocity was considered better estimated from the Takagi-Sugeno FIS model. The model proposed by Adoko and Wu (2012) is therefore recommended for use in predicting tunnel convergences until improved ones become available. However, it should not be a replacement for in-situ measurement of convergence. In simple terms, the model can be used in conjunction with convergence monitoring programs for decision making purposes.

Coming back to the work by Adoko et al. (2011) referred to earlier, 135 datapoints were used for the Mamdani model. The model was noted to capture tunnel diameter convergence reasonably well. However, its main shortcoming was the poor prediction of convergence velocity. The authors have indicated that research is ongoing to improve the model capacity. They have embarked on growing the dataset to ultimately define ideal parameters to be used as membership inputs into the fuzzy model (Adoko et al., 2011).

The case studies presented above support that fuzzy methods simplify the complexity of solving geotechnical problems compared to traditional methods. Indeed, Tay and Lim (2006) as well as Yazdani-Chamzini (2014) pointed out that expert knowledge and experience are beneficial since risk evaluation, prioritisation, and ranking are permitted in fuzzy models. However, the models are usually empirical and should therefore be modified when adopted in a different environment or field of study. This therefore presents room for improvement regarding the application of fuzzy theory in geotechnical engineering and tunnelling. Most importantly, the successful implementation of a fuzzy model is strongly dependent on the dataset and the input membership functions. It is critical to adequately divide the dataset into two subsets: one for model development and the other for testing and validation. Finally, the understanding of tunnel geometry, surrounding rock mass, support conditions, and ground engineering conditions plays a vital role in developing a successful fuzzy model. Expert knowledge also needs to be correctly infused with realistic decision-making functions in mind.

2.5. Ground characteristics and support reaction curves.

The management and conservation of road tunnels can be improved by having a better understanding of how their conditions change over time. The interaction between the rock mass and the tunnel support has been studied using ground characteristic curves and support reaction lines. The support system can either be rigid or flexible. Rigid support results in low radial deformation due to high stiffness. In contrast, flexible support leads to high

radial deformation as the stiffness is low (Lu et al., 2022). To achieve a stable tunnel, the support system must be very stiff. However, this is sometimes not economically viable. Hence the need for intermediate stiffness support system. This has been practiced by researchers such as (Sandrone and Labiouse, 2010). Their research demonstrated how the tunnel long-term stability conditions are affected by the delayed behaviors of the final lining and rock mass.

Calculating the Support Reaction Curve (SRC) and Ground Reaction Curve (GRC) is necessary for the convergence-confinement method. In general, the geometry of the opening, the mechanical characteristics of the rock mass, and the support elements in use, all affect how both curves are shaped. Structural elements supporting the opening that are more rigid have a tendency to resist deformations and spread out loads more evenly. As a result, the SRC and GRC may become flatter and more uniform (see Figure 2.8). In contrast, if the elements are more flexible, they may show greater deflections and deformations under load. As a result, the SRC and GRC may exhibit nonlinear or more variable curves (Lu et al., 2022).

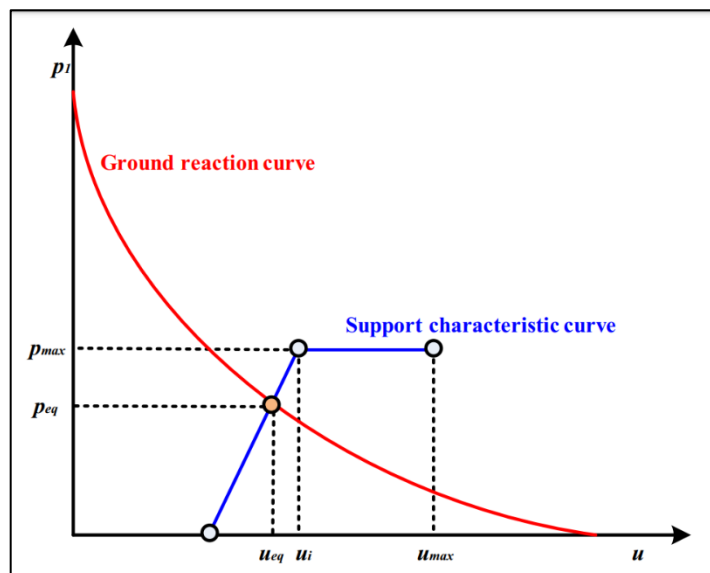


Figure 2.8: Ground reaction curve (GRC) and Support Reaction Curve (SRC) (Lu et al., 2022)

It is important to firstly understand the behaviour of the rock mass and the behaviour of the support system individually before understanding their interaction.

2.6. Comparison of measurement methods for tunnel convergence

The process of tunnel construction involves the moving of ground material (rocks or soil). The excavation process disturbs the equilibrium of the surrounding ground. Consequently, ground movement occurs until a new equilibrium state is reached. Ground deformation occurs during construction and after the completion of the excavation. The rate of deformation depends on the type of surrounding ground or rock and the stress levels in the vicinity of the excavation. In this section, four methods used specifically for monitoring the deformation of the tunnel walls (i.e., hanging and side walls) are discussed. The four methods are: total station, laser scanner, photogrammetry, and wireless sensors. They are also compared in terms of precision as well as capital and operating costs.

2.6.1. Method 1: Total station

Total stations have predominantly been used in tunnelling to measure and monitor tunnel convergence. They are primary surveying instruments used in underground and surface surveys to measure and record the location (distance and direction) of objects such as the tunnel face, walls, and target points.

Five to seven targets evenly mounted along the tunnel (side walls and hanging wall) are generally required to determine tunnel convergence using a total station. According to Erlandsson (2020), at least one of the targets must be mounted on the highest level of the tunnel profile (i.e., the crown). The total station is then used to measure the distance and direction of the targets in order to generate their coordinates. This process is repeated in multiple setup locations which can be at an average distance of 15m to 20m

apart. The average distance is however dependent upon the properties of the ground in which the tunnel is excavated. The main reason for repeating the same procedure at different setup positions is to achieve precise coordinates for the targets.

Various total stations are available on the market; however, a total station of 'class T1' is required to measure deformation. This class implies that the standard uncertainty on the vertical and horizontal angles of 0.15 milligon (mgon is a unit of measure for angles that is equal to 0.001 gon) is allowed. and for distances and convergence specifically, it stands at 1mm + 1ppm (Luo et al., 2016).

There exist automatic and manual total stations. Manual total stations require advanced skills and experience to yield quality results, and this could be a limiting factor. In contrast, automatic total stations require minimal skills. However, measurements of the first target need to be taken manually in order for the total station to recognise other targets relative to the first target. After that, the total station can measure the rest of the targets evenly distributed in the tunnel automatically. Automatic total stations are more costly compared to manual total stations (Erlandsson, 2020). In terms of monitoring, Figure 2.9 illustrates how four total station positions can be set up for the collection of four sets of measurements.

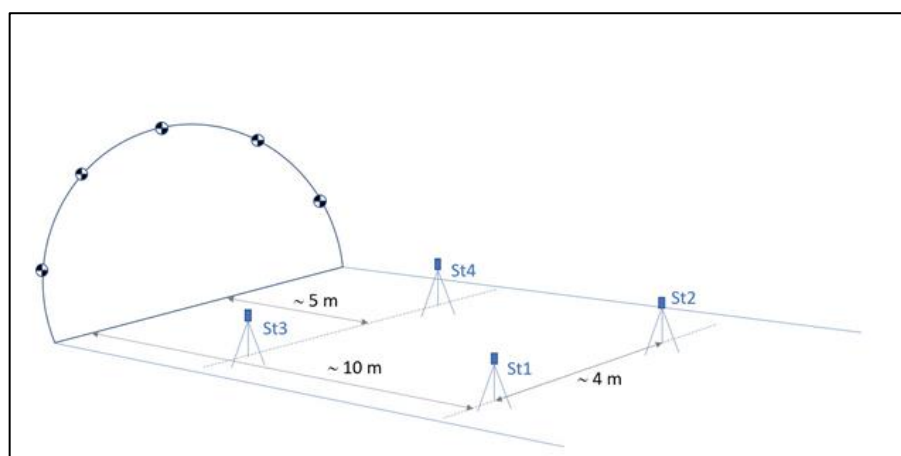


Figure 2.9: Schematic illustration of the total station measurement set-up with four different instrument positions (Erlandsson, 2020)

From the setup presented in Figure 2.9, the measured quantities include the distance, horizontal angle, vertical angle and the direction from each total station and each target. Though the exercise can be finished earlier with fewer measuring points, the quality of the final results is still compromised. Most of the time, limited equipment supply compromises final results.

2.6.2. Method 2: Laser scanner

Historically, laser scanners have not been widely used for measuring and detecting deformation. However, they are now gaining popularity because they can scan or measure more points compared to the conventional methods (Li et al., 2015). Conventional methods for deformation measurement including tape extensometers and total stations have been commonly used in mining and tunnelling to measure convergence.

Laser scanning is basically an advanced approach of capturing details of an existing structure (e.g., tunnel, mining panel, building). The instrument beams laser light and scan the surrounding multiple times so that the results are presented in three-dimensional point clouds. The point clouds consist of information that can later be processed into a map representing the shape and size of the precisely scanned objects.

Like with total station, laser scanning also involves the mounting of targets along the tunnel at regular intervals. Figure 2.10 shows the laser scanner setup. Laser scanning is fast and safe; however, the disadvantage of this method is that laser scanners are more expensive than total stations. Moreover, ambient light may combine with the laser and impair the accuracy of the scan since laser scanners use laser light to record data.

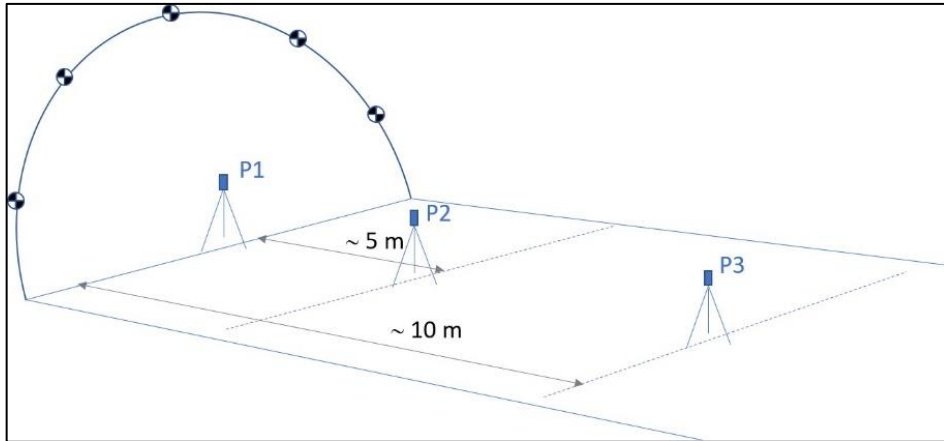


Figure 2.10: Schematic illustration of the laser scanner setup with three different instrument positions (Erlandsson, 2020)

Laser scanning also has an acceptable level of accuracy. Literature has showed that with laser scanning of tunnels, the accepted level of accuracy is $\pm 5\text{mm}$ (Kavvada, 2005; Scaioni et al., 2014).

2.6.3. Method 3: Photogrammetry

Photogrammetry is the process of converting photograph images into point cloud data to create a two-dimensional or three-dimensional model. This process generally relies on specialised software programmes. In essence, the software imports pixel data of a photo from a normal camera. Photogrammetry is therefore a technique whereby images captured by a normal camera are processed by a software into a three-dimensional model using point cloud data (Erlandsson, 2020). The procedure is more similar to laser scanning since both methods use cloud point data to create the final product. The most prominent advantage of the photogrammetric technique is the relatively low cost of the required equipment when compared to the two previous methods discussed (i.e., total station and laser scanning). The setup used for capturing photos for the photogrammetry method is illustrated in Figure 2.11.

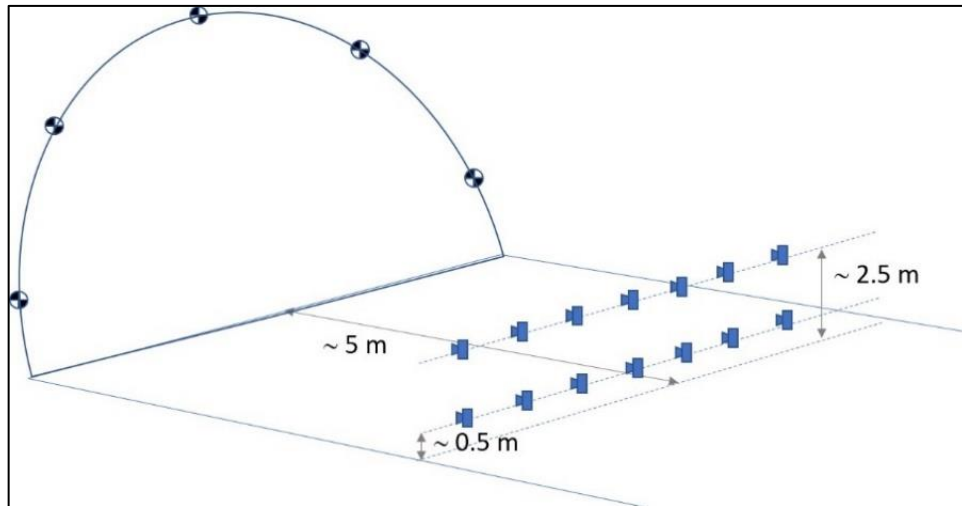


Figure 2.11: Schematic illustration of capturing photos for the photogrammetry method (Erlandsson, 2020)

In terms of accuracy, photogrammetry is different from the total station and laser scanner methods. It uses dimensionless measurements that in turn bring a level of ambiguity associated with the scale of the three-dimensional image created. To remedy the ambiguity, at least one known distance must be captured on the scene. This may be for example the distance between two targets or an object which is clearly visible. Therefore, capturing the scene can enhance the photogrammetric measurements and scale thereof. Also critical are the technical specifications to enhance accuracy applicable to photogrammetry. These include camera quality and resolution, object, size of object, and image plane geometry (Alhaddad et al., 2019; Scaioni et al., 2014; Erlandsson, 2020).

2.6.4. Method 4: Wireless sensors

Wireless sensors have recently been applied to deformation monitoring (Benoit et al., 2014; Marsella and Scaioni, 2018). This is mainly because the associated exercise does not really need personnel to be physically present in the field. Measurements can be taken remotely. Wireless technology is used as a replacement of wired sensors to transfer the data recorded by the sensors to a centralised database.

Prior to the wireless technology, wired sensors were placed and wired along the tunnel to collect relevant data. With advanced technology, tunnels can be fitted with internet connection so that data can be accessed wherever, at any time, provided there is internet connection. This means that tunnel deformation monitoring can be conducted continuously (Gama, 2004).

Wireless sensor methods may involve electric resistance strain gauges or fibre optic sensors mounted on steel arches which forms part of the tunnel support system. These sensors can detect any movement that occurs on the steel arches and any deformation of the tunnel. The cost of the entire system is relatively high compared to the previous three methods. This is mainly because stable network is required for smooth data transfer.

2.6.5. General conclusions of the four tunnel convergence measurement techniques.

The overall findings after comparing the four measurement methods of tunnel convergence are summarised in Table 2.5. The comparison was based on three parameters: deformation measurement uncertainty (at confidence level of 95%), cost of equipment to be used, and labour costs.

Table 2.5: Uncertainty at 95% confidence and cost for four deformation measurement methods (After Erlandsson, 2020)

Measurement method	Displacement (95% confidence)	Cost of equipment	Labour costs
Method 1: Total station	Horizontal: 3mm	Medium	Low
	Vertical: 2mm		
Method 2: Laser scanner	Horizontal: 5mm	Medium	Low
	Vertical: 3mm		
Method 3: Photogrammetry	Horizontal: 43mm	Medium	Low
	Vertical: 24mm		

Method 4: Wireless sensors	Convergence: 1mm	High	Very Low
----------------------------	---------------------	------	-------------

Photogrammetry showed very high measurement uncertainty. In contrast, the uncertainty measurements for other methods ranges between 1mm and 5mm. The first three methods are within the same equipment cost range and the uncertainty measurements are horizontal and vertical. Although displacement in wireless sensors is given as a convergence, the method appears to be more precise (1mm). This means that the displacement is in the direction normal to the tunnel surface (Erlandsson, 2020). The cost of equipment required in wireless sensor method is very high compared to the other methods. It can be concluded from the comparison of the four methods that the level of precision is directly proportional to the cost of equipment needed.

2.7. Concluding remarks

Rock mass classification has established itself as a great tool for rock engineering designs. Rock mass classification methods are capable of producing reliable input data relating to rock mass properties. Such input data is generally required for numerical modelling. The traditional rock mass classification methods presented in this literature review all have limitations. However, when applied with the understanding of their limitations, they are valuable tools for the research.

Looking at tunnelling, the excavation process entails moving the ground from the surrounding rock mass. The equilibrium stress around the excavation is disturbed as a result. The ground then readjusts to a new stress equilibrium leading to the steady displacement and convergence of the tunnel. Displacement and convergence occur in the tunnel during and after tunnel construction. Recently, fuzzy inference systems have been

used in tunnelling to analyse not only displacement and convergence but also the overall tunnel stability.

Since the first introduction of fuzzy theory in the 19th century, it has opened up room for continuous research and application in various fields. Fuzzy set theory is now finding wide application in geotechnical engineering with research in this field continuing to date. From the review, it has become evident that, as a subset of fuzzy set theory, fuzzy inference system (FIS) can be seen as the most popular technique in rock engineering. It has indeed been adopted for the resolution of several geomechanical challenges faced in surface and underground excavations. For example, FIS has found use in the estimation of the convergence and convergence velocity of high-speed railway tunnels with promising outcomes (Adoko et al., 2011 & 2012). Secondly, several algorithms are available for the implementation of FIS. However, the review noted that most researchers opt for the Mamdani technique whereas the Takagi-Sugeno technique is also capable of addressing similar geotechnical problems with competing effectiveness, accuracy, and reliability. Research is needed to further develop available and new techniques. Thirdly, the number of datapoints required to build an FIS model should be large enough to cater for the development itself as well as the validation of the model. Fourthly, from an FIS perspective, assigning membership function for input variables is key to ensuring the success of the model. However, the review revealed the need for further research to identify membership functions appropriate for specific geomechanics problems. Research is also needed around the around the three key conceptual aspects of FIS: rule base, database, and reasoning mechanism. Lastly, the incorporation of neural network in fuzzy set systems has shown improvements in terms of the application of FIS to geomechanics. Continuous research on this theme is expected to minimise the limitations and deficiencies associated with fuzzy set theory.

Talking about the monitoring of tunnel convergence, four prevalent methods were compared: total station, laser scanner, photogrammetry, and wireless

sensors. Based on the appraisal of their measurement precision, equipment cost and labour cost, it was concluded that precision is directly proportional to the cost of the associated equipment and setup. This is a limiting factor especially for wireless sensors that are on the upper side of the price scale.

The study of tunnel convergence as a function of time is still in its early stages. According to the literature, tunnel convergence can be observed over time, but the cost of the necessary equipment makes this difficult. This thesis hypothesise that it is possible to comprehend tunnel stability by developing a method of estimating microfracture distribution and total displacement. Researchers will then be able to gather useful data on tunnel convergence prediction as a result of this. A review of the literature reveals that FIS has potential, but significant progress must still be made before it can be considered acceptable. Empirical methods like GSI have some limitations. The use of microfractures to create a predictive chart is therefore explored in this thesis because it is more cost-effective and accessible to the researcher.

This research proposes an alternative avenue to analyse convergence in shallow tunnels. The researcher explored the use of thin sections and micro fracture analysis to develop a predictive chart for fracture distribution along the tunnel. Instead of using FIS and monitoring equipment, the researcher uses ML and advanced geomechanics approach to bridge the gap.

3. Chapter 3: Materials and Methodology

In this chapter, the methodology followed for data collection pertaining to this thesis is explained in detail. This includes field measurements and observations, laboratory experiments and analysis, traditional rock slope analysis, and failure probability analysis for tunnels. Lastly, procedures followed for estimating rock mass properties, kinematic analysis and slope stability analysis are detailed.

3.1. Introduction

The data collection methodology followed in this thesis encompasses desktop study, field observations, field measurements, experimental tests and numerical simulations.

As a starting point, a desktop study was strategically chosen to be the first method of data collection to lay a good foundation for the research. This was achieved by gathering and reviewing relevant books, journal papers and conference papers dealing with tunnel stability analysis and associated stability analysis approaches. The desktop exercise developed a better understanding with regards to the nature of data to be collected from the field observations and laboratory experiments to achieve the objectives of this thesis. The desktop study also served the purpose of identifying meaningful computer programs that can be used to analyse the collected data.

Secondly, field observation and measurements were performed. At this stage, geological discontinuities were identified and observed. The possible areas of rockfall were also identified from the geological features. Field observations were mainly focused on geological discontinuities; rock types; possible rockfall; and tunnel conditions. In terms of field measurements, scanline mapping was conducted following a detailed structural mapping protocol. Upon completion of mapping, rock samples were collected for

further characterisation. This specifically hinged on the microscopic analysis of samples by means of thin sections.

The last phase of the experimental endeavour involved the kinematic analysis, on the one hand, and stress-strain relationship analysis, on the other. These were performed to evaluate the slope stability for the rock mass in the vicinity of the tunnel as well as the stability of the tunnel itself. The following rock engineering software programs were used for the purpose: DIPS (note that the correct marketing name is "Dips" but to avoid confusion we use "DIPS" in this thesis), Optum G2 and Phase2. From the simulation work, the outputs pertaining to stress-strain relationship and kinematic analyses were used to develop a predictive deformation curve of the road tunnels. Incidentally, the two aforementioned analyses made it possible to develop a predictive stability analysis chart with proposed tunnel support systems.

In the subsequent sections, the methodology adopted in data collection for this thesis succinctly is described in detail. The phases introduced above are broken down and presented with applicable information. In terms of laboratory testing, all procedures and protocols followed are described. For the numerical simulation work, the selected software packages are presented in terms of input and output parameters as well as how each package was set up for the intended purpose. Finally, the data set analysis is discussed while corresponding results are made sense of in the next and later chapters.

3.2. Field observations and measurements

Field observations and measurements were conducted at the Hendrik Verwoerd Tunnels (Figure 3.1). This exercise was carried out to collect valuable information that was used to validate the simulation results for this study. The use of field data establishes opportunities for practical interpretations of numerical calculations illustrative of the behaviour of rocks and rock mass. Field observations involved observing inside and outside of

the tunnels, measurements of rock mass properties and geological mapping. These are explained in detail in the next two subsections.

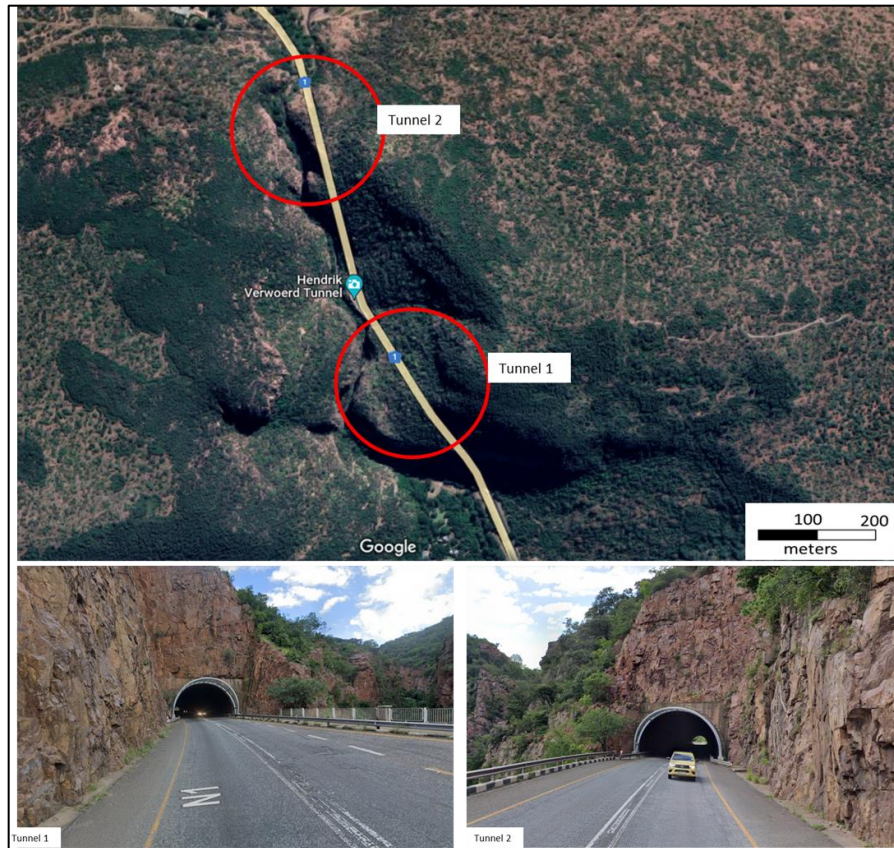


Figure 3.1: Areal map of the study area (Google Maps, 2022)

3.2.1. Observations

Visual observations were conducted along the Henrik Verwoerd Tunnels in Limpopo. The visual observation exercise was divided into two parts. The first part was to look at the conditions of the rock mass in the vicinity of the tunnel. The second part of the observation was to look at the condition of the tunnel itself. In other words, observations were conducted inside and outside the tunnel. When observing outside the tunnel, the main focus was on the rock type, geological discontinuities and their infill, slope height, the possibility of rockfalls and the general conditions of the rock mass. In contrast, observations inside the tunnel were mainly focused on the cracks,

water seepage, evidence of deformation and the general tunnel conditions. These observations are further analysed in Chapter 4.

3.2.2. Field measurements

Field measurements were conducted to attain the rock mass properties and rock samples were also collected for further laboratory analysis. A tape measure (Figure 3.2a) was used to measure the distance along the side of the tunnel where rock samples were collected. Point number 1 was on the skin of the tunnel. The subsequent points were separated by 0.5 m. A tape was stretched from the tunnel face to the back of the face while marking intervals of 0.5m from the tunnel backward. Both the right and left sides of the tunnel had samples collected; 14 samples from the right side and 10 samples from the left side, respectively. A geological hammer (Figure 3.2b) was used to remove rock samples for the sample collection process to be smoothed. Each rock sample was placed in a sample bag (Figure 3.2c); then, the sample bag was labelled and packaged to avoid mix-ups. Collected rock samples were taken to the laboratory for thin section experiments and micro fracturing analysis. The experiment analysis is covered later in Section 3.3.

Geological mapping was conducted to collect rock mass properties and discontinuities present in the rock mass. Discontinuities identified included joints and parting planes (see Figure 3.3). A clinometer (Figure 3.2d) was used to measure the dip of the geological structures whereas the dip direction was measured using the pocket compass (Figure 3.2e). This information was recorded in the field notebook (Figure 3.2f) to be further used for the desktop analysis of the results. The dip and dip direction of the

structures were further analysed and displayed on a stereonet using the DIPS software.

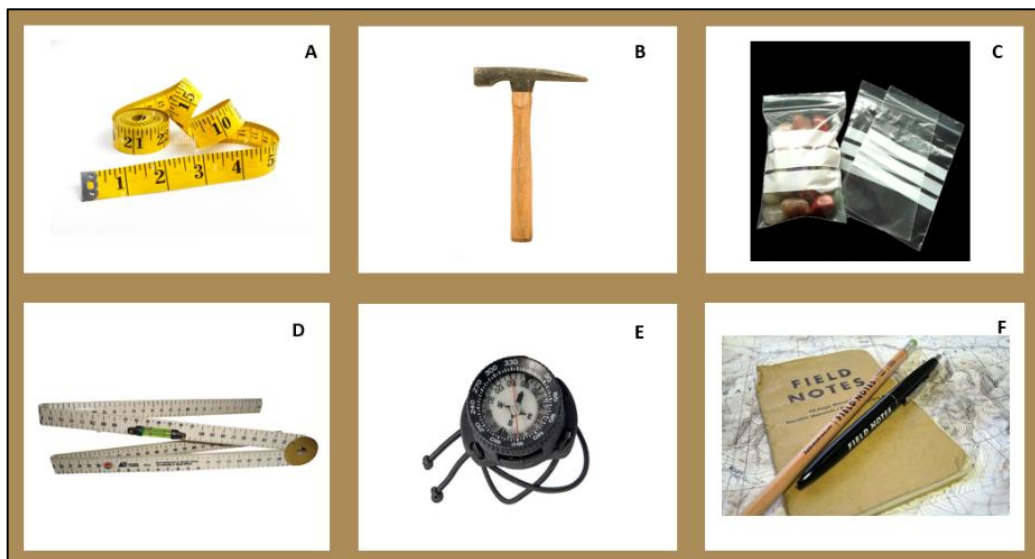


Figure 3.2: Geological tools used for field measurements. (a) Tape measurement, (b) Geological hammer, (c) Sample bag, (d) Clino ruler, (e) Compass, (f) Field notebook and pen

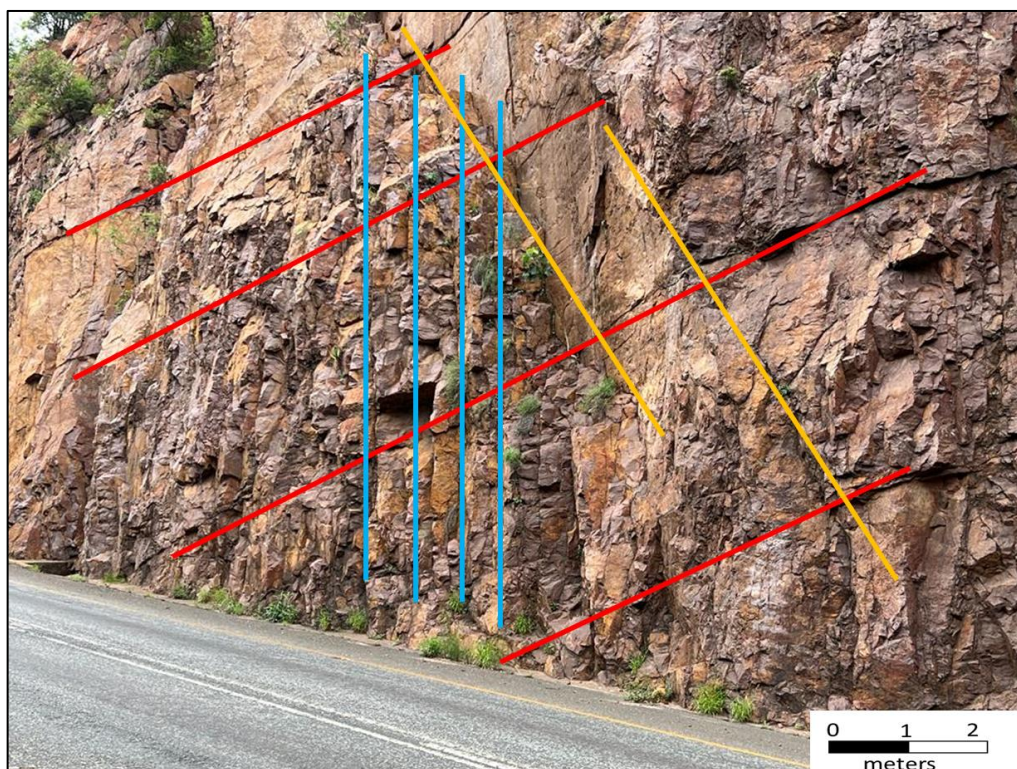


Figure 3.3: Jointed rock mass in the periphery of the tunnels

The field observations and measurements were coupled with geological mapping. This was performed to obtain and gather geotechnical information that was later used as input data for numerical simulations. In Section 2.1 of Chapter 2, four traditional methods of rock mass classification were reviewed. These are the Q-system by Barton et al. (1974), the geomechanics classification (RMR) system by Bieniawski (1973, 1976 & 1989), Mining Rock Mass Classification (MRMR) system by Laubscher (1975, 1990 & 1993), and the Geological Strength Index (GSI) by Hoek (1994). The abovementioned traditional methods were considered to classify the rock mass quality in the periphery of the Hendrik Verwoerd tunnels. Nonetheless, GSI technique was found to be more efficient during field observation and measurement, hence it was adopted. The exercise sought to accurately characterise and attribute parameter ratings using the relative rating charts. Because an understanding of rock properties and rock strength is critical for this doctoral study, this exercise was suggested to help the researcher create an exhaustive description of the rock mass at hand.

Furthermore, scanline mapping method was used to collect geotechnical parameters summarised in Table 3.1.

Table 3.1: Field measurement geotechnical parameters

Geotechnical property	Symbol	Units of measurement
Dip		Deg (°)
Dip direction		Deg (°)
Joint set number	J_n	
Joint spacing	J_s	mm
Joint infilling	J_I	-
Joint water reduction factor	J_w	-
Joint aperture	J_A	mm
Joint persistence	J_P	m

Information provided in Table 3.1. was used as input data in numerical simulations at a later stage of this research. Most rock engineering software requires this information as input data for stability analysis (e.g., DIPS, RS2, Swedge, Unwedge, etc). Moreover, the information in Table 3.1. was also used to quantify the rock mass in the vicinity of the tunnels. The compilation of this information in conjunction with the relative slope stability and tunnel stability analysis is critical for the development of tunnel stability charts and the design of tunnel support systems.

This doctoral research is not geological in nature. However, it took cognisance of how vital it is to understand the geology of the area of study in order to link it to the behaviour of the rock mass present. This was one of the motivations for conducting scanline mapping.

Scanline mapping is a technique used to record and describe geological discontinuities on an exposed rock mass. In other words, a straight line is drawn, or a tape is extended over an exposed surface of the rock mass. All discontinuities intersecting the straight line or tape are recorded and described (ISRM, 1981; Priest, 2004). The properties of the geological discontinuities along the scanline were recorded. Figure 3.4 shows a schematic diagram of the scanline mapping technique. The image provided in Figure 3.5 was modified after Harrison and Hudson (1997). It describes the terminologies of geotechnical parameters collected along the scanline. The procedure for scanline mapping was carried out as per Gumedde and Stacey (2007). A scanline was drawn along the sidewalls of the tunnel to measure geotechnical parameters of the rock mass (see Figure 3.6).

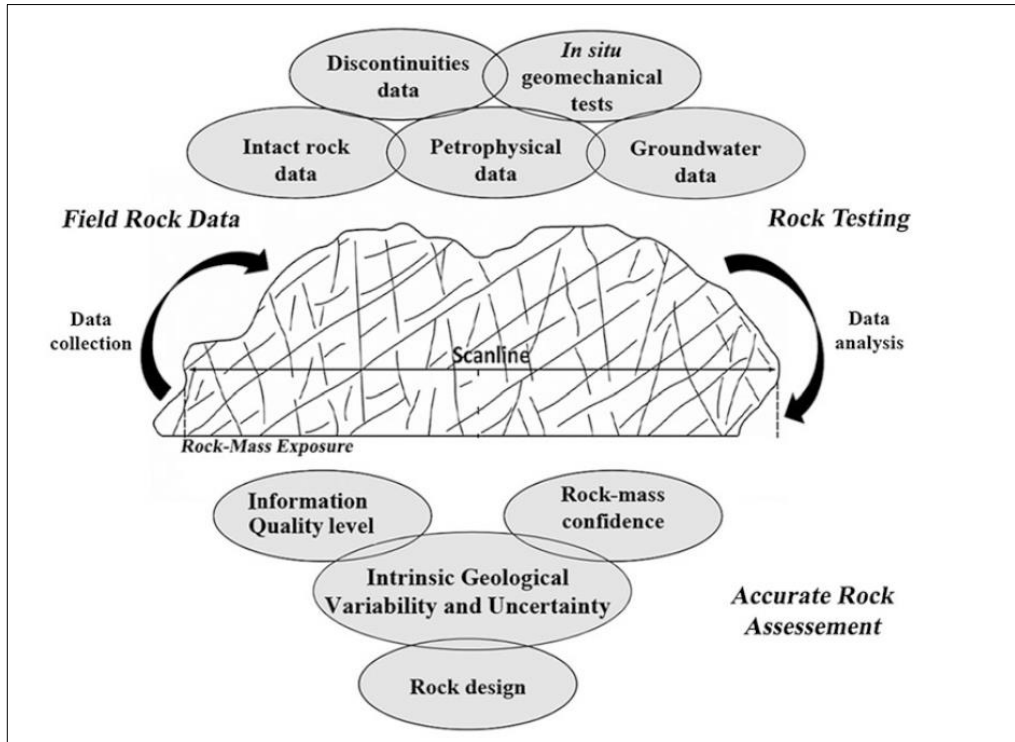


Figure 3.4: Scanline mapping technique for geotechnical data collection (Chaminé et al., 2015)

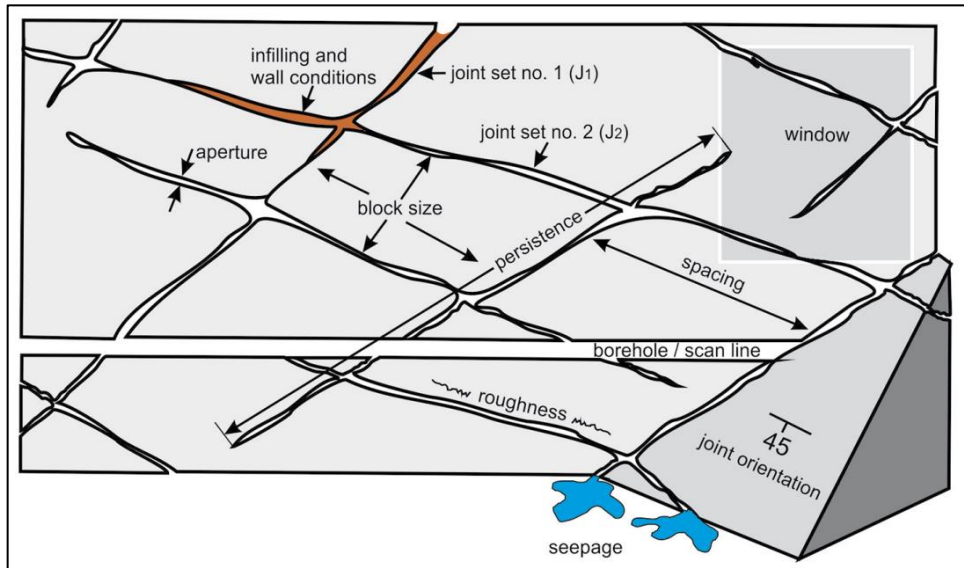


Figure 3.5: Scanline mapping and terminologies for rock mass properties (After Harrison and Hudson, 1997)

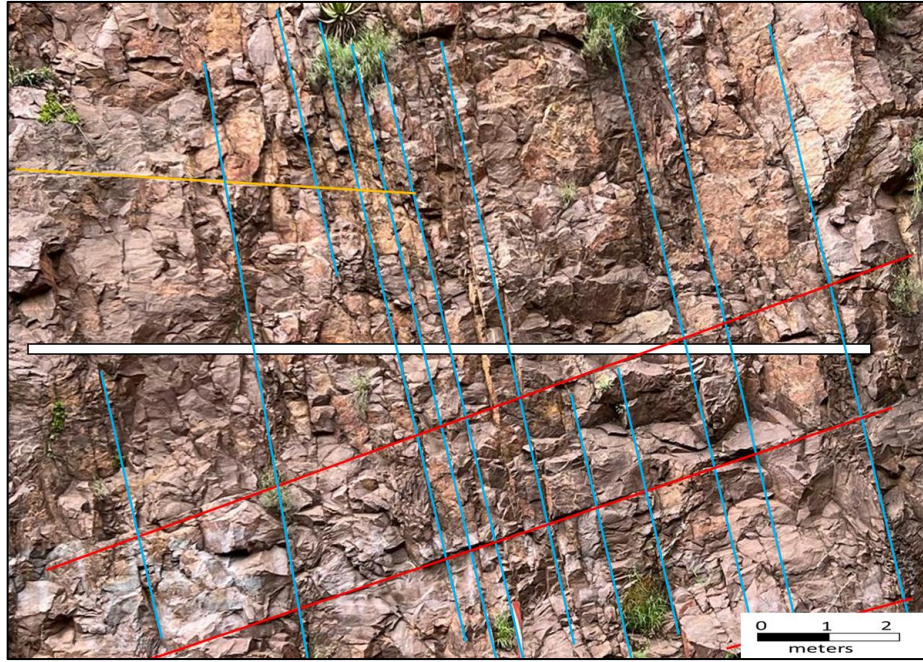


Figure 3.6: Scanline mapping in the periphery of the tunnels

3.3. Laboratory experiments and analysis

Laboratory tests are critical in the field of rock engineering. They assist in understanding the strength and composition of the rock material. This information is very key for design and decision-making purposes.

One set of laboratory experiments was carried out in this research. It entailed the laboratory analysis of microscopic fractures. Rock samples were collected along the sides of the tunnels.

The collected rock samples were sent to the laboratory and prepared. The preparation process involves cutting of the samples using the cutting machine (Figure 3.7a). The cut piece of rock must be flat and smooth before polishing commences. The cut piece of rock is firstly polished using coarse silicon carbide powder to remove the rough surface. Secondly, the rock is polished using fine silicon carbide powder to further smoothen the surface. The course and fine silicon carbide powder is shown in Figure 3.7c. While polishing, the cut rock piece is pressed against the surface with the silicon carbide powder mixture. The movement must form the shape of the number

eight in order to even the pressure applied (see Figure 3.7d). After polishing, the rock is placed on a glass slide to check for air bubbles. The presence of air bubbles implies that more polishing is needed. In absence of air bubbles, the rock is then put to dry as shown in Figure 3.7b.



Figure 3.7: Thin section preparation at the laboratory. (a) Cutting machine, (b) Drying process, (c) Course and fine silicon carbide powder, and (d) Polishing

After the rock has dried up, the polished side was fixed to a glass and UV light was used to dry up the fixture on the glass (Figure 3.8a). After drying, the other side of the rock was also polished until it was thin. Thin section rock samples should be almost $30\ \mu\text{m}$ thick (Sturm, 2010). Grinding and polishing took place until the block was about $30\ \mu\text{m}$ thick (Figure 3.8b). The thin section was then covered with a thin glass as shown in Figure 3.8c.

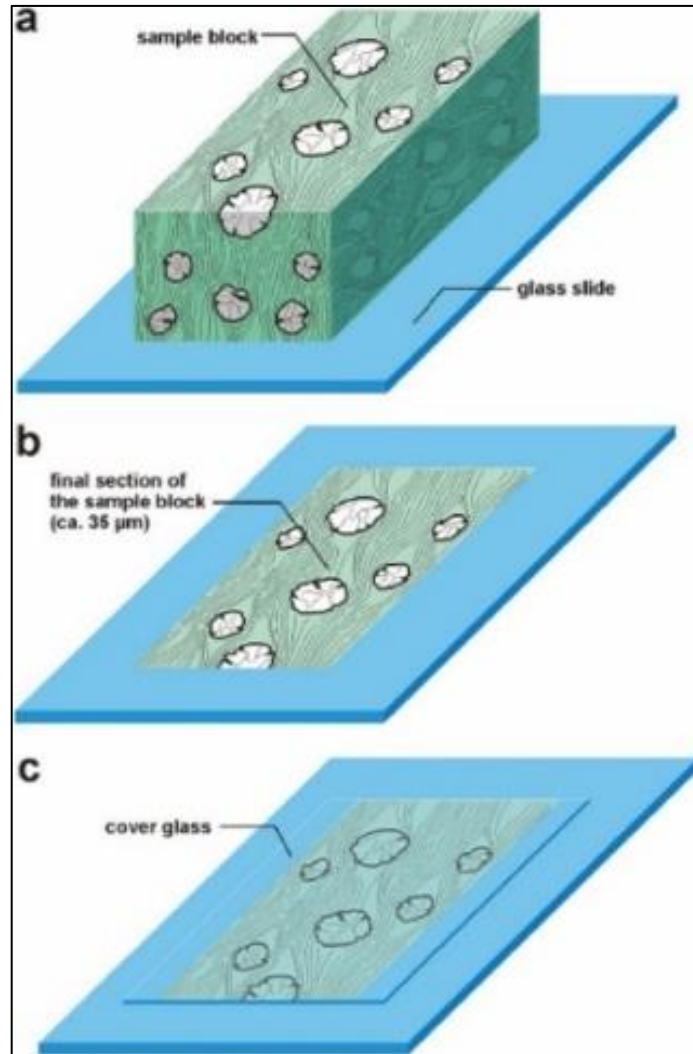


Figure 3.8: Schematic diagram of thin section preparation. (a) Sample block with one polished side fixed on glass, (b) Final 35µm thick section of the sample block, (c) Thin section covered by glass on both sides (Sturm, 2010)

Thin sections are usually mounted to a glass slide and can only be viewed and analysed through a microscopic lens. To analyse a thin section under a microscopic lens, the following parameters are considered: colour, grain size, grain shape and micro fractures. The thin section technique is an analytical approach that enables researchers to identify the mineral composition of the rock, observe structural features present and also interpret the environmental conditions under which the rock was formed. Indeed, the thin section experiment permits researchers to describe the distribution and development of fractures. In this research, the microscopic

analysis of fractures was conducted for tunnels in a shallow hard rock mining environment (road tunnels in this case).

3.4. Data analysis using Machine Learning

Machine Learning (ML) is part of artificial intelligence in data science. In simple terms, ML uses data to answer questions. The use of data in this case can be referred to as training, whereas answering questions can be referred to as prediction (MathWorks, 2022).

ML can be categorised into two groups. The first group is known as unsupervised learning while the second refers to supervised learning. The two groups differ based on the type of input data and the objectives of the output (Alloghani et al., 2020).

Unsupervised learning comes with a lot of unknown data and a lot of variables. As such, in order to solve a problem, ML determines hidden patterns in the data by grouping it into subsets showing similar characteristics. In contrast, there is a series of known variables available with supervised learning. And in this case, supervised learning algorithm learns the relationship of the available data in order to solve a problem. Classical examples of supervised learning algorithms are regression and decision trees (see Figure 3.9).

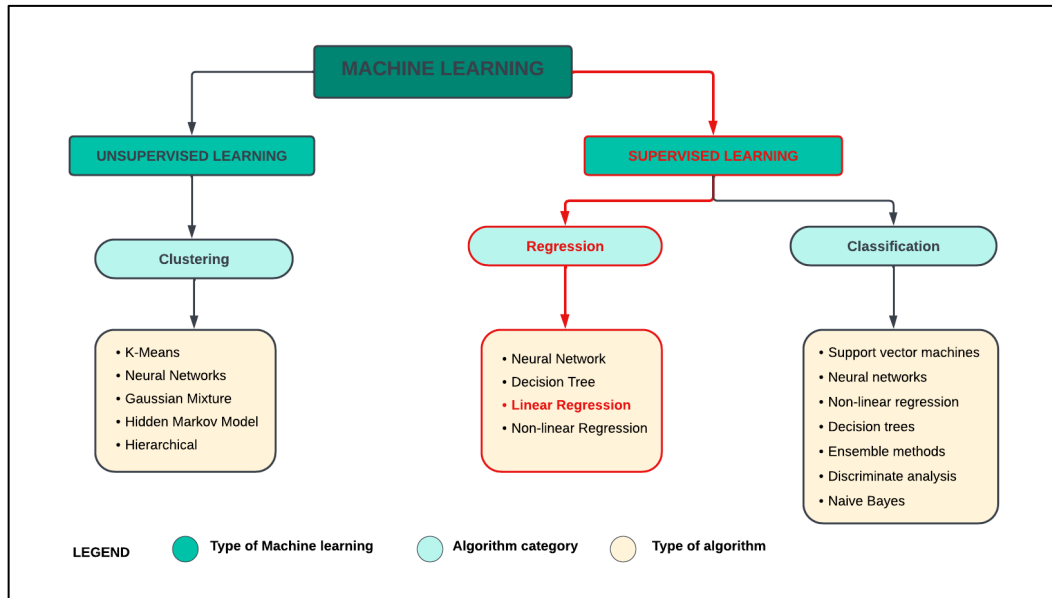


Figure 3.9: Machine Learning Flowchart (Modified after MathWorks, 2022)

Regression algorithms seek to explain or predict the unknown dependent variable, based on the known independent variables. This algorithm used independent variables to model the relationship with dependent variables. The relationship is presented using a regression line which is a line of best fit. The modelled relationship can either be positive or negative (Bunker and Thabtah, 2017; MathWorks, 2022). A positive relationship means that the dependent variable is directly proportional to the independent variable. In contrast for negative relationship, when the independent variable increases, the dependent variable decreases.

In this thesis, linear regression was used to develop a predictive model for fracture distribution along the tunnel. A flowchart of the learning type, algorithm category and algorithm type used in this thesis is illustrated in red in Figure 3.9. The results and outcomes of the linear regression of data consisting of total number of fractures along the tunnel is presented and discussed later in Chapter 5.

3.5. Numerical simulation work

Numerical simulations have been used quite extensively in geotechnical engineering. Their underlying principle has been used to mimic the behaviour of various systems that consist of complex mathematical models and later analyse the outputs using classical mathematical tools. In mining and civil engineering, numerical simulations are used to analyse the behaviour of the rock mass and its impact on the stability of the excavations or infrastructures. They are also used to evaluate and determine the deformation, and displacement of various types of excavations subjected to loading. Numerical simulations are therefore ideal for analysing the stress and deformation relationship in tunnelling. They are supported by computerised software programmes that encapsulated the mathematical description of the behaviour of the tunnel.

Simulation and numerical analysis of excavations can be conducted using three main methods: Boundary Element Method (BEM), Finite Element method (FEM), and Finite Difference method (FDM). In BEM, only the boundary of the excavation is divided into elements. Both the finite element and boundary element methods work by dividing the geometry into elements. In FDM, the body is discretised with a two- or three-dimensional grid (Ghadimi Chermahini and Tahghighi, 2019; Kanik and Gurocak, 2018; Rehman et al., 2020).

In rock engineering, researchers mostly resort to numerical modelling and simulations to analyse the stress-deformation interaction. Likewise, in this thesis, numerical simulation is employed to analyse and predict the behaviour of the tunnel subjected to load. This is achieved by using rock engineering software programs such as DIPS, Optum G2 and RS2. These software packages require input data that speaks to the mechanical properties of the rocks as explained in Sections 3.2 and 3.3. The mechanical properties of the rock used as input data are summarised in Table 3.2.

Table 3.2: Mechanical properties of the rock

Mechanical Properties of the rock	Symbol	Units
Density	ρ	kg/m ³
Unit weight	γ	kN/m ³
Young's modulus	E	Pa
Poisson's ratio	ν	
Uniaxial compressive strength	UCS	Pa
Shear strength	τ	Pa
The angle of internal friction	ϕ	deg (°)
Cohesion	c	Pa

This section outlines the numerical modelling techniques and software that was used to analyse the tunnel deformation and equilibrium states for this thesis. Firstly, the procedure for estimation of rock mass properties using RocLab is detailed. Furthermore, the kinematic analysis and rock slope stability analysis are described as the two methods of analysis of choice for this doctoral thesis.

3.5.1. Estimating rock mass properties using RocLab

RocLab is a Rocscience software used to determine rock mass strength parameters. In this thesis, RocLab was used to determine the strength parameters of the rock mass in the vicinity of the tunnels in the study area. The rock mass strength parameters are estimated based on GSI using the generalised Hoek-Brown parameters (detailed in Section 2.1.4 of Chapter 2).

A new project was set up to define the rock mass properties of the slope in the vicinity of the tunnels. Intact uniaxial compressive strength was estimated based on the rock type as indicated in Figure 3.10.

Field Estimate of Strength	Examples	Strength (MPa)
Specimen can only be chipped with a geological hammer.	Fresh basalt, chert, diabase, gneiss, granite, quartzite.	>250
Specimen requires many blows of a geological hammer to fracture it.	Amphibolite, sandstone, basalt, gabbro, gneiss, granodiorite, limestone, marble, rhyolite, tuff.	100-250
Specimen requires more than one blow of a geological hammer to fracture it.	Limestone, marble, phyllite, sandstone, schist, shale.	50-100
Cannot be scraped or peeled with a pocket knife, specimen can be fractured with a single blow from a geological hammer.	Claystone, coal, concrete, schist, shale, siltstone.	25-50
Can be peeled with a pocket knife with difficulty, shallow indentation made by firm blow with point of a geological hammer.	Chalk, rocksalt, potash.	5-25
Crumbles under firm blows with point of a geological hammer, can be peeled by a pocket knife.	Highly weathered or altered rock.	1-5
Indented by thumbnail.	Stiff fault gouge.	0.25-1

Uniaxial Compressive Strength (σ_{ci}): MPa

Figure 3.10: Estimating intact uniaxial compressive strength in RocLab

GSI value was chosen based on the visual observations at the study area. RocLab is equipped with the GSI chart as illustrated in Figure 3.11. Numerous material constant values for intact rock (m_i) are available within the software. They are selected based on the rock type as presented in Figure 3.12).

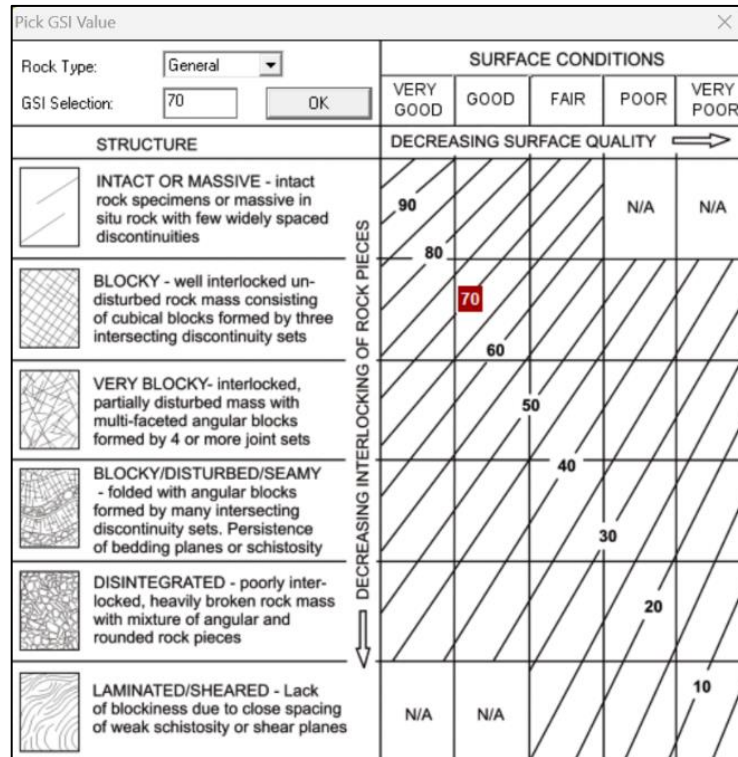


Figure 3.11: Choosing GSI number in RocLab

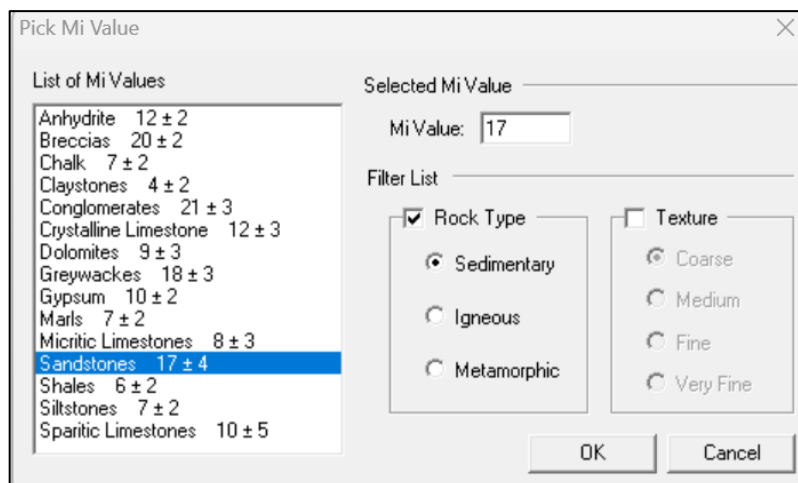


Figure 3.12: Choosing the mean constant value (m_i) in RocLab

The disturbance factor D (refer to Section 2.1.4 of Chapter 2) is applicable in two scenarios, including tunnels and slopes. Although the scope of this thesis is in tunnelling, the exposed rock mass at the study area was the slope rock mass between the two tunnels. Therefore, the disturbance factor category applicable in this case was slope.

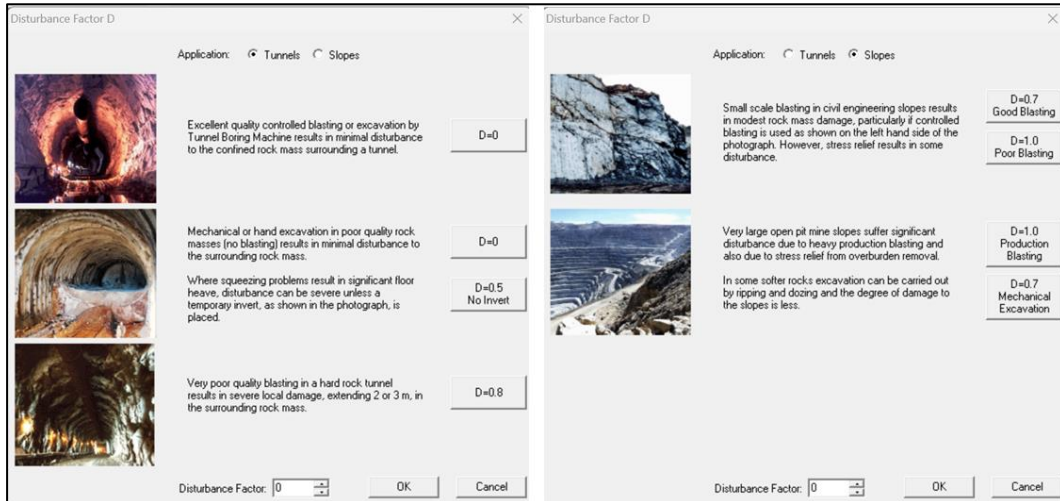


Figure 3.13: Choosing disturbance factor (D) in RocLab

Finally, the estimated rock mass properties are presented in the form of graphs of normal stress (σ_n) vs shear stress (τ) and minor principal stress (σ_3) vs major principal stress (σ_1) as illustrated in Figure 3.14.

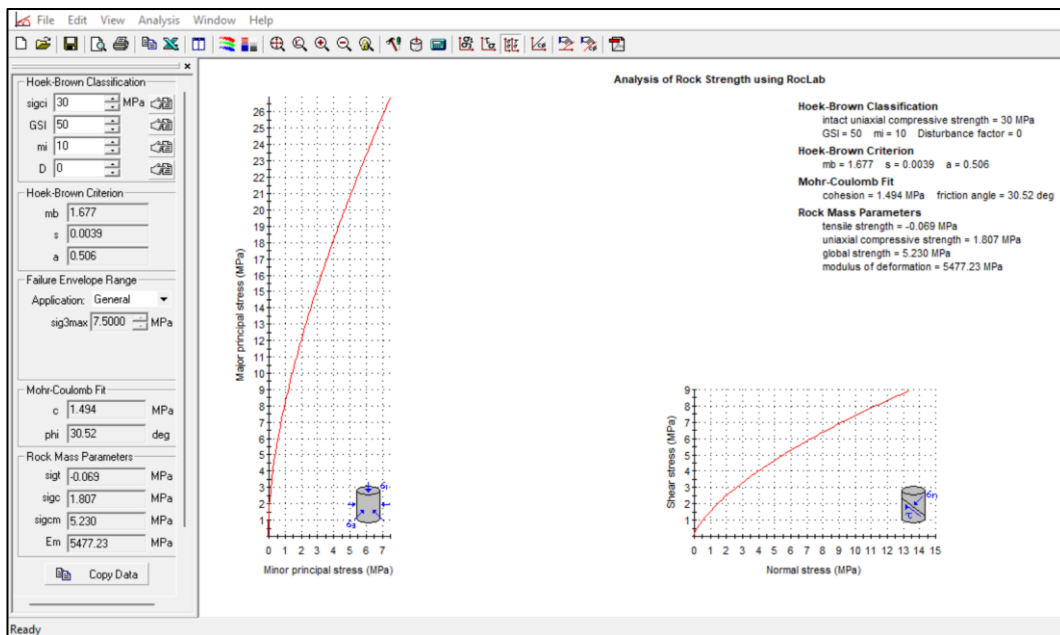


Figure 3.14: Rock mass strength parameters estimated in RocLab

3.5.2. Kinematic analysis

Kinematics analysis was used in this thesis to describe the possible failure modes in the vicinity of the tunnel based on the observed geological

structures such as joints (refer to Section 3.2.2). DIPS is one of the most popular rock engineering software programs used to visualise orientation-based geological data. The software uses stereonet to plot and display the dip and dip direction of structures. The kinematic analysis feature in DIPS enables the user to easily evaluate the possible rock slope failure and stability modes (Rocscience Inc, 2002). These include toppling, planar, and wedge failure modes. Figure 3.15 illustrates how a new DIPS file was created. The input data required is the dip and dip direction of the excavation, and/or geological discontinuities.

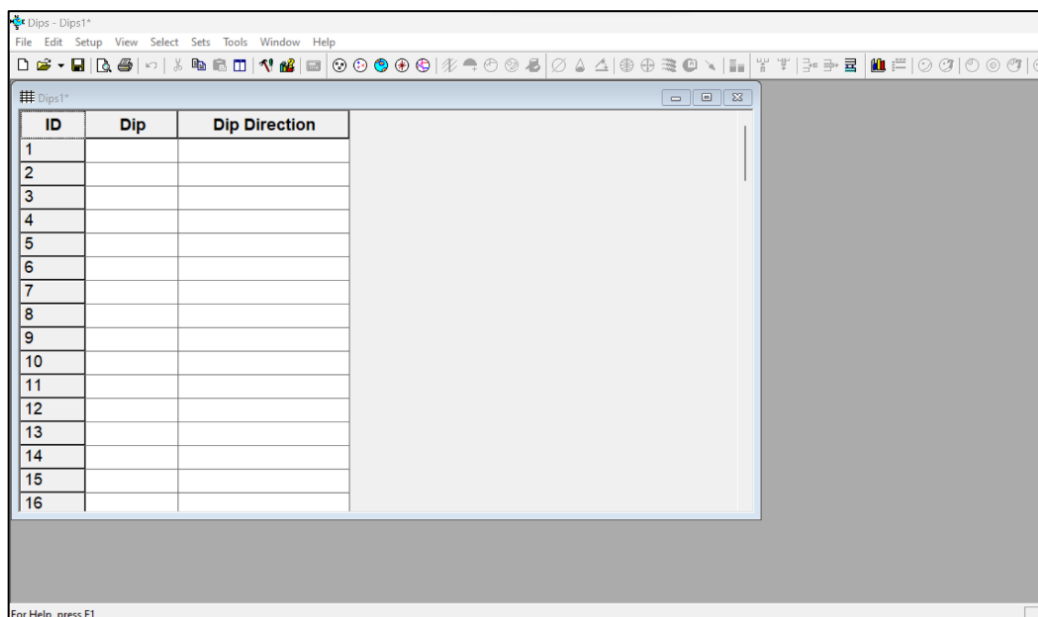


Figure 3.15: Creating a DIPS file.

Results in DIPS can be presented as scatter plots, pole plots, contour plots, rosette plots and major plane plots. Examples of scatter plots and contour plots is shown in Figure 3.16. To visualise the possible rock failure modes such as wedge failure, major plane plots are used (see Figure 3.17). In this thesis, the dip and dip direction data were collected through scanline mapping, along the sides of the tunnel. DIPS was used to predict the possible slope failure modes in the periphery of the tunnel based on the observations made.

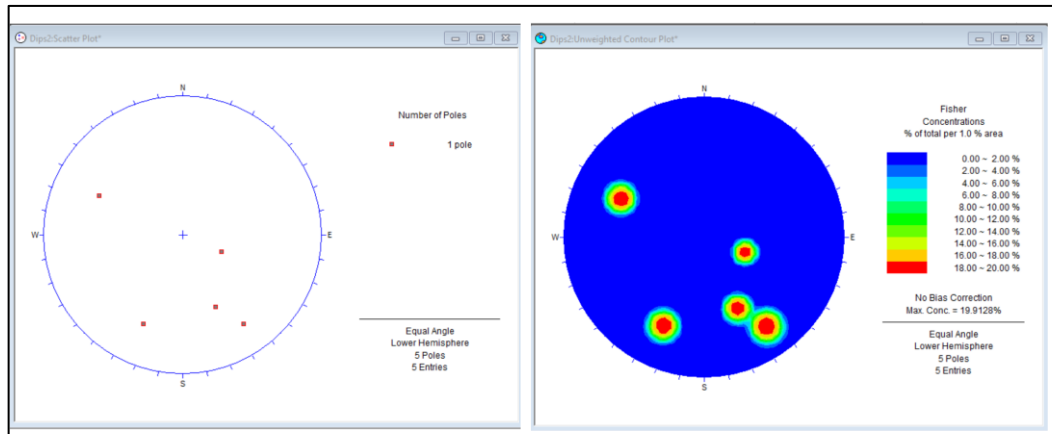


Figure 3.16: Example of scatter plots and contour plots in DIPS

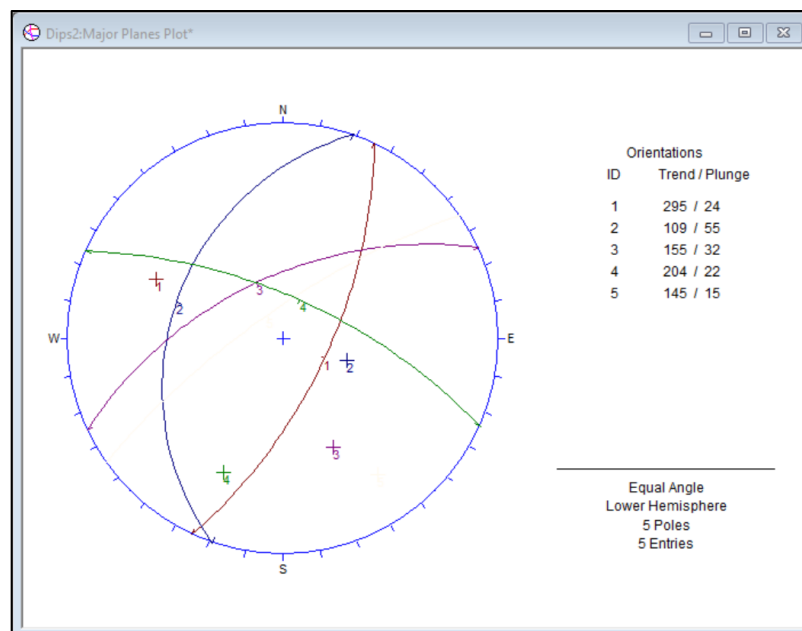


Figure 3.17: Example of major plane plots in DIPS

3.5.3. Rock slope stability analysis

Rock slope stability analysis is a critical aspect of rock engineering because it assesses the risk of instability and the consequences of failure. Moreover, in rock stability analysis, measures to stabilise the slopes are suggested as a remedial action. The numerical simulation software that was employed for the analysis of slope stability is described in this subsection. This includes ground reaction curve, support design, stress analysis in two and three

dimensions, and potential modes of failure resulting from structural instability.

3.6. Strength reduction factor

Optum G2 is a commercial rock engineering software that uses finite element technique to solve geotechnical problems. This software is commonly used to analyse the deformation and strength of engineering excavations. Its application has been evident in slope stability, tunnelling, dams and retaining walls. There are various types of analysis to choose from in Optum G2. These include but are not limited to limit analysis and strength reduction.

For this thesis, the strength reduction analysis was used to assess the stability of the tunnel in fractured ground conditions. An example of tunnel simulation on Optum G2 and the results there of is illustrated in Figure 3.18 and Figure 3.19 respectively.

ADAPT STEP	ITR	REDUCTION FACTOR	STABILITY
1	1	1.000E+00	Unstable
1	2	5.000E-01	Unstable
1	3	2.500E-01	Stable
1	4	3.750E-01	Unstable
1	5	3.125E-01	Unstable
1	6	2.500E-01	Stable
1	7	2.813E-01	Stable
1	8	2.969E-01	Stable
1	9	3.047E-01	Stable
1	10	3.086E-01	Unstable
1	11	3.066E-01	Unstable
1	12	3.047E-01	Stable
2	1	3.047E-01	Stable
2	2	3.323E-01	Stable
2	3	3.623E-01	Unstable
2	4	3.473E-01	Unstable
2	5	3.323E-01	Stable
2	6	3.398E-01	Unstable
2	7	3.360E-01	Stable
2	8	3.379E-01	Stable
3	1	3.379E-01	Stable
3	2	3.467E-01	Stable
3	3	3.557E-01	Stable
3	4	3.650E-01	Unstable
3	5	3.603E-01	Unstable

Figure 3.18: Strength reduction factor simulation running on Optum G2

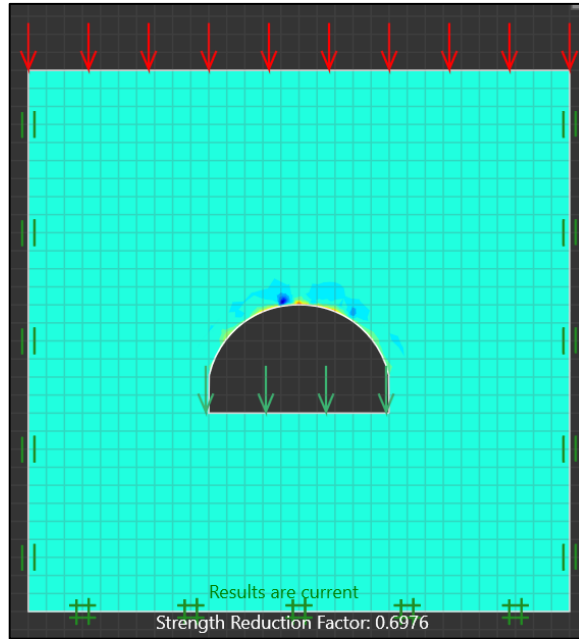


Figure 3.19: Example of SRF simulation on tunnel in Optum G2

Tunnel one was simulated using Optum G2 to assess the effects of fracturing on strength reduction factor. The results from this simulation are discussed at length in Section 6.2 (Chapter 6).

3.7. Tunnel deformation analysis using RS2

RS2 (previously known as Phase 2) is a two-dimension finite element programme provided by Rocscience. It was created specifically to assess the stability of geotechnical structures like tunnels, slopes, and others. Advanced numerical modelling tools are available in RS2 to simulate how soil and rock masses will behave under various loading and boundary conditions. It is used in rock engineering to evaluate stresses and assess the suitability of various support systems for underground excavations. In this thesis, RS2 was used to analyse the effects of fracturing on tunnel stability, focusing mainly on the strength factor and total displacement around the tunnel.

A new project (Figure 3.20) was set in place to render the necessary simulations. There are seven steps that need to be taken in order to set up a new project. Firstly, the general settings are assigned to the project where

the analysis type, solver type and units are defined (see Figure 3.21). For this thesis, the analysis was chosen as plain strain with Gaussian Elimination solver type. The units are metric, and stresses are represented in Mega Pascals. Secondly, the stages of the project were set to be 10. This was done to distribute the internal pressure in 10 stages. The remaining five aspects to be defined include stress analysis, ground water, statistics, strength reduction and finally the project summary.

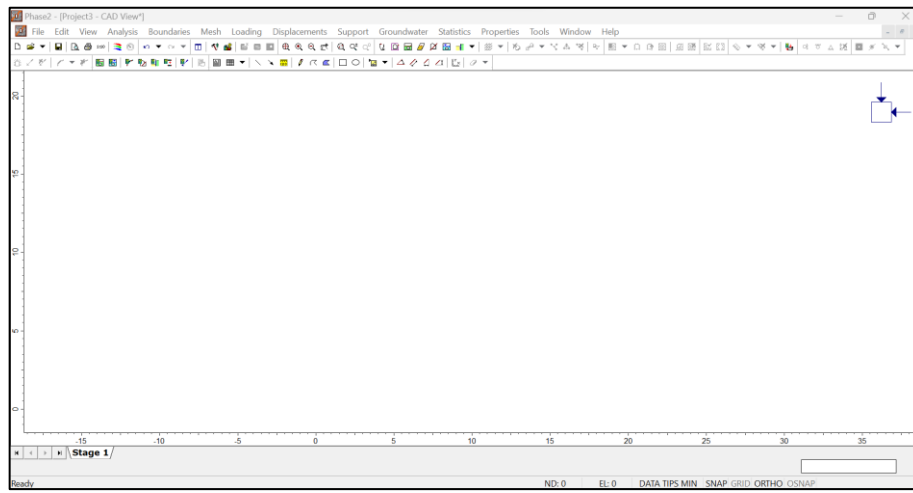


Figure 3.20: Starting a new project in RS2

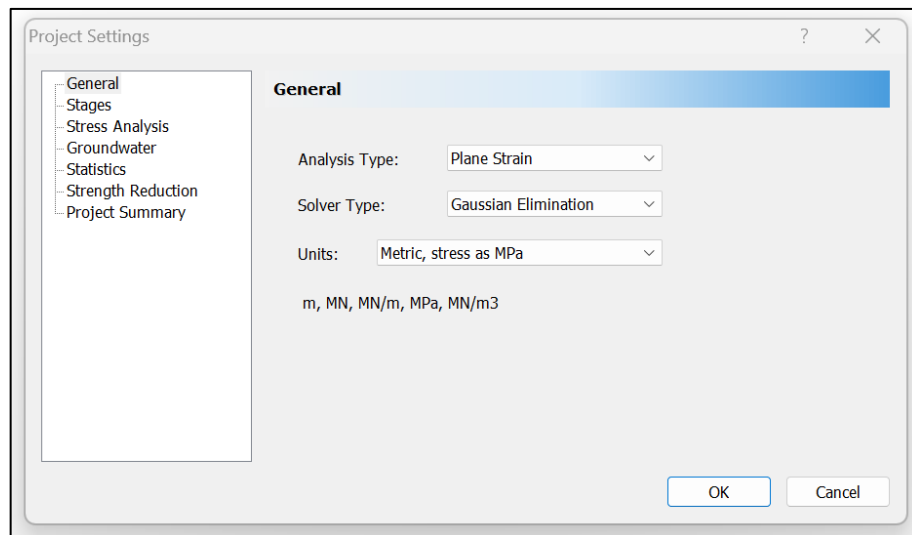


Figure 3.21: General project settings in RS2

The excavation and external boundaries were defined, simulating the tunnel geometry at the area of study for this thesis. To get the actual shape of the tunnel, firstly a line with X, Y coordinates (0,0; 10,0) was defined. Secondly

a three-point arch was drawn using the following coordinates (0,0; 5,7.5; 10,0). The number of segments on the arch were set to 100 (Figure 3.22). The middle point represents the height of the tunnel in the middle which is 7.5m. The external boundary was defined with an expansion factor of 3 (see Figure 3.22). The excavation and external boundary were defined as illustrated in Figure 3.23.

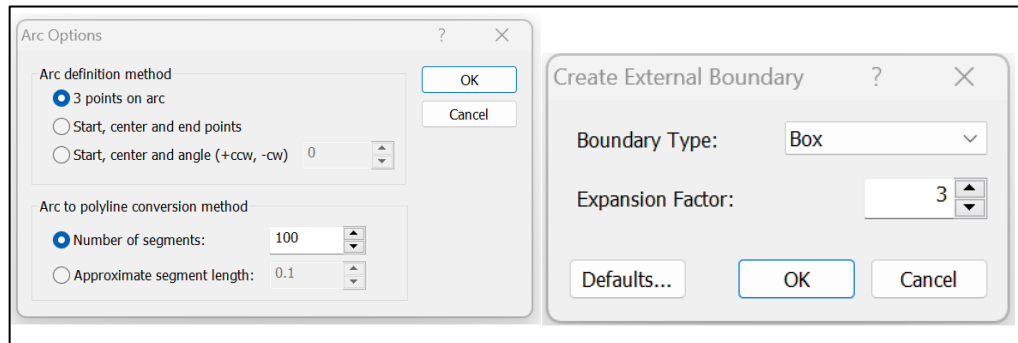


Figure 3.22: Defining the arch and external boundary

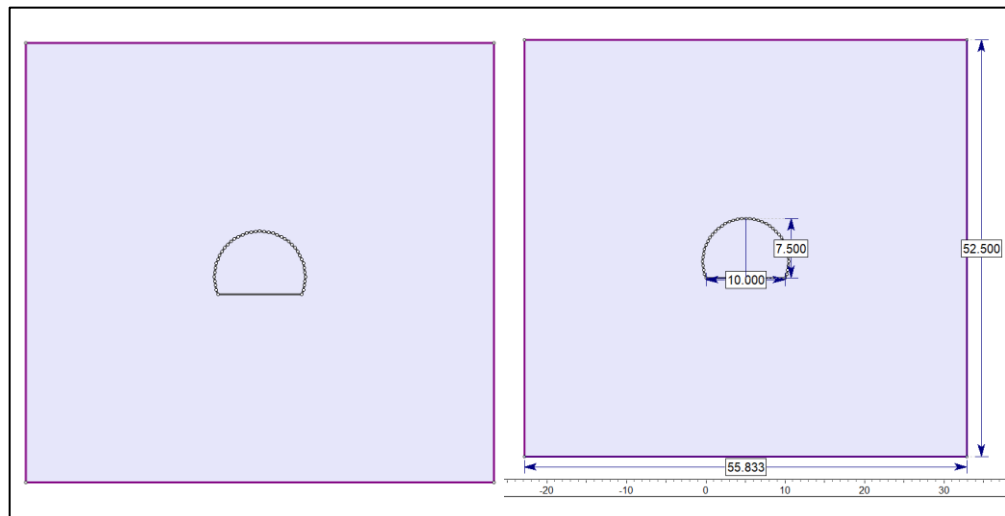


Figure 3.23: Excavation and external boundary defined.

Depending on the rock mass, joint properties can be defined in RS2. (See example in Figure 3.24). However, for this thesis, the different fracturing intensities were assigned for each zone. Thereafter, mesh set up was conducted where the mesh was defined by graded type mesh with 6 noded triangles at 0.1 grading factor. The mesh was then discretised (Figure 3.25).

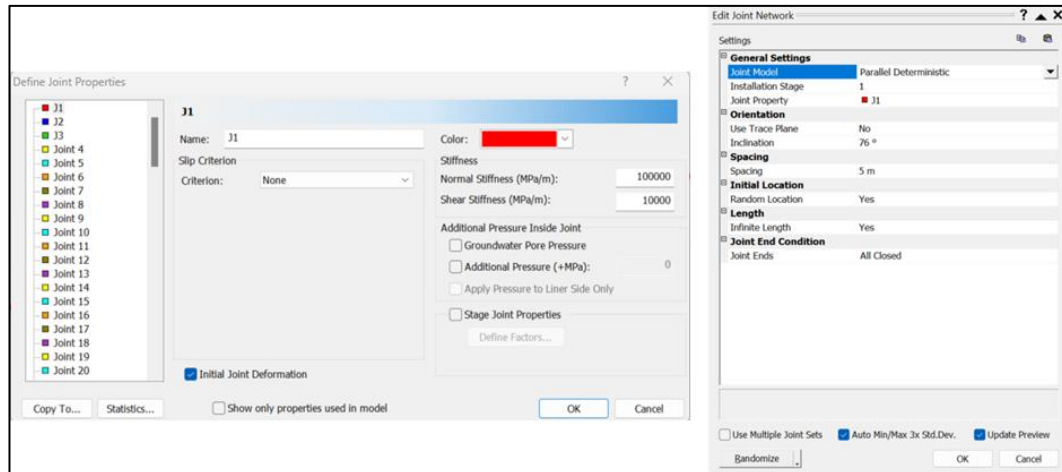


Figure 3.24: Illustration of how joint properties and joint network are defined in RS2

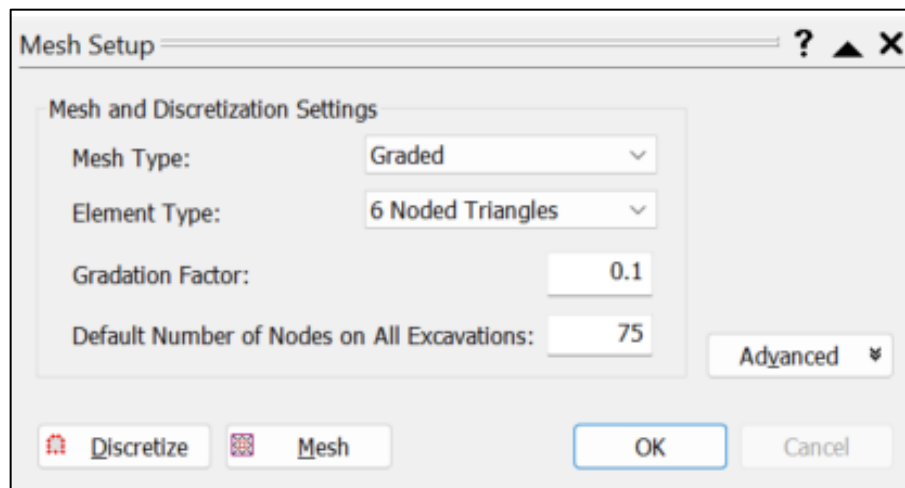


Figure 3.25: Mesh set up in RS2

Upon completing the mesh setup, the field stress properties were defined. Since the tunnel is in a shallow environment, the gravity field stress type was selected over constant field stress type which is applicable to deep mining environments to represent reality. At shallow depths, the K ratio (horizontal to vertical stress ratio) tends to be higher. However, in this study the site-specific effective k ratio was considered to be 0.5 as it considers the reduction in vertical stress near the ground surface (Figure 3.26). The effective stress ratio is defined as the ratio of the effective horizontal stress to the effective vertical stress. It considers the influence of pore water pressure and the stress distribution within the rock mass.

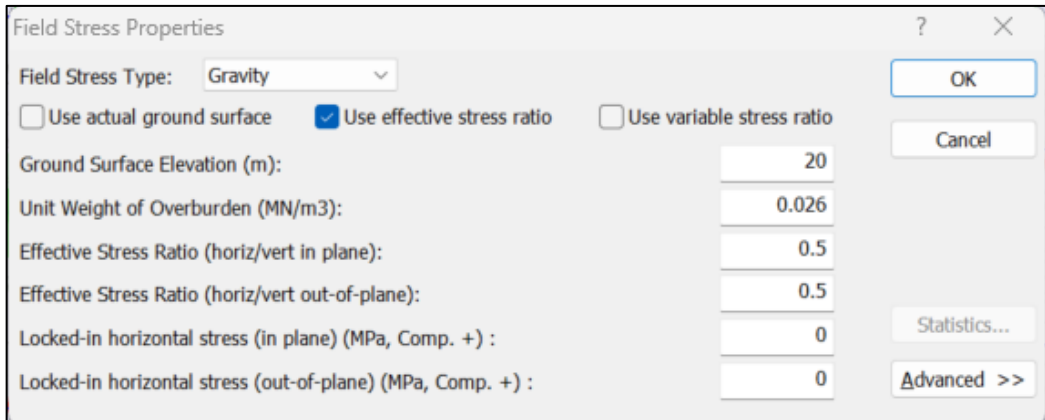


Figure 3.26: Field stress set up in RS2

The rock mass properties were defined based on the generalised Hoek-Brown failure criterion (Figure 3.27). This input data was estimated using RocLab as explained in the previous section. Finally, the simulation is computed to interpret the results. An example of computing in RS2 is illustrated in Figure 3.28.

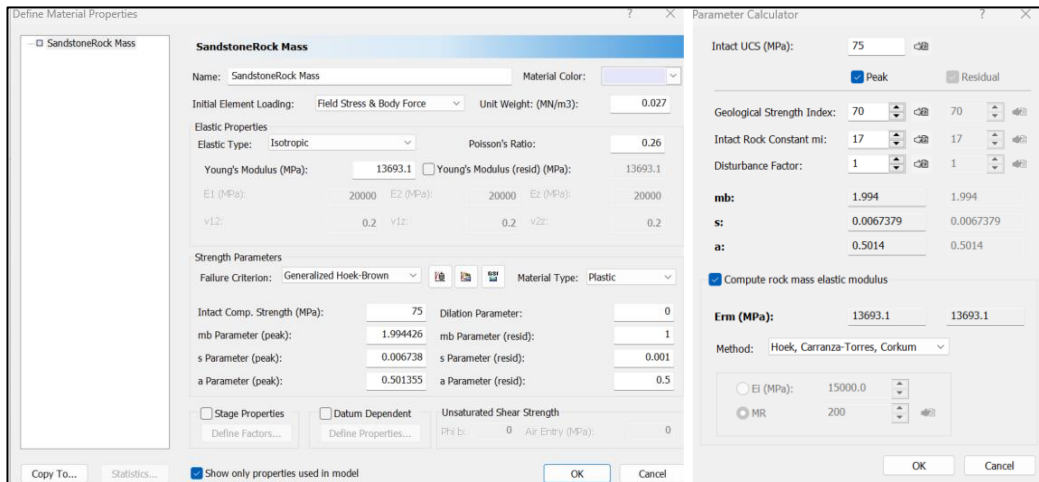


Figure 3.27: Defining rock mass properties in RS2

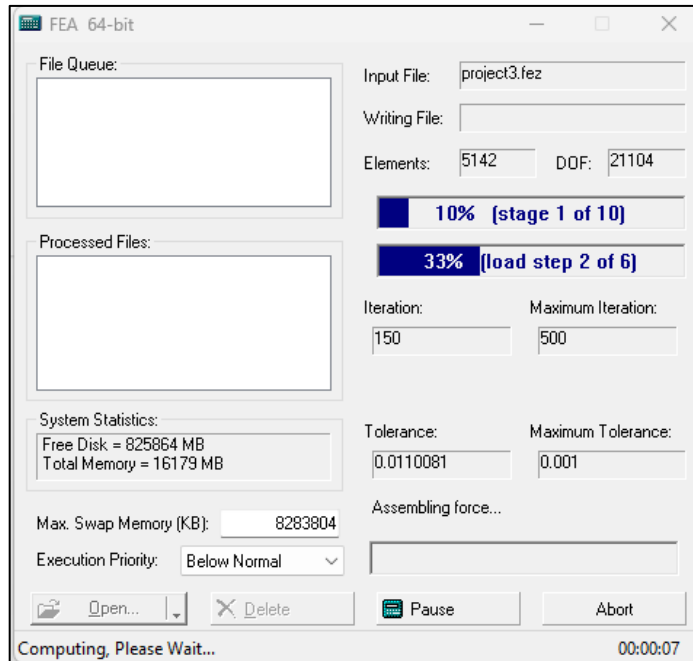


Figure 3.28: Example of computing in RS2

3.8. Limitations and challenges

It was initially intended to scan across the tunnel with Ground Penetrating Radar (GPR). Due to high purchasing as well as rental cost of the equipment, the experiment was not conducted. Instead, the initially intended experiment was supplemented with microscopic fracture analysis using geological techniques. Following that, it was anticipated that at least one core from the tunnel wall be obtained. This was later found to be logistically impossible; hence, a laboratory experiment was used to support the analysis.

Despite the laboratory work done, it was wished to use Particle Flow Code (PFC0 3D) for phenomenological simulations. Unfortunately, a version of the software package was not yet available with the functionalities. This may be a topic for future research as recommended in Chapter 7.

Plans were initially put in place with necessary municipal clearances for the collection of rock samples from both Tunnels One and Two. However, samples were later not collected from Tunnel Two for safety reasons.

Instead, mapping was conducted online using Google Maps for rock mass in the vicinity of Tunnel Two under restricted access. In general, Google Maps is a useful tool that offers reliable and accurate information for the majority of the needs of users. Nevertheless, it is essential to use critical judgment and double-check data when using the service. Google Maps can be supplemented with local information, official sources, and other map services to ensure the highest level of accuracy in particular situations.

Last, it was challenging to manually count the number of fractures considering that there are several categories of fractures to be identified from the thin sections. Moreover, from one sample, an average of 4 images are analysed. Hence, it is deemed important for researchers to explore image analysis in this area.

4. Chapter 4: Field Observations and Measurements

This chapter is devoted to the quantitative interpretation of the results stemming from the field observations and measurements presented in Section 3.2 of Chapter 3.

The chapter starts with a description of the observed rock mass and the conditions of the tunnel. The structural analysis and development of joint sets is then discussed. Intersection of discontinuities such as bedding planes and joints, form blocks of rocks with potential to fail (wedges) are identified next. Rock interlocking and resistance are decreased by falling rock blocks. In this chapter, structural controlled failure is covered. Possible failure modes such as wedge, planar, and toppling failure are explained. Finally, these modes of failure are analysed by means of stereographic projections.

4.1. Introduction

The quality of a rock mass is defined by several factors such as rock strength, the presence and characteristics of geological discontinuities: conditions of ground water, weathering and alteration. In rock engineering, discontinuity surveys are usually conducted on site to quantify the rock mass quality. Rock characteristics such as strength, deformability, and permeability are influenced by the presence of discontinuities within a rock mass (Chaminé et al., 2015).

Scanline technique (presented in Section 3.2.2) is one reliable mapping technique commonly used to acquire field data for the estimation of rock mass quality. In this technique, a straight line is drawn on the exposed rock mass as illustrated in Figure 3.6 (see Chapter 3) and all discontinuities intersecting the line are measured and described.

When an excavation is made in the rock mass, the stresses in the surrounding rock are redistributed until equilibrium is reached. Indeed, the

presence of geological discontinuities influence to some degree the stability of the excavation. The more geological discontinuities are present, the weaker the rock mass quality. Similarly, the behaviour of the rock mass is highly influenced by the rock properties and the level of disturbances present in that rock mass. When tunnels are excavated in a specific rock mass, its behaviour is therefore dependent upon numerous factors including rock properties, and discontinuities. It is therefore critical in this thesis to observe the discontinuities present in the rock mass and its influence on the tunnel stability. This is achieved through analysing the possible failure modes that can occur based on the quality of rock mass in the vicinity of the tunnels. The possible failure modes include wedge failure, planar failure and toppling failure.

4.2. Observations

The observations section of the thesis was based on the two Hendrik Verwoerd tunnels along the N1 road. In this regard, ground conditions and tunnel conditions were observed in both cases. Indeed, the focus was on the geological features and rock mass conditions at the vicinity of the tunnel. Furthermore, the condition of the tunnel from the tunnel faces and inside the tunnel were also considered. A detailed analysis of the observation data is documented in Section 4.2.1 and 4.2.2.

4.2.1. Observations on Tunnel One

The description of the observation results from Tunnel One is divided into two subsections. Visual observations were conducted inside and outside of the tunnel. Nonetheless, not many observations were conducted inside the tunnel due to lack of light and for safety reasons. The first subsection therefore provides detailed information regarding rock mass properties at the vicinity of the tunnel. The second subsection provides a description of the conditions of the tunnel.

4.2.1.1. Conditions of rock mass at the vicinity of Tunnel One

The conditions of the rock mass in the vicinity of tunnel one was observed. The rock mass is characterised by multiple joints, fractures, and bedding planes. These discontinuities resulted in very blocky rock mass conditions. Although a large part of the surrounding rock mass was blocky, the right side of the tunnel was core competent and intact as opposed to the left side of the tunnel (see Figure 4.1). Zooming to the left side, which was very blocky, it was observed that the very top part of the tunnel rock mass was supported with wire mesh (see Figure 4.2a). This is to minimise the topsoil and highly weathered rock from falling. A near vertical fracture was also observed with no infill material (see Figure 4.2b). When multiple discontinuities intersect, they have potential to form blocks of rock which may fall due to gravitational force. Likewise, evidence of rock falls was observed in the periphery of the tunnel on the left side. One block of rock dislodged from the top of the tunnel and fell on the net as shown in Figure 4.2(c). This block of rock could have fallen on one of the vehicles passing through the tunnel. Nonetheless, the tunnel is supported with a steel structure that has an aerial coverage in the form of a net or mesh, hence the rock was caught on the net. The second evidence of rock fall was observed on the floor (Figure 4.2d). Indeed, intersection of multiple discontinuities result in blocks of rocks with potential to fall and cause harm.

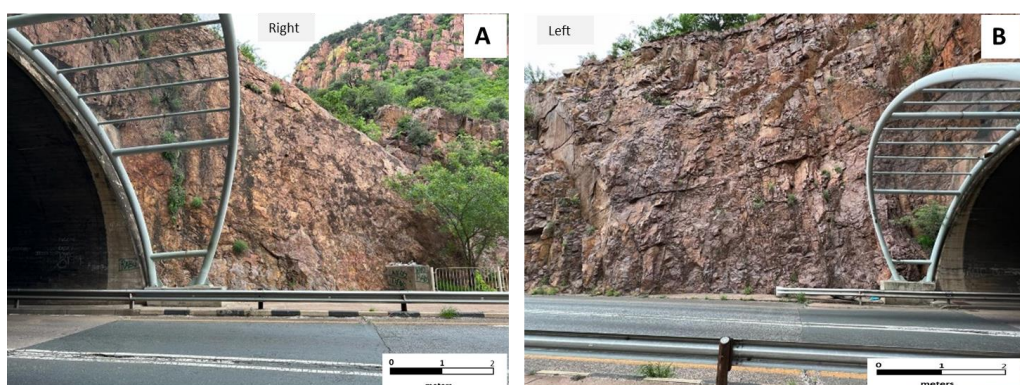


Figure 4.1: Rock mass conditions on the right side (A) and the left side (B) of Tunnel One



Figure 4.2: Rock mass conditions in the vicinity of Tunnel One: (a) Blocky weathered ground supported with wire mesh; (b) Fractured rock on the top of the tunnel; (c) Evidence of rock fall from the top of the tunnel; and (d) Evidence of rock fall on the left side of the tunnel

4.2.1.2. Observation of the conditions within Tunnel One

The tunnel is supported with concrete lining in the inside. Along the joining sections of the concrete lining, there is evidence of water seepage (see Figure 4.3). The water source is expected to be rainfall since the tunnel is located in a tropical climate zone. From the outside, the tunnel is supported with a steel structure that has an aerial coverage in the form of a net or mesh. Overall, Tunnel One was observed to be in a good condition.



Figure 4.3: Evidence of water seepage in Tunnel One

4.2.2. Observations on Tunnel Two

The description of observations on Tunnel Two is also divided into two subsections. The first subsection provides detailed information regarding rock mass observations at the vicinity of the tunnel. The second subsection provides description of the condition of the tunnel within or along the tunnel walls.

4.2.2.1. *Conditions of rock mass at the vicinity of Tunnel Two*

Visual observations were conducted on the rock mass in the vicinity of Tunnel Two. The rock mass observed consisted of multiple geological discontinuities intersecting to create very blocky ground conditions. These discontinuities include joints, parting planes and fractures. The blocky rock mass in the periphery of Tunnel Two was partially supported with rock bolts and wire mesh (Figure 4.4a). The identified discontinuities serve as a passage for water and organic material to penetrate. Hence there is evidence of vegetation along the rock mass (Figure 4.4b). The presence of water and continuously growing vegetation in the rock mass weakens the

rock shear strength along the discontinuities. Consequently, rock failure occurs. In Figure 4.4c, it can be seen that the discontinuities around the tunnel are closely spaced. This means that the potential blocks of rocks formed are very small. Numerous small blocks of rocks were identified caught up on the wire mesh on the top of the tunnel (Figure 4.4d). No large blocks were identified dislodged around the tunnel as it was the case with Tunnel One.

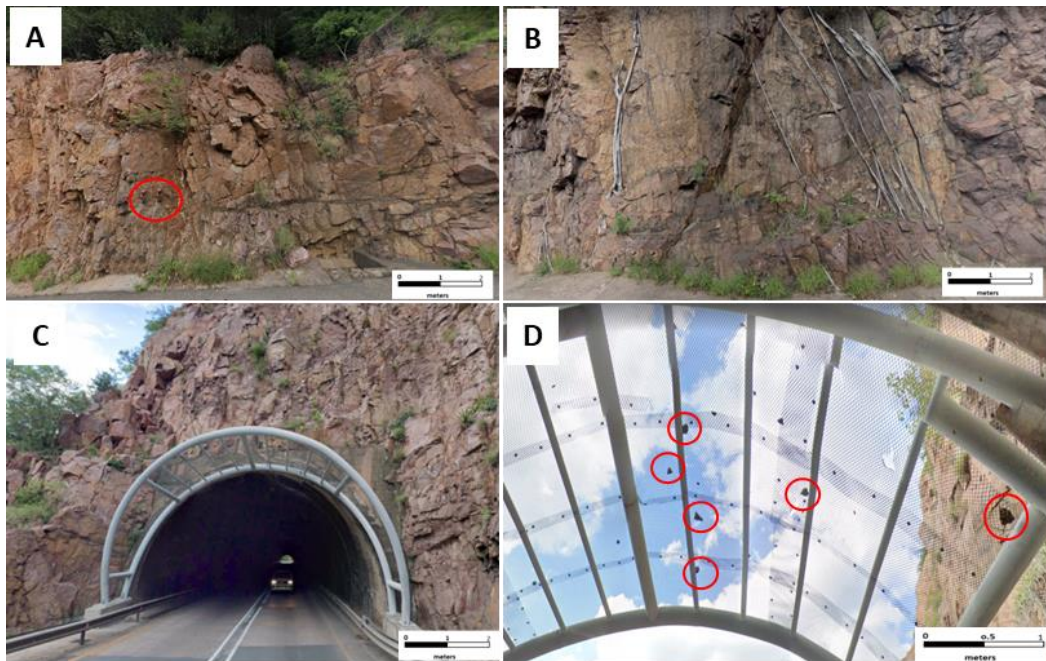


Figure 4.4: Rock Mass conditions in the vicinity of Tunnel Two. (a) blocky rock mass supported with rock bolts and wire mesh; (b) blocky side wall with evidence of vegetation; (c) blocky rock mass around the tunnel entrance; (d) evidence of rock falls

4.2.2.2. Observation of the conditions within Tunnel Two

Visual observations were conducted inside Tunnel Two. The tunnel is supported with concrete lining. Along the tunnel concrete lining joints, traces of water seepages were identified. This means that rainwater seeps through the rock mass discontinuities from the top of the tunnel (see Figure 4.5). Although the tunnel conditions were stable, the continuous water seepage can be a problem in a long run.



Figure 4.5: Evidence of water seepage in Tunnel Two

4.3. Field measurements and analysis

Field measurements were conducted on the rock mass in the periphery of the tunnels. The techniques followed during this exercise are detailed in Section 3.2. Scanline mapping technique was used to collect discontinuity survey data. Section 3.2.2 provides more detail on the technique.

In addition, the rock mass quality was quantified using one of the traditional methods known as the geological strength index (GSI). This method is explained in detail in Section 2.1.4. The ability of GSI to quantitatively describe the rock mass quality based on geological observations and fewer numerical values made it the preferred choice over Q-system, RMR, and MRMR. The latter three methods require more numerical values and rock samples for laboratory testing of UCS. Hence Q-system, RMR and MRMR were not considered.

Scanline mapping was conducted in the vicinity of the tunnel in order to acquire geotechnical parameters of the discontinuities. As already mentioned, the rock mass in the periphery of the tunnels is characterised by multiple joints, fractures and bedding planes. When these discontinuities intersect, they form blocks of rocks, hence the ground conditions are very blocky.

4.3.1. Rock mass rating using GSI for Tunnel One

Geological strength index observations were conducted on the left, right and top portions of the tunnel (Figure 4.6a). It can already be seen from the image that the three portions mentioned above do not necessarily possess the exact same geological disturbances. The frequency of geological discontinuities also varies. Rock mass on the top portion of the tunnel (Figure 4.6b) is characterised by joints and parting planes. These discontinuities resulted in blocky ground conditions with well interlocked undisturbed blocks. Moreover, the joint surface conditions are good due to rough and slightly weathered surfaces. As a result, the GSI value corresponding to these conditions is 70. Thus, the rock mass on the top portion of the tunnel can be classified as good based on Hoek (1994).



Figure 4.6: GSI rock mass rating on tunnel one: (a) tunnel one with all three sides visible, (b) Top portion of tunnel one, (c) right side of tunnel one, (d) left side of tunnel one.

The right side of the tunnel (Figure 4.6c) is characterised by minimal rock mass structures that are widely spaced, making the rock mass to be massive and intact. The joint surface conditions in this case were observed to be slightly un-weathered. These observations resulted in GSI value of 76. As a result, the rock mass on the right side can be classified as very good based on Hoek (1994). Zooming into the left side of the tunnel (Figure 4.6d) the rock mass is characterised by multiple jointing structures causing very blocky ground and interlocked partially disturbed rock mass. The joint surface conditions show that the rock mass is weathered, and the joint surfaces are altered. In accordance with the chart by Stacey (2001) shown in Chapter 2, Figure 2.2, the GSI value of the left side of the tunnel is 65. Overall, the rock mass around tunnel one is blocky but interlocked. Therefore, the average GSI value for this rock mass is 70.

4.3.2. Rock mass rating using GSI for Tunnel Two

Geological strength index observations were also conducted on the left, top and right portions of Tunnel Two.

As can be seen in Figure 4.7a, the rock mass is characterised by multiple jointing causing very blocky ground conditions. The left portion of the tunnel is very blocky and consist of interlocked partially disturbed blocks of rocks. The joint surface quality on the left side of the tunnel is influenced by rough slightly unweathered surfaces (Figure 4.7b). According to Stacey (2001), the rockmass on the left side of tunnel two is classified as good and the corresponding GSI value is 65. Jointing is persistent also on the top portion of the tunnel (Figure 4.7c). The top portion is characterised by partially interlocked rock pieces. Therefore, the GSI value of the top part of the tunnel corresponding to the chart (Figure 2.2 in Chapter 2) is 68. Lastly, the right side is also very blocky, and the rock pieces are partially interlocked (Figure 4.7d). The behaviour of the right side is similar to the top portion. Therefore, the rockmass on the left side of tunnel two is very blocky with corresponding GSI value equal to 68. Overall, the rock mass in the periphery of tunnel

two can be classified as good, with corresponding average GSI value of 67 based on Hoek (1994).



Figure 4.7: GSI rock mass rating on Tunnel Two: (a) tunnel one with all three sides visible, (b) left side of tunnel two, (c) top portion of tunnel two, (d) right side of tunnel two.

To sum up the rock mass conditions in the periphery of the tunnels. It can be concluded that for Tunnel One, the right side is less disturbed by geological discontinuities as opposed to the left side and the top portion. In contrast, the left side is more disturbed and very blocky as opposed to the top and right portions of tunnel two. To further comprehend the rock mass behaviour around the tunnel, it was considered critical to look at the effects of micro-fracturing and mineralogy on the rock strength. Micro-fracturing is discussed at length in Chapter 5. Nonetheless, rock mass properties were estimated based on the observations as presented in the next sub-section.

4.3.3. Rock mass properties estimation for Tunnel One

Rock mass properties for Tunnel One slope were estimated using RocLab software. The field observations were conducted on a sandstone rock mass which is blocky but well intact.

One can argue that the blocky ground conditions are due to partial metamorphism on the exposed rock mass. Therefore, the intact uniaxial compressive strength was estimated to be 75MPa. The field observation gave an insight of the geological strength index which in this case was estimated to be 70 (see Figure 4.8 and refer to Figure 2.3 in Section 2.1.4 of Chapter 2).

Sandstone has constant value m_i ranging between 4-17. Therefore, for tunnel one slope, the m_i value was estimated to be 17. The disturbance factor was estimated for the slope in the periphery of Tunnel One. Based on the field observations, one can argue that there was poor blasting during the construction of the tunnel. As a result, the disturbance factor in the periphery of tunnel 1 was estimated to be 1. The rock mass properties for slope in the periphery of Tunnel One is given in Table 4.1.

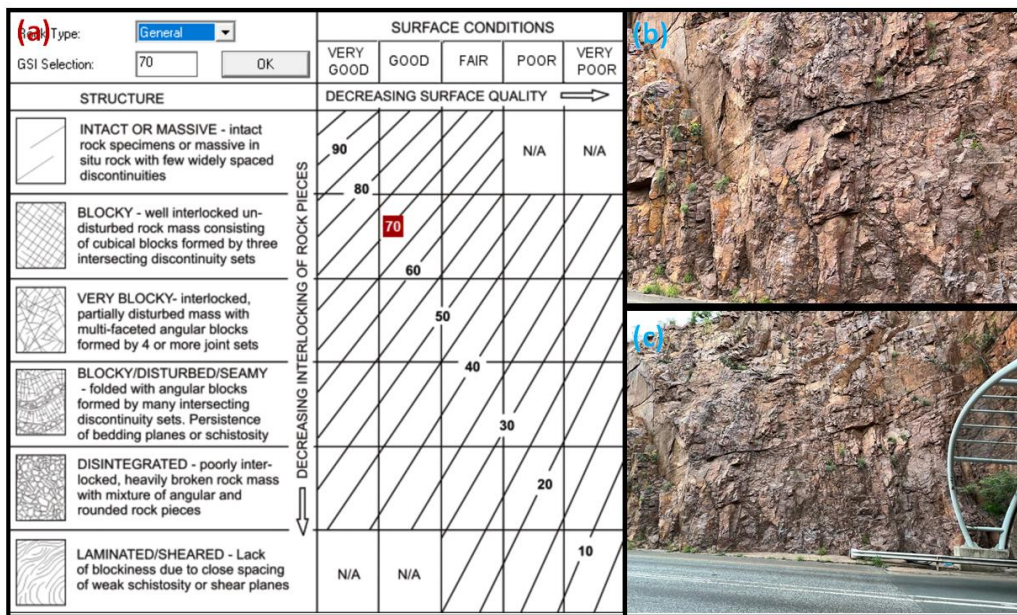


Figure 4.8: GSI estimation for the rock mass slope of Tunnel One

To summarise the estimated rock mass properties, the rock mass slope of Tunnel One has a uniaxial compressive strength of 6.11 MPa, a global strength of 14.7 MPa and the tensile strength is -0.25 MPa. The modulus of deformation is 13.69 GPa while the cohesion and friction angle based on Mohr-Coulomb fit were found to be 0.75 MPa and 60.5° respectively.

Table 4.1: Rock mass properties estimation for Tunnel One through the means of RocLab

Hoek-Brown classification		
δ_{ci}	75	MPa
GSI	70	
m_i	17	
D	1	
Hoek-Brown criterion		
m_b	1.99443	
s	0.00673795	
a	0.501355	
Failure envelope range		
Application	Slopes	
δ_{3max}	0.269187	MPa
γ	0.026	MN/m ³
Slope Height	10	m
Mohr-Coulomb fit		
c	0.755469	MPa
ϕ	60.5458	degrees
Rock mass parameters		
δ_t	-0.253379	MPa
UCS	6.1148	MPa
δ_{cm}	14.7143	MPa
E	13693.1	MPa

Simulation was conducted using the estimated rock properties to evaluate the effects of principal stresses, and shearing stress against minor stress on the slope. The results of the simulation are shown in Figure 4.9 and Figure 4.10 respectively. In Figure 4.9 the relationship between minor and major principal stresses is illustrated whereas Figure 4.10 shows the relationship between shearing stress and normal stress.

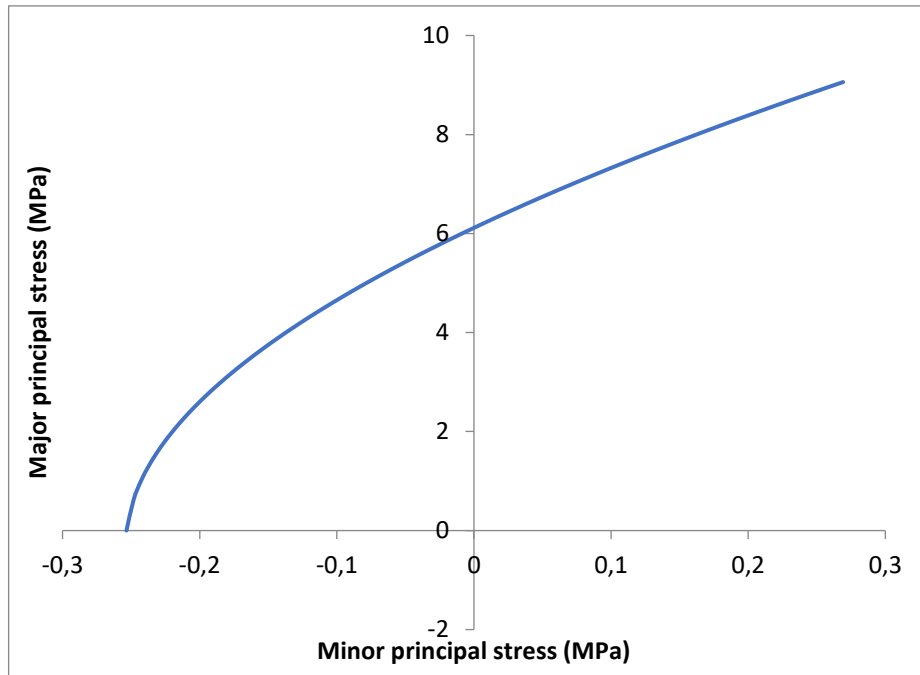


Figure 4.9: Principal stresses for the Tunnel One slope

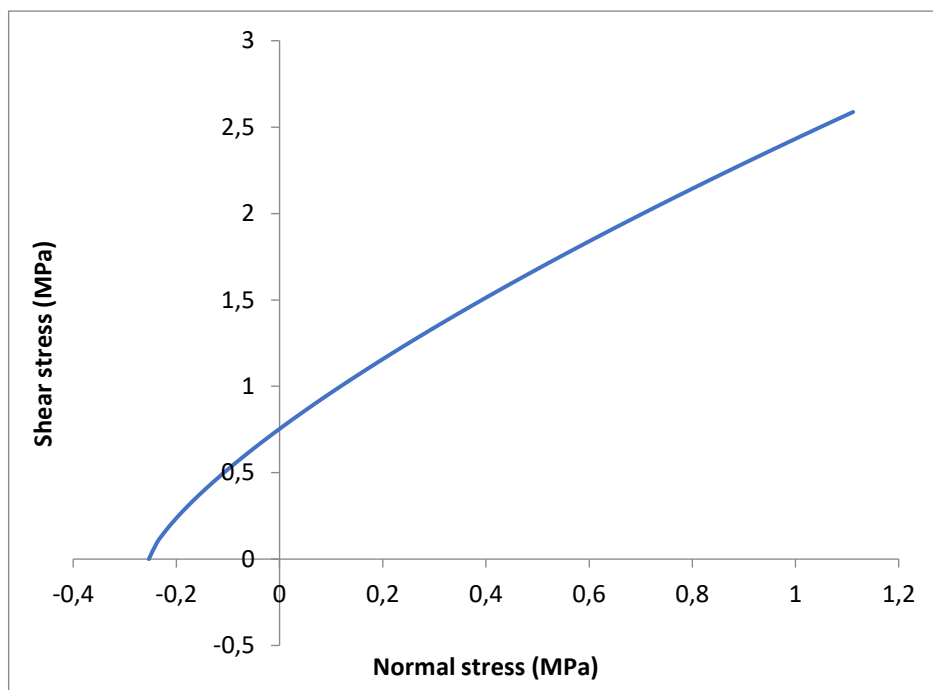


Figure 4.10: Normal stress vs shear stress for Tunnel One

4.3.4. Rock mass properties estimation for Tunnel Two

The rock mass properties for Tunnel Two were also estimated using RocData. A similar approach followed to estimate rock mass properties for

tunnel one was also applied here. Tunnel Two was also excavated in the same rock type (sandstone). However, the rock mass conditions in this area are intact but very blocky as opposed to rock mass in the periphery of tunnel one. Thus, intact uniaxial compressive strength and geological strength index were estimated to be 75MPa and 67 respectively (see Figure 4.11). Similarly, m_i value for sandstone ranges between 4-17. Therefore, m_i value was also estimated to be 17 for Tunnel Two. The slope in the periphery of tunnel two is a result of poor blasting, hence the disturbance factor of 1. The estimated rock mass properties for this slope are presented in Table 4.2.

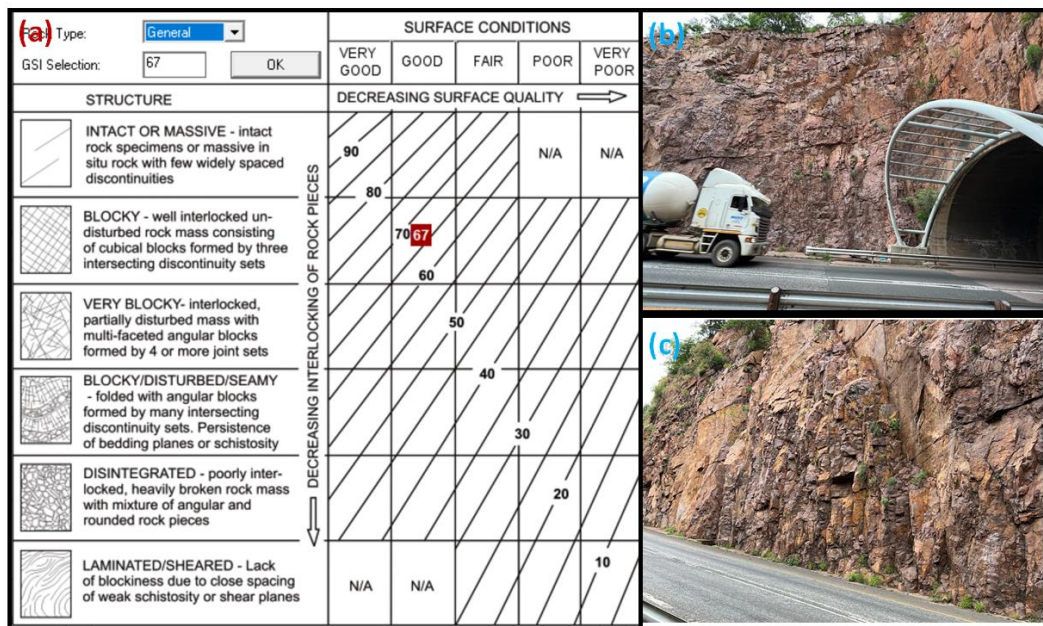


Figure 4.11: GSI estimation for tunnel two rock mass slope

Table 4.2: Rock Mass properties estimation for Tunnel Two through the means of RocLab

Hoek-Brown classification		
δ_{ci}	75	MPa
GSI	67	
m_i	17	
D	1	
Hoek-Brown criterion		
m_b	1.60974	

s	0.004087	
a	0.501702	
Failure envelope range		
Application	Slopes	
δ_{3max}	0.266296	MPa
γ	0.026	MN/m ³
Slope Height	10	m
Mohr-Coulomb fit		
c	0.591622	MPa
ϕ	59.9973	degrees
Rock mass parameters		
δ_t	-0.19041	MPa
UCS	4.74991	MPa
δ_{cm}	13.0505	MPa
E	11521.3	MPa

Rock mass properties estimation for tunnel two show that the uniaxial compressive strength, global strength, and tensile strength are 4.75MPa, 13.05MPa, and -0.19MPa respectively. These values are not far off from the estimated values for tunnel one. Likewise, Mohr-Coulomb fit showed that the friction angle and cohesion for this slope are 0.59MPa and 60° respectively. This is a validation that the tunnels were indeed excavated in the same rock mass using the same excavation process.

The estimated rock mass properties were also used to simulate the relationship between normal and shear stress together with minor and principal stresses. The simulation results are given in Figure 4.12 and Figure 4.13.

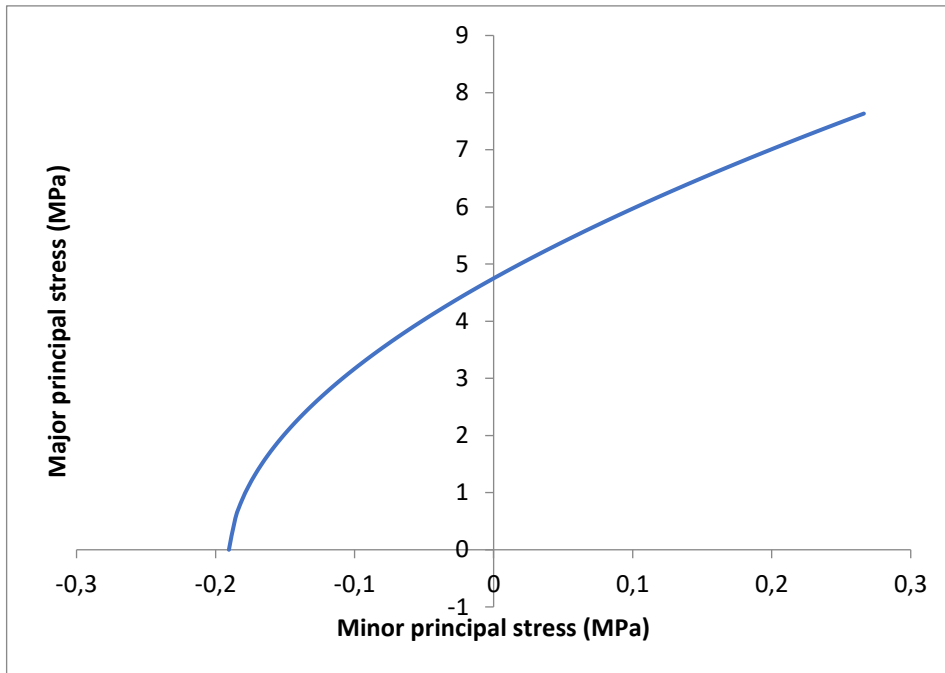


Figure 4.12: Principal stresses for the Tunnel Two slope

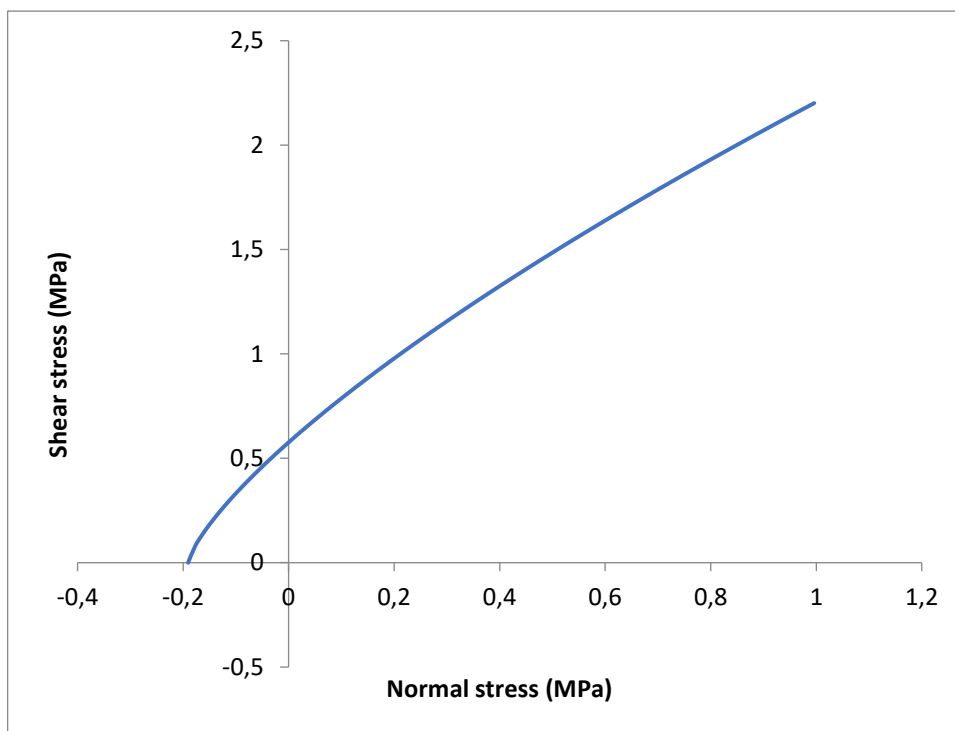


Figure 4.13: Normal stress vs shear stress for Tunnel Two

In conclusion, rock mass properties are critical for detailed kinematic analysis purposes. The analysis of possible failure modes depends on the specific rock properties of the particular rock slope. Furthermore, rock mass

properties are essential for use as input data in simulation programmes for further analysis to be carried out for this study.

4.4. Structural analysis and development of joint sets

Rock slopes occur naturally or because of engineering activities such as development of roads, buildings, dams, and mines. These slopes need to be stabilised as per the specific project requirements. For this thesis, the rock slopes of interest were created as a result of engineering project (tunnelling). This section discusses the structural analysis and the development of joint sets along the rock mass in the vicinity of the tunnels. This exercise paves way to identifying the possible modes of failure that can be expected in the rock mass and consequently the possible stabilising mechanisms.

The presence of geological discontinuities within a rock mass may lead to structurally controlled instability. Scanline mapping was conducted in the vicinity of tunnel one and tunnel two (Figure 4.14).

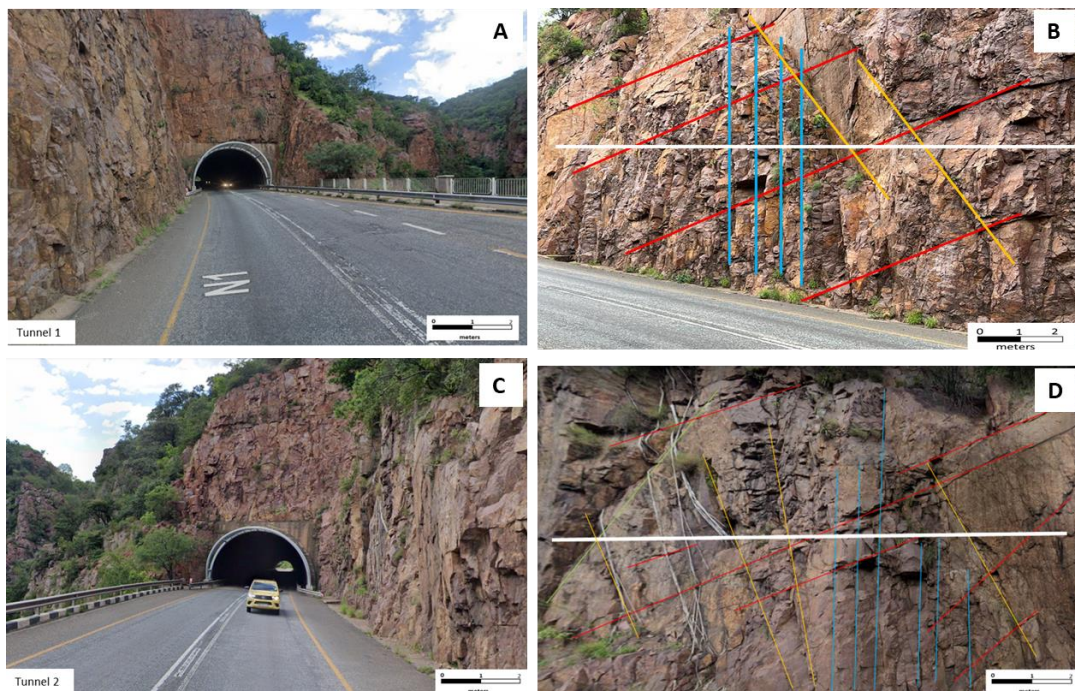


Figure 4.14: Scanline mapping in the vicinity of the tunnels

4.4.1. Developing joint sets of the tunnels

The dominant sets obtained from the scan line mapping exercise are available as raw data in APPENDIX A. To create sets on DIPS, the collected data was examined using the Fisher concentration method available within the software. As explained in section 3.5.2 (Chapter 3), DIPS is a geotechnical software used for statistical analysis of orientation data. The analysis in Dips software can be categorised into three categories: namely, kinematic analysis, rosette plots, and three-dimensional stereo-sphere. The 3D stereo-sphere allows the user to plot poles, planes and contours in three-dimensional hemisphere view. Kinematic analysis in DIPS is used to plot the dip and dip directions of the slope and discontinuities based on field data. This allows the user to determine the mode of failure of which the slope is susceptible to. The modes of failure include planar, wedge, and toppling failure modes. Rosettes are used to view the strike density and frequency of measured data.

Structurally controlled instability in a rock mass may be a result of jointing, bedding planes, faults and other geological discontinuities. The manner in which these structures interact may cause blocks of rock to either slide or fall, depending on the orientation of both the slope and the discontinuities. To assess the likelihood of such failures, kinematics analysis is used.

Tunnels developed in highly jointed rock mass in shallow depths are more likely to experience rock falls. This is because when multiple joints intersect, they form blocks of rocks which can fall or slide from the roof or the side walls depending on where the wedge is created. Measures must be taken to support these wedges to prevent instability of the excavation.

4.4.2. Kinematic failure analysis

The kinematic analysis function in DIPS is one of the commonly used techniques to perform kinematic analysis for slope stability. In this section, DIPS was used to perform kinematic analysis of joints using orientation data collected from the field to determine if the slope is susceptible to failure

modes such as planar failure, wedge failure and toppling failure. During the construction of the stereonet, the input data collected in the field was exported from excel to a DIPS file format. Three sets were generated as shown in Table 4.3.

Table 4.3: Joint sets developed based on mapping data

	Set	Dip	Dip direction
1	Set (weighted)	14°	246°
2	Set (weighted)	71°	328°
3	Set (weighted)	74°	90°

The sets developed based on mapping data are further interpreted in Figure 4.15 and Figure 4.16 which shows the pole plots of mapped discontinuities and contour plots of mapped discontinuities respectively. The plots in Figure 4.17 indicate mean discontinuity planes and face planes. These stereographic techniques can be used as input to deterministic or probabilistic limit equilibrium calculations to determine a safety factor or probability of failure for potential blocks or wedges.

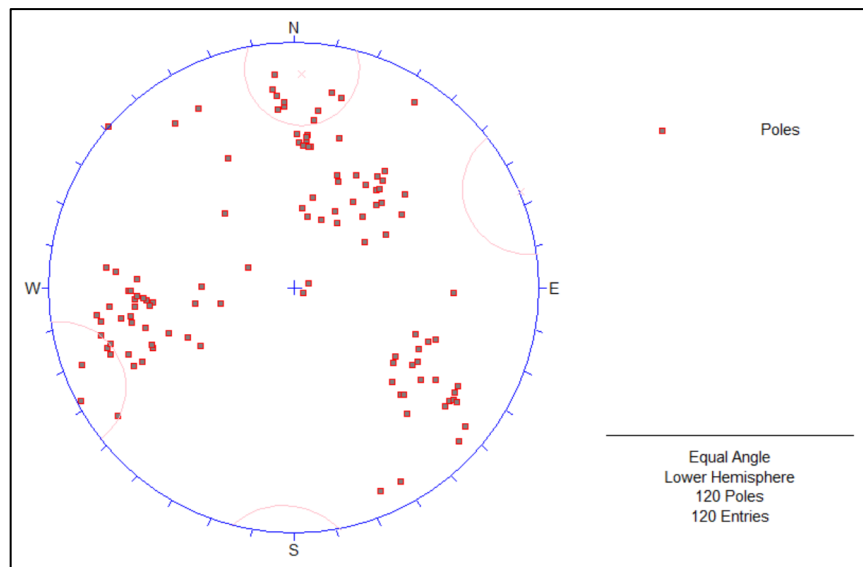


Figure 4.15: Pole plots of mapped discontinuities

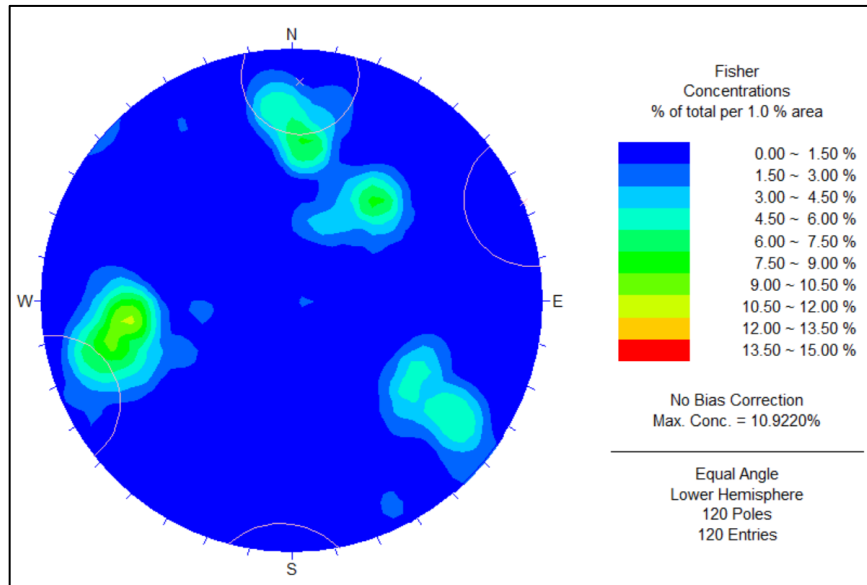


Figure 4.16: Contour plots of mapped discontinuities

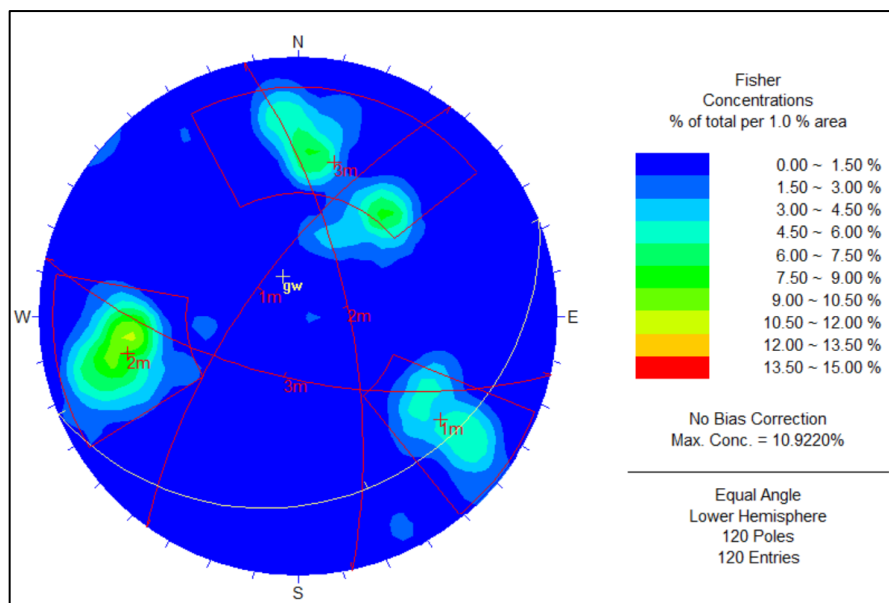


Figure 4.17: Contour plot with mean discontinuity planes and face planes

The resulting plots of the study area are presented in the next subsections alongside their analysis and discussion. The main aim behind setting up the kinematic stereonet was to analyse the modes of failure on the rock slope and some of its physical attributes.

Results from kinematic analysis show that there are several modes of failure expected in the rock slope around the periphery of the tunnels. These

include planar failure, toppling failure, and wedge failure. These failure modes are discussed next.

4.4.2.1. Planar analysis

Planar failure in rock slopes occurs when four main geometric conditions are met according to Wyllie and Mah (2004). These conditions are:

- The plane on which sliding takes place must strike parallel to the slope face (i.e., within approximately $\pm 20^\circ$)
- The sliding plane must daylight in the slope face (i.e., the plane dip angle must be less than the slope dip angle)
- The plane dip angle must be greater than the friction angle of the slope.
- The sliding surface top-end must intersect the top end of the slope or terminate in a tension crack.

The regions delineated in Figure 4.18 indicate poles prone to planar failure. Poles in set 3 are at risk of planar failure. These poles meet the four criteria mentioned above; hence, planar failure may be expected in this area.

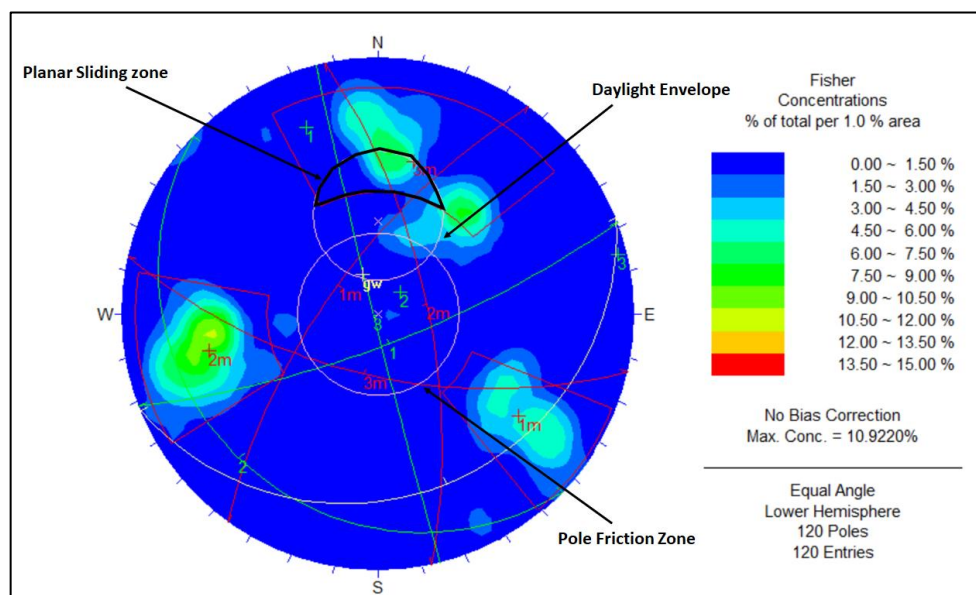


Figure 4.18: Planar failure analysis using DIPS.

4.4.2.2. Toppling Analysis

It takes a combination of various mechanisms which occur over time for toppling failure to occur in rock slopes. Toppling failure depends on the occurrence of steeply dipping continuous joint sets striking parallel to the slope face. Generally, for continuous joint sets dipping at 60-95 degrees, toppling failure can be anticipated.

Kinematic results showed that the rock slope in the area of study is susceptible to toppling failure. In this area, multiple steeply dipping joint set were identified. The toppling region is denoted in Figure 4.19. This means that the poles identified within this region are at risk of toppling failure (i.e., poles for set 1).

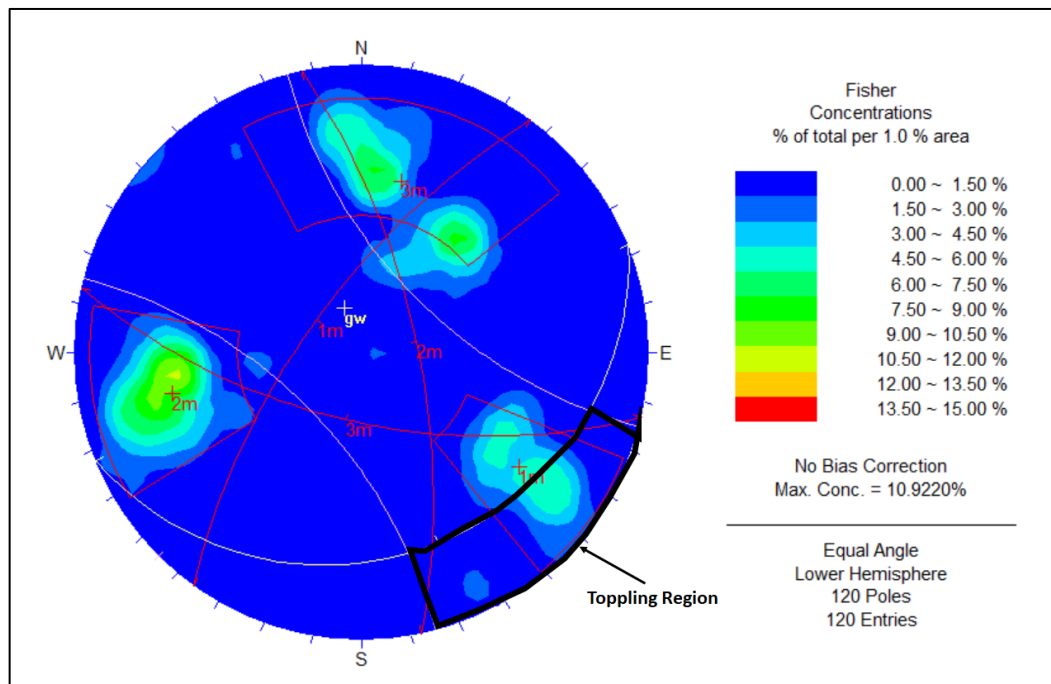


Figure 4.19: Toppling failure analysis using DIPS.

4.4.2.3. Wedge Analysis

For wedge failure to occur, certain geometric conditions must be met. These include the intersection of two planes, the line of intersection dipping in a direction out of the slope face for sliding to occur, the dip of the line of

intersection must be smaller than the dip of the slope face, and the dip of the line of intersection must be within the wedge sliding zone (friction circle).

When using stereonet, wedges can be identified at the point of intersection of planes. In Figure 4.20 the points of intersection of sets are indicated with black dots. Therefore, a potential unstable wedge is formed at the point of intersection of the three major sets (i.e., sets 1 and 2; sets 1 and 3; and sets 2 and 3). One may argue that the wedges formed in the study area are big. This is indeed supported by results from visual observations conducted at the study area as documented in the previous sections of this chapter. Furthermore, the zone of wedge sliding is represented by the enclosed friction cone in Figure 4.20.

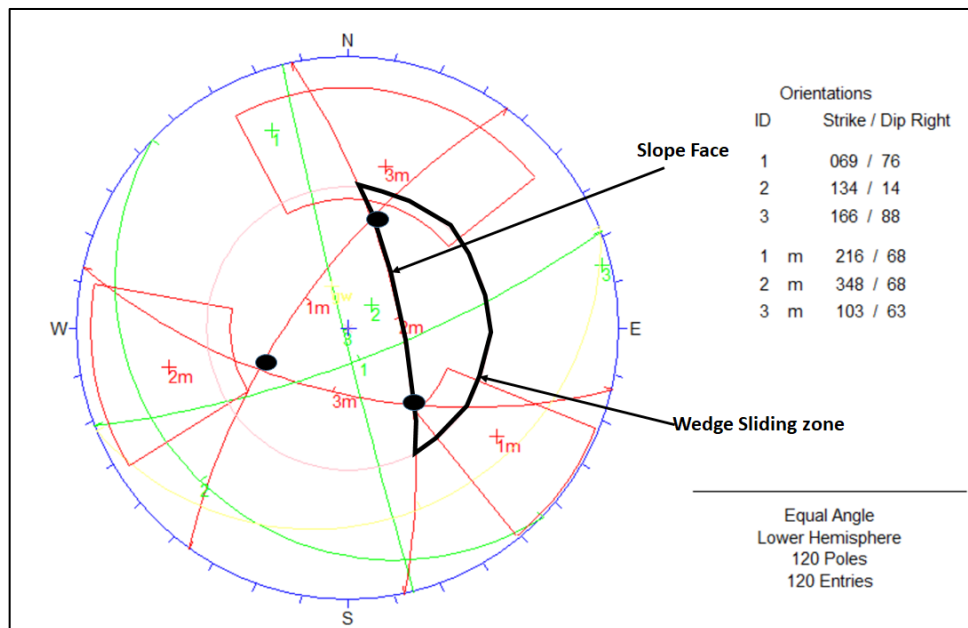


Figure 4.20: Wedge failure analysis using DIPS

Overall, the kinematic analysis exercise indeed shows that the area of study is susceptible to various modes of failure depending on the orientation of the joints and the slope. The failure modes identified include, planar, wedge, and toppling failure.

4.5. Establishing the rock mass failure models

The modes of rock slope failure depend on the geometric interaction of the discontinuities present in the rock mass. For example, the presence of joints, fractures and bedding planes. The four most common rock slope failure modes are wedge failure, planar failure, toppling failure and circular failure. For the purpose of this thesis, only the three modes of failure (toppling, wedge, and planar failure) are discussed. Circular failure is excluded since it is more suitable for soft soils. This is because the scope of this thesis is limited to shallow hard rock mining environment where such failure mode is not prevalent (Wyllie and Mah, 2004; Kolapo et al., 2022). That is the reason why the subsections below only deal with toppling, wedge, and planar failure modes.

4.5.1. Toppling Analysis

Toppling failure involves the rotation of columns or of rock along an existing sliding surface at the base of a slope. The columns or blocks of rocks rotate along the slope toe and overturn (topple). This mode of failure is more significant on mountain slopes and open pit mines. The blocks and columns of rocks that fail in a toppling manner are created through several factors. These include erosion, weathering and changes in force that act on the rock.

A schematic representation of toppling failure is illustrated in Figure 4.21. Prior to failure, the blocks and columns of rock are compact and intact (Figure 4.21a). With time exposed rock surface is weathered and eroded; thus, it begins to be weak (see Figure 4.21b). When the fixed blocks begin to move, the tallest columns of blocks topple, and slight bending takes place (Figure 4.21c). This is driven by the centre of gravity. The gaps between the columns of rocks increases with time, and the tension cracks become wider at the top and decreases towards the toe of the slope as shown in Figure 4.21d (Cundall, 1971).

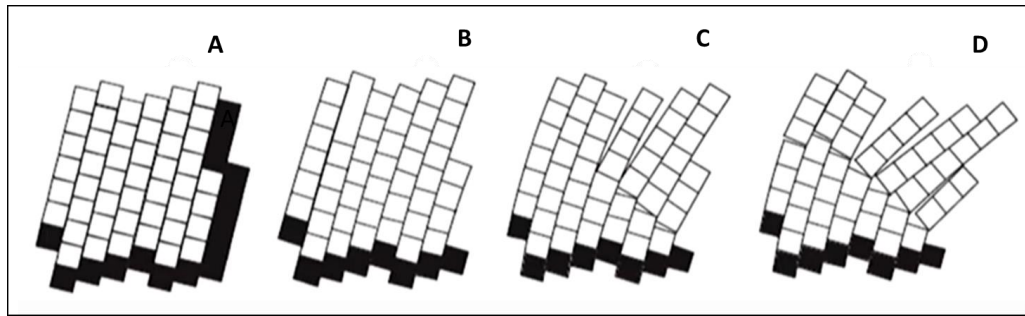


Figure 4.21: Schematic illustration of toppling failure (Cundall, 1971)

Field identification of toppling failure is observed looking along the strike direction. The bending and rotating columns and blocks of rocks (topples) are easily identified in the field when observing from the strike direction (Wyllie and Mah, 2004). This approach was also used to identify along the periphery of the tunnel where toppling failure is most expected.

Prior to toppling failure analysis, it is critical to understand the type of toppling because there are two methods of toppling failure analysis. The two types of toppling are block toppling and flexural toppling. Block toppling occurs in strong rock where individual columns are created by a set of steeply dipping discontinuities (dipping into the face). The column height in this case is defined by the second set of orthogonal discontinuities (joints) that are widely spaced. In flexural toppling, continuous columns of rocks are separated by well-developed steeply dipping discontinuities (joints). The discontinuities break in flexure as they bend forward. In this case, orthogonal joints are not present as it was the case with block toppling (Wyllie and Mah, 2004).

4.5.2. Wedge analysis (for single and multi-tetrahedral wedges)

A wedge is formed in-between two planes of discontinuities. Wedge failure involves sliding of a block of rock along the intersection line of two planar discontinuities. Wedge failure is the most observed kind of failure in most blocky ground conditions in surface and underground mining environments. This is mainly because the geological conditions that yield this type of failure are mostly common in most mining environments. For example, multiple

jointing, parting planes and faults are prominent in shallow hard rock mining environments. Wedge failure is similar to planar failure. However, in wedge failure, two or more planes of discontinuities within a rock mass must intersect.

A typical example of a wedge failure simulated in Swedge software is shown in Figure 4.22. In this Swedge example, the two planes intersecting daylight at the toe of the slope and the top of the slope forms a tension crack. Take note that the factor of safety of this wedge is 0.358 because the expected wedge is very small.

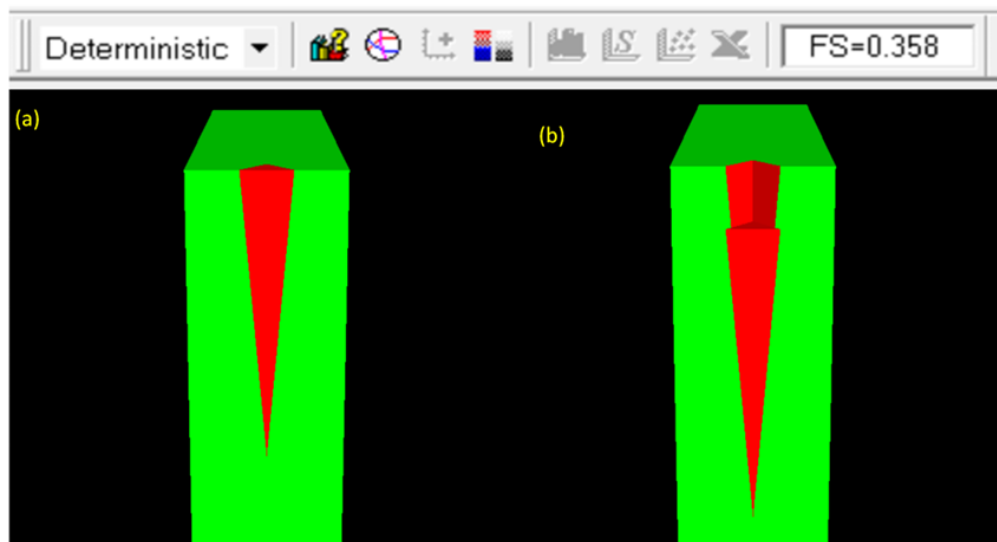


Figure 4.22: Wedge failure using deterministic analysis using Swedge

Wedge failure can also result from two or more joints intersecting where the dip angle of one joint is more than the friction angle of the slope surface and one of the joints intersect the slope plane (Wyllie and Mah, 2004). Observations were conducted in the vicinity of the tunnels to identify where wedge failure is more likely to occur.

4.5.3. Planar failure

Planar failure is more common in sedimentary rocks (Raghuvanshi, 2017). Plane failure is similar to wedge failure. However, in plane failure there is only one plane as opposed to two or more in wedge failure (Wyllie and Mah,

2004). In plane failure, the block of rock slides along a single plane. This plane may be a bedding plane, striking parallel to the face or dipping onto the face.

In Figure 4.23 and Figure 4.24, the rock slope in the periphery of the tunnel is simulated. The identified bedding plane has a factor of safety equal to 8.948, meaning the slope is stable. According to Hoek and Bray (1981), plane failure is rare to occur in a rock mass consisting of multiple discontinuities. This is because the geometrical conditions for plane failure to occur indicate that there is only one plane along which failure will occur.

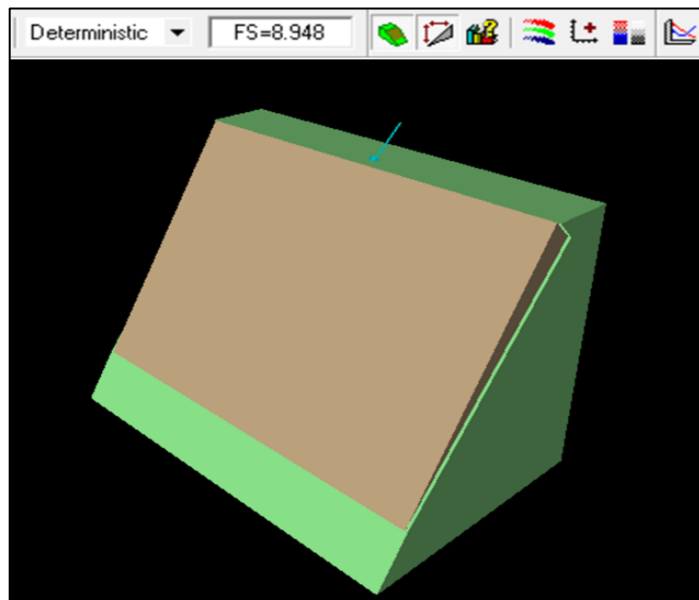


Figure 4.23: Simulated representation of plane failure using deterministic analysis.

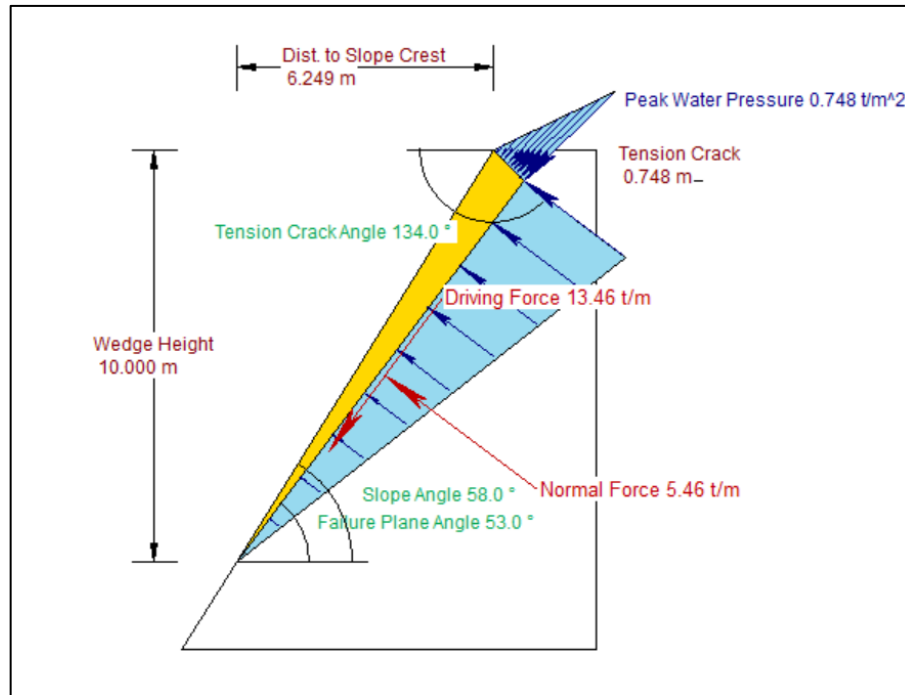


Figure 4.24: Simulation of planar failure on the rock slope in the periphery of the tunnels

4.6. Conclusion

In conclusion, this chapter discussed the observations and measurements conducted at the site. The rock mass and condition of the tunnel were described in detail.

The rock mass in the vicinity of the tunnels was found to be characterised by multiple joints and bedding planes, creating blocky ground conditions. Structurally controlled instability in tunnels and slope instability were also identified and explained in this chapter.

Finally, three common structurally controlled modes of failure were identified as plausible around the tunnels. These are the wedge, plane, and toppling failure modes. The three failure modes were then discussed using computer analysis tools. Stereographic projections were created to show that the three modes of failure are plausible for the rock mass around the tunnels.

Overall, the field measurements and observations made in this chapter aided the researcher in estimating the rock mass properties on RocLab. In Chapters 5 and 6, the estimated rock mass properties are used for numerical simulations.

5. Chapter 5: Developing an Empirical Chart for Fracturing Distribution in Shallow Tunnels

This chapter discusses the results from the laboratory experiments on thin sections presented in Section 3.3 of Chapter 3. The results are presented in the form of images showing the microfractures identified in the rock mass along the tunnel. These fractures are then analysed and used to develop an empirical fracture distribution chart. The chart is specifically intended for use in shallow hard rock mining environments.

5.1. Introduction

In order to understand the influence of micro-fracturing on rock strength, it is critical to first understand the possible fracturing mechanisms available in a rock. The mechanism of rock fracture is such that the stress in a rock exceeds its strength. Similarly, microfractures or cracks follow the same principle.

Microfractures are small and cannot be seen with a naked eye. They are only visible under a microscopic lens. Microcracks are said to initiate when the stress within the local rock exceeds the strength therein (Nur and Simmons, 1970). When the minimum principal stress exceeds the elastic tensile strength in a rock, a narrow opening is created forming a crack (Anders et al., 2014). With time, the crack provides a pathway for gases or fluids to infiltrate and create a cavity in the rock. At times, the fluids contain minerals which build up in the cracks as infilling material. The infilling material ultimately weakens the rock by propagating the cracks.

The process of rock failure is governed by two primary mechanisms: the shear failure and the tensile failure. Brittle material such as rocks and concrete tend to be sensitive because of inconsistency of their mechanical behaviour known as anisotropy (Ghamgosar, 2017).

The direction of propagation of fractures in a rock is governed by the maximum stress concentration. This means that the microfractures or cracks will grow and propagate in the direction perpendicular to the maximum tensile stress in the rock (Hoek and Bieniawski, 1965). According to Rodríguez et al. (2016), the growth and propagation of microfractures reduces the overall stiffness of the rock resulting in large scale failure after some time. Anders et al. (2014) argued that studying microscopic fractures within the rock aids the researcher understands the overall mechanical strength of the rock. In this light, micro-fracturing patterns and their distribution were analysed to gain a better understanding of the overall rock strength of the area of study. This was used to characterise the behaviour of the rock mass around the tunnels in line with the objectives of this doctoral research.

Generally, the mechanical properties in rocks are nonhomogeneous. Moreover, rock masses contain numerous geological disturbances such as joints, faults, parting planes and fractures. As a result, it is quite challenging for engineers to deal with rocks as opposed to other engineering material used in mining or civil projects (e.g., construction of a tunnel). For this reason, it is critical to understand the behaviour of rock together with the formation and propagation of microfractures. This information is vital for investigating the mechanical responses of rocks when subjected to different loading conditions.

Rock samples collected from the left and right sides of Tunnel One were taken to the laboratory and prepared for thin sections. This exercise was conducted to analyse and assess the effects of micro-fracturing on rock strength. This section focuses on micro-fracturing analysis and the results obtained from the laboratory experiment are discussed. The discussion compares the microfractures on the left and right sides of the tunnel. In addition, microfractures that occur nearer and farther from the tunnel are also compared. To conclude this chapter, the development of an empirical chart for fracture distribution along the tunnel is presented. This is based on

the results of data stemming from microscopic analysis also covered in this chapter.

5.2. Micro-fracturing analysis

The procedure followed to prepare rock samples for thin section laboratory experiment is given in Section 3.3 in Chapter 3. In this section, the experiment results are presented in the form of microscopic images. These results are analysed and discussed in the following subsections. Micro-fracturing is looked at in a small scale and later analysed in a large scale to understand the effects of micro fracturing on the tunnel.

According to Lim and Martin (2010), there exist three main types of microscopic fractures. These are the grain boundary cracks; inter-angular cracks; and trans-angular cracks.

Grain boundary cracks are characterised with the boundaries of the grain in a rock. On the other hand, inter-angular cracks are identified by lying within the mineral grain. Lastly, trans-angular cracks are identified by crossing different mineral grains and boundaries. These types were used to analyse micro-fracturing in both the left and right sides of Tunnel One.

5.2.1. Micro-fracturing analysis on the right side of tunnel one.

From the right side of the tunnel, 14 samples were collected spaced from the tunnel backwards at an interval of 0.5m. The distribution of microcracks from the back to the front is given in this section. Figure 5.1 shows the microfractures at Point number 1 (refer to Section 3.2.2 of Chapter 3). The thin section in this image exhibits all three types of micro-fracturing; namely, grain boundary (GB) cracks represented in orange; inter-angular (IA) cracks represented in red; and trans-angular (TA) cracks represented in blue. Physical observations on the right side of the tunnel showed that the rock mass is more intact with minimal geological disturbances. Nonetheless, the images of the thin section show that there are some IA cracks and TA

cracks. Figure 5.2 is a point 0.5m away from the first point whereas Figure 5.3 is 1.0 m away. It can be seen that the intensity of micro-fracturing has increased. The intensity of trans-angular fractures is more visible in Figure 5.3. Likewise, there is evidence of inter-angular fractures and minimal grain boundary fractures visible.

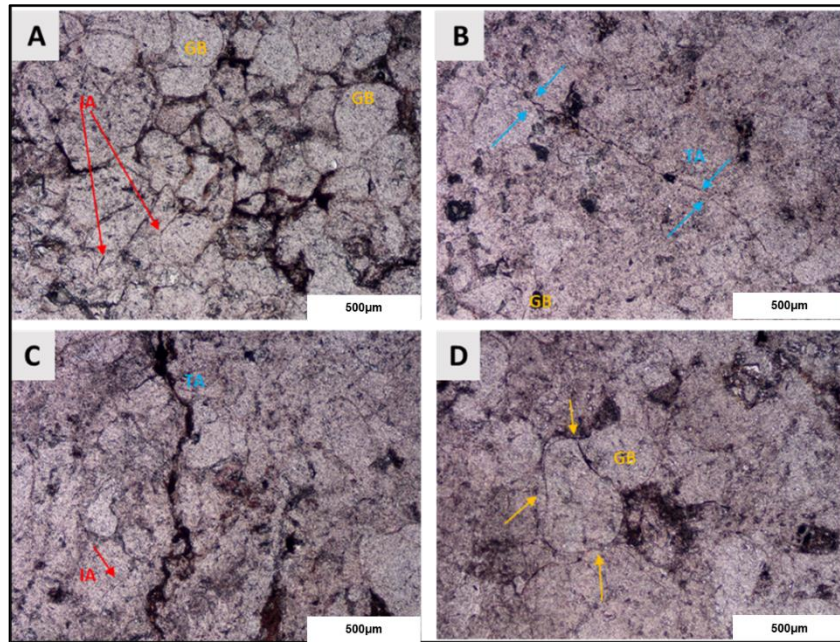


Figure 5.1: Microcracks at Point 1 on the right side of Tunnel One

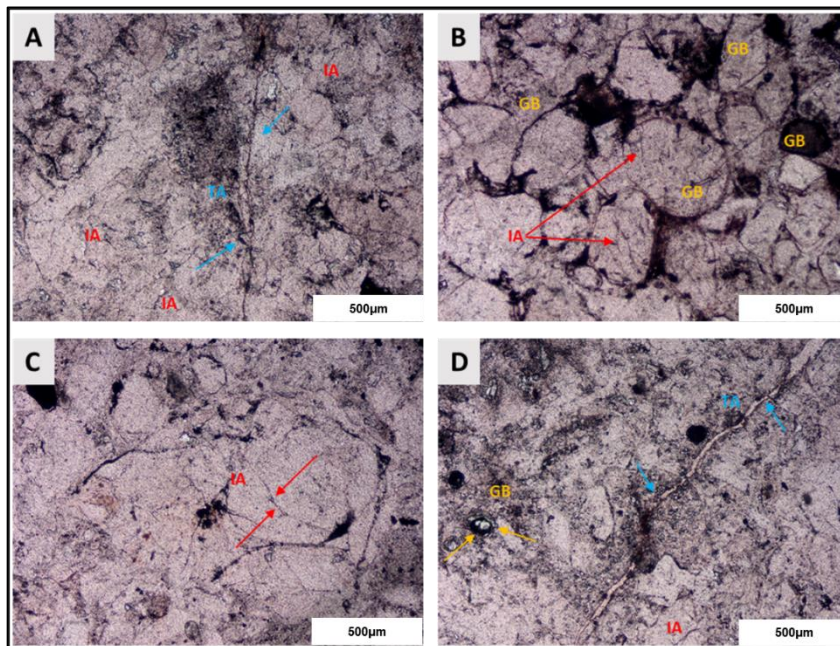


Figure 5.2: Microcracks at Point 2 on the right side of Tunnel One

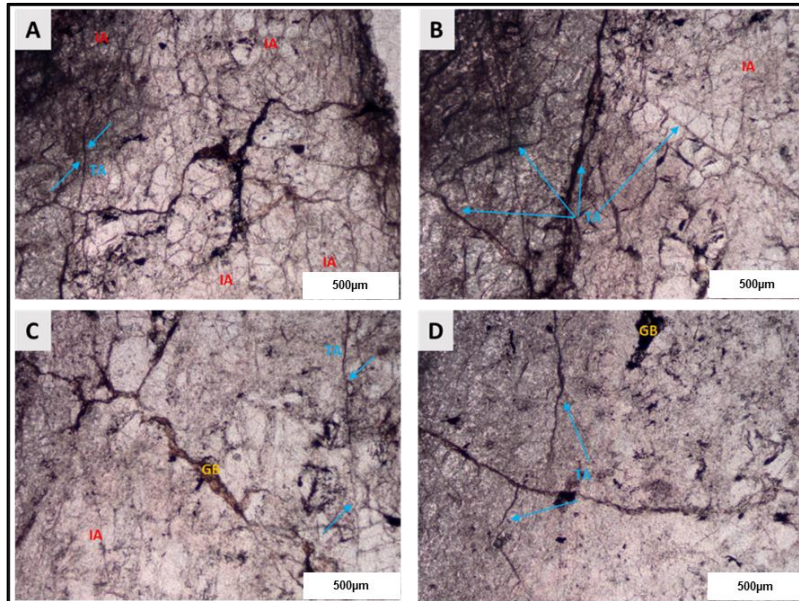


Figure 5.3: Microcracks at Point 3 on the right side of Tunnel One

Let us move to the middle portion which are Point 7 and 8 and talk about Figure 5.4 and Figure 5.5 respectively. These images clearly show the grain boundary cracks identified on the rock mass. Although there is evidence of inter-angular fracturing, there are no trans-angular crack visible at Point 7. It can be seen that this portion of the rock mass is more intact which confirms to the visual observation alluded to in the previous sections (Figure 5.4). In contrast, Figure 5.5 shows numerous trans-angular micro cracks.

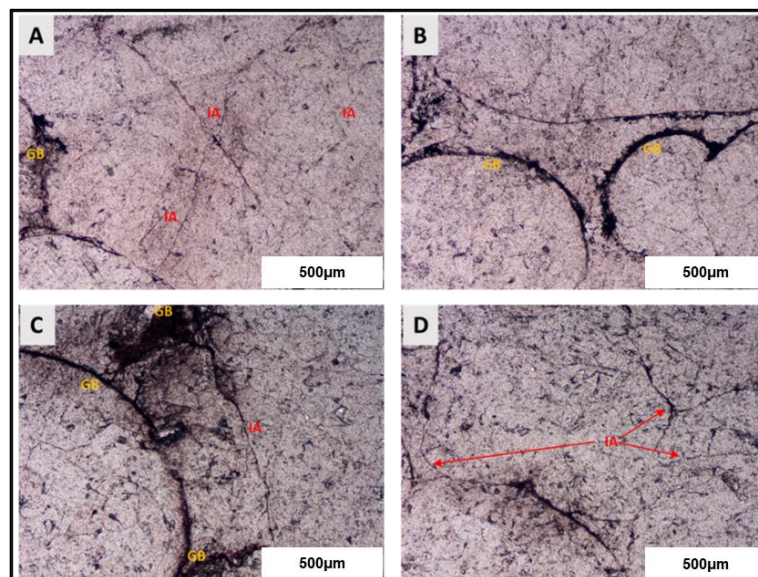


Figure 5.4: Microcracks at Point 7 on the right side of Tunnel One

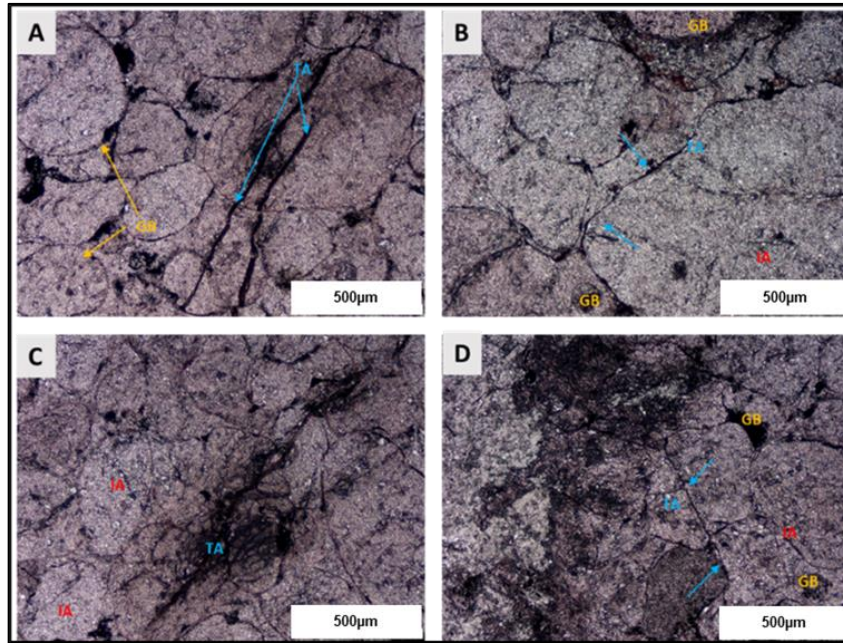


Figure 5.5: Microcracks at Point 8 on the right side of Tunnel One

Towards the face of the tunnel, the microcracks tend to be more intense. Points 13 and 14 (i.e., Figure 5.6 and Figure 5.7) exhibit all three categories of cracks. However, the most dominant category of microfractures visible is the grain boundary cracks, followed by the trans-angular cracks and last the inter-angular cracks.

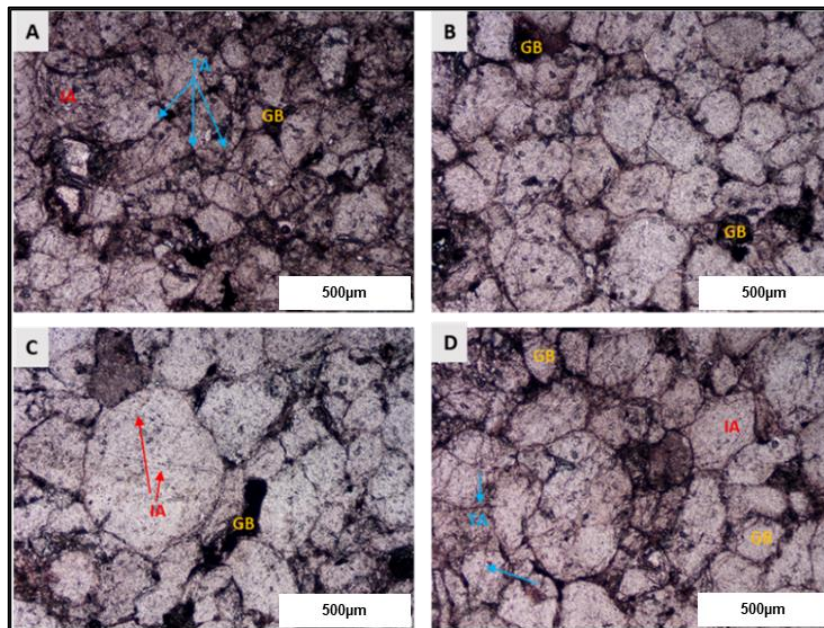


Figure 5.6: Microcracks at Point 13 on the right side of Tunnel One

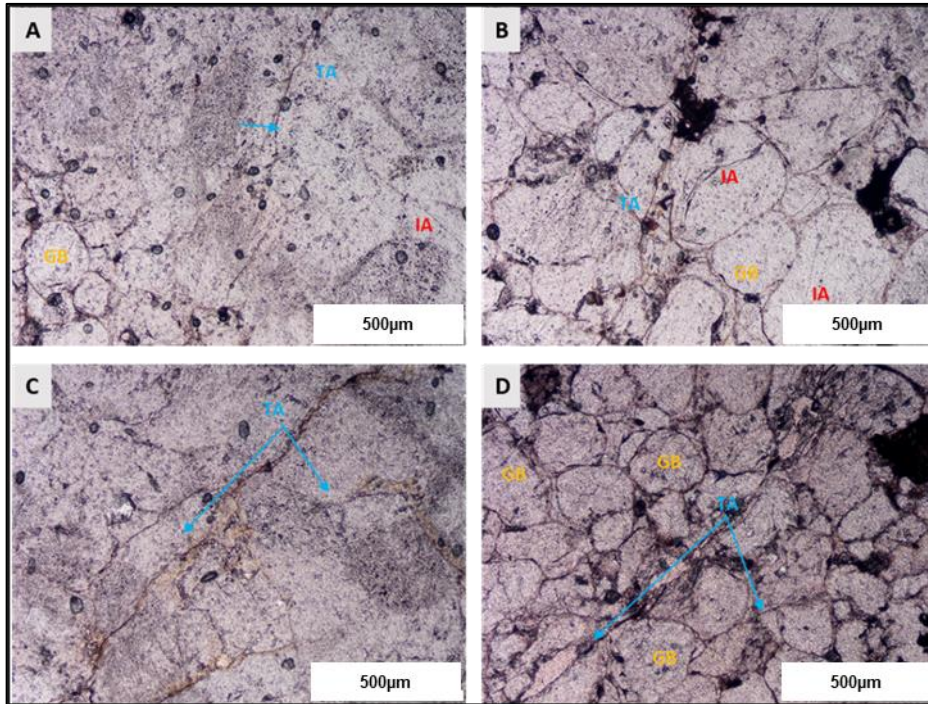


Figure 5.7: Microcracks at Point 14 on the right side of Tunnel One

5.2.2. Micro-fracturing analysis on the left side of Tunnel One

From the left side of the tunnel, 10 samples were collected spaced from the tunnel backwards at an interval of 0.5m. The distribution of microcracks from the back forward is given in this section.

Figure 5.8 shows the microfractures at Point number 1. The thin section in this image exhibits all three types of micro-fracturing, i.e., the grain boundary (GB) cracks represented in orange; inter-angular (IA) cracks represented in red; and trans-angular (TA) cracks represented in blue. Visually, the left side of the tunnel was observed to be very blocky. The microfractures also concur with the visual observations. These images shows that trans-angular fractures are more dominant followed by grain boundary fractures and lastly inter-angular fractures (see Figure 5.8, Figure 5.9, and Figure 5.10). Although these points are at an interval of 0.5m, they exhibit similar microfractures since the rock mass is jointed and very blocky.

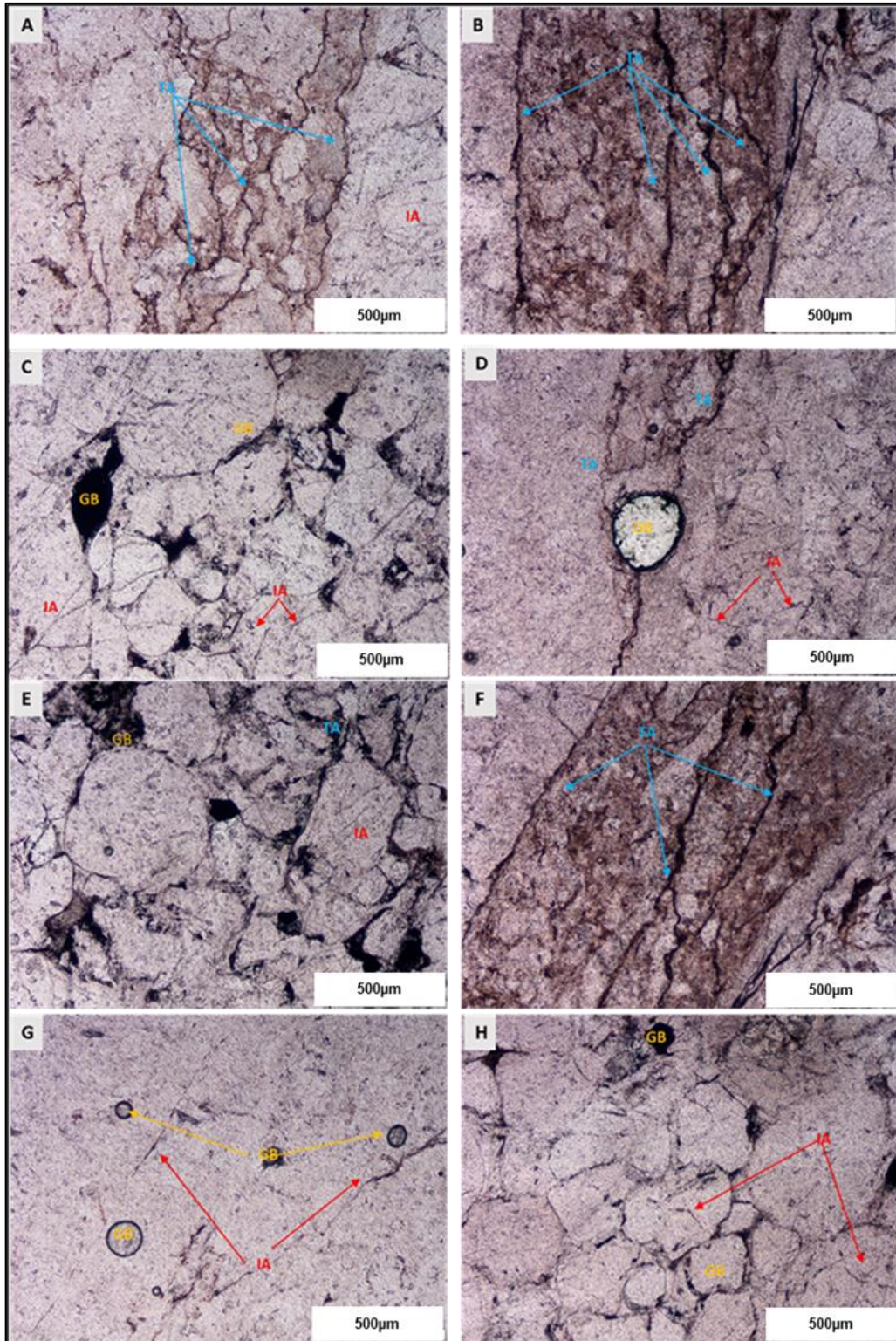


Figure 5.8: Microcracks at Point 1 on the left side of Tunnel One

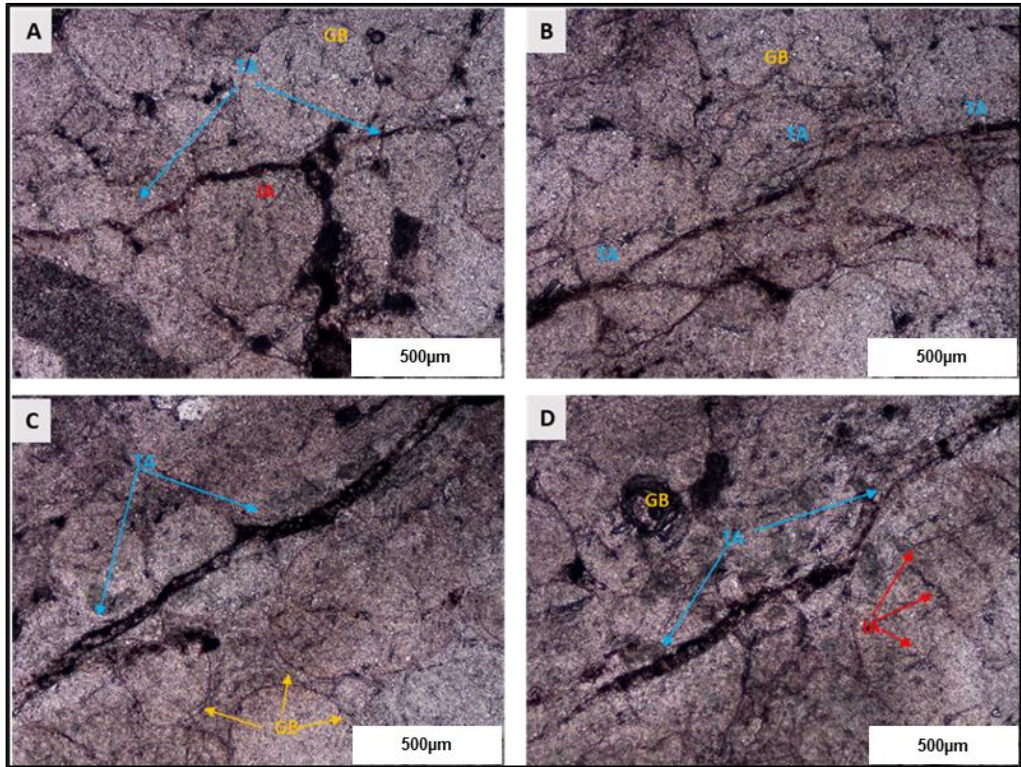


Figure 5.9: Microcracks at Point 2 on the left side of Tunnel One

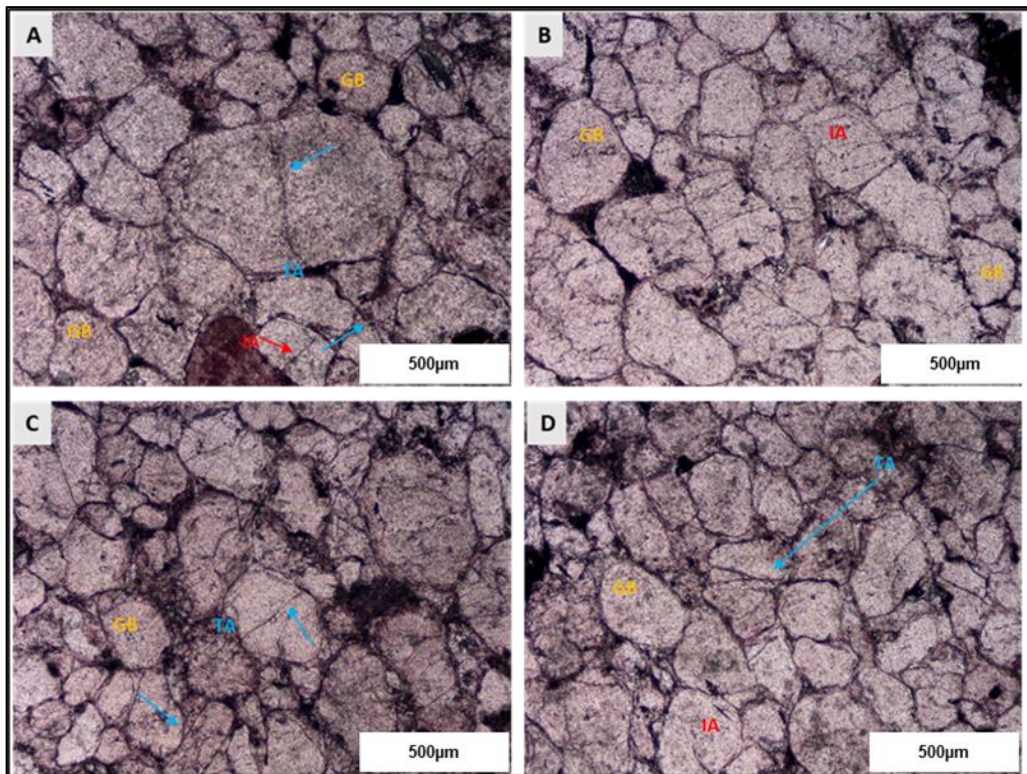


Figure 5.10: Microcracks at Point 3 on the left side of Tunnel One

The middle portions are represented by Points 5 and 6 which correspond to Figure 5.11 and Figure 5.12 respectively. In this portion of the rock mass, there are more trans-angular cracks and grain boundary cracks than inter-angular cracks. One can argue that the inter-angular cracks propagated with time into trans-angular cracks, judging from the physical observation made together with the thin section microfracture images below (i.e., Figure 5.11 and Figure 5.12). Similarly, point 10 which is located towards the tunnel face shows the same attributes (Figure 5.13). The rock mass has more trans-angular cracks, followed by grain boundary cracks and minimal inter-angular cracks.

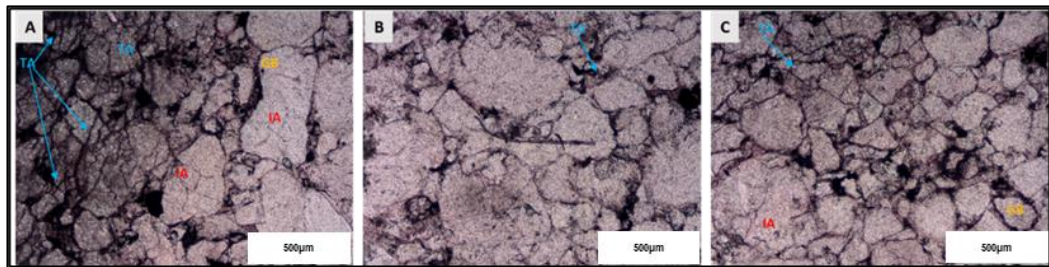


Figure 5.11: Microcracks at Point 5 on the left side of Tunnel One

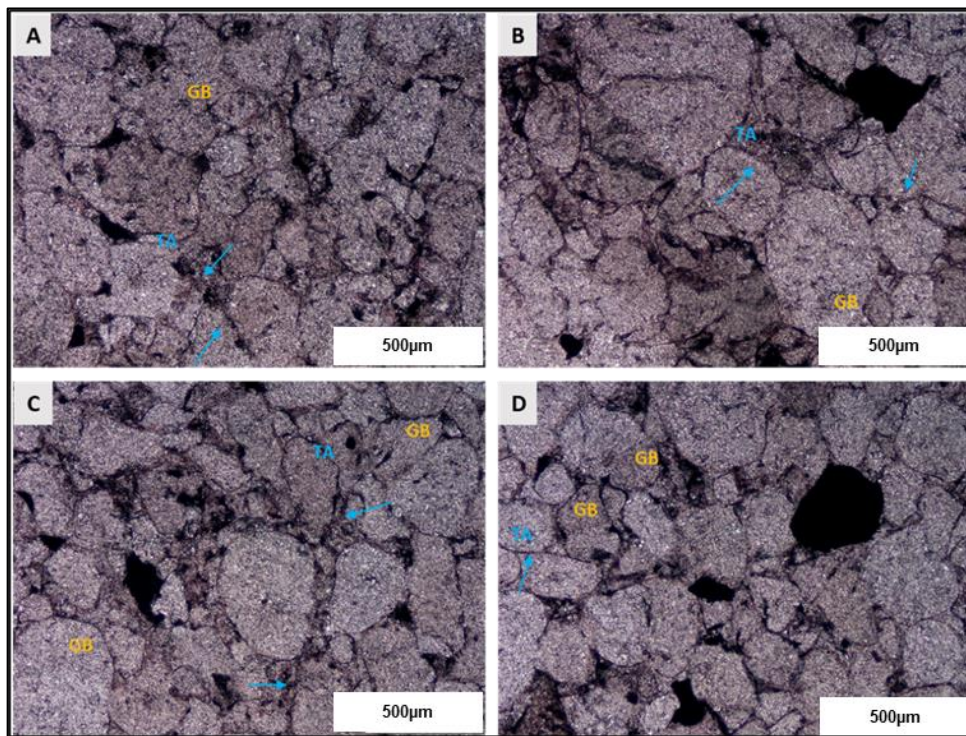


Figure 5.12: Microcracks at Point 6 on the left side of Tunnel One

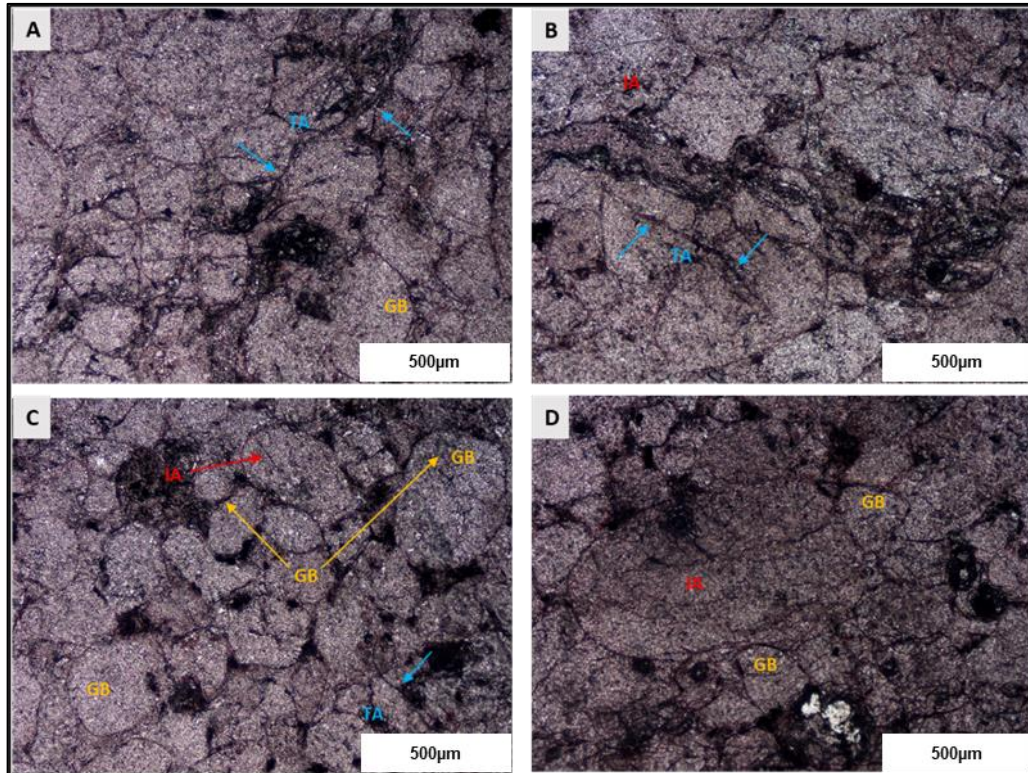


Figure 5.13: Microcracks at Point 10 on the left side of Tunnel One

Both the left and right sides of the tunnel consist of the three main microfractures, i.e., grain boundary (GB) cracks; inter-angular (IA) cracks; and trans-angular (TA) cracks. The difference between the two sides is the persistence and frequency of occurrence of these fractures. It was also noticed that the microfractures concur with physical observations. Therefore, microscopic analysis is critical to enhance the understanding of the behaviour of the rock mass. For this reason, it becomes now important to zoom out and analyse rock fractures based on the microscopic results obtained. The next section briefly explains this notion.

5.3. Rock failure analysis on a large scale

Rock failure is governed by external factors such as anisotropy, heterogeneity, stress states, surrounding environment and discontinuities (Ghamgosar, 2017). Rock failure can also occur from the failure process of a crack initiated in the rock (Stacey, 1981). In this case, a new surface is opened up and filled with material from fluid or gasses passing through the

crack. With time the crack propagates and results in a fracture. The fracture can be identified in an 'intact' rock collected for laboratory testing by, say, uniaxial compressive strength test. This crack creates a possible failure plane for the rock specimen when subjected to uniaxial compressive stress. Ultimately, the crack propagates over time and has potential to cause failure. A possible wedge failure is indicated in Figure 5.14 below. This scenario assumes a jointed rock mass where a tunnel is excavated. The microfracture propagated over time and intersected the joint plane resulting in a possible wedge failure. In essence, Figure 5.14 shows the notion of rock fracturing from a microscopic failure through laboratory scale failure to macro- failure at field-scale.

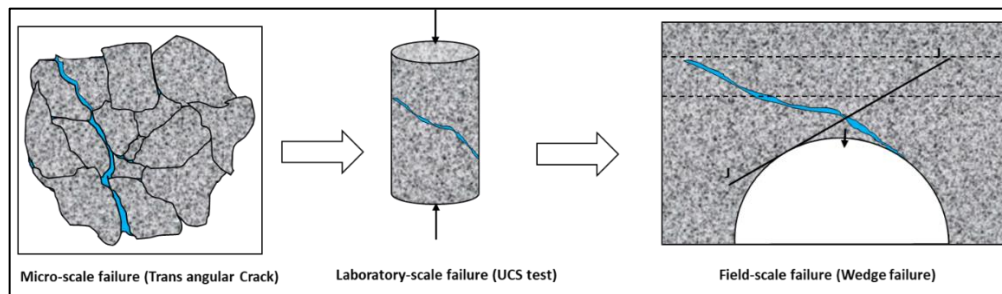


Figure 5.14: Rock fracturing from micro to macro scale (Modified after Ghamgosar, 2017)

An understanding of the mechanism of rock fracture served as the foundation for the micro-fracturing analysis of the left and right sides of tunnel one (see Section 5.2). With the understanding of rock fracturing propagating from micro to macro scale, it was found critical to propose an empirical chart for fracture distribution and the effects of fracture distribution on strength factor and total displacement in shallow tunnels. These concepts are discussed in Section 5.4 (next section) and Section 6.3 in Chapter 6.

5.4. Development of an empirical chart of fracture distribution

To develop an empirical chart for fracture distribution around the tunnel, microscopic data was used. The total number of fractures was analysed on

both the left and right side of the tunnel. This data is provided in APPENDICES B1 and B2.

For each point, there are four images while in each image, the identified cracks were classified into three categories: grain boundary cracks, inter-angular cracks, and trans-angular cracks. At each point, the total number of cracks per category was determined. The summarised total number of fractures identified for both the right and left sides of the tunnel are presented in Table 5.1 and Table 5.2 respectively. It can be seen that the number of cracks closer to the tunnel face is higher than that away from the tunnel face. Overall, the total number of cracks on the right side is greater than on the left as more samples were collected on the left than on the right. Nonetheless, from both sides, it can be concluded that the trans-angular cracks are more dominant than grain boundary and inter-angular cracks.

Table 5.1: Total number of fractures for right side of tunnel one

TOTAL NUMBER OF FRACTURE FOR RIGHT SIDE OF THE TUNNEL				
Position along the tunnel	Grain boundary cracks	Inter-angular cracks	Trans-angular cracks	Total number of cracks
Point 1	29	19	48	96
Point 2	29	19	36	84
Point 3	16	31	36	83
Point 4	21	21	34	76
Point 5	22	22	23	67
Point 6	16	24	27	67
Point 7	13	29	21	63
Point 8	19	15	18	52
Point 9	15	14	17	46
Point 10	12	25	9	46
Point 11	20	13	13	46
Point 12	11	18	14	43
Point 13	12	14	17	43
Point 14	16	12	14	42

TOTAL	251	276	327	854
-------	-----	-----	-----	-----

TOTAL NUMBER OF CRACKS	
(GB)_Grain boundary cracks - Found on the boundary of a grain	251
(IA)_Inter-angular cracks - Found within the grain	276
(TA)_Trans-angular cracks - Cut across different mineral grains and boundaries	327

Table 5.2: Total number of fractures for left side of Tunnel One

TOTAL NUMBER OF FRACTURE FOR LEFT SIDE OF THE TUNNEL				
Position along the tunnel	Grain boundary cracks	Inter-angular cracks	Trans-angular cracks	Total number of cracks
Point 1	13	15	51	79
Point 2	12	18	43	73
Point 3	27	22	23	72
Point 4	20	29	18	67
Point 5	5	6	53	64
Point 6	13	10	30	53
Point 7	12	10	31	53
Point 8	12	24	12	48
Point 9	11	25	14	50
Point 10	19	7	21	47
TOTAL	144	166	296	606

TOTAL NUMBER OF CRACKS	
(GB)_Grain boundary cracks - Found on the boundary of a grain	144
(IA)_Inter-angular cracks - Found within the grain	166
(TA)_Trans-angular cracks - Cut across different mineral grains and boundaries	296

The total number of cracks from both sides of Tunnel One was combined and used to develop a predictive model for fracture distribution along the tunnel. The combined total number of fractures is summarised in Table 5.3. Supervised ML was then used to analyse this data. Linear regression algorithm was used to develop a predictive model. A predictive analysis approach was strategically chosen since it was best suited for this type of analysis.

Table 5.3: Total number of fractures around Tunnel One

Position along the tunnel	Distance from the tunnel in (m)	Total number of cracks on the left	Total number of cracks on the right	Total number of cracks around the tunnel
Point 1	0	79	96	175
Point 2	0.5	73	84	157
Point 3	1	72	83	155
Point 4	1.5	67	76	143
Point 5	2	64	67	131
Point 6	2.5	53	67	120
Point 7	3	53	63	116
Point 8	3.5	48	52	100
Point 9	4	50	46	96
Point 0	4.5	47	46	93
Point 11	5	-	46	46
Point 12	5.5	-	43	43
Point 13	6	-	43	43
Point 14	6.5	-	42	42

Supervised ML (linear regression) also works well in cases where historical data and patterns are available for use in forecasting the future. As is the case in this study, the number of fractures from the outside of the tunnel is known. To predict the number of fractures inside the tunnel, the predictive analysis approach is therefore ideal. The predictive model and corresponding plots are detailed in APPENDICES B3 and B4 respectively.

From the modelling effort, a simple linear regression equation with coefficient of distribution R^2 of 96.25% was developed:

$$y = mx + b = -21.749x + 174.97 \quad (5.1)$$

$$R^2 = 0.9625 \quad (5.2)$$

This regression model in Equation (5.1) represents the number of cracks (y) as a function of the distance along the tunnel (x). Also note that m and b are the expected slope and projected intercept respectively.

The regression model was further used to develop an empirical chart for fracture distribution along the tunnel. This model applies specifically to shallow tunnels. Figure 5.15 illustrates the empirical chart mentioned above. The number of fractures expected at the face of the tunnel is extremely high. This is mainly because the rock mass at this position is mostly exposed. Thus, more fractures occur as there is continuous weathering on the exposed rock mass.

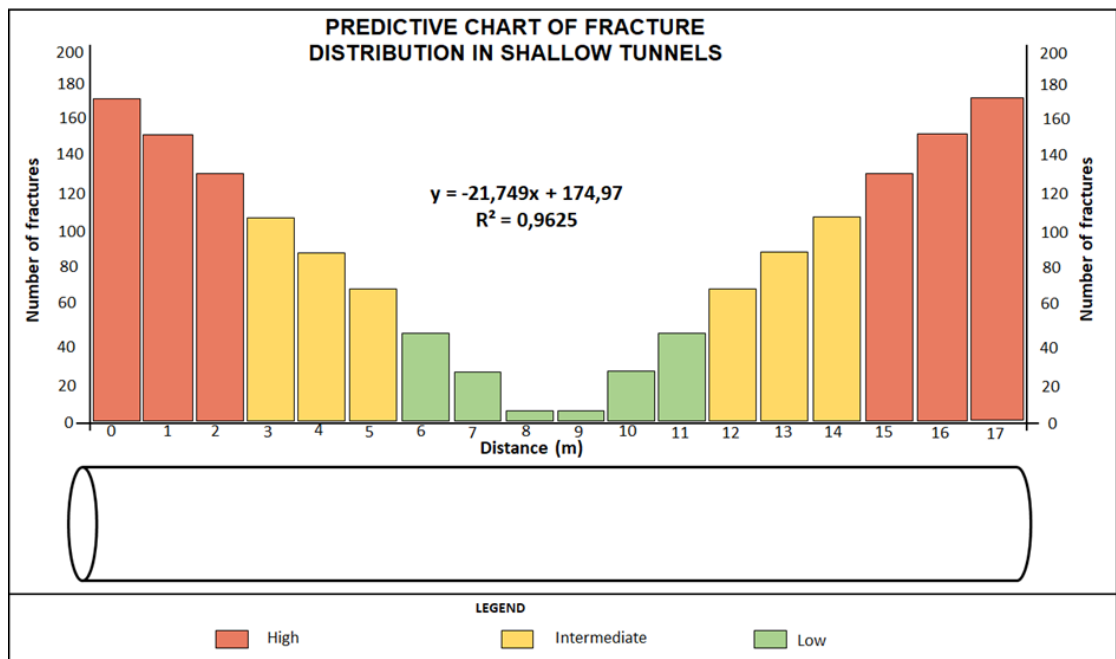


Figure 5.15: Predictive chart of fracture distribution in shallow tunnels

Moving towards the middle, number of fractures also tend to decrease from intermediate to very low (represented in orange and green respectively in Figure 5.15). The lessening in number of fractures expected is a result of

minimal or no weathering at all in this portion of the tunnel. Since this is a road tunnel, similar fracture distribution is expected to happen when moving outside the tunnel at the other end, hence the chart is symmetrical about the y-axis (see Figure 5.15). Three zones can be identified within the tunnel based on the degree of fracturing. Little to no fracturing is symbolised by Zone 1 (green), intermediate fracturing is defined by Zone 2 (yellow), and highly fractured portion is represented by Zone 3 (red) in Figure 5.15.

5.5. Conclusion

This chapter detailed how microfractures were characterised and used to model fracture distribution in shallow tunnels. Various traditional rock mass classification was considered and GSI was used to rate the rock mass in the periphery of the tunnel. It was noted that the left side of the tunnel consists of numerous geological disturbances as opposed to the right side which was more intact. In addition to field measurements and observations, rock samples were collected from both sides of the tunnel. These samples were prepared for thin section laboratory experiment.

The results obtained from the thin sections were analysed using microfracturing analysis with the understanding of rock fracture mechanism. Three main microfractures were evident. These are the grain boundary cracks, inter-angular cracks, and trans-angular cracks. Distribution of microfractures on the right side showed that there are more trans-angular cracks followed by grain boundary cracks when moving from the back to the face of the tunnel. Similarly, the frequency of trans-angular cracks and grain boundary cracks was noted on the left side of the tunnel. In both sides there is some evidence of inter-angular fracturing. However, these fractures were not as dominant as the TA and GB. Results from thin section analysis were further used to develop an empirical chart of fracture distribution in shallow tunnels. It was observed from the predictive model used that the number of fractures at the entrance of the tunnel is high (Zone 3), and it reduces to intermediate (Zone 2) and ultimately low in the middle portions of the tunnel

(Zone 3). This distribution is symmetrical in the y-axis as a similar trend is observed from the middle moving to the other end of the tunnel. To validate the predictive model developed in this chapter, simulations are conducted in Chapter 6, where various depths of fractures are simulated to determine the safety factor and deformation of the tunnel. The simulations are run for the tunnel with and without lining material.

It can be stated that the concept of rock fracture is a fundamental feature in rock engineering and rock mechanics. This component requires a comprehensive understanding of the mechanical behaviour of rocks subjected to different stress levels. An understanding of the principles of failure mechanisms of rocks is critical to solving most geo-mechanical problems.

6. Chapter 6: Effects of Fracture Distribution on Tunnel Stability

This chapter aims at addressing the effects of fracture distribution on tunnel stability looking at the strength factor and total displacement. Each zone (refer to Section 5.4 in Chapter 5) is assessed individually to comprehend its effect. This helped to later develop a support strategy for each zone. The proposed support strategy is validated using support capacity diagrams. Lastly, comparison is done on the major principal stress and total displacement for each zone before and after support installation. Simulations in this chapter were rendered in Optum G2 and RS2.

6.1. Introduction

Tunnel responds to the deformation of the rock mass with time. In this section, tunnel stability is assessed with and without support for three different zones. The first zone is characterised by little or no fractures, second zone is moderately fractured, and the third zone is highly fractured. It is believed that the tunnel stability differs in the three zones based on the fracture distribution and intensity.

Support designed for road tunnels in shallow environments should not be too stiff nor too flexible. Moreover, support should not be applied too early or too late. Hence, the introduction of time dependent deformation analysis and ground reaction curves in support design of tunnels.

6.2. Effects of fracturing on shallow tunnels using Optum G2

The tunnel simulations were conducted on a tunnel with dimensions as shown in Figure 6.1. This exercise was to comprehend the effect of fracturing on tunnel stability along the length of the tunnel. As seen from the Predictive chart of fracture distribution in shallow tunnels presented in Chapter 5, the tunnel can be divided into three zones. Each zone was simulated individually to comprehend the effect of fracture distribution on

the strength reduction factor. Simulations were conducted using Optum G2 for each zone.

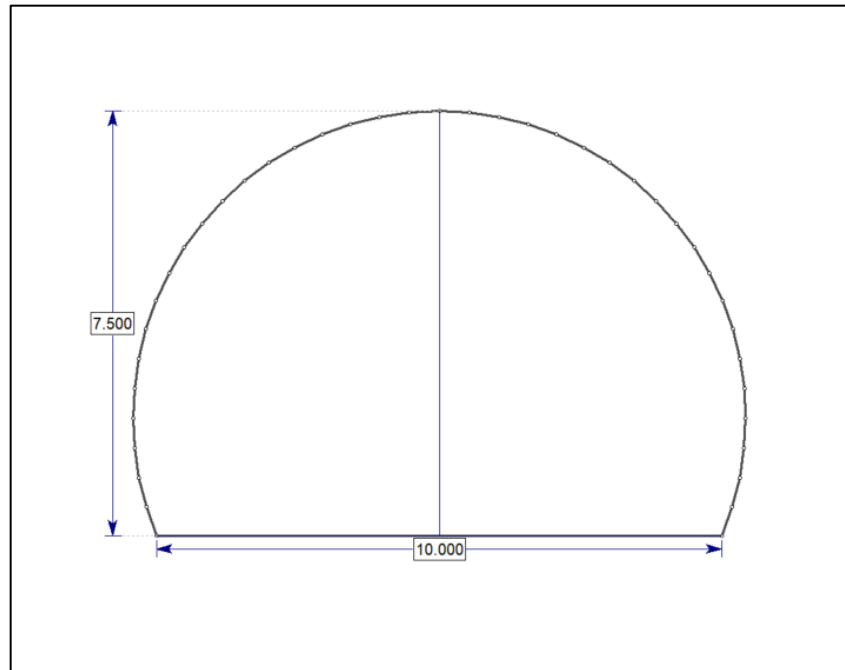


Figure 6.1: Tunnel simulation dimensions

The tunnel was divided into three zones namely Zone 1 (little or no fracturing), Zone 2 (moderately fractured) and Zone 3 (highly fractured) as explained in Section 5.4 (Chapter 5). Results from the simulation for Zone 1 are illustrated in Figure 6.2. When the rock mass has little or no fractures, the tunnel can stay stable over a period. Figure 6.2a show the initial condition of the tunnel. In Figure 6.2b and Figure 6.2c, the fractures start to propagate after a period of time. It is important to note that the time period required for fractures to start propagating in a tunnel can vary significantly depending on several factors. These factors include the specific geological conditions, the stress state of the surrounding rock mass, the excavation method, and the support system in place. It is difficult to provide a precise timeframe that universally defines when fractures will start propagating, as it can differ from one project to another. The ultimate propagation of the fractures can result in very small blocks of rocks forming (Figure 6.2d). These blocks have the potential to fall under the influence of gravity if support is not installed to stabilise the tunnel.

In general, the surrounding rock mass needs some time to adjust to the new stress distribution brought on by tunnel construction after it has been excavated. During this period, which can range from hours to days or even longer, the fractures may not propagate immediately. However, as time progresses, the stress redistribution, and the effects of various factors such as groundwater flow, cyclic loading, or external influences may lead to the propagation of fractures.

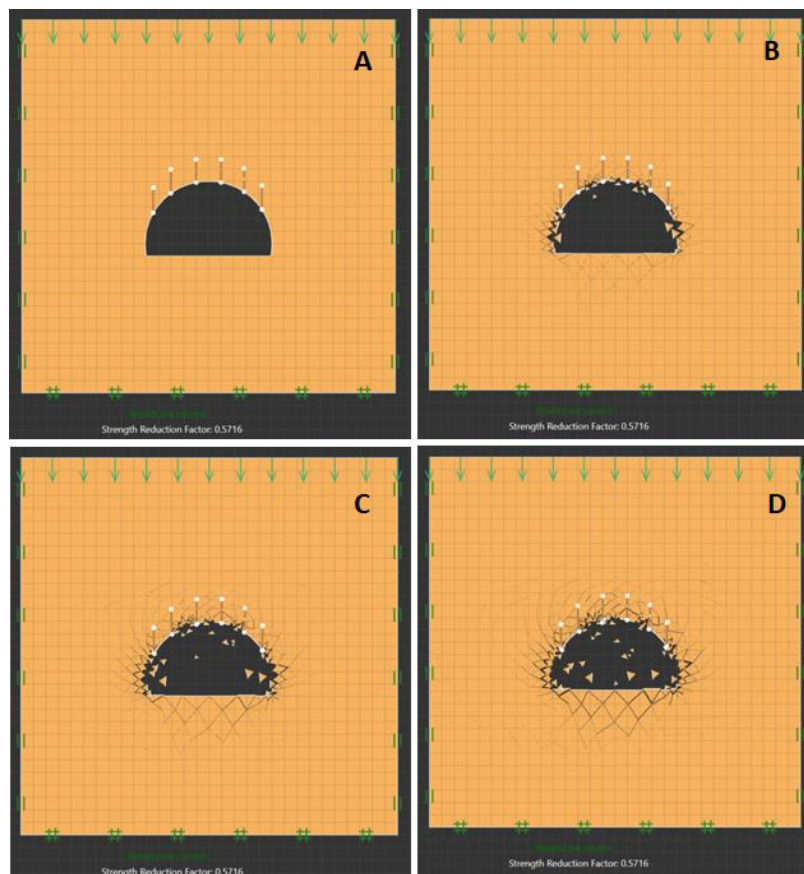


Figure 6.2: Fracture distribution in Zone 1 using Optum G2

Similarly, in Zone 2 and Zone 3 when the rock mass is moderately fractured or highly fractured respectively, the tunnel will be stable in the initial stage (Figure 6.3a and Figure 6.4a). However, the fractures will spread with time and intersect forming blocks of rocks that can potentially fall under the influence of gravity. In Zone 2, the potential blocks of rocks are marginally smaller than the potential blocks of rocks formed in Zone 3 (Figure 6.3b-c and Figure 6.4b-c). Lastly, the propagation of fractures in Zone 3 is more

intense when compared to Zones 1 and 2. It can be seen that the fractures spread on both the sidewalls, hanging wall and also on the footwall (Figure 6.3d and Figure 6.4d).

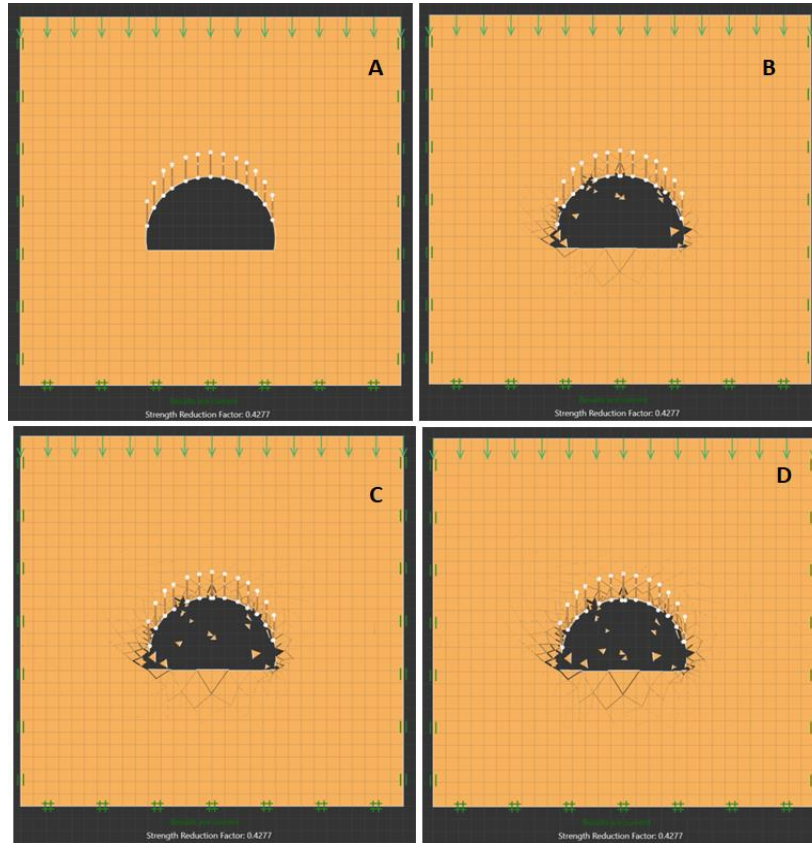


Figure 6.3: Fracture distribution in Zone 2 using Optum G2

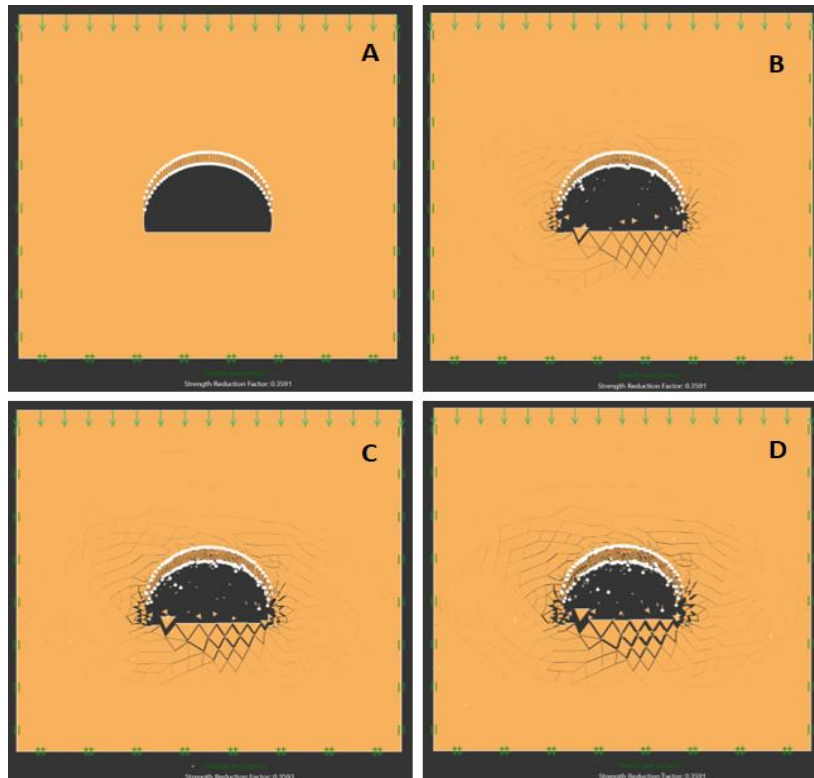


Figure 6.4: Fracture distribution in Zone 3 using Optum G2

For the three zones in Figure 6.2 – Figure 6.4, the strength reduction factors were also recorded for various lengths of fractures. The fracture lengths were found to range from 1m to 5m. For each fracture length, three sets of simulations were done. The Optum G2 simulations described in Section 3.6 (Chapter 3) were used to produce the strength reduction factor (SRF) values in Table 6.1. The SRF method is a numerical technique used to assess the stability of tunnels and other geotechnical structures. It involves reducing the strength parameters of the soil or rock mass incrementally until a failure mechanism is identified. SRF is a measure of the initial strength to reduced strength at failure ratio. By applying this method, engineers can evaluate the factor of safety against failure and identify potential failure modes (Hammah et al., 2005; Gupta et al., 2016).

To evaluate the stability of shallow tunnels during construction and subsequent service, the shear strength reduction (SSR) and SRF methods are used. These techniques enable engineers to assess the safety factor against failure and identify potential failure mechanisms, such as excessive

deformations, excessive convergence, or surrounding ground shear failure (Diederichs et al., 2007). Engineers can forecast the magnitude and distribution of deformations, such as tunnel convergence, heave, and settlement, by considering the reduced shear strength of the rock mass. This data is essential for assessing the compatibility of the tunnel with adjacent structures and infrastructure (Kaya et al., 2016). The histogram in Figure 6.5 visually contrasts how fracture length affects the strength reduction factor for each of the three Zones.

Table 6.1: Strength reduction factor for fracture distribution along the tunnel

Fracture size	SRF (Little or no fracturing)	SRF (Moderately fractured)	SRF (Highly fractured)
1m	0.565	0.433	0.359
2m	0.572	0.428	0.352
3m	0.565	0.430	0.354
4m	0.564	0.422	0.351
5m	0.559	0.424	0.357

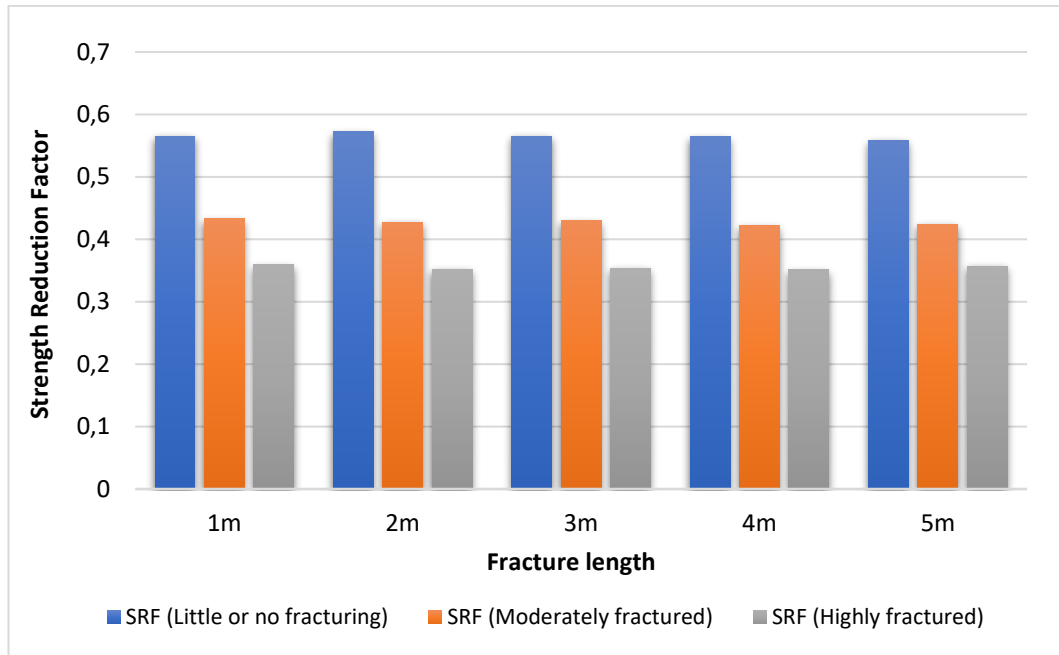


Figure 6.5: Strength reduction factor and fracture distribution along tunnel one.

In all the three zones, the tunnel cannot be considered stable since the strength reduction factor is less than 1. However, when there is little or no fracturing, the strength reduction factor ranges between 0.56 and 0.89. In Zone 2 and Zone 3, the average strength reduction factor was found to be 0.43 and 0.36 respectively.

Based on the simulations conducted in Optum G2, the predictive chart of fracture distribution in shallow tunnels can be improved to incorporate the expected strength reduction factor as shown in Figure 6.6.

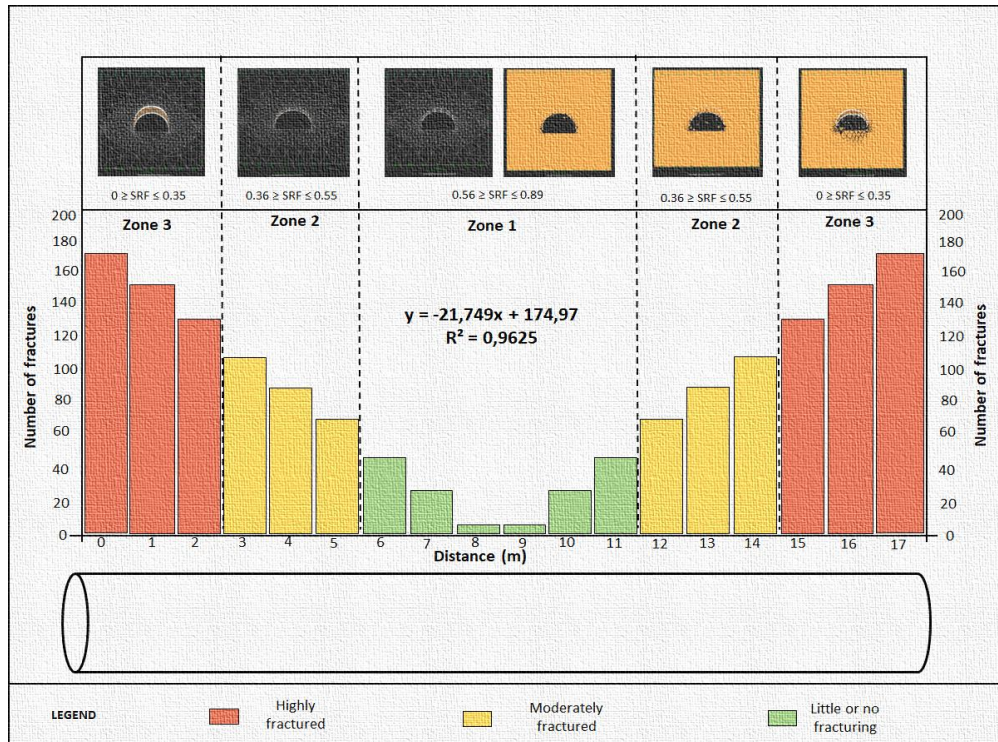


Figure 6.6: Predictive chart of fracture distribution and relative strength reduction factor per zone in shallow tunnels

These simulations show that there is indeed a need for support and particularly areal support in the form of concrete lining for tunnels. This should cater for small blocks or rocks formed on the immediate sidewalls and hanging wall of the tunnel. The concrete lining would also enhance the long-term stability of the road tunnel. In the next section, different types of concrete lining are simulated using RS2.

6.3. Effects of fracture distribution on strength factor and total displacement in shallow tunnels

The stability of road tunnels is critical. In this section, the effect of fracturing on strength factor and total displacement is simulated using the RS2 software. The aim is to understand the change in strength factor and the expected displacement caused by three zones of fracturing identified in the previous section. The simulation results are presented as follows:

6.3.1. Total displacement around the tunnel in RS2

Simulations were initially set as presented in Section 3.7 (Chapter 3). This section now run the simulations and generate results to understand the effects of fracture distribution along the tunnel on strength factor and total displacement. The methodology followed to run the simulations is detailed in Section 3.7. From the predictive model in Equations (5.1) and (5.2) (Section 5.4 of Chapter 5), the tunnel was divided into three zones based on the intensity of fracturing. Likewise, simulations and analysis of the effect of fracture distribution on strength factor and total displacement was divided into three zones. Figure 6.7 shows the simulated section view of fracture distribution in each zone.

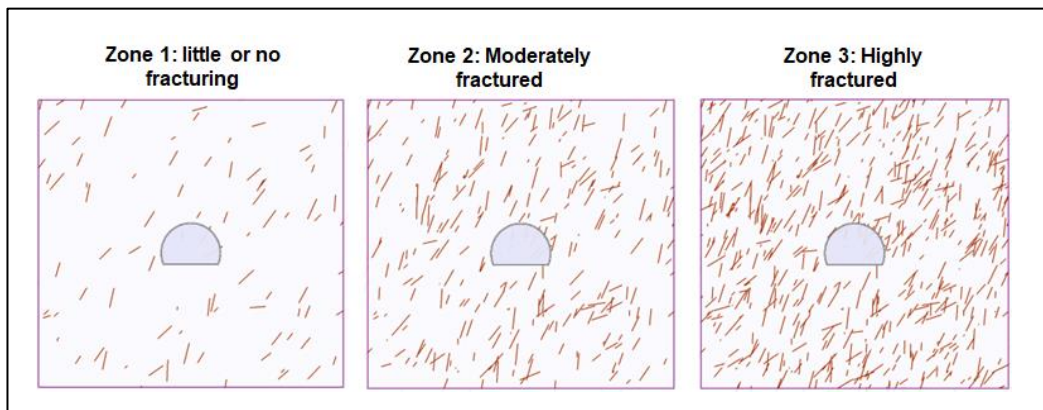


Figure 6.7: Section view of fracture distribution along the tunnel in different zones

The strength factor in all three Zones is similar. In stage 1, the support pressure is at 100%; hence, the strength factor is at maximum. When the support pressure is reduced, the strength factor also reduces. This is visible on the sidewalls of the tunnels in stage 2 where support pressure is 80%. The strength factor continuously reduces and propagates towards the hanging wall. This is visible between stage 5 and 10 where the support pressure decreases from 10% to 0% respectively. The above explained trend (i.e., reduced support pressure results in decreased strength factor) is evident in Zones 1, 2 and 3 as shown in Figure 6.8 – Figure 6.10.

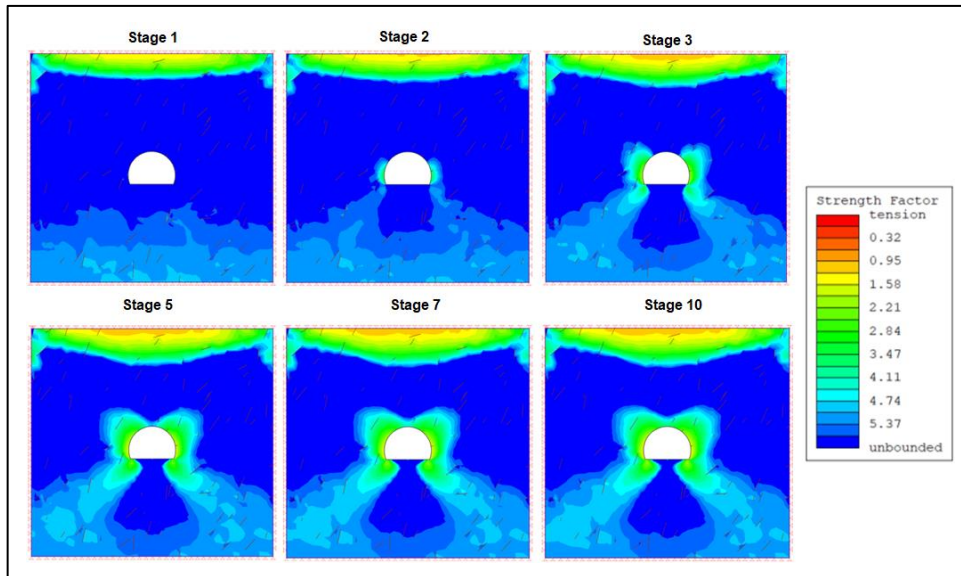


Figure 6.8: Simulated strength factor in various stages of Zone 1

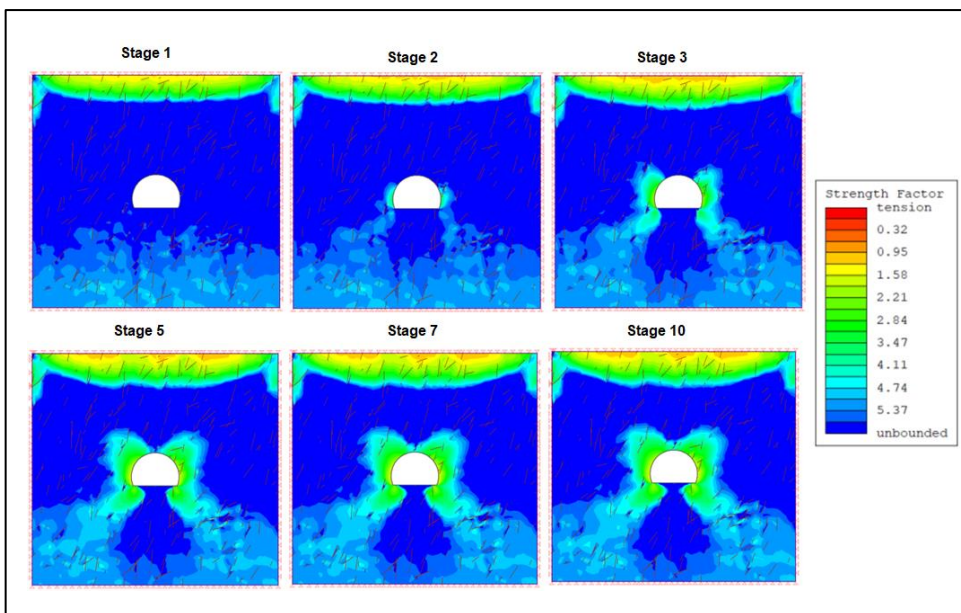


Figure 6.9: Simulated strength factor in various stages of Zone 2

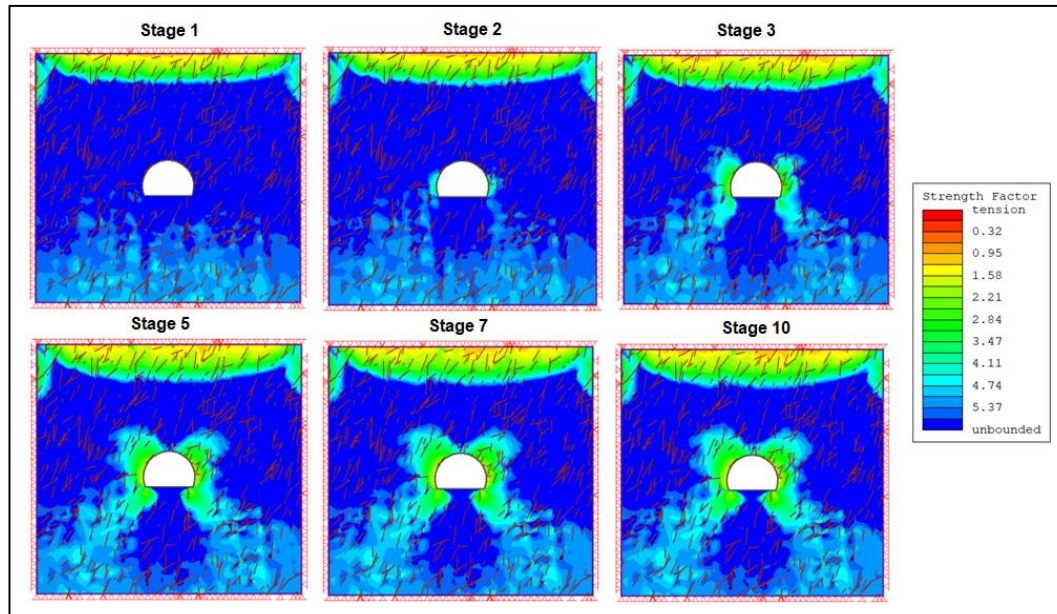


Figure 6.10: Simulated strength factor in various stages of Zone 3

The distribution of fractures, including their orientations, densities, and persistence, affects the mechanical behaviour of the rock mass and its response to tunnel excavation and support installation. Fractures act as planes of weakness, reducing the overall strength and cohesion of the rock mass. By applying the SRF method in the presence of fracture distribution, the weakened zones and failure mechanisms that may be associated with fracture propagation can be accounted for. This enables a more accurate evaluation of tunnel stability and helps design suitable support measures to reduce potential failure risks brought on by fractures.

It is important to note that the incorporation of fracture distribution and the determination of an appropriate SRF value require site-specific data, including geological mapping, fracture characterisation, and geotechnical investigations. These inputs, combined with engineering judgment and experience, allow for a comprehensive analysis of the interaction between fracture distribution and the SRF method to ensure the stability of the tunnel structure. In summary, the strength factor deteriorates from the side walls to the crown of the tunnel when the support pressure decreases. As a result, this can have negative implications on the overall stability of road tunnels with time. Therefore, when designing the tunnel support, the effect of

fractures on strength factor needs to be taken into consideration to prolong the life span of the tunnel and enhance stability.

6.3.2. Total displacement around the tunnel in RS2

Total displacement in tunnels is critical to simulate since it gives an insight of the expected deformation caused by the surrounding rock mass. To understand the effect of fracturing on total displacement, analysis was conducted from the skin of the excavation 10m into the immediate rock mass on three sides of the tunnel. These include the crown, and two side walls (left and right) as shown in Figure 6.11. This exercise was done for Zones 1, 2 and 3.

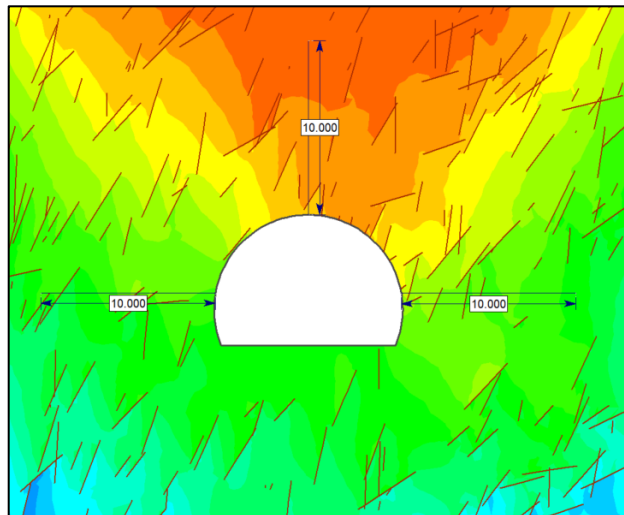


Figure 6.11: Total displacement analysis on three sides of the tunnel

The overall total displacement for each zone is summarised in stages as indicated in Figure 6.12 to Figure 6.14. With the understanding that the simulations are for shallow tunnelling environments, it is expected that total displacement will be concentrated on the crown of the tunnel. The stability of shallow excavations is highly influenced by the weight of the overburden as opposed to deep mining environments where the stability is influenced by the field stress. It is evident from the simulated results that total displacement is greater on the crown of the tunnel.

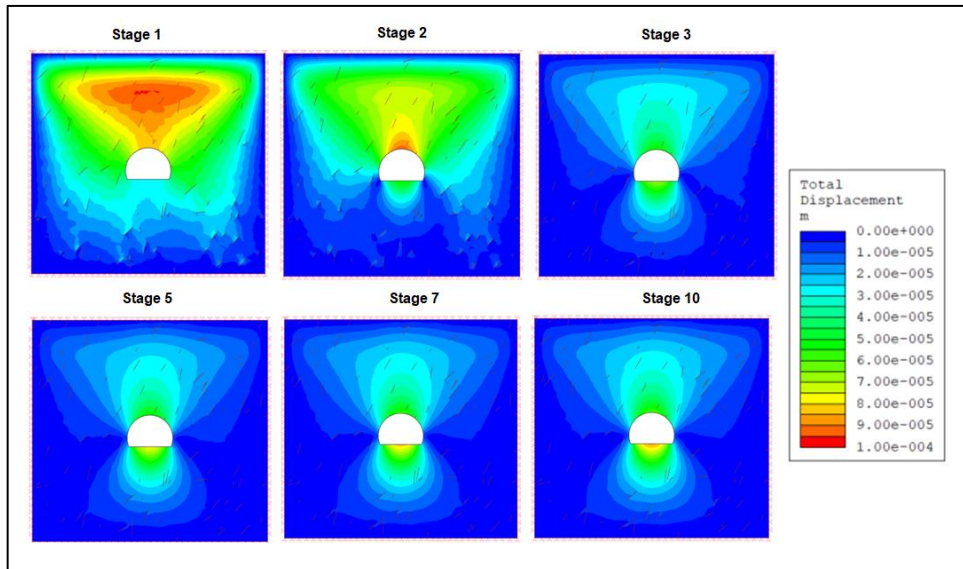


Figure 6.12: Simulated total displacement in Zone 1 using RS2

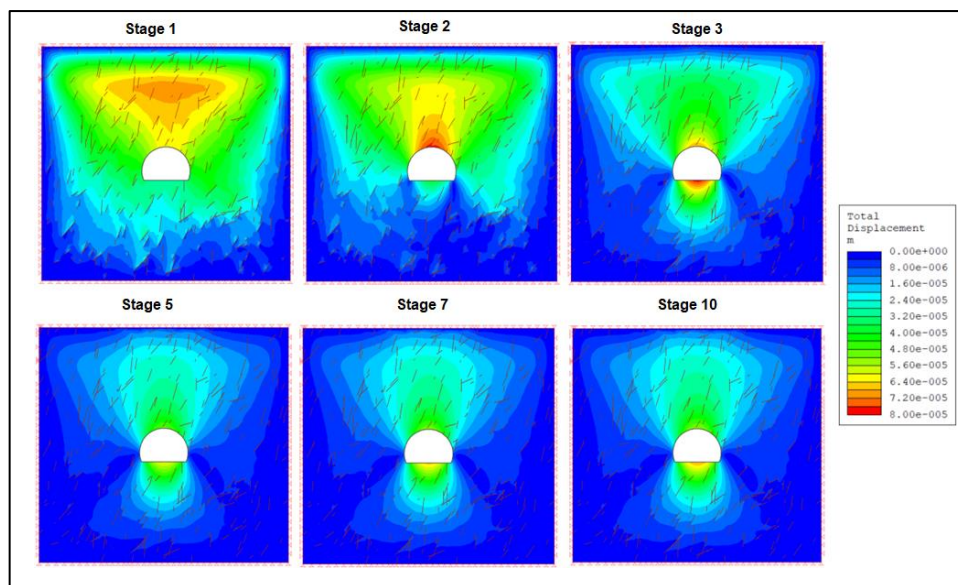


Figure 6.13: Simulated total displacement in Zone 2 using RS2

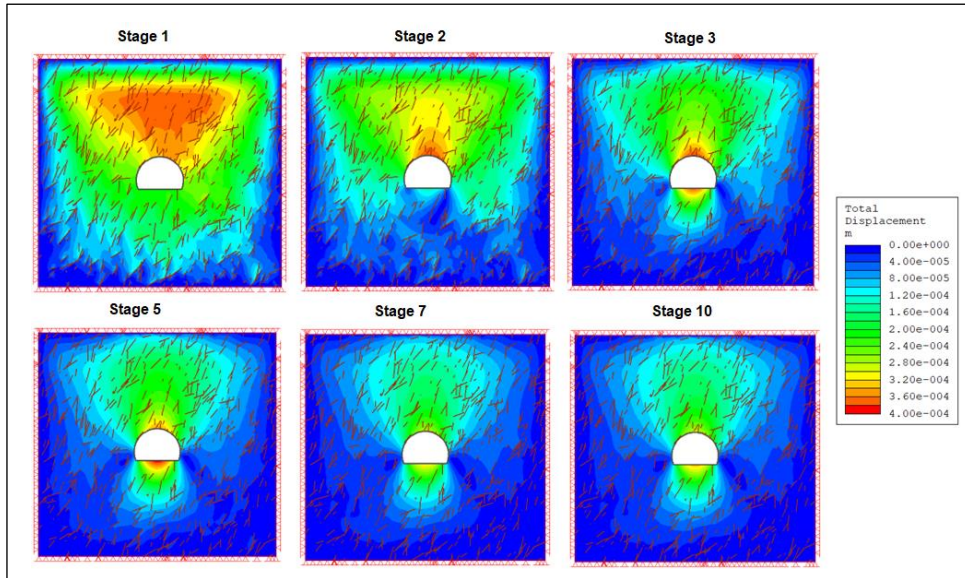


Figure 6.14: Simulated total displacement in Zone 3 using RS2

Total displacement for the crown, and sidewalls was analysed in six points (i.e., $n_1 = 0$; $n_2 = 0.5\text{m}$, $n_3 = 1\text{m}$, $n_4 = 2\text{m}$, $n_5 = 5\text{m}$, and $n_6 = 10\text{m}$) including the tunnel skin. These results are presented in graphs (see Figure 6.15 to Figure 6.17). The total displacement is very high at the skin of the excavation. This displacement steadily decreases as the distance from the skin of the excavation increases.

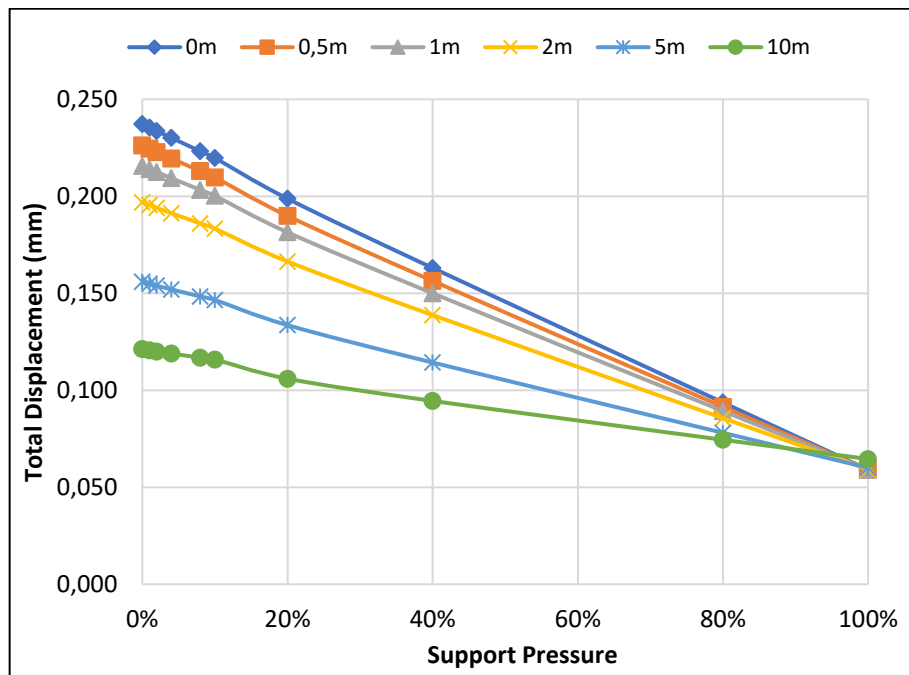


Figure 6.15: Total displacement on the tunnel crown Zone 1

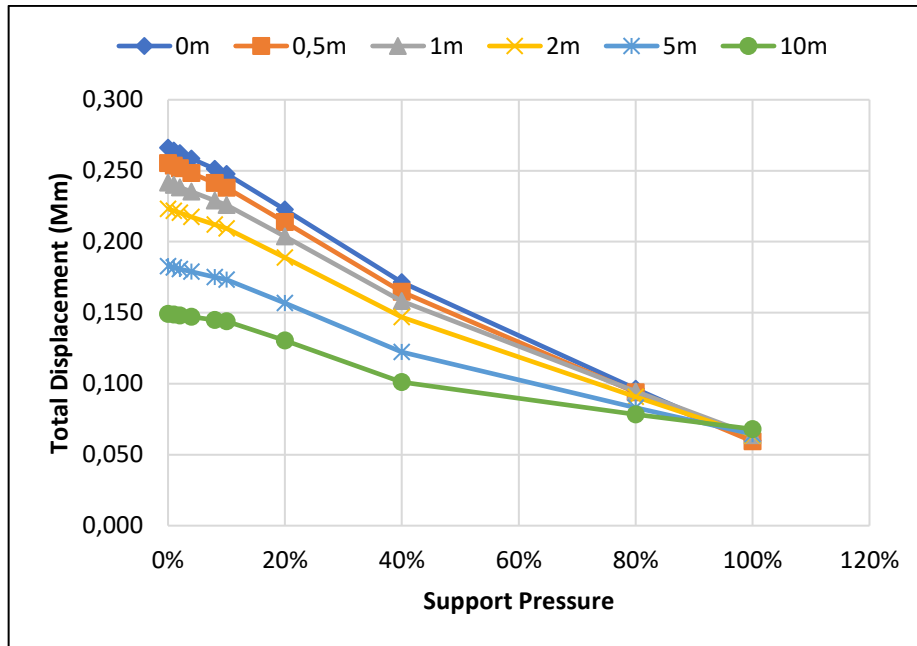


Figure 6.16: Total displacement on the tunnel crown Zone 2

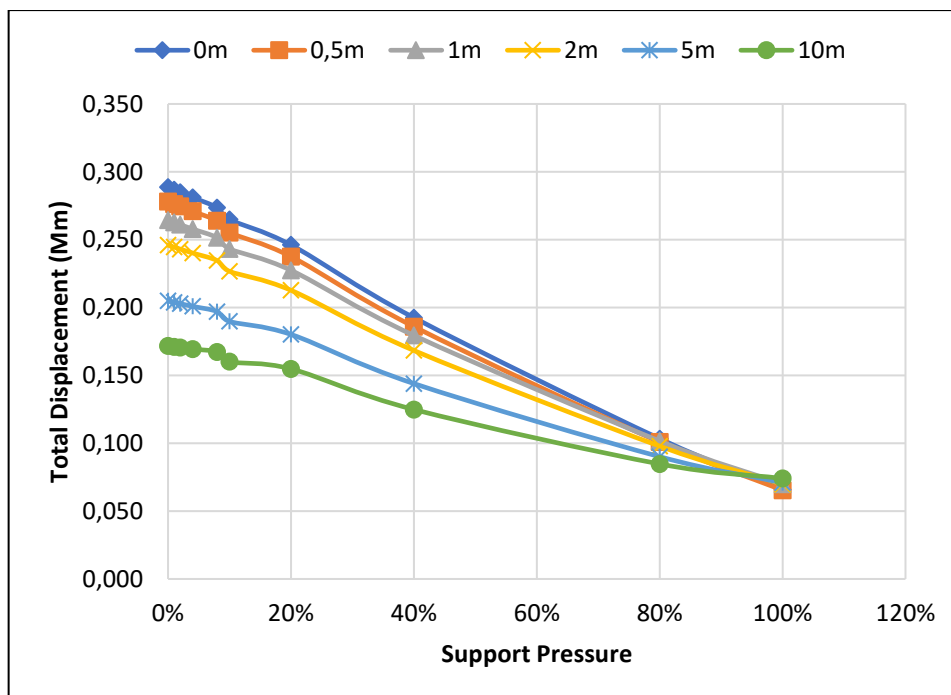


Figure 6.17: Total displacement on the tunnel crown in Zone 3

A similar approach was applied to analyse the total displacement on the left and right sidewalls of the simulated tunnel. The results of these analysis are presented in graphs in APPENDICES C1 – C3. The total displacement trends on the left and right sidewalls are similar. The total displacement in all three zones is higher on the skin of the tunnel and reduces when moving

away from the tunnel. However, unlike on the tunnel crown, the magnitude of total displacement on the sidewalls is reduced, ranging from 0.09mm in Zone 3 to 0.07mm in Zone 1.

Furthermore, a comparison of total displacement on the crown of the tunnel for the three zones was conducted on the skin of the excavation. It is evident in Figure 6.18 that highly fractured zone (Zone 3) is prone to more total displacement on the crown of the tunnel. The total displacement decreases when the fractures decrease (from Zone 2 to Zone 1).

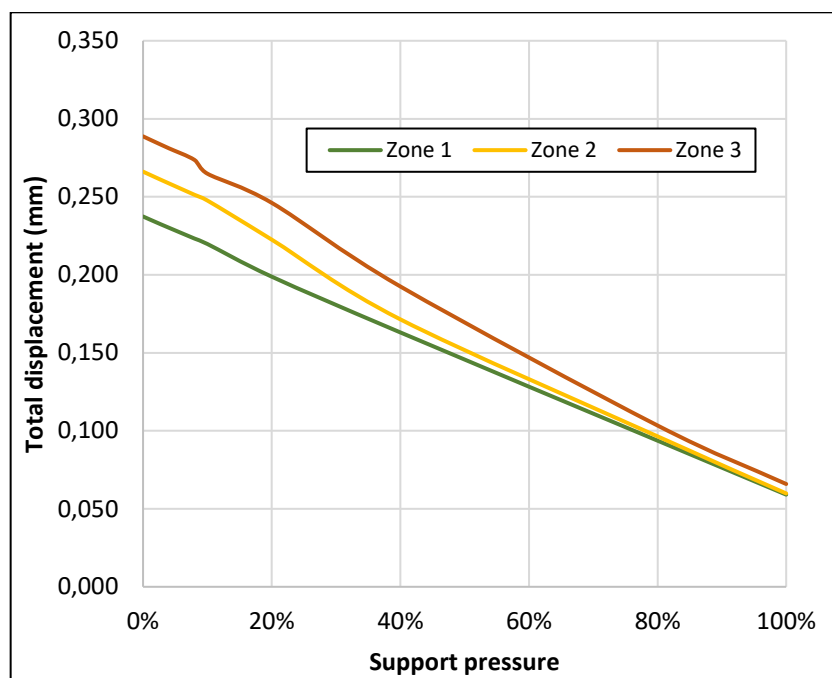


Figure 6.18: Total displacement on the tunnel crown

Similarly, the total displacement on the skin of the excavation was compared for both side walls. The comparisons are presented in Figure 6.19 and Figure 6.20. In Zone 3, the total displacement on both sidewalls is concentrated. This gradually reduces as the fracturing intensity reduces. Although the support pressure is 100%, displacement is still expected to happen on the sidewalls.

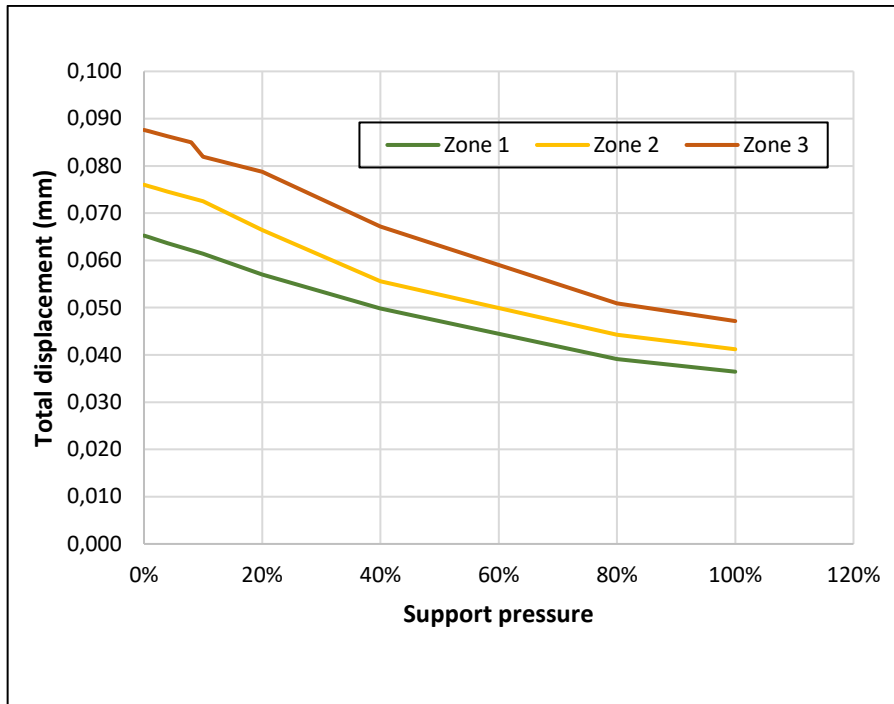


Figure 6.19: Total displacement on the left sidewall

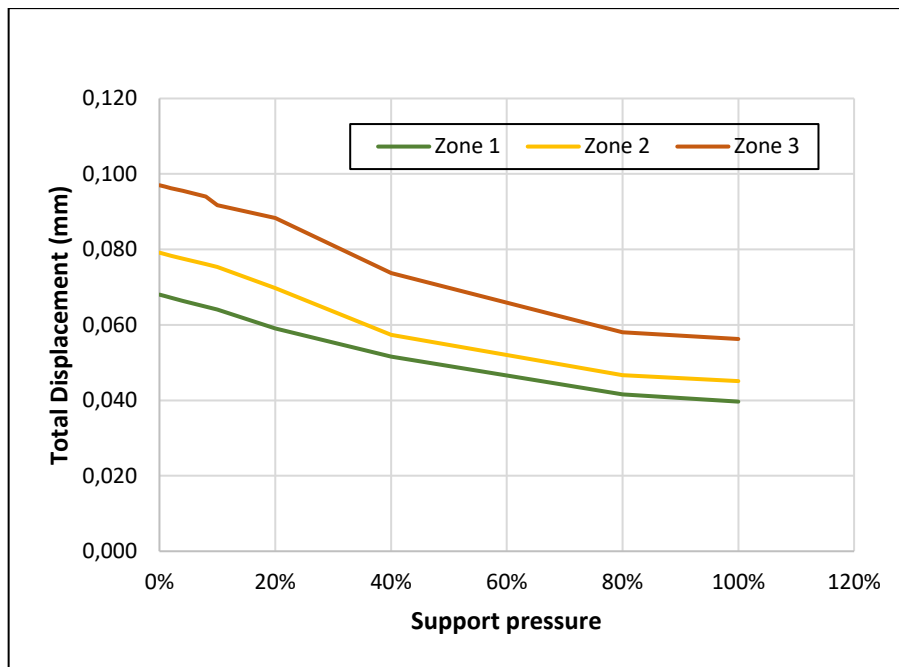


Figure 6.20: Total displacement on the right sidewall

Owing to the identified displacements in Zones 1-3, there is need for support lining to enhance stability and minimise the expected displacement that can happen when support pressure is 100%.

6.4. Design of tunnel lining based on factor of safety.

Having identified the zones prone to high displacement, it is critical to design support lining that will enhance the stability of the tunnel and reduce the possibility of fracturing. This section proposes a tunnel lining support system for shallow tunnels based on the predictive model developed in this study. Table 6.2 summarises the support lining parameters used for the support design. The proposed support design parameters were selected in RS2, from the basis that the Hendrik Verwoerd tunnels are supported with roof bolts and reinforced concrete.

Table 6.2: Support design parameters

Lining composite		
Support unit type	Properties	Value
Liner 1: Geosynthetic	Tensile modulus	0.2MN/m
Liner 2: Reinforced concrete	Equivalent Young's modulus	36063.6MPa
	Equivalent thickness	0.2m/0.3m/0.4m
Bolt parameters		
End anchored bolt	Diameter	19mm
	Length	2m
	Spacing	1m
	Tensile capacity	0.1 MN
	Young's modulus	200000 MPa

Prior to support installation in Zone 1, major principal stresses are very high on the bottom corners of the tunnel (Figure 6.21a). However, upon installation the level of stress slightly decreases (Figure 6.21b). Similarly, the total displacement before and after support was compared as shown in Figure 6.22. The installed support has reduced the total displacement on the skin of the tunnel.

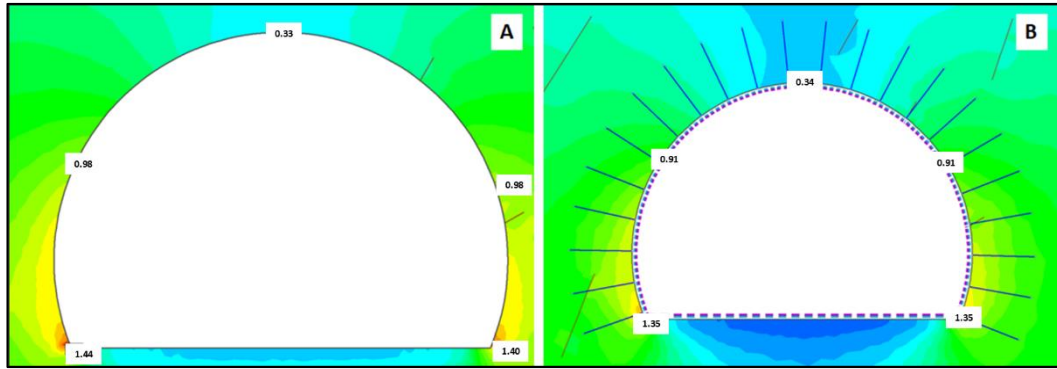


Figure 6.21: Major Principal stress in Zone 1 before and after support installation

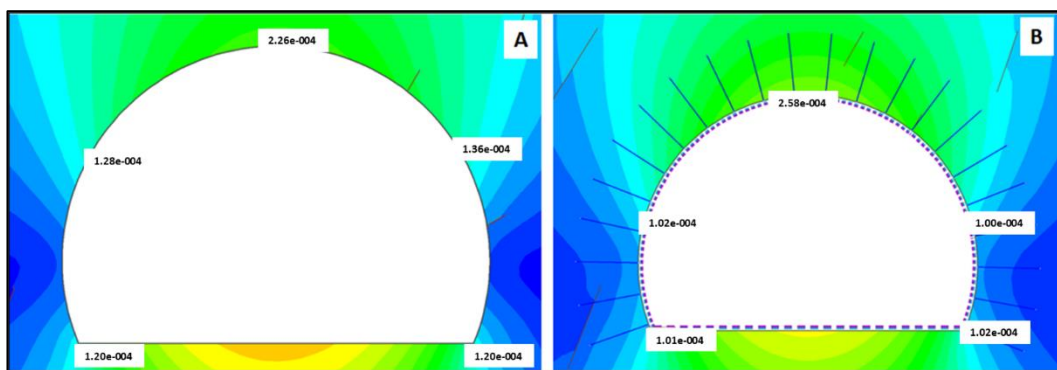


Figure 6.22: Total displacement in Zone 1 before and after support installation

Support capacity diagrams were used to determine feasibility of the proposed reinforced concrete lining to stabilise the tunnel. This technique assesses each part of the tunnel boundary for a given factor of safety. For this thesis, the benchmark factor of safety is 1. Nonetheless, the support will be tested against a range of factors of safety (i.e., 1 to 1.6). The support capacity diagrams are plotted with envelopes of the benchmark factor of safety. Four diagrams are used to analyse the overall stability of the tunnel upon application of the lining support. If the computed liner values fall outside or on the envelope, the proposed lining material would not be able to support the tunnel to its required stability. For a lining material to be acceptable, all the computed values must fall within the envelope.

In Zone 1, the reinforced concrete lining thickness was set to be 0.2m because the zone is characterised by little or no fracturing. Support capacity diagrams for Zone 1 are presented in Figure 6.23.

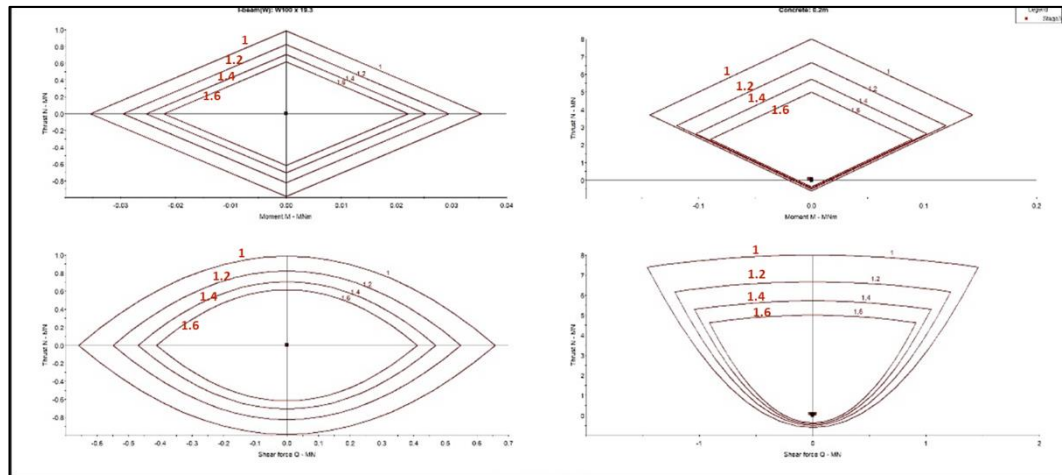


Figure 6.23: Support capacity diagrams for Zone 1

The support capacity diagrams for Zone 1 indicate that for all the points simulated on the tunnel lining, there is no outlier. The proposed support lining is stable; hence all the points are within the boundaries of the factor of safety.

The same support properties used in Zone 1 were used to evaluate major principal stress and total displacement in Zone 2 and 3. The only difference is that the concrete lining thickness was increased from 0.2m to 0.3m and 0.4m in Zone 2 and Zone 3 respectively. The change in concrete thickness is proposed to cater for the expected fracturing intensity when transitioning from Zone 2 to Zone 3. Figure 6.24 to Figure 6.27 show the effectiveness of the proposed support in lowering the major principal stress and total displacement around the tunnel skin.

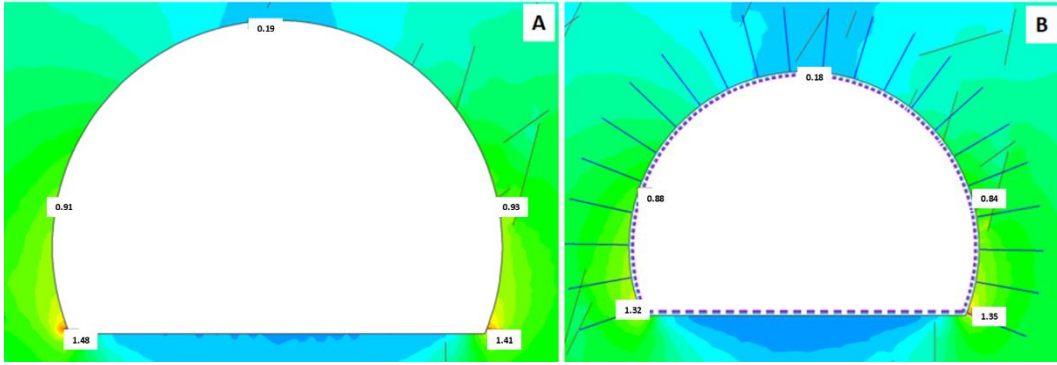


Figure 6.24: Major principal stress in Zone 2 before and after support installation

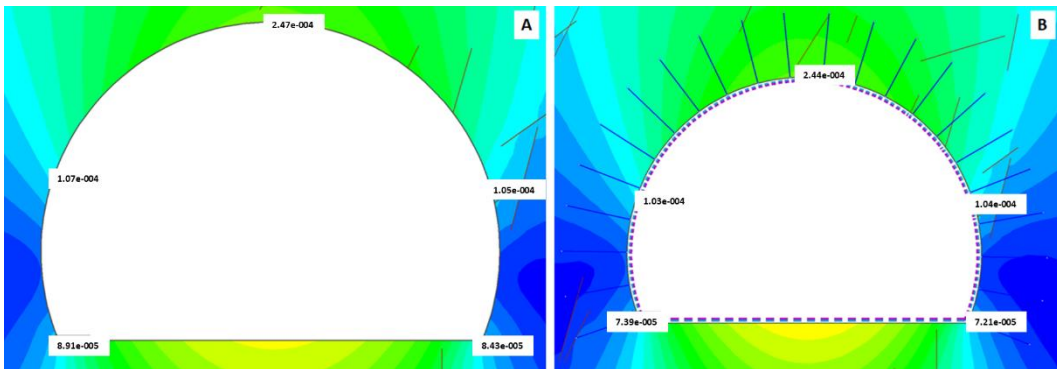


Figure 6.25: Total displacement in Zone 2 before and after support installation

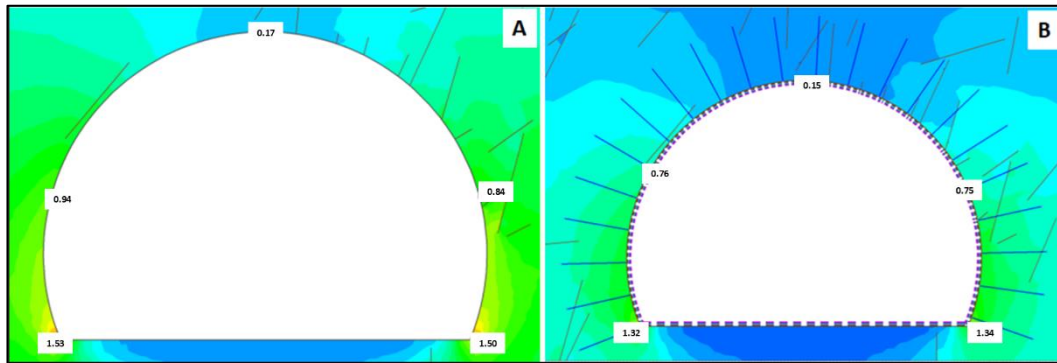


Figure 6.26: Major principal stress in Zone 3 before support installation

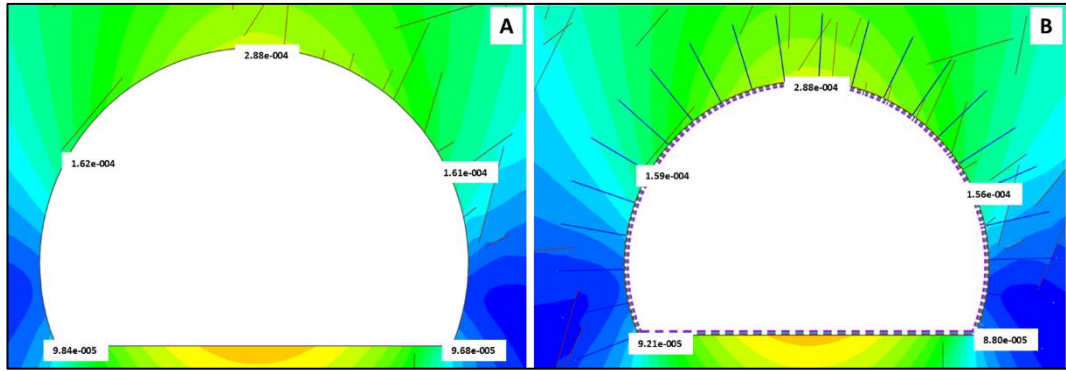


Figure 6.27: Total displacement in Zone 3 before and after support installation

Likewise, support capacity diagrams were used to evaluate the proposed support for Zone 2 and Zone 3 where the concrete lining thickness is 0.3m and 0.4m respectively. In both cases, the proposed support is stable (see Figure 6.28 and Figure 6.29).

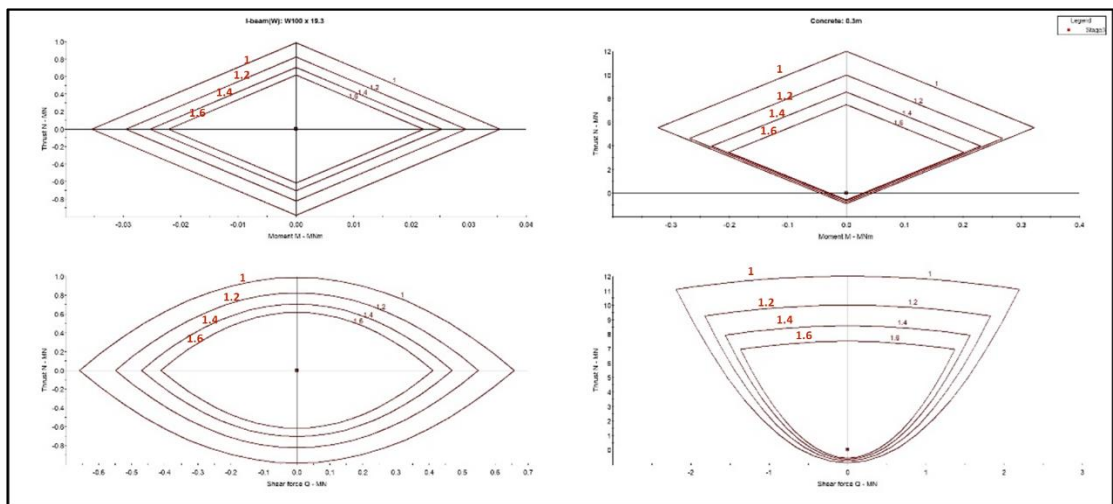


Figure 6.28: Support capacity diagrams for Zone 2

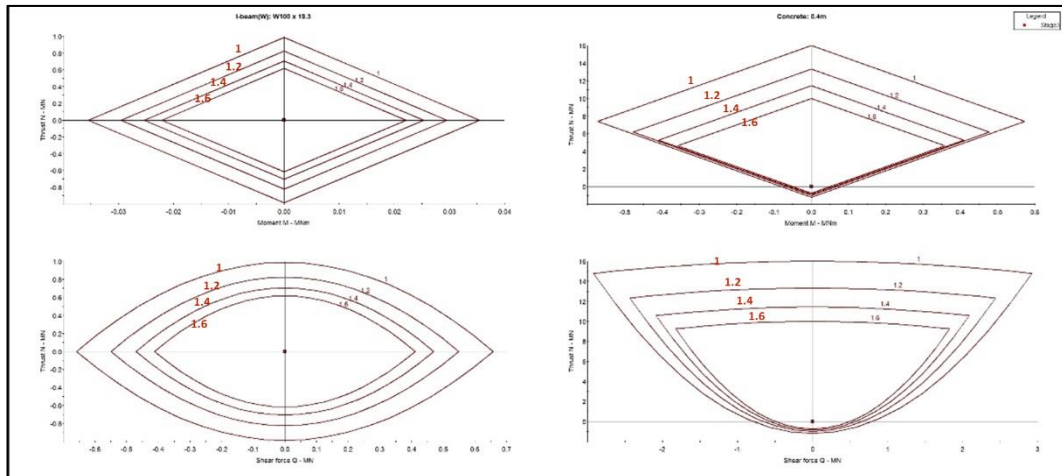


Figure 6.29: Support capacity diagrams for Zone 3

To summarise this section, it can be concluded that the proposed support lining is applicable to shallow tunnels. The following major stresses and total displacements are evidence that increasing the concrete lining improves the overall effects of fracturing on tunnel stability. According to Figure 6.30, the values of the major principal stresses and total displacement were entered into Table 6.3 and Table 6.4, respectively, for each point on the tunnel skin. Readings were taken before and after support installation for each point in each zone. Table 6.3 and Table 6.4 summarise the total displacements and major principal stress before and after support installation respectively. Figure 6.30, on the other hand, illustrates the points evaluated before and after support installation.

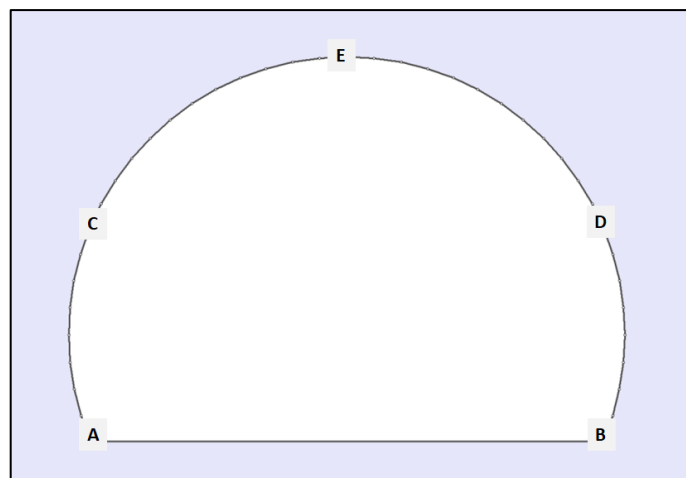


Figure 6.30: Points evaluated before and after support installation.

According to Figure 6.30, the values of the major principal stresses and total displacement were entered into Table 6.3 and Table 6.4, respectively, for each point on the tunnel skin. Readings were taken before and after support installation for each point in each zone. After the support is provided, there is a corresponding increase in displacement in Zone 1 column E. Because of confinement effects, arching effects, stiffness contrast, and load redistribution, the provision of support in a shallow tunnel may result in an increase in principal stress and displacement.

Table 6.3: Major principal stresses (in MPa) before and after support installation

Zone	Position along the tunnel					
		A	B	C	D	E
1	<i>Before</i>	1.44	1.40	0.98	0.98	0.33
	<i>After</i>	1.35	1.35	0.91	0.91	0.34
2	<i>Before</i>	1.48	1.41	0.91	0.93	0.19
	<i>After</i>	1.32	1.35	0.88	0.84	0.18
3	<i>Before</i>	1.53	1.50	0.94	0.84	0.17
	<i>After</i>	1.32	1.34	0.76	0.75	0.15

Table 6.4: Total displacement (m) before and after support installation

Zone	Position along the tunnel					
		A	B	C	D	E
1	<i>Before</i>	0.000120	0.000120	0.000128	0.000136	0.000226
	<i>After</i>	0.000101	0.000102	0.000102	0.000100	0.000258
2	<i>Before</i>	0.000089	0.000084	0.000107	0.000105	0.000247
	<i>After</i>	0.000074	0.000072	0.000103	0.000104	0.000244
3	<i>Before</i>	0.000098	0.000097	0.000162	0.000161	0.000288
	<i>After</i>	0.000092	0.000088	0.000159	0.000156	0.000288

6.5. Conclusions

This chapter aimed at understanding the effects of fracturing on strength factor and total displacement of shallow tunnels. This was achieved by conducting simulations using Optum G2 and RS2 software packages. Results obtained from rendered simulations using the selected computer programmes indicated that indeed fracturing has an impact on the overall tunnel stability.

Firstly, the strength reduction factor analysis conducted in Optum G2 show that when there is no support installed the tunnel is not stable. SRF in all three zones was found to be below 1. Hence the need for support is critical. Moreover, areal support in the form of reinforced concrete is deemed important for such environments.

Secondly, the total displacement simulations rendered in RS2 show that total displacement is concentrated at the skin of the tunnel and lessens when moving away from the tunnel. Similarly, the major principal stresses were analysed around the tunnel before and after support installation. Results show that the proposed support for each zone can stabilise the tunnel based on the factor of safety rendered using support capacity diagrams.

In conclusion, the effects of fracturing in the three zones of the tunnel pose varying threats to the overall stability of the tunnel. Through observing the effect of fracturing in each zone separately, it can be concluded that the three zones of road tunnels should be treated differently. This will enable researchers to design appropriate support system for long term stability.

7. Chapter 7: Conclusions and Recommendations for Future Research

Road tunnels are engineering structures which evolve with time. The effective design and continuous stability analysis of such structures is critical for their long-term use. The main aim of this thesis was to predict fracture distribution along road tunnels using the Hendrik Verwoerd tunnels along the N1 in the Limpopo Province as case studies. This chapter seeks to summarise the overall findings of the thesis.

7.1. Summary of the thesis

This thesis explored the use of machine learning together with advanced geomechanics approaches as an alternative to fuzzy inference systems to establish tunnel deterioration. The application of machine learning and advanced geomechanics approaches was suggested to improve the design of support lining. The Hendrik Verwoerd tunnels along the N1 in Limpopo Province, South Africa, were used as case studies for this thesis. Data was collected at the site by means of field observations and measurements. In addition, rock samples were collected for thin section laboratory experiment.

The rock mass around the periphery of the tunnels was assessed using finite element modelling approaches. Field measurements were conducted at the study area, and mapping of geological structures was done on the exposed slope of the tunnels. Kinematic analysis was used to determine the possible modes of failure along the exposed rock mass in the vicinity of the tunnel. The rock mass behaviour around the tunnel was primarily rated through GSI method. This was used to later estimate the rock mass properties in the periphery of the tunnel using the RocLab software. In this software, the Hoek-Brown parameters were estimated. These properties were later used as input data for numerical simulations.

A predictive model for fracture distribution along road tunnels was developed using supervised machine learning (linear regression). To develop a predictive model, images from the thin section laboratory experiment were analysed. The analysis was grounded on micro-fracturing with the understanding of rock fracture mechanism. Three key microfractures were identified, which are grain boundary (GB) cracks, inter-angular (IA) cracks and trans-angular (TA) cracks. The distribution of these fractures was studied for both the left and right side of the tunnel. Total number of fractures in the vicinity of the tunnel were high and reduced when moving away from the tunnel. Machine learning was used to develop a predictive model for fracture distribution. A linear regression algorithm was applied to predict the fracture distribution within the tunnel. This algorithm is best suitable for predictive models provided there is historical known data. In this thesis, the trend of fracture distribution on the slope of the tunnels was used as historical data to develop a predictive model. Finally, a predictive chart for fracture distribution in shallow tunnels was developed. The model demonstrated that the expected number of fractures is extremely high at the tunnel face and gradually decreases to intermediate and finally low levels in the middle portions of the tunnel.

It is a typical occurrence in shallow tunnelling to have a large number of fractures at the tunnel face as shown in the model. The rock mass surrounding a shallow tunnel excavation is significantly disturbed and the distribution of stress is altered, which can cause fracturing. The rock mass around the tunnel gradually adapts to the changes in stress and displacement as it moves deeper into the ground and farther away from the face. Moving towards the middle of the tunnel, the number of fractures decreases as a result of this adjustment process, which lowers the possibility of additional fractures developing. It is important to note that the precise number of fractures can vary depending on a number of factors. These factors include the particular geological conditions, the excavation technique, the support system used, and the level of tunnel construction expertise. Overall, the high number of fractures at the tunnel face and the

gradual decrease towards the middle portions of the tunnel is a well-recognised behaviour in shallow tunnelling. This behaviour draws attention to the significance of implementing appropriate support measures to ensure the stability and safety of the tunnel structure.

The intensity of fracturing affects the total displacement of the tunnel. The effect of fracturing on total displacement was evaluated using RS2 software. For each zone the total displacement was evaluated from the skin of the excavation to 10m away from the excavation. This evaluation was conducted on the crown and side walls of the tunnel. Results from the simulation in this study showed that there is more displacement on the crown of the excavation. On the side walls there is minimal displacement observed, which fades away when the distance from the tunnel increases. Furthermore, when comparing total displacement on the skin of the tunnel for each Zone, it was found that Zone 3 is prone to more total displacement than Zones 1 and 2. This is because of the intensity of fracturing expected in Zone 3. In essence, the higher the fracturing intensity, the more the total displacement is expected. Additionally, it is anticipated that exposed rock will fracture more frequently than non-exposed rock (i.e., less fracture at the middle of the road tunnels and more at the entrance).

The best support lining for shallow road tunnels was suggested. Based on the predictive model and the total displacement analysis, it was deemed essential that support be designed for each zone individually. The proposed support comprises of rock bolts and reinforced concrete lining. The major principal stress and total displacement on the skin of the tunnel were compared before and after support installation. Although the bolt length, diameter, strength and concrete properties used in the three Zones is the same, the lining thickness differs. In Zone 3, the proposed lining was 0.4m because the ground is highly fractured in this zone. In Zones 1 and 2, the lining thickness was proposed to be 0.2m and 0.3m respectively. The suggested support was further evaluated using support capacity diagrams.

In all three zones, the proposed support was within factor of safety envelope range (1-1.6). Therefore, the support will stabilise the tunnel.

7.2. Techniques, analysis, and findings

In this section, the analysis and findings of the study are presented, focusing on the techniques employed, analysis statements, and other key observations. The aim is to provide a comprehensive understanding of the selected methods and their implications for tunnel stability. This section also presents the arguments and results obtained through the analysis, highlighting their significance and relevance to the research objectives.

The first technique utilised in this study was field observation and geotechnical data collection. This data includes geological information, rock properties, and any available data on fractures or discontinuities. Geotechnical data is critical because it serves as input for numerical modelling. Finite element modelling provides a powerful tool to assess the behaviour of the rock mass around tunnel peripheries. It allows engineers to evaluate the influence of various factors on stability, deformations, and stress redistribution. The insights gained from these models can inform support design, excavation sequencing, and risk mitigation strategies for tunnel construction and operation.

The second technique was to use microfractures to understand the fracture distribution along shallow tunnels. The presence and distribution of fractures can affect the stability analysis of the tunnel. Fractures act as planes of weakness in the rock mass, reducing its overall strength and cohesion. When conducting stability analysis, it is important to consider the orientation, spacing, and persistence of fractures to accurately assess the stability of the tunnel. The influence of geological conditions on tunnel stability was evident. The analysis statements revealed variations in the behaviour of different rock formations, emphasizing the need for site-specific assessments and tailored support designs. The presence of fractures influences the design and selection of appropriate support

measures. Fractured rock masses may require additional support elements, such as rock bolts, shotcrete, steel ribs, or ground anchors, to stabilise the tunnel and prevent rock mass deformation or collapse.

Lastly, the effect of fracturing on total displacement was assessed and support strategy was suggested. Assessing the effect of fracturing on total displacement was important for understanding the behaviour and stability of a tunnel. Fractures can contribute to increased displacement by allowing the surrounding rock mass to deform more easily or by causing localised instabilities. Once the impact of fracturing on total displacement was evaluated, a support strategy was suggested to mitigate the potential risks. The suggested support strategy was based on a comprehensive understanding of the geological and geotechnical conditions, analysis of the predicted displacements and fracturing patterns. Ultimately, the support strategy aims to provide a stable and safe environment for the tunnel, considering the potential effects of fracturing on total displacement and ensuring the long-term performance of the structure.

In summary, the analysis and findings presented in this section demonstrate the effectiveness of the selected techniques in assessing tunnel stability. The arguments put forward support the notion that a method that can accurately estimate total displacement and examine the distribution of microfractures can result in a thorough comprehension of tunnel stability. By developing such a method, important insights into the complex nature of microfracture distribution and its effect on tunnel integrity can be gained. Furthermore, by precisely determining total displacement, the stability of the tunnel construction as a whole can be effectively evaluated. This hypothesis states that this research may considerably improve the understanding of tunnel stability and take precautions to assure safe and long-term underground infrastructure through using a reliable technique for predicting microfracture distribution and total displacement.

7.3. Original contribution

In this thesis, thin section analysis was used to gather data for microfracturing that is expected in the rock mass. Most researchers tend to lean towards traditional methods of data collection when conducting such research. In this thesis a different avenue was explored to utilise micro fracture and project the results from a micro scale to a large scale. This was achieved with ML where supervised learning was applied. Linear regression was used to develop a predictive model based on the data extracted from micro fracture images that were analysed. The model estimates the number of cracks (y) as a function of the distance along the tunnel (x) as expressed in Equation (5.1) in Chapter 5.

Upon developing the predictive model, simulations were rendered to further comprehend the effect of fracturing on road tunnels. This aided the researcher to propose a support mechanism for each zone of the tunnel. The proposed support comprises of rock bolts and reinforced concrete lining. Regarding reinforced concrete lining, the thickness of the lining varies by 0.1m. If lining thickness in Zone 1 is 0.2m, lining thickness in Zone 2 and Zone 3 should be 0.3m and 0.4m respectively. This was proposed to cater for different predicted fracturing intensities. Therefore, the tunnel can remain stable over time.

This thesis hypothesised that by devising a technique for estimating microfracture distribution and total displacement, tunnel stability can be understood (Section 2.7 of Chapter 2). Indeed, the hypothesis has been proven. The findings from the research done in this thesis bring forth useful data on tunnel convergence prediction based on fracture distribution analysis.

7.4. Overall conclusion of the thesis

The purpose of this thesis was to predict the fracture distribution along road tunnels through advanced geomechanics approaches and machine

learning. The Hendrik Verwoerd tunnels were used as case studies to achieve this.

Based on the findings from the field observations and measurements; laboratory experiments, and numerical simulations executed, it can be concluded that fracturing has an impact on tunnel stability. Therefore, the effect of fracturing and fracture distribution along road tunnels should be considered in the support design. Designing support for each zone individually based on the predictive model and total displacement analysis is a prudent approach in tunnel engineering. By considering the unique characteristics and behaviour of each zone, the support system can be tailored to address the specific challenges and ensure the overall stability of the tunnel. A typical and reliable combination for tunnel support is rock bolts and reinforced concrete lining. Typically, rock bolts are used to strengthen the surrounding rock mass and add strength and stability. On the other hand, reinforced concrete lining gives the tunnel structural support and aids in distributing the loads that are placed on it. By combining rock bolts and reinforced concrete lining, the proposed support system addresses both the reinforcement of the rock mass and the structural integrity of the tunnel. Rock bolts help stabilise the surrounding rock, reducing the likelihood of fractures and rockfall, while the reinforced concrete lining provides a robust structural element to withstand the applied loads and maintain the shape of the tunnel.

The specific design and implementation of the support system would depend on various factors, including the geological conditions, the anticipated loads, and the available construction techniques. The proposed strategy should be considered as a starting point towards detailed analysis and design of the appropriate support for shallow road tunnels. Generally, if the overall proposed lining for a new road tunnel is designed to be 0.3m then the inner portion (referred to as Zone 1) should have lining of 0.3m thick. Zone 2 should have a lining 0.4m (0.3m + 0.1m) thick and Zone 3 should have 0.5m (0.3m + 0.2m) thick. This approach is suggested to

enhance the stability of the tunnel over a period of time. Finally, the expertise of geotechnical engineers and tunnel designers is crucial in determining the appropriate design parameters and ensuring the effectiveness of the proposed support system.

7.5. Recommended future research.

Based on the findings in this thesis, the following is suggested for future research:

- Alternative avenues of solving complex tunnelling problems without the use of Fuzzy set theory.
- Using Particle Flow Code (PFC0 3D) for phenomenological simulations.
- The use of image analysis on microfracture results from thin section laboratory experiment to classify and quantify micro fractures.
- Predicting road tunnel deformation through GPR scanning and advanced geo-mechanical approaches.

LIST OF REFERENCES

Abbas, D., Mohammad, A., Farhang, S., 2011. Assessment of rock slope stability using the Fuzzy Slope Mass Rating (FSMR) system. *Applied Soft Computing*, vol. 11, no. 8, pp. 4465 – 4473.

Adoko, A.C., Zuo, Q.-J., Wu, L., 2011. A fuzzy model for high-speed railway tunnel convergence prediction in weak rock. *Electronic Journal of Geotechnical Engineering*, vol. 16, pp. 1275 – 1295.

Adoko, A.C., Gokceoglu, C., Wu, L., Zuo, Q.J., 2013a. Knowledge-based and data driven fuzzy modelling for rockburst prediction. *International Journal of Rock Mechanics and Mining Sciences*, vol. 61, pp. 86 – 95.

Adoko, A.C., Wang, H., Jiao, Y.Y., Seitsh, I.T., 2016. Developing the Ground Index (GI) for rock collapse assessment in tunneling. *The 50th US Rock Mechanics/Geomechanics Symposium*, Houston, 26 – 29 June 2016, Houston, Texas, American Rock Mechanics Association.

Adoko, A.C., Wu, L., 2011. Fuzzy inference systems-based approaches in geotechnical engineering – a review. *Electronic Journal of Geotechnical Engineering*, vol. 16, no. 1, pp. 1543 – 1558.

Adoko, A.C., Wu, L., 2012. Estimation of the convergence of high-speed railway tunnel in weak rock using an Adaptive Neuro-Fuzzy Inference Systems (ANFIS) approach. *Journal of Rock Mechanics and Geotechnical Engineering*, vol. 4, no. 1, pp. 11 – 18.

Adoko, A.C., Yagiz, S., 2018. Fuzzy inference system-based for TBM field penetration index estimation in rock mass. *Geotechnical and Geological Engineering*, vol. 37, no. 3, pp. 1533 – 1553

Adoko, A.C., Jiao, Y.Y., Wu, L., Wang, H., Wang, Z.H., 2013b. Predicting tunnel convergence using Multivariate Adaptive Regression Spline and Artificial Neural Network. *Tunnelling and Underground Space Technology*, vol. 38, pp. 368 – 376.

Aksoy, C.O., 2008. Review of rock mass rating classification: Historical developments, applications, and restrictions. *Journal of Mining Science*, vol. 44, no. 1, pp. 51 – 63.

Alhaddad, M., Dewhirs, M., Soga, K., Devriendt, M., 2019. A new photogrammetric system for high-precision monitoring of tunnel deformations. *Proceedings of the Institution of Civil Engineers – Transport*, vol. 172, no. 2, pp. 81 – 93.

Ali, F.C., Abdulkadir, C., Candan, G., 2012. Some applications of Adaptive Neuro-Fuzzy Inference System (ANFIS) in geotechnical engineering. *Computers and Geotechnics*, vol. 40, pp. 14 – 33.

Alloghani, M., Al-Jumeily, D., Mustafina, J., Hussain, A., Aljaaf, A.J, 2020. A systematic review on supervised and unsupervised machine learning algorithms for data science. In: Berry, M.W., Mohamed A., Yap, B.W. (Eds). *Supervised and Unsupervised Learning for Data Science*. Springer International Publishing, Cham, pp. 3 – 21.

Anders, M.H., Laubach, S.E., Scholz, C.H., 2014. Microfractures: A review. *Journal of Structural Geology*, vol. 69, pp. 377 – 394.

Asadi, M., 2016. Optimized Mamdani fuzzy models for predicting the strength of intact rocks and anisotropic rock masses. *Journal of Rock Mechanics and Geotechnical Engineering*, vol. 8, pp. 218 – 224.

Azimi, Y., Osanloo, M., Aakbarpour-Shirazi, M., Aghajani, B.A., 2010. Prediction of the blastability designation of rock masses using fuzzy sets. *International Journal of Rock Mechanics & Mining Sciences*, vol. 47, no. 7, pp. 1126 – 1140.

Barker, O.B., Brandl, G., Callaghan, C.C., Erikson, P.G., van der Neut, M., 2006. The Soutpansberg and Waterburg Groups and the Blouberg formation. In: Anhaeusser, M.R., Thomas, C.R., Johnson, R.J. (Eds). *The*

Geology of South Africa, Geological Society of South Africa, pp. 301 – 324, Council for Geosciences, Pretoria.

Barton, N., Lien, F., Lunde, J., 1974. Engineering classification of rock masses for the design of tunnel support. *Rock Mechanics*, vol. 6, no. 4, pp. 189 – 236.

Basarir, H., Karpuz, C., Tutluoğlu, L., 2007. A fuzzy logic based rippability classification system. *Journal of the Southern African Institute of Mining and Metallurgy*, vol. 107, no. 12, pp. 817 – 831.

Benoit, L., Briole, P., Martin, O., Thom, C., 2014. Real-time deformation monitoring by a wireless network of low-cost GPS. *Journal of Applied Geodesy*, vol. 8, no. 2, pp. 119 – 128.

Bieniawski, Z.T., 1973. Engineering classification of jointed rock masses. *Transaction of the South African Institution of Civil Engineers*, vol 15, pp. 335 – 344.

Bieniawski, Z.T., 1974. Geomechanics classification of rock masses and its application in tunneling. *International Society of Rock Mechanics (ISRM)*, Denver, pp. 27 – 32.

Bieniawski, Z.T., 1979. The geomechanics classifications in rock engineering applications. *International Congress on Rock Mechanics*, Montreux, pp. 41 – 48.

Bieniawski, Z.T., 1988. Rock mass classification as a design aid in tunneling. *Tunnels and Tunnelling International*, vol. 20, no. 7, pp. 19 – 22.

Bieniawski, Z.T., 1989. *Engineering rock mass classifications: a complete manual for engineers and geologists in mining, civil, and petroleum engineering*. John Wiley and Sons, ISBN: 978-0-471-60172-2.

Bieniawski, Z.T., 1976. Rock mass classification in rock engineering. Bieniawski, Z.T., Eds., Symposium Proceedings of Exploration for Rock Engineering, no. 1, pp. 97 – 106, Balkema, Cape Town.

Black, M., 1937. Vagueness: An exercise in logical analysis. Philosophy of Science, vol. 4, no. 4, pp. 427 – 455.

Blej, M., Azizi, M., 2016. Comparison of Mamdani-type and Sugeno-type fuzzy inference systems for fuzzy real time scheduling. International Journal of Applied Engineering Research, vol. 11, no. 22, pp. 11071 – 11075.

Boidy, E., 2002. Modélisation numérique du comportement différé des cavités souterraines. Thèse de Doctorat. Université Joseph Fourier-Grenoble I, Grenoble.

Boidy, E., Bouvard, A., Frederic, P., 2002. Back analysis of time-dependent behaviour of a test gallery in claystone. Tunnelling and Underground Space Technology, vol. 17, no. 14, pp. 415 – 424.

Brandl, G., 1981. The geology of the Messina area. Sheet 2230, Messina: Geology Survey of South Africa. Report number, 35.

Brandl, G., 1986. The geology of Pieterburg area. Explain. Sheet 2230, Geology Survey of South Africa, Pietersburg, Report number, 43.

Brown E.T., Bray, J.W., Landanyi, B., Hoek, E., 1983. Ground response curves for rock tunnels. Journal of Geotechnical Engineering, vol. 109, no. 1, pp. 15 – 39.

Bunker, R., Thabtah, F., 2017. A machine learning framework for sport result prediction. Applied Computing and Informatics, vol. 15, no. 1, pp. 27 – 33.

Cao, B. T., Freitag, S., Meschke, G., 2018. A fuzzy surrogate modelling approach for real-time. International Journal of Reliability and Safety, vol. 12, no. 1/2, pp. 187 – 217.

Carranza-Torres, C., Fairhurst, C., 2000. Application of the convergence-confinement method of tunnel design to rock-masses that satisfy the Hoek-Brown failure criterion. *Tunnelling and Underground Space Technology*, vol. 15, no. 2, pp. 187 – 213.

Çelikyılmaz, A., Turksen, I. B., 2009. Modeling uncertainty with fuzzy logic with recent theory and applications. Springer-Verlag, Berlin Heidelberg.

Chaminé, H.I., Afonso, M.J., Ramos, L., Pinheiro, R., 2015. Scanline sampling techniques for rock engineering surveys: Insights from intrinsic geologic variability and uncertainty. In: *Engineering Geology for Society and Territory*, Springer International Publishing, Switzerland, pp. 357 – 361.

Chen, C.-F., Xiao, Z.-Y., Zhang, G. B., 2011. Stability assessment model for epimetamorphic rock slopes based on adaptive neuro-fuzzy inference system. *Electronic Journal of Geotechnical Engineering*, vol. 16 (Bund. A), pp. 93 – 107.

Chetan, S., 2021. CS Electrical and Electronics, Electrical, Electronics, Programming, Technology. [Online] Available at: <https://www.cselectricalandelectronics.com/what-is-fuzzy-logic-working-advantages-disadvantages-applications/> [Accessed 26 May 2021].

Compilation, G., 2007. TB 10121-2007 Technical code for monitoring measurement of railway tunnel. China Railway Press, Beijing.

Cristescu, N., Hunsche, U., 1998. Time effects in rock mechanics. Wiley, West Sussex.

Cristescu, N., 1985. Viscoplastic creep of rocks around horizontal tunnels. *International Journal of Rock Mechanics, Mineral Science and Geomechanics Abstracts*, vol. 22, no. 6, pp. 453 – 459.

Cristescu, N., 1988. Viscoplastic creep of rocks around a lined tunnel. *International Journal of Plasticity*, vol. 4, no. 4, pp. 393 – 412.

Cristescu, N., 1994. Time effect in rocks surrounding a horizontal tunnel. In: Nelson, P.P., Laubach, S.E., (Eds). Proceedings of the 1st NARMS Symposium Rock Mechanics. Models and Measurements. Challenges from Industry, Balkema, Rotterdam, pp. 657 – 664.

Cundall, P.A., 1971. Computer model for simulating progressive large-scale movements in blocky rock systems. Society for Rock Mechanics (ISRM), International Society for Rock Mechanics, France.

Dai, T., Xie, D., Yao, H., Li, G., 2011. Establishment of grey system model about tunnel surrounding rock convergence and information renewal GM(1,1) model forecasting. In: Proceedings of the International Conference on Remote Sensing, Environment and Transportation Engineering (RSETE 2011), Springer, Berlin, pp. 310 – 314.

Deere, D.U., Hendron, A.J., Patton, F.D., Cording, E.J., 1967. Design of surface and near surface construction in rock. Failure and Breakage of Rock, Proceedings of the 8th US Symposium of Rock Mechanics, New York, pp. 237 – 302.

Diederichs, M.S., Lato, M., Quinn, P., Hammah, R., 2007. Shear strength reduction approach for slope stability analyses. Rock Mechanics: Meeting Society's Challenges and Demands, pp. 319 – 327.

Dubois, D., Prade, H., 2012. Gradualness, uncertainty and bipolarity: Making sense of fuzzy sets. Fuzzy Sets and Systems, vol. 192, pp. 3 – 24.

Elbaz, K., Shen, S., Zhou, A., Yuan, D., Xu, Y., 2019. Optimization of EPB shield performance with adaptive neuro-fuzzy inference system and genetic algorithm. Applied Sciences, vol. 9, no. 4, pp. 1 – 17.

Erlandsson, O., 2020. Comparison of total convergence measurement methods. Master's Dissertation, KTH, School of Architecture and the Built Environment (ABE), Real Estate and Construction Management, Sweden.

Frenelus, W., Peng, H., Zhang, J., 2021. Long-term degradation, damage and fracture in deep rock tunnels: A review on the effect of excavation methods. *Frattura ed Integrità Strutturale*, vol. 15, pp. 128 – 150.

Gama, C.D., 2004. A method for continuous monitoring of tunnel deformations during construction and service phases. *EUROCK2004*, Salzburg, pp. 251 – 254.

Ghadimi Chermahini, A., Tahghighi, H., 2019. Numerical finite element analysis of underground tunnel crossing an active reverse fault: a case study on the Sabzkouh segmental tunnel. *Geomechanics and Geoengineering*, vol. 14, no. 3, pp. 155 – 166.

Ghamgosar, M., 2017. Micromechanical and microstructural aspects affecting rock damage, fracture and cutting mechanisms. Doctor of Philosophy Thesis. University of Queensland, Australia.

Ghasemi, E., Ataei, M., 2013. Application of fuzzy logic for predicting roof fall rate in coal mines. *Neural Computing and Applications*, vol. 22, no. 1, pp. 311 – 321.

Gökceoğlu, C., Yesilnacar, E., Sonmez, H., Kay, A., 2004. A neuro-fuzzy model for modulus of deformation of jointed rock masses. *Computers and Geotechnics*, vol. 31, no. 5, pp. 375 – 383.

Gökceoğlu, C., Zorlu, K., 2004. A fuzzy model to predict the uniaxial compressive strength and the modulus of elasticity of a problematic rock. *Engineering Applications of Artificial Intelligence*, vol. 17, no. 1, pp. 61 – 72.

Google Maps, 2022. Google. [Online] Available at:
<https://www.google.com/maps/place/Hendrik+Verwoerd+Tunnel./@-24.3058559,27.5829743,7z/data=!4m6!3m5!1s0x0:0x1eb517e994a7d550!4b1!8m2!3d-22.915636!4d29.9278755!5m1!1e4> [Accessed 23 05 2022].

Grima, A.M., Bruines, P.A., Verhoef, P.N.W., 2000. Modeling tunnel boring machine performance by neuro-fuzzy methods. *Tunnelling and Underground Space Technology*, vol. 15, no. 3, pp. 259 – 269.

Grimstad, E., Barton, N., 1993. Updating of the Q-system for NMT. Norwegian Concrete Association, Fagernes, Oslo, Norway, pp. 44 – 66.

Gumede, H., Stacey, T.R., 2007. Measurement of typical joint characteristics in South African gold mines and the use of these characteristics in the prediction of rock falls. *Journal of the Southern African Institute of Mining and Metallurgy*, vol. 107, no. 5, pp. 335 – 344.

Gupta, V., Bhasin, R.K., Kaynia, A.M., Kumar, V., Saini, A.S., Tandon, R.S., Pabst, T., 2016. Finite element analysis of failed slope by shear strength reduction technique: a case study for Surabhi Resort Landslide, Mussoorie township, Garhwal Himalaya. *Geomatics, Natural Hazards and Risk*, vol. 7, no. 5, pp.1677 – 1690.

Hammah, R.E., Yacoub, T.E., Corkum, B.C., Curran, J.H., 2005, June. The shear strength reduction method for the generalized Hoek-Brown criterion. In: *ARMA US Rock Mechanics/Geomechanics Symposium* (pp. ARMA-05). ARMA.

Harrison, J.P., Hudson, J.A., 1997. Discontinuities. In: *Engineering rock mechanics: An introduction to principles*. Pergamon, Oxford, pp. 113 – 139.

Hartono, I., 2016. Optimization of Tsukamoto Fuzzy Inference System using Fuzzy Grid Partition. *International Journal of Computer Science and Network*, vol. 5, no. 5, pp. 786 – 791.

Hazrati Aghchai, M., Moarefvand, P., Salari Rad, H., 2020. On analytic solutions of elastic net displacements around a circular tunnel. *Journal of Mining and Environment*, vol. 11, no. 2, pp. 419 – 432.

Hoek, E., Brown, E.T., 2018. The Hoek–Brown failure criterion and GSI – 2018 Edition. *Journal of Rock Mechanics and Geotechnical Engineering*, vol. 11, no. 3, pp. 1 – 19.

Hoek, E., 1994. Strength of rock and rock masses. *ISRM News Journal*, vol. 2, no. 2, pp. 4 – 16.

Hoek, E., Bieniawski, Z.T., 1965. Brittle rock fracture propagation in rock under compression. *International Journal of Fracture Mechanics*, vol. 1, no. 3, pp. 137 – 155.

Hoek, E., Bray, J.D., 1981. *Rock slope engineering*, 3rd Edition. Taylor and Francis, London and New York.

Hoek, E., Carranza-Torres, C., Corkum, B., 2002. Hoek-Brown failure criterion. 2002 Edition, *Proceedings of NARMS-Tac*, Toronto.

Høien, A.H., Nilsen, B., Olsson, R., 2019. Main aspects of deformation and rock support in Norwegian road tunnels. *Tunnelling and Underground Space Technology*, vol. 86, pp. 262 – 278.

Hoseinie, S.H., Ataei, M., Osanloo, M., 2009. A new classification system for evaluating rock penetrability. *International Journal of Rock Mechanics and Mining Sciences*, vol. 46, no. 8, pp. 1329 – 1340.

Hudson, J.A., Harrison, J.P., 2005. *Engineering rock mechanics. An introduction to the principles*. Pergamon, Amsterdam.

International Society for Rock Mechanics (ISRM), 1981. Basic geotechnical description of rock masses. *International Journal of Rock Mechanics Mining Science Geomechanics*, vol. 18, pp. 85 – 110.

Iphar, M., Goktan, R.M., 2006. An application of fuzzy sets to the Diggability Index Rating Method for surface mine equipment selection. *International Journal of Rock Mechanics & Mining Sciences*, vol. 43, no. 2, pp. 253 – 266.

Jakubec, J., Laubscher, D., 2000. The MRMR rock mass rating classification system in mining practice. Proceedings of the 3rd International Conference and Exhibition on Mass, Brisbane, Australia, pp. 413 – 421.

Jalalifar, H., Mojedifar, S., Sahebi, A.A., Nezama, H., 2011. Application of the adaptive neuro-fuzzy inference system for prediction of a rock engineering classification system. Computers and Geotechnic, vol. 38, no. 6, pp. 783 – 790.

Jang, J.R., Sun, C.T., Mizutani, E., 1997. Neuro-fuzzy and soft computing, a computational approach to learning and machine intelligence. Prentice Hall.

Jang, J., Gulley, N., 1997. MATLAB: Fuzzy Logic Toolbox User's Guide. The Math-Works, pp. 19 – 127.

Javad, M., Amin, Z.S., Hamid, T., 2015. Adaptive-neuro fuzzy inference system (ANFIS) model for prediction of blast-induced ground vibration. Science International (Lahore), vol. 27, no. 3, pp. 2079 – 2091.

Juang, C.H., Jhi, Y.-Y., Lee, D., 1998. Stability analysis of existing slopes considering uncertainty. Engineering Geology, vol. 49, no. 2, pp. 111 – 133.

Kacewicz, M., 1987. Fuzzy slope stability method. Mathematics Geology, vol. 19, no. 8, pp. 757 – 767.

Kalantary, F., Ardalan, H., Nariman-Zadeh, N., 2009. An investigation on the Su–NSPT correlation using GMDH type neural networks and genetic algorithms. Engineering Geology, vol. 104, no. 1 – 2, pp. 144 – 155.

Kang, Y., Wang, J., 2010. A support-vector-machine-based method for predicting large deformation in rock mass. Proceedings of the 7th International Conference on Fuzzy Systems and Knowledge Discovery, FSKD 2010. Institute of Electrical and Electronics Engineers (IEEE) Computer Society, Yantai, Shandong, China, pp. 1176 – 1180.

Kanik, M., Gurocak, Z., 2018. Importance of numerical analyses for determining support systems in tunneling: A comparative study from the Trabzon-Gumushane tunnel. *Journal of African Earth Sciences*, vol. 143, pp. 253 – 265.

Kavvadas, M.J., 2005. Monitoring ground deformation in tunnelling: Current practice in transportation tunnels. *Engineering Geology*, vol. 79, no. 1 – 2, pp. 93 – 113.

Kaya, A., Akgün, A., Karaman, K., Bulut, F., 2016. Understanding the mechanism of slope failure on a nearby highway tunnel route by different slope stability analysis methods: a case from NE Turkey. *Bulletin of Engineering Geology and the Environment*, vol. 75, pp. 945 – 958.

Kayadelen, C., Taşkıran, T., Günaydın, O., Fen, M., 2009. Adaptive neuro-fuzzy modeling for the swelling potential of compacted soils. *Environmental Earth Sciences*, vol. 59, no.1, pp. 109 – 115.

Khademi, H.J., Shahriar, K., Rezai, B., Bejari, H., 2010. Application of fuzzy set theory to rock engineering classification systems: an illustration of the rock mass excavability index. *Rock Mechanics and Rock Engineering*, vol. 43, no. 3, pp. 335 – 350.

Khadka, S.S., Maskey, R.K., 2017. Stability analysis and design of rock support for tunnel and cavern of Kathmandu University Geo-lab. *Kathmandu University Journal of Science, Engineering and Technology*, vol. 13, no. 1, pp. 1 – 19.

Kolapo, P., Oniyide, G.O., Said, K.O., Lawal, A.I., Onifade, M., Munemo, P., 2022. An overview of slope failure in mining operations. *Mining*, vol. 2, no. 2, pp. 350 – 384.

Laubscher, D.H., 1975. Class distinction in rock masses. *Coal, Gold, and Base Minerals of South Africa*, vol. 23, no. 6, pp. 37 – 50.

Laubscher, D.H., 1990. A geomechanics classification system for the rating of rock mass in mine design. *Journal of the South African Institute of Mining and Metallurgy*, vol. 9, no. 10, pp. 257 – 273.

Laubscher, D.H., 1993. Planning mass mining operations. *Comprehensive rock engineering: Principles, practices and projects*. Hudson, J. (Eds.), Pergamon Press, vol. 2, pp. 547 – 583.

Laubscher, D.H., Jakubec, J., 2001. The MRMR rock mass classification for jointed rock masses. Colorado, SME, Littleton, pp. 455-463.

Li, C., Lu, X., Zhu, N., Lu, Y., Wu, Y., Li, G., 2015. Continuously extracting section and deformation analysis for subway tunnel based on LiDAR points. *Acta Geodaetica et Cartographica Sinica*, vol. 44, no. 9, pp. 1056 – 1062.

Li, Y., Li, X., Zhang, C., 2006. Displacement prediction method of surrounding rock in tunnel based on BP neural network. *Chinese Journal of Rock Mechanics and Engineering*, vol. 25, no. 1, pp. 2969 – 2973.

Lim, S.S., Martin, C.D., 2010. Core dinking and its relationship with stress magnitude for Lac Du Bonnet granite. *International Journal of Rock Mechanics and Mining Science*, vol. 47, pp. 254 – 264.

Liu, K.Y., Qiao, C.S., Wang, S.D., 2008. Study on the GA-ANIFIS intelligence model for nonlinear displacement time series analysis of long and large tunnel construction. *Proceedings of the International Young Scholars' Symposium on Rock Mechanics – Boundaries of Rock Mechanics Recent Advances and Challenges for the 21st Century*. Taylor and Francis/Balkema, pp. 667 – 671, Beijing, China.

Liu, Z.-J., Huang, Y., Zhou, D., Ge, H., 2017. Analysis of external water pressure for a tunnel in fractured rocks. *Geofluids*, vol. 2017, Article ID 8618613, pp. 1 – 11.

Lu, W., Sun, H., Song, S., Ma, W., Wu, Y., Guo, X., 2021. Mechanical analysis of arch support and rock–arch interaction considering arch failure

mechanism. Iranian Journal of Science and Technology, Transactions of Civil Engineering, vol. 46, pp. 353 – 365.

Luo, Y., Chen, J., Xi, W., Zhao, P., Qiao X., Deng, X., Liu, Q., 2016. Analysis of tunnel displacement accuracy with total station. Measurement, vol. 83, pp. 29 – 37.

Mahdevari, S., Torabi, S.R., 2012. Prediction of tunnel convergence using artificial neural networks. Tunnelling and Underground Space Technology, vol. 28, pp. 218 – 228.

Mamdani, E.H., Assilian, S., 1975. An experiment in linguistic synthesis with a fuzzy logic controller. International Journal of Man-Machine Studies, vol. 7, no. 1, pp. 1 – 13.

Mao, G., Xia, Y., Liu, L., 2011. Time series forecasting of tunnel surrounding rock displacement. Proceedings of the International Conference on Civil Engineering and Building Materials (CEBM 2011). Trans Tech Publications, pp. 1789 – 1793, Kunming, China.

Marinos, V., Marinos, P., Hoek, E., 2005. The geological strength index: applications and limitations. Bulletin of Engineering Geology and the Environment, vol. 64, pp. 55 – 65.

Marsella, M., Scaioni, M., 2018. Sensors for deformation monitoring of large civil infrastructures. Sensors, vol. 18, no. 11, pp. 3941 – 3945.

MathWorks Inc, 2010. MATLAB fuzzy logic toolbox user's guide (version R2010a). MathWorks Inc., Massachusetts, USA.

MathWorks, 2022. Machine Learning in MATLAB. [Online] Available at: <https://www.mathworks.com/help/stats/machine-learning-in-matlab.html> [Accessed 14 November 2022].

Matos, Y.M.P., Dantas, S., Barreto, G.A., 2019. A Takagi-Sugeno fuzzy model for predicting the clean rock joints shear strength. Revista Escola de

Minas (REM)-International Engineering Journal, vol. 72, no. 2, pp. 193 – 198.

Mishra, D.A., Basu, A., 2013. Estimation of uniaxial compressive strength of rock materials by index tests using regression analysis and fuzzy inference system. *Engineering Geology*, vol. 160, pp. 54 – 68.

Monjezi, M., Rezaei, M., 2011. Developing a new fuzzy model to predict burden from rock geo-mechanical properties. *Expert Systems with Application*, vol. 38, no. 8, pp. 9266 – 9273.

Monjezi, M., Rezaei, M., Yazdian Varjani, A., 2009. Prediction of rock fragmentation due to blasting in Gol-E-Gohar iron mine using fuzzy logic. *International Journal of Rock Mechanics & Mining Sciences*, vol. 46, pp. 1273 – 1280.

Murnawan, M., Virgana, R., Lestari, S., 2021. Comparison of Sugeno and Tsukamoto fuzzy inference system method for determining estimated production amount. *Turkish Journal of Computer and Mathematics Education*, vol. 12, no. 8, pp. 1467 – 1476.

Nguyen, V.U., 1985. Some fuzzy set applications in mining geomechanics. *International Journal of Rock Mechanics and Mining Sciences and Geomechanics Abstracts*, vol. 22, no. 6, pp. 369 – 379.

Nguyen, V.U., Ashworth, E.A., 1985. Rock mass classification by fuzzy sets. In: *26th US Symposium on Rock Mechanics*, Rapid City, SD, pp. 937 – 945.

Norwegian Geotechnical Institute (NGI), 2015. Using the Q-system – Rock mass classification and support design. NGI Publication, Oslo, Norway.

Nur, A., Simmons, G., 1970. The origin of small cracks in igneous rocks. *International Journal of Rock Mechanics and Mining Sciences*, vol. 7, no. 3, pp. 307 – 314.

Ozsan, A., Karakus, M., 2006. Site investigations and convergence measurements for a twin metro tunnel driven in Ankara clay, Turkey. Proceedings of the 10th IAEG International Congress (IAEG2006), Paper No. 504.

Palmstrom, A., 1982. The volumetric joint count – A useful and simple measure of the degree of rock mass jointing. IAEG Congress, New Delhi, pp. V.221 – V.228.

Palmstrom, A., Broch, E., 2006. Use and misuse of rock mass classification systems with particular reference to the Q-System. Tunnels and Underground Space Technology, vol. 21, pp. 575 – 593.

Panet, M., 1979. Time-dependent deformations in underground works. Proceedings of the 4th International Congress on Rock Mechanics, Montreux, Francois, vol. 3, pp. 279 – 290.

Panet, M., 1995. Le calcul des tunnels par la méthode convergence-confinement. Presses d'Ecole Nationale des Ponts et Chaussées, Paris.

Park, K.H., Kim, Y.J., 2006. Analytical solution for a circular opening in an elastic-brittle-plastic rock. International Journal of Rock Mechanics and Mining Sciences, vol. 43, no. 4, pp. 616 – 622.

Priest, S.D., 2004. Determination of discontinuity size distributions from scanline data. Rock Mechanics and Rock Engineering, vol. 37, no. 5, pp. 347 – 368.

Provenzano, P., Ferlisi, S., Musso, A., 2004. Interpretation of a model footing response through an adaptive neural fuzzy inference system. Computers and Geotechnics, vol. 31, no. 3, pp. 251 – 266.

Raghuvanshi, T.K., 2017. Plane failure in rock slopes – A review on stability analysis techniques. Journal of King Saud University – Science, vol. 31, no. 1, pp. 1 – 20.

Rahman, M.S., Wang, J., 2002. Fuzzy neural network models for liquefaction prediction. *Soil Dynamics and Earthquake Engineering*, vol. 22, no. 8, pp. 685 – 694.

Rangel, J.L., Iturrarán-Viveros, U., Gustavo Ayala, A., Cervantes, F., 2005. Tunnel stability analysis during construction using a neuro-fuzzy system. *International journal for numerical and analytical methods in geomechanics*, vol. 29, no. 15, pp. 1433 – 1456.

Rehman, S., Meheub, S., Shyamal, D., Haroon, 1040 S., Xuang, S., Kashif, I., Jie, D., 2020. Assessing subsidence susceptibility to coal mining using frequency ratio, statistical index and Mamdani fuzzy models: evidence from Raniganj coalfield, India. *Environmental Earth Sciences*, vol. 79, no 16, pp. 1 – 18.

Rocscience Inc, 2002. Dips user guide. [Online] Available at: <https://www.rocscience.com/help/dips/tutorials/tutorials-overview/tutorial-01-dips-quick-start> [Accessed May 2022].

Rodríguez, P., Arab, P.B., Celestino, T.B., 2016. Characterization of rock cracking patterns in diametral compression tests by acoustic emission and petrographic analysis. *International Journal of Rock Mechanics & Mining Sciences*, vol.83, pp. 73 – 85.

Saepullah, A., Wahono, R.S., 2015. Comparative analysis of Mamdani, Sugeno and Tsukamoto method of fuzzy inference system for air conditioner energy saving. *Journal of Intelligent Systems*, vol. 1, no. 2, pp. 143 – 147.

Sandrone, F., 2008. Analysis of pathologies and long-term behaviour of Swiss National Road tunnels. Thèse EPFL no. 4019, École Polytechnique Fédérale de Lausanne, Lausanne.

Sandrone, F., Labiouse, V., 2010. Analysis of the evolution of road tunnels equilibrium conditions with a convergence-confinement approach. *Rock Mechanics Rock Engineering*, vol. 43, pp. 201 – 218.

Sandrone, F., Labiouse, V., Mathier, J.F., 2007. Data collection for Swiss road tunnels maintenance. *Felsbau*, vol. 1, pp. 8-14.

Sari, M., 2016. Estimating strength of rock masses using fuzzy inference system. *Rock Mechanics and Rock Engineering: From the past to the future*, Ulusay et al. (Eds.), Eurock 2016, ISRM International Symposium, Cappadocia, Turkey, vol. 1, pp. 129 – 134.

Scaioni, M., Barazzetti, L., Giussani, A., Previtali, M., Roncoroni, F., Alba, M.I., 2014. Photogrammetric techniques for monitoring tunnel deformation. *Earth Science Informatics*, vol. 7, no. 2, pp. 83 – 95.

Sezer, E.A., Pradhan, B., Gökçeoğlu, C., 2011. Manifestation of an adaptive neurofuzzy model on landslide susceptibility mapping: Klang valley, Malaysia. *Expert Systems with Applications*, vol. 38, no. 7, pp. 8208 – 8219.

Sönmez, H., Gökçeoğlu, C., Ulusay, R., 2003. An application of fuzzy sets to the Geological Strength Index (GSI) system used in rock engineering. *Engineering Applications of Artificial Intelligence*, vol. 16, no. 3, pp. 251 – 269.

Stacey, T.R., 1981. Simple extension strain criterion for fracture of brittle rock. *International Journal of Rock Mechanics and Mining Sciences*, vol.18, no. 6, pp. 469 – 474

Stacey, T.R., 2001. Best practice rock engineering handbook for “other” mines. The Safety in Mines Research Advisory Committee (SIMRAC), Braamfontein

Stein, S., Geller, R.J., Liu, M., 2012. Why earthquake hazard maps often fail and what to do about it. *Tectonophysics*, pp. 1 – 25.

Sugeno, M., 1985. Industrial applications of fuzzy control. Elsevier Science Pub. Co., Amsterdam.

Sun, J., Li, T., Hung, R., Wang, F., 2003. Design of fuzzy inference system for classification of underground construction surrounding rock. Journal of Engineering Geology, vol.11, no. 3, pp. 269 – 274.

Tay, K.M., Lim, C.P., 2006. Fuzzy FMEA with a guided rules reduction system for prioritization of failures. International Journal of Quality and Reliability Management, vol. 23, no. 8, pp. 1047 – 1066.

Trimble User Community, 2013. Trimble S8 total station data sheet. [Online] Available at: <https://totalstations.co/wp-content/uploads/2017/07/Trimble-S8-Edited-1.pdf> [Accessed 15 October 2022].

Tsukamoto, Y., 1979. An approach to fuzzy reasoning method. Advances in fuzzy set theory and applications. Elsevier, North-Holland.

Tutmez, B., Kahraman, S., Günaydin, O., 2007. Multifactorial fuzzy approach to the sawability classification of building stones. Construction and Building Materials, vol. 21, no.8, pp. 1672 – 1679.

Vadapalli, P., 2021. Fuzzy inference system: Overview, applications, characteristics, structure and advantages. [Online] Available at: <https://www.upgrad.com/blog/fuzzy-inference-system/> [Accessed 15 March 2022].

Walia, N., Singh, H., Sharma, A., 2015. ANFIS: Adaptive neuro-fuzzy inference system – A Survey. International Journal of Computer Applications, vol.123, no. 13, pp. 32 – 38.

Wang, M.-W., Chen, G.-Y., Jin, J.-L., 2011. Risk evaluation of surrounding rock stability based on stochastic simulation of multi-element connection number and triangular fuzzy numbers. Chinese Journal of Geotechnical Engineering, vol. 33, no. 4, pp. 643 – 647.

Wu, Z.Z., 2010. Stochastic medium predicting model of ground movement tunneling based on non-uniform convergence mode. *Zhongnan Daxue Xuebao (Ziran Kexue Ban)/Journal of Central South University (Science and Technology of Mining and Metallurgy)*, vol.41, pp. 2005 – 2010.

Wyllie, D.C., Mah, C.W., 2004. *Rock slope engineering*, 4th Edition. Taylor and Francis, London and New York.

Xie, C., Nguyen, H., Bui, X.-N., Nguyen, V.-T., Zhou, J., 2021. Predicting roof displacement of roadways in underground coal mines using adaptive neuro-fuzzy inference system optimized by various physics-based optimization algorithms. *Journal of Rock Mechanics and Geotechnical Engineering*, vol. 13 no. 6, pp. 1452 – 1465.

Yazdani-Chamzini, A., 2014. Proposing a new methodology based on fuzzy logic for tunnelling risk assessment. *Journal of Civil Engineering and Management*, vol. 20, no.1, pp. 82 – 94.

Zadeh, L.A., 1965. Fuzzy sets. *Information and Control*, vol. 8, pp. 338 – 353.

Zadeh, L.A., 1975. The concept of a linguistic variable and its application to approximate reasoning Part I. *Information Sciences*, vol. 8, pp. 199 – 249.

Zhang, L., 2017. Chapter 5 – Rock Masses. In: L. Zhang, Eds. *Engineering Properties of Rocks*. Second Edition. Butterworth-Heinemann, pp. 137 – 171, Tucson, Arizona.

Zhou, L., Liu, B., Fan, Y., 2018. The effect of radial cracks on tunnel stability. *Geomechanics and Engineering*, vol. 15, no. 2, pp. 721 – 728.

Zimmermann, H. J., 2010. Fuzzy set theory. *Wiley Interdisciplinary Reviews: Computational Statistics*, vol. 2, no. 3, pp. 317 – 332.

APPENDIX

Appendix A: Mapping Data

Dip Direction	Dip
140	61
340	85
85	76
340	57
101	78
356	66
125	54
125	54
334	72
84	78
87	73
351	44
216	65
348	68
342	77
332	89
352	78
335	51
228	69
338	72
334	69
345	64
337	64
1	41
354	60
350	71
328	48
219	84
350	77
247	84
353	66
241	84
355	62
104	77

338	64
359	68
211	76
182	66
348	34
213	69
353	61
216	76
206	59
123	84
87	74
356	63
213	76
215	77
92	61
97	69
209	5
3	65
359	67
146	56
346	78
343	76
350	68
350	68
354	74
357	65
85	72
63	61
211	61
118	39
150	47
107	65
112	33
223	85
41	90
200	63
96	36
24	23
102	41
124	35

98	72
136	53
85	72
94	60
95	64
95	62
214	53
125	46
47	45
111	52
113	50
225	63
130	55
134	44
127	59
213	60
97	60
201	56
218	76
215	78
165	7
224	58
5	72
340	77
135	51
96	60
54	79
101	33
62	79
119	55
118	39
91	64
6	75
202	61
346	78
130	59
147	38
95	63
217	54
135	51

128	62
346	78
324	83
224	64
131	56
85	82
116	36
125	36
124	40
123	40
130	49
161	60
83	65
105	33
127	12
94	60
31	46
107	65
213	82
124	40
123	40
130	49
161	60
83	65
105	33
234	66
234	73
225	60
236	67
236	67
229	77
2	48
13	59
354	61
125	54
125	54
334	72
84	78
87	73
91	69

216	65
348	68
342	77
332	89
352	78
335	51
226	52
115	35
210	66
131	58
170	79
155	54
340	58
129	90
337	65
94	69
246	50
59	48
64	49
97	33
106	76
51	44
237	58
232	57
99	70
233	51
210	80
223	65
340	60
230	68
228	27
127	51
336	66
215	62
224	58
39	57
17	56
146	46
124	80
91	67

Appendix B: Micro-fracturing data and predictive model

B1: Number of fractures for right side of the tunnel

NUMBER OF FRACTURE FOR RIGHT SIDE OF THE TUNNEL												
Position	SLIDE A			SLIDE B			SLIDE C			SLIDE D		
	Grain Boundary cracks	Inter-Angular cracks	Trans-angular cracks	Grain Boundary cracks	Inter-Angular cracks	Trans-angular cracks	Grain Boundary cracks	Inter-Angular cracks	Trans-angular cracks	Grain Boundary cracks	Inter-Angular cracks	Trans-angular cracks
Point 1	15	4	28	8	6	4	2	4	9	4	5	7
Point 2	10	8	19	6	5	7	8	3	8	5	3	2
Point 3	3	7	10	2	7	11	6	9	8	5	8	7
Point 4	6	6	7	5	6	8	6	5	10	4	4	9
Point 5	5	8	6	8	6	6	5	4	6	4	4	5
Point 6	2	7	5	7	5	7	4	3	5	3	9	10
Point 7	3	4	5	3	5	6	5	8	5	2	12	5
Point 8	6	3	2	3	2	4	7	7	6	3	3	6
Point 9	5	2	6	2	6	4	5	3	2	3	3	5
Point 10	2	8	2	6	5	2	2	5	2	2	7	3
Point 11	3	2	5	6	3	3	5	3	3	6	5	2
Point 12	2	6	5	4	6	2	2	3	4	3	3	3
Point 13	3	3	6	2	4	3	4	3	5	3	4	3
Point 14	5	4	2	2	2	4	5	3	4	4	3	4
TOTAL	70	72	108	64	68	71	66	63	77	51	73	71

(GB)_Grain boundary cracks - Found on the boundary of a grain

(IA)_Inter-angular cracks - Found within the grain

(TA)_Trans-angular cracks - Cut across different mineral grains and boundaries

B2: Number of fractures for left side of the tunnel

NUMBER OF FRACTURE FOR LEFT SIDE OF THE TUNNEL												
	SLIDE A			SLIDE B			SLIDE C			SLIDE D		
	Grain Boundary cracks	Inter-Angular cracks	Trans-angular cracks	Grain Boundary cracks	Inter-Angular cracks	Trans-angular cracks	Grain Boundary cracks	Inter-Angular cracks	Trans-angular cracks	Grain Boundary cracks	Inter-Angular cracks	Trans-angular cracks
Point 1	3	3	22	3	5	8	3	5	15	4	2	6
Point 2	4	9	12	2	0	9	4	5	9	2	4	13
Point 3	6	6	4	8	4	7	8	9	7	5	3	5
Point 4	8	7	3	5	9	5	3	10	6	4	3	4
Point 5	2	4	14	2	0	17	1	2	22	0	0	0
Point 6	4	3	11	2	0	8	3	2	7	4	5	4
Point 7	2	3	9	6	3	7	2	2	6	2	2	9
Point 8	3	4	4	3	8	3	2	7	2	4	5	3
Point 9	2	3	3	2	7	5	2	6	4	5	9	2
Point 10	2	1	5	4	2	4	4	2	7	9	2	5
TOTAL	36	43	87	37	38	73	32	50	85	39	35	51

(GB)_ Grain boundary cracks - Found on the boundary of a grain

(IA)_ Inter-angular cracks - Found within the grain

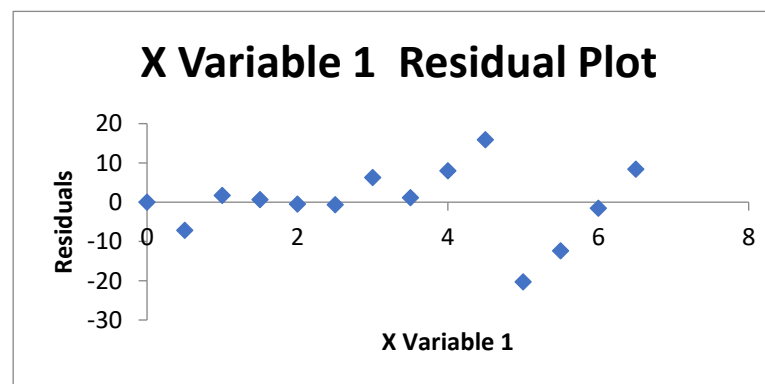
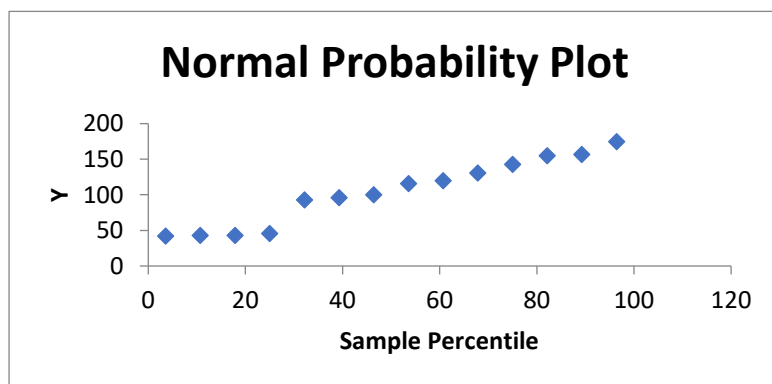
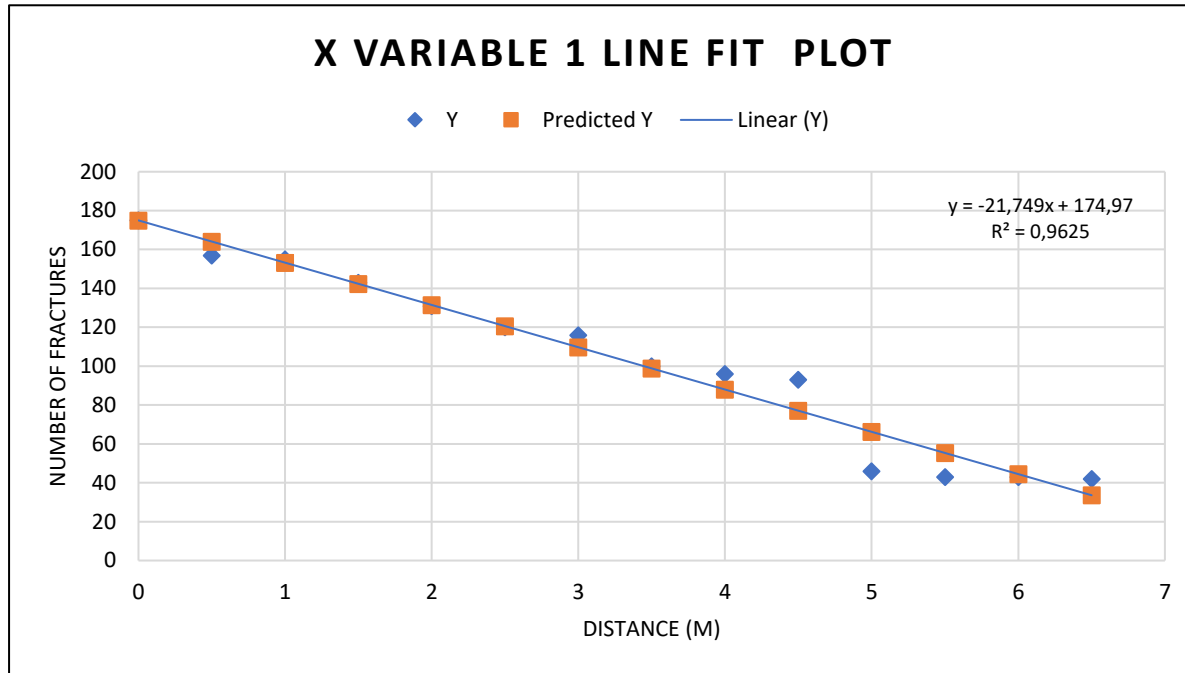
(TA)_ Trans-angular cracks - Cut across different mineral grains and boundaries

B3: Predictive model

SUMMARY OUTPUT								
<i>Regression Statistics</i>								
Multiple R	0,981096							
R Square	0,962549							
Adjusted R Square	0,959428							
Standard Error	9,33982							
Observations	14							
ANOVA								
	<i>df</i>	<i>SS</i>	<i>MS</i>	<i>F</i>	<i>Significance F</i>			
Regression	1	26904,07	26904,07	308,4189	6,33E-10			
Residual	12	1046,787	87,23223					
Total	13	27950,86						
	<i>Coefficients</i>	<i>Standard Error</i>	<i>t Stat</i>	<i>P-value</i>	<i>Lower 95%</i>	<i>Upper 95%</i>	<i>Lower 95.0%</i>	<i>Upper 95.0%</i>
Intercept	174,9714	4,736153	36,94379	9,92E-14	164,6522	185,2906	164,6522	185,2906
X Variable 1	-21,7495	1,238448	-17,5619	6,33E-10	-24,4478	-19,0511	-24,4478	-19,0511
RESIDUAL OUTPUT					PROBABILITY OUTPUT			

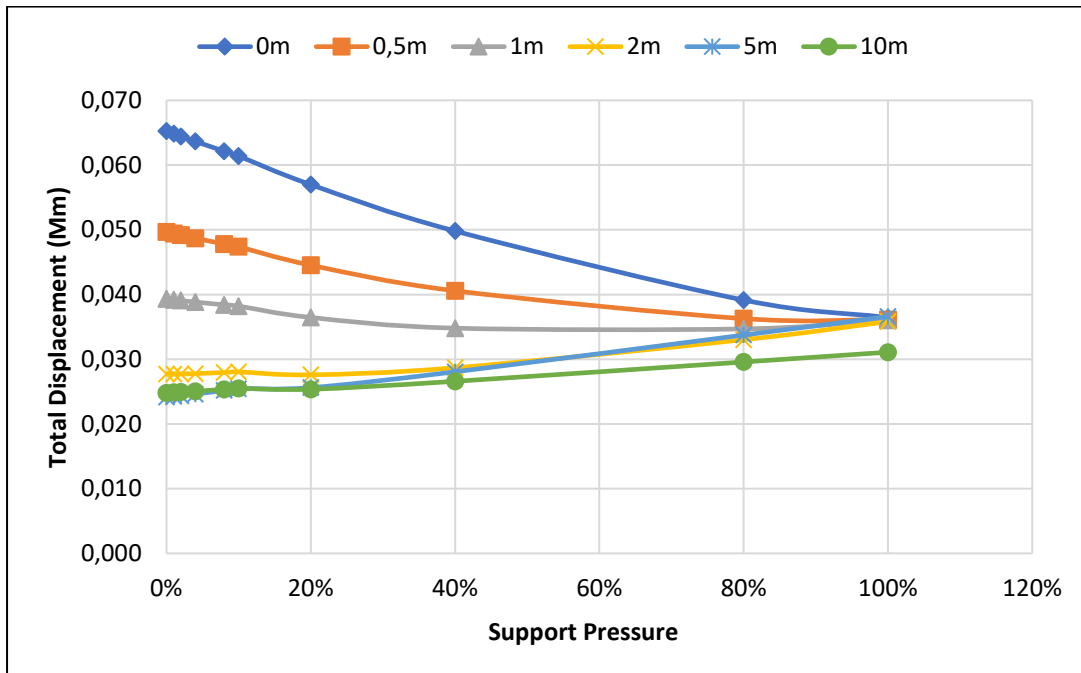
<i>Observation</i>	<i>Predicted Y</i>	<i>Residuals</i>	<i>Standard Residuals</i>	<i>Percentile</i>	<i>Y</i>
1	174,9714	0,028571	0,003184	3,571429	42
2	164,0967	-7,0967	-0,79086	10,71429	43
3	153,222	1,778022	0,198143	17,85714	43
4	142,3473	0,652747	0,072742	25	46
5	131,4725	-0,47253	-0,05266	32,14286	93
6	120,5978	-0,5978	-0,06662	39,28571	96
7	109,7231	6,276923	0,699503	46,42857	100
8	98,84835	1,151648	0,12834	53,57143	116
9	87,97363	8,026374	0,894462	60,71429	120
10	77,0989	15,9011	1,772024	67,85714	131
11	66,22418	-20,2242	-2,25379	75	143
12	55,34945	-12,3495	-1,37623	82,14286	155
13	44,47473	-1,47473	-0,16434	89,28571	157
14	33,6	8,4	0,936099	96,42857	175

B4: Predictive model plots

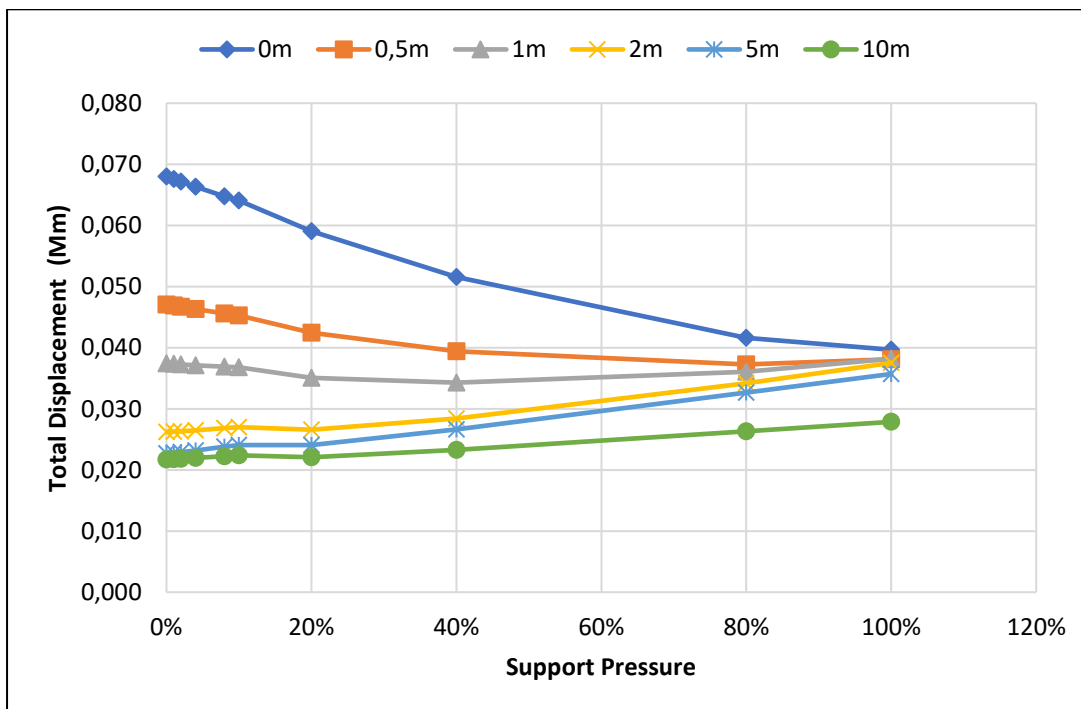


APPENDIX C: Total displacement

C1: Total Displacement on tunnel sidewalls in Zone 1

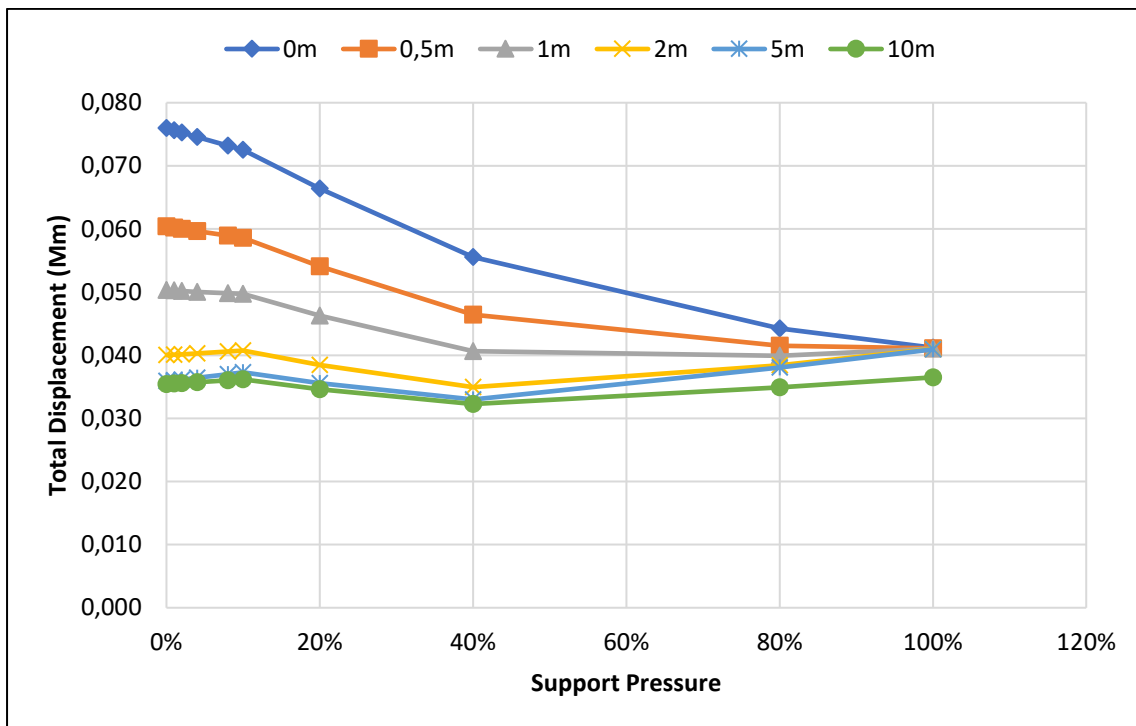


Total displacement on the left sidewall in Zone1

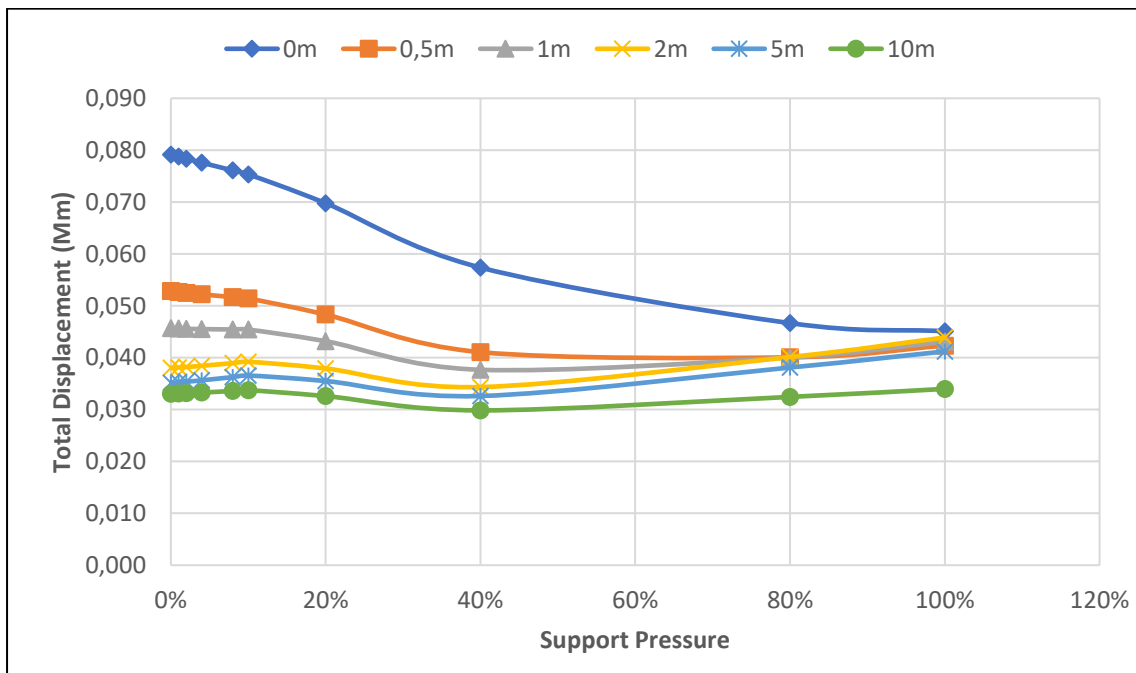


Total displacement on the right sidewall in Zone1

C2: Total Displacement on tunnel sidewalls in Zone 2

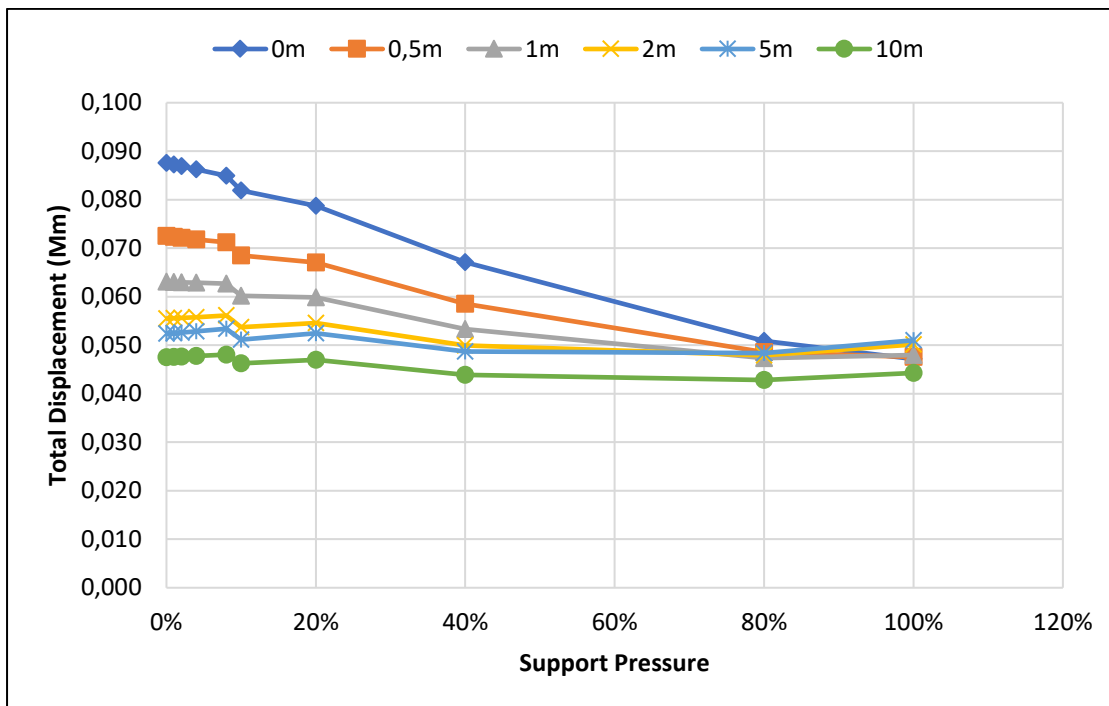


Total displacement on the left sidewall in Zone2

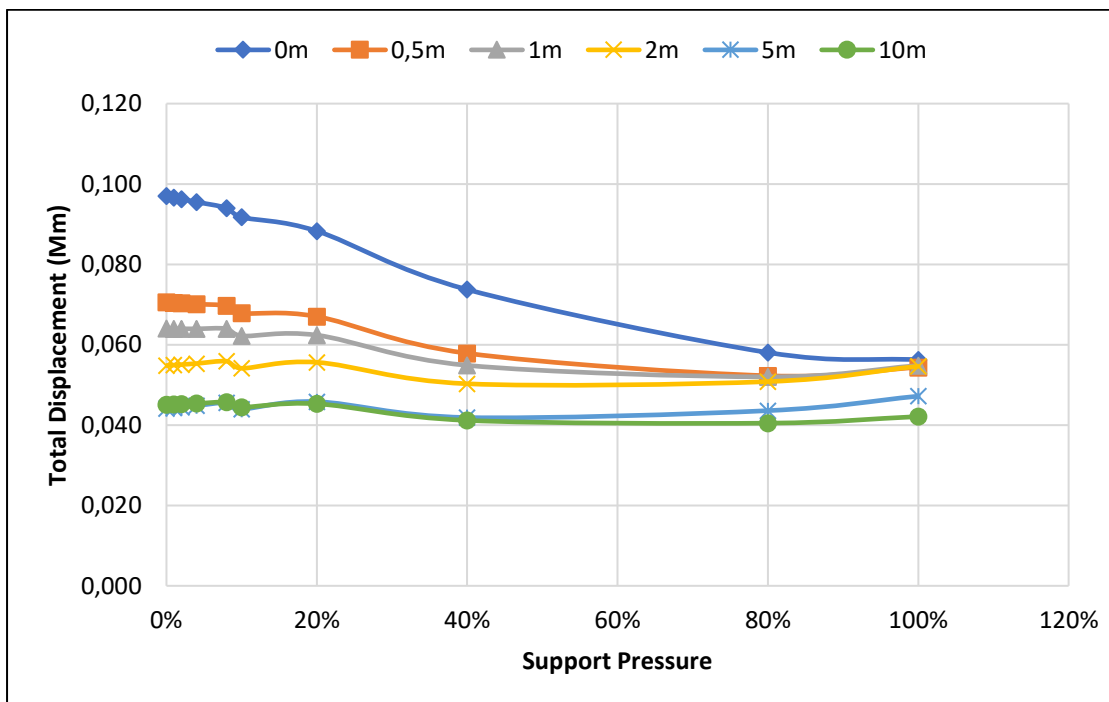


Total displacement on the right sidewall in Zone2

C3: Total Displacement on tunnel sidewalls in Zone 3



Total displacement on the tunnel left side wall in Zone 3



Total displacement on the tunnel right side wall in Zone 3